

UNIVERSIDAD DE CANTABRIA



ESCUELA DE DOCTORADO DE LA UNIVERSIDAD DE CANTABRIA  
DOCTORADO EN INGENIERÍA QUÍMICA DE LA ENERGÍA Y DE PROCESOS

**ADVANCED ELECTROCHEMICAL AND PHOTOCHEMICAL  
TECHNOLOGIES FOR THE TREATMENT OF POLY- AND  
PERFLUOROALKYL SUBSTANCES (PFASs) IN WATER**

*Tecnologías electroquímicas y fotoquímicas avanzadas para el  
tratamiento de sustancias poli- y perfluoroalquílicas (PFASs) en agua*

Memoria de tesis doctoral presentada para optar al título de Doctor por  
la Universidad de Cantabria

Presentada por:

**Beatriz Gómez Ruiz**

Dirigida por:

**Prof. Dra. Ana María Urtiaga Mendia**

**Dra. Nazely Diban Gomez**

Santander, 2018



*Programa de Doctorado en Ingeniería Química, de la Energía y de  
Procesos (BOE núm. 16, de 19 de enero de 2015. RUCT: 5601000)*

The research described in this thesis was conducted at the Environmental and Bioprocess Technologies (EBT) Research Group in the Department of Chemical and Biomolecular Engineering at the University of Cantabria.

This research was financially supported by the Spanish Ministry of Economy and Competitiveness and the European Regional Development Fund through the projects: CTM2013-44081-R (RETOS-FEDER, UE), “Development of innovative technologies for the treatment of perfluorinated contaminants in water”; and, CTM2016-75509-R (RETOS-FEDER, UE), “Advanced strategies for the integration of membranes and electrocatalytic and photocatalytic processes for the elimination of persistent pollutants”. The author of the thesis would also like to express her gratitude to the Spanish Ministry of Economy and Competitiveness for the FPI postgraduate research grant (BES-2014-071045) and a predoctoral mobility grant for conducting short stays in R&D Centers (EEBB-I-17-12384). This research stay was developed in the Department of Civil and Environmental Engineering at Colorado School of Mines (United States of America) over the period June-September 2017, under the supervision of Professor Timothy J. Strathmann.

Due to all of these, a warm thanks towards these institutions is extended.



This doctoral thesis is presented in the form of compendium of interrelated scientific articles published in international journals indexed in the Journal Citation Reports (JCR):

- **B. Gomez-Ruiz**, N. Diban, A. Urriaga, Comparison of microcrystalline and ultrananocrystalline boron doped diamond anodes: Influence on perfluorooctanoic acid electrolysis, *Separation and Purification Technology*, 208 (2019), 167-177. Quartile Q1 in Category *Engineering, Chemical* (22/137)
- **B. Gomez-Ruiz**, S. Gómez-Lavín, N. Diban, V. Boiteux, A. Colin, X. Dauchy, A. Urriaga, Boron doped diamond electrooxidation of 6:2 fluorotelomers and perfluorocarboxylic acids. Application to industrial wastewaters treatment, *Journal of Electroanalytical Chemistry*, 798 (2017), 51–57. Quartile Q1 in Category *Chemistry, Analytical* (17/81)
- **B. Gomez-Ruiz**, S. Gómez-Lavín, N. Diban, V. Boiteux, A. Colin, X. Dauchy, A. Urriaga, Efficient electrochemical degradation of poly- and perfluoroalkyl substances (PFASs) from the effluents of an industrial wastewater treatment plant, *Chemical Engineering Journal*, 322 (2017), 196-204. Quartile Q1 in Category *Engineering, Chemical* (3/50)
- **B. Gomez-Ruiz**, P. Ribao, N. Diban, M.J. Rivero, I. Ortiz, A. Urriaga, Photocatalytic degradation and mineralization of perfluorooctanoic acid (PFOA) using a composite TiO<sub>2</sub>-rGO catalyst, *Journal of Hazardous Materials*, 344 (2017), 950–957. Quartile Q1 in Category *Engineering, Environmental* (5/50)





# ACKNOWLEDGEMENTS

---

Deseo expresar mi más sincero agradecimiento a mis directoras de tesis, la Prof. Dra. Ane Miren Urtiaga Mendía y la Dra. Nazely Diban Gómez, por la confianza que depositaron en mí para desarrollar este trabajo, pero sobre todo por su ayuda, comprensión y paciencia durante toda esta etapa investigadora. Especialmente, gracias por todo el tiempo invertido tanto en enseñarme la metodología de trabajo en los laboratorios, así como, el tratamiento de resultados, con valiosas sugerencias y marcando los caminos oportunos para dar lugar a la obtención de buenos resultados y publicaciones.

I would like to acknowledge Prof. Dr. Timothy J. Strathmann for giving me the opportunity to work in the Department of Civil and Environmental Engineering at Colorado School of Mines (USA). I would like to highlight his help, advice and support to develop the work. Moreover, I would also like to thank to Raul Tenorio for helping me with the photochemical treatments and support in the lab. Also, I am very grateful to Juliane Brown for the complex analysis of PFASs of my samples. Finally, I would like to show my gratitude to Hooman, Andrea, Rudy and Johan, to let me be a part of your international group with lots of memories and adventures. It was a positive experience for me professionally and personally.

Me gustaría también mostrar mi agradecimiento al personal técnico y profesorado del Departamento de Ingenierías Química y Biomolecular de la Universidad de Cantabria. Especialmente, quiero agradecer a Sonia Gómez Lavín toda la ayuda a lo largo de la tesis en la compleja preparación

y análisis de muestras, y también, por su contribución en la cooperación con el grupo dirigido por el Dr. Xavier Dauchy en el Laboratoire d'Hydrologie de Nancy (ANSES).

Ampliar mi agradecimiento a todos los compañeros del departamento, soy muy afortunada de haber compartido este periodo con personas dispuestos a dejar su trabajo por ayudarte y escucharte en cualquier momento.

No puedo dejar de dar las gracias a mis amigos por apoyarme siempre, y saber escucharme, aunque muchas veces no sepan de que les hablo.

Finalmente, quiero dar las gracias a toda mi familia, pero especialmente a mis padres, por enseñarme a que es posible caer y levantarse, por apoyarme en cada decisión y animarme a luchar hasta el final. A mi hermano por apoyarme, escucharme y sobre todo hacerme reír de cosas que solo tú y yo entenderemos. Y finalmente a Héctor, por su incondicional apoyo y fuerza en todo momento, por elegir ser mi acompañante de este viaje que es la vida.

A todos, ¡MUCHAS GRACIAS!

# ABSTRACT

---

Nowadays one of the most important challenges that the scientific community has to address, lies in the sustainable management of available water resources. However, water resources are currently threatened due to the increased release of anthropogenic pollutants of emerging concern from industrial and non-industrial sectors. Among these contaminants, poly- and perfluoroalkyl substances (PFASs) have been extensively released to the environment due to their use in a wide variety of industrial and household applications for 50 years. Furthermore, the extreme environmental persistence, global distribution and bio-accumulation of PFASs have resulted in increasing attention by the international regulatory bodies dealing with environmental issues for the last few years.

Not only the conventional water treatments are not capable of efficiently removing these hazardous substances, but also the concentration of certain PFASs could even rise after the breakdown of labile PFASs precursors in those processes. As a result, the development of environmentally friendly technologies to treat emissions of PFASs and polluted water with low-cost and high efficiency is crucial.

Over the last few decades, advanced oxidation processes (AOPs) have appeared as non-conventional techniques able to strengthen the oxidation ability for the degradation of recalcitrant compounds. AOPs are technologies based on redox reactions that involve the generation of reactive oxidizing species. Within this category, electrochemical and

photochemical approaches have become promising technologies for PFAS removal due to the capability to mineralize organic matter.

On the one hand, it is well-known that the anodic material strongly influences both selectivity and efficiency of the electrochemical process. Boron doped diamond (BDD) anodes have attracted interest for water treatment due to their unique properties such as inert surface with low adsorption properties, remarkable corrosion stability, long life span and high oxygen evolution overpotential, which lead to powerful oxidation conditions for the removal of organic compounds. Previous research has dealt with model solution of single PFASs using high initial concentration. However, either the role of the chemical and morphological features of the anode surface on the electro-oxidation pathways of PFASs or the electrochemical treatment of PFASs in real wastewaters have not been addressed yet.

On the other hand, photochemical technologies typically operate at ambient temperature and pressure, and minimize the generation of secondary pollution. Although  $\text{TiO}_2$  is extensively used for heterogeneous photocatalysis due to its photostability and low cost, most of the previous studies revealed the limited performance of  $\text{TiO}_2$  for PFASs degradation. Nevertheless, composite catalysts based on the combination of  $\text{TiO}_2$  and other materials, such as noble metals and carbon-based materials have become as alternative catalysts to improve the photoactivity of  $\text{TiO}_2$ . Within the homogeneous photocatalysis, UV photolysis of persulfate has demonstrated the ability to degrade PFASs by the sulfate radicals promoted. However, a new class of photo-reduction treatments has recently arisen as a promising alternative for PFASs defluorination. The activation of sensitizer (e.g., iodide or sulfite) by UV light involves the

generation of powerful hydrated electrons ( $e_{aq}^{\cdot-}$ ). These  $e_{aq}^{\cdot-}$  species can react rapidly with the electronegative fluorine atoms that act as reductive reaction centers, resulting in different degradation pathways conventional oxidative processes.

Based on the previous background, the work developed in this thesis aims to evaluate different electrochemical and photochemical strategies for the treatment of persistent PFASs in water. The first chapter of this thesis includes an overview to PFASs and the main fundamentals and challenges of the proposed water treatments. The chemical reagents, experimental set-ups and procedures, together with the analytical methods are described in Chapter 2. Chapter 3 summarizes the main results of the scientific publications done over the doctoral period. Specifically, a morphological, chemical and electrochemical comparison of commercial BDD anodic materials against the degradation of PFOA model solutions was initially included (scientific publication 1). Following this study, the application of microcrystalline BDD anode to remediate PFASs polluted industrial wastewaters under the effect of complex matrix composition with high background organic load was evaluated. The understanding of the electrochemical reaction mechanisms involved and the potential formation of undesired oxidation by-products, such as chlorinated species, were also investigated (scientific publications 2 and 3). Furthermore, the viability of photo-assisted technologies was initially studied by a photocatalyst prepared with  $TiO_2$  and reduced graphene oxide towards the degradation of PFOA in model solutions (scientific publication 4). Additionally, the capability of sequential oxidative/reductive photochemical strategies to remove a complex mixture of PFASs contained in a model aqueous film-forming foam (AFFF) impacted groundwater was examined. The oxidative treatment consisted of UV irradiation with sodium persulfate to generate

sulfate radicals, whereas the UV reductive process used sodium sulfite as the sensitizer to generate hydrated electrons (manuscript under elaboration). Finally, chapter 4 comprises the main conclusions of the thesis.

Hoy en día uno de los principales retos al que tiene que enfrentarse la comunidad científica radica en la generación de conocimiento para el desarrollo de una gestión sostenible de los recursos hídricos disponibles. Sin embargo, estos recursos se están viendo actualmente amenazados debido al incremento de contaminantes emergentes de origen antropogénico procedentes tanto de sectores industriales como de otro tipo de fuentes contaminantes. Entre estos compuestos, las sustancias poli- y perfluoroalquílicas (PFASs) han sido ampliamente liberadas al medio ambiente debido a su uso en una amplia variedad de aplicaciones industriales y domésticas desde hace más 50 años. Debido a la extrema persistencia en el medio ambiente, la distribución mundial y la bioacumulación que presentan los PFASs, los organismos de vigilancia medioambiental y reguladores han aumentado la atención hacia estos compuestos en los últimos años.

Además de que los tratamientos de agua convencionales no son capaces de degradar estas sustancias nocivas eficientemente, la concentración de algunos PFASs podría incluso aumentar tras la descomposición de los precursores de estos compuestos en este tipo de tratamientos. Como resultado, es crucial el desarrollo de tecnologías innovadoras, respetuosas con el medio ambiente, para el tratamiento de aguas contaminadas y emisiones de PFASs con bajo coste asociado y alta eficiencia.

Durante las últimas décadas, los procesos de oxidación avanzada (POAs) han surgido como técnicas no convencionales capaces de

fortalecer la habilidad de oxidación para la eliminación de contaminantes recalcitrantes. Los POAs son tecnologías basadas en reacciones redox que dan lugar a la generación de especies oxidantes reactivas. Dentro de esta categoría, las estrategias fotoquímicas y electroquímicas se han convertido en tecnologías prometedoras para la eliminación de PFASs debido a su capacidad de mineralización de la materia orgánica.

Por un lado, el material anódico influye fuertemente en la selectividad y en la eficiencia del proceso electroquímico. Los ánodos de diamante dopados con boro (BDD) han atraído gran interés para el tratamiento de agua debido a sus propiedades únicas, como una superficie inerte que proporciona bajos valores de adsorción, extraordinaria estabilidad a la corrosión, larga vida útil y alto sobrepotencial para la evolución del oxígeno, lo que conduce a condiciones altamente oxidantes para la eliminación de compuestos orgánicos. Los trabajos ya publicados han tratado disoluciones modelo de compuestos perfluorados individuales con elevada concentración inicial. Sin embargo, el papel que desempeñan las características morfológicas y químicas de la superficie del ánodo sobre las reacciones de electro-oxidación de PFOA, así como el tratamiento electroquímico de PFASs en aguas residuales reales no ha sido abordado.

Por otro lado, las tecnologías fotoquímicas generalmente operan a temperatura y presión ambiente, y minimizan la generación de contaminantes secundarios. A pesar de que el catalizador  $\text{TiO}_2$  es ampliamente utilizado en fotocatalisis heterogénea debido a su estabilidad y bajo coste, la mayoría de los resultados previos revelaron una fotoactividad muy escasa del  $\text{TiO}_2$  para la degradación de PFASs. Sin embargo, los catalizadores compuestos por la combinación de  $\text{TiO}_2$  con metales nobles o de transición, o con materiales de carbono, han surgido como

potenciales catalizadores para mejorar el comportamiento fotocatalítico del  $\text{TiO}_2$ . Dentro de las tecnologías de fotocatálisis homogénea, la fotólisis de persulfato mediante luz UV ha demostrado la habilidad de degradar PFASs debido a los radicales sulfato generados. Sin embargo, una nueva clase de tratamientos de foto-reducción han surgido como una alternativa prometedora para la defluoración de PFASs. Así, la activación de agentes reductores, como el sulfito, por luz ultravioleta da lugar a la generación de electrones hidratados ( $e_{\text{aq}}^{\cdot-}$ ). Estas especies  $e_{\text{aq}}^{\cdot-}$  pueden reaccionar rápidamente con los átomos de flúor altamente electronegativos que actúan como centros de la reacción reductiva, dando lugar a vías de degradación diferentes de los procesos oxidativos convencionales.

En base a los estudios previos, el trabajo desarrollado en esta tesis tiene como objetivo evaluar diferentes estrategias electroquímicas y fotoquímicas para el tratamiento de PFASs en agua. El primer capítulo de esta tesis incluye una perspectiva general de los PFASs así como los principales fundamentos y retos de los tratamientos de agua propuestos en este trabajo. Los reactivos químicos, sistemas y procedimientos experimentales, junto con los métodos analíticos, son descritos en el capítulo 2. El capítulo 3 resume los principales resultados de las publicaciones científicas realizadas durante el periodo doctoral. Inicialmente se muestra la comparación morfológica, química y electroquímica de diferentes materiales anódicos de BDD, para la degradación de PFOA de disoluciones modelo (publicación científica 1). Tras este estudio, se evaluó la aplicación del ánodo de BDD microcristalino para el tratamiento de mezclas de PFASs presentes en aguas residuales industriales, bajo el efecto de una composición compleja de la matriz acuosa caracterizada por una elevada carga orgánica. Además, se investigaron las posibles reacciones electroquímicas, así como la

formación de sustancias nocivas, como algunas especies cloradas, durante los tratamientos (publicaciones científicas 2 y 3). La viabilidad de las tecnologías fotoquímicas fue inicialmente estudiada mediante la degradación de PFOA de disoluciones modelo con un catalizador compuesto preparado con  $\text{TiO}_2$  y óxido de grafeno reducido (publicación científica 4). Por otro lado, se estudió la capacidad de diferentes técnicas fotoquímicas de oxidación y reducción para la eliminación de una mezcla compleja de PFASs presentes en espumas anti-incendios. El proceso de oxidación se basó en el uso de radiación UV y persulfato de sodio para generar radicales sulfato, mientras que la técnica de reducción consistió en la fotólisis de sulfito de sodio como sintetizador de electrones hidratados (manuscrito en elaboración). Finalmente, el capítulo 4 está constituido por las principales conclusiones de la tesis.

# TABLE OF CONTENTS

<b>Acknowledgements</b>	<b>V</b>
<b>Summary / Resumen</b>	<b>VII</b>
<b>Chapter 1. Introduction</b>	<b>1</b>
1.1. Poly- and per-fluoroalkyl substances (PFASs)	3
1.2. Terminology and classification of PFASs	4
1.3. Emissions and global occurrence	9
1.4. Toxicity and legislative framework	14
1.5. Advanced technologies for PFASs treatments	16
1.6. Research approach and thesis structure	25
1.7. References	29
<b>Chapter 2. Materials and methods</b>	<b>41</b>
2.1. Chemical reagents	43
2.2. Electrochemical oxidation treatment	44
2.3. Photocatalytic technology	51
2.4. Homogeneous photochemical techniques	56
2.5. Analytical methods	60
2.6. References	63
<b>Chapter 3. Results summary</b>	<b>67</b>
3.1. Electrochemical oxidation	69
3.2. Heterogeneous photocatalysis	102

3.3. Homogeneous photocatalysis	117
3.4. Assessment of the energy consumption	138
3.5. References	144
<b>Chapter 4. Conclusions</b>	<b>155</b>
<hr/>	
4.1. Final remarks and future work	157
4.2. Conclusiones y trabajo futuro	163
<b>Chapter 5. Scientific publications</b>	<b>173</b>
<hr/>	
5.1. Scientific publication 1. (Gomez-Ruiz et al., <i>Separation and Purification Technology</i> , 2019)	175
5.2. Scientific publication 2. (Gomez-Ruiz et al., <i>Journal of Electroanalytical Chemistry</i> , 2017)	193
5.3. Scientific publication 3. (Gomez-Ruiz et al., <i>Chemical Engineering Journal</i> , 2017)	203
5.4. Scientific publication 4. (Gomez-Ruiz et al., <i>Journal of Hazardous Materials</i> , 2018)	221
<b>Chapter 6. Annexes</b>	<b>239</b>
<hr/>	
Annex I. Scientific publication in preparation	241
Annex II. Congress contributions	289
Annex III. Dissemination activities	291







# **INTRODUCTION**





## **1.1. Poly- and per-fluoroalkyl substances (PFASs)**

Water pollution is a severe global challenge that has increased in both developed and developing countries, harming human development as well as the physical and environmental health of billions of people [1]. Indeed, water resources are currently threatened due to increasing presence of anthropogenic pollutants from industrial and non-industrial sectors. Every day, about 2 millions of tons of sewage, industrial and agricultural waste are discharged into world's water without prior treatment or under poor wastewater management [2].

Among water contaminants, emerging contaminants are unregulated or not completely regulated organic compounds even in the most developed countries, and they have now raised significant concerns to public health professionals and environmental engineers and scientists due to their environmental persistence and the potential hazard to the human health [3,4]. Among these persistent organic pollutants, poly- and per-fluoroalkyl substances (PFASs) are chemicals of anthropogenic origin that have been manufactured since the 1950s. These compounds consist of a partially or fully fluorinated alkyl chain of varying length (typically C<sub>4</sub> to C<sub>16</sub>) and a hydrophilic end group (e.g. carboxylic, sulfonic, sulfonamide or phosphonic). These compounds have been historically made by two major manufacturing methods, electrochemical fluorination (ECF) and telomerization. ECF produces a mixture of compounds including branched, linear, and cyclic isomers of various chain lengths, while telomerization produces primarily straight chain (linear) PFASs with an even number of carbons, such as fluorotelomer-based surfactants or perfluoroalkyl substances [5,6].

The C-F bond, which is predominant in PFASs molecular structure, is the shortest and strongest bond in organic chemistry. This molecular structure provides PFASs unique physical-chemical properties, such as the amphiphilic character and extraordinary thermal and chemical stability which have led to their use in a wide range of industrial, commercial and household applications. Furthermore, the suitable properties of these recalcitrant compounds make difficult to find equally effective replacement chemicals for some applications, specifically for aqueous film-forming foams (AFFF) that are used for fire fighting. As a result, PFASs have been highly used as additives in surface treatment processes, polymerization aids and surfactants, etc. Polymer applications included oil repellents, food packaging and stain guard products for carpets, textile or furnishings [5]. PFASs are used as surfactants in fluoropolymer manufacture, cosmetics, electronics, coatings, AFFFs and other facilities handling large volumes of flammable liquid hydrocarbons [6–8].

## **1.2. Terminology and classification of PFASs**

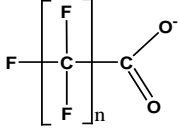
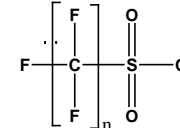
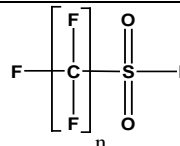
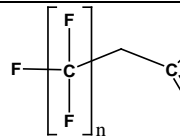
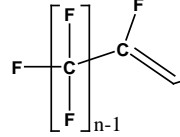
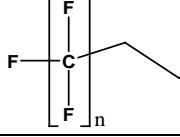
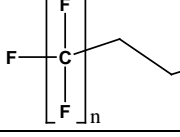
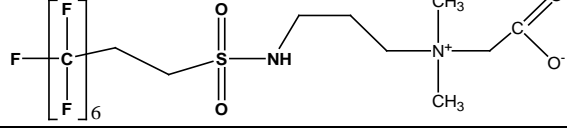
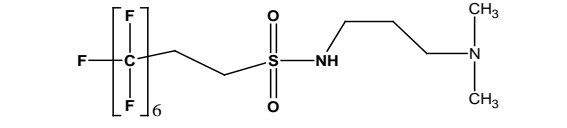
PFASs are defined as compounds that contain the perfluoroalkyl moiety  $C_nF_{2n+1}-$ , and they are divided in two main groups [6]:

- Perfluoroalkyl substances: aliphatic substances for which all the H atoms attached to C atoms in the alkyl chain have been replaced by F atoms, except those H atoms whose substitution would modify the nature of any functional groups present (e.g. hydroxyl -OH). PFAA is commonly used to denote perfluoroalkyl acids.

- Polyfluoroalkyl substances: aliphatic substances for which all H atoms attached to at least one (but not all) C atoms have been replaced by F atoms; they still contain the perfluoroalkyl moiety  $C_nF_{2n+1}$ . The nomenclature of partially fluorinated alkyl chains must indicate the number of fluorinated and unfluorinated carbons, e.g. the “6:2” nomenclature states that the alkyl chain is formed by 8 carbon atoms, six carbons are fully fluorinated and two carbons are bonded to hydrogen atoms.

Table 1.1 lists the molecular structure and acronyms of the groups of PFASs addressed in this thesis, which consisted of perfluorinated carboxylic acids (PFCAs), perfluorinated sulfonic acids (PFSA), and polyfluorinated compounds, such as fluorotelomer sulfonic acids (FTSAs), fluorotelomer carboxylic acids (FTCAs), fluorotelomer unsaturated carboxylic acids (FTUCAs) and fluorotelomer sulfonamides (6:2 FTAB or M4). Even though most PFASs have very low acid dissociation constant ( $pK_a$ ) [9,10], the acronyms used in this document maintain the original abbreviation with the “A” related to “acid” to refer both the protonated and ionized forms (e.g. PFOA is also used for perfluorooctanoate).

**Table 1.1.** Chemical structure by compound class of most relevant PFASs.

Compound Name	Chemical structure	n
Perfluoroalkyl carboxylic acids (PFCAs)		3-13
Perfluoroalkane sulfonic acids (PFSAs)		4-10
Perfluorooctane sulfonamide (FASAs)		4-10
Fluorotelomer carboxylic acids (n:2 FTCAs)		4-8,10
Fluorotelomer unsaturated carboxylic acids (n:2 FTUCAs)		6,8,10
Fluorotelomer alcohols (n:2 FTOHs)		4,6,8,10
Fluorotelomer sulfonic acids (n:2 FTSA)		4,6,8,10
6:2 Fluorotelomer sulfonamide alkylbetaine (6:2 FTAB)		
6:2 Fluorotelomer sulfonamide propyl N,N dimethylamine (M4)		

### Perfluoroalkyl carboxylic acids (PFCAs)

These compounds contain a fluorinated carbon chain with a terminal carboxylic acid functional group, with a general chemical formula  $C_nF_{2n+1}COOH$  (Table 1.1). The alkyl chain of PFCAs can typically contain from 2 to 14 carbon atoms. PFCAs have  $pK_a$  in the range 0–1 and they will be predominantly present as dissociated anions in environmental media which typically have pH above 4 [9,10]. PFCAs generally exhibit high water solubility and low vapor pressure, a sum of characteristics that promote their transportation in the aquatic environment. Water solubility and vapor pressure decrease with the carbon chain length [8,11].

### Perfluoroalkyl sulfonic acids (PFSAs)

Perfluoroalkyl sulfonic acids is one of the most important families of significance along with PFCAs. PFSAs have the generic formula  $C_nF_{2n+1}SO_3H$  (Table 1.1). PFSAs are suggested to have negative  $pK_a$  values and exist in aqueous solution as dissociated anions [9,10]. They possess moderate water solubility which decreases with carbon chain length, and low vapor pressure [8].

### Perfluoroalkyl sulfonamides (FASAs)

FASAs contain a fully fluorinated alkyl chain with a terminal sulfonamide group (Table 1.1). Perfluorooctane sulfonamide (FOSA) is the most detected compound ( $C_8F_{17}SO_2NH_2$ ) of this group. It is produced by reacting a primary amine with perfluorooctane sulfonyl fluoride ( $R_8SO_2F$ ) [5]. FASAs are considered precursors of PFSAs and PFCAs, due to their oxidation and biotransformation into these latter compounds [12,13].

### Fluorotelomers (FT)

Fluorotelomers are polyfluorinated substances which contain unfluorinated carbons between the perfluoroalkyl moiety and the hydrophilic end group. The main fluorotelomers are listed in Table 1.1. Fluorotelomer carboxylic acids (n:2 FTCAs) exhibit a  $-\text{CH}_2-$  group between the fully fluorinated alkyl chain and the carboxylic acid end group,  $\text{C}_n\text{F}_{2n+1}\text{CH}_2\text{COOH}$ . Similarly, fluorotelomer unsaturated carboxylic acids (n:2 FTUCAs) contain a double-bond structure between the perfluoroalkyl moiety and the carboxylic acid end group,  $\text{C}_n\text{F}_{2n+1}\text{CFCHCOOH}$ . Fluorotelomer sulfonic acids (n:2 FTSA) possess the fully fluorinated alkyl chain and the ethyl group bonded to the sulfonic acid end group,  $\text{C}_n\text{F}_{2n+1}\text{CH}_2\text{CH}_2\text{SO}_3\text{H}$ . Fluorotelomer alcohols (n:2 FTOHs) have the generic formula  $\text{C}_n\text{F}_{2n+1}\text{CH}_2\text{CH}_2\text{OH}$ , which contain a terminal hydroxyl group upon the ethyl group. Additionally, novel fluorotelomer sulfonamide-based chemicals have been progressively introduced in different applications specially for AFFFs, as alternatives of C8 perfluorinated compounds, e.g. 6:2 FTAB and M4 (Table 1.1) [14]. The molecular structure typically contains a polyfluorinated chain with a sulfonamide end group bonded to an alkyl chain that contains different groups, such as, betaine moiety [15–17].

Depending on the alkyl moiety and the head group of these compounds, vastly different physicochemical properties and subsequent environmental fate can be obtained. Fluorotelomers or fluorotelomer sulfonamide-based chemicals can have a negatively charged carboxylic or sulfonic acid head group, positively charged quaternary ammonium head group or amphoteric head group, such a betaine. As a result, uncharged neutral compounds (zwitterionic species) would be much less water soluble and may partition

to solid phases or volatilize into atmosphere, while charged PFASs mainly end up into the aquatic environment. Exceptionally, FTOHs and FOSAs were also dominant compounds in air due to their low water solubility and high vapor pressure [18].

Fluorotelomer-based compounds contain abstractable H atoms within the alkyl chain which promotes the environmental oxidation, typically into PFCAs or PFSA as degradation byproducts [19–22]. This has resulted in an increasing attention on fluorotelomers as precursors of persistent PFASs in the environment.

### **1.3. Emissions and global occurrence**

As a result of the wide PFASs manufacturing and use, these compounds are released to the environment by several ways: (i) during synthesis, (ii) incorporation into final products, (iii) distribution of the products to consumers, (iv) use of the product by the consumers and (v) during disposal. Prevedouros et al. [23] estimated that the total global emissions from direct (manufacture, use, consumer products) and indirect (PFAS impurities and/or precursors) sources were 3200-7300 tonnes up to 2006. Similarly, total C<sub>4</sub>-C<sub>14</sub> PFCAs emissions of 2610-21400 tonnes were estimated during 1951-2015, and 20-6420 tonnes are expected to be released from 2016-2030 [24]. The majority of PFCAs discharge resulted from fluoropolymer manufacture and use. Nowadays, environmental emissions of PFASs still occur through a variety of pathways and diffuse sources, such as from production sites, downstream industry, use of fire-fighting foams, via wastewater effluents or via consumer product use and disposal [25].

Due to their high volume of emissions and the resistance to abiotic and biotic degradation, PFASs have been globally found in water, atmosphere, soil and even in animals and humans [18,23,26]. Water is the major non-biota environmental compartment of concern because of the human exposure through PFASs contamination of drinking water, particularly near industrial sites [27,28] or fire-fighting training areas [21,29], as well as near landfill sites and wastewater treatment plants (WWTPs) [30,31]. Figure 1.1 shows a brief outline of PFASs transport and fate in the environment.

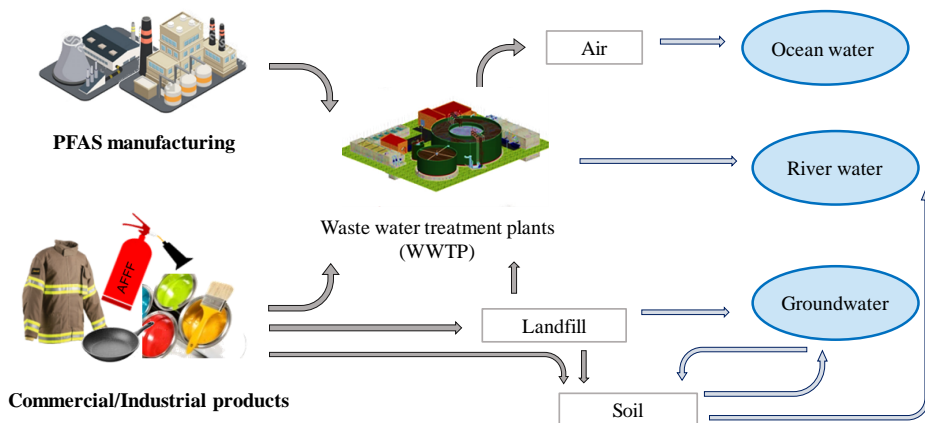


**Figure 1.1.** Diagram of PFASs transport and fate in the environment.

PFOA and PFOS are the most detected of PFAS compounds in the aquatic environment with not uniform distribution. Table 1.2 provides an overview of PFOA and PFOS concentrations in the different aquatic compartments detailed below.

**Table 1.2.** Summary of PFOA and PFOS concentrations ( $\text{ng.L}^{-1}$ ) in different aquatic compartments: ocean water, surface water, industrial/municipal WWTPs, landfill leachates and AFFF-impacted groundwater.

Source	[PFOA] ( $\text{ng.L}^{-1}$ )	[PFOS] ( $\text{ng.L}^{-1}$ )	Reference
Ocean water		0.01-0.1	[23,32]
Surface waters (Japan, USA, Europe, China)	0.9-173	0.9-30	[33–35]
Surface waters (China)	0.24-320	0.02-730	[36]
Industrial wastewater (USA)	50-525,000	198-1,400	[28,37–41]
Municipal WWTP (USA)	58-1050	3-68	[38]
Landfill leachates (USA, Europe)	10-8,900	50-3,200	[30,42]
Landfill leachates (China)	281-214,000	1,150-6,020	[42,43]
AFFF-impacted water	1.7-4,470	1.3-42,000	[29,44–47]

Whereas PFOA and PFOS levels in ocean water typically vary between 10-100  $\text{pg.L}^{-1}$ , coastal waters have a range between 0.2 and 20  $\text{ng.L}^{-1}$  [23,32,48]. On the contrary, levels in surface water of developed countries can be several orders of magnitude higher [7,48]. It has been reported that PFOS and PFOA concentrations in surface waters in Japan were in the ranges of 0.9-4 and 0.9-22  $\text{ng.L}^{-1}$ , respectively [33]. In Northeast U.S.A, Sinclair et al. [34] found PFOA and PFOS concentrations in surface water of New York State around 10–173 and 0.8–30  $\text{ng.L}^{-1}$ , respectively. Berger et al. [35] reported concentrations of <1  $\text{ng.L}^{-1}$  for PFOS and 7.8  $\text{ng.L}^{-1}$  for PFOA in European Nordic Countries. In respect of China, ranges of concentrations of PFOS in coastal seawaters of Hong Kong, the Pearl River Delta, and Korea were 0.02-730  $\text{ng.L}^{-1}$ , while those of PFOA were 0.24-320  $\text{ng.L}^{-1}$  [36].

There was a possible link between this contamination with manufacturing and use of PFASs in those countries. Industrial sites may introduce these chemicals into the aquatic environment via direct release into the rivers or sewage treatment plants. In this way, PFASs concentrations in the industrial effluents can range from  $\text{ng.L}^{-1}$  to  $\text{mg.L}^{-1}$ . 3M company, the major manufacturer of perfluorooctanyl compounds for more than 40 years, caused contamination of municipal wells ranging from 0.05 to  $1 \mu\text{g.L}^{-1}$  of PFOA and to  $1.4 \mu\text{g.L}^{-1}$  of PFOS, tested near the 3M manufacturing facilities (Minnesota) from 2005 to 2008 [37,49]. Additionally, elevated PFOS levels of 198–1,090  $\text{ng.L}^{-1}$  found in Lake Onondaga (Northeast USA) were related to the high volume of industrial wastewater discharges from several industries located along the lake [38].

Moreover, WWTPs are another important source along with industrial contributions. PFASs cannot be removed efficiently in conventional treatments in WWTPs, and the partial biodegradation of labile PFASs precursors can increase concentrations in the treated effluent relative to the influent [28,30,50]. Dauchy et al. [28] have recently detected 51 different PFASs in an industrial wastewater treatment plant that receives the emissions of one fluorochemicals manufacturing facility in the north of France. The study found that 6:2 FTAB was the predominant PFAS with a concentration ranging from 4 to  $45.5 \text{ mg.L}^{-1}$ . Municipal WWTPs typically contain lower levels of PFASs in the influent, effluent and sludge than industrial wastewaters [51]. Sinclair et al. [38] measured concentrations of several PFASs in six WWTPs in New York State, showing that PFOA was the predominant PFAS compound with concentrations from 58 to  $1050 \text{ ng.L}^{-1}$ . PFOA could occur up to hundreds of  $\text{ng.L}^{-1}$  in wastewaters not

impacted by fluorochemical manufacture, whereas its level was 7-fold greater in the plants that treated daily industry wastes.

Landfills that receive consumer products contribute to PFAS pollution, as these compounds can reach landfill leachates with the potential of migration to groundwater or other aquatic environments [43]. In addition, WWTPs and landfills are also emission sources of semivolatile PFASs to the ambient air [25]. Hamid et al. [42] have recently reported concentrations of PFAAs in the range of 1-1800 ng.L<sup>-1</sup> in leachates of several European countries. Fuertes et al. [30] also observed that PFOA was the predominant PFAS component in raw leachates of landfill sites located in the north of Spain, followed by shorter-chain PFCAs, due to their increasing use as alternative to C8 PFASs. However, PFHxA become the most abundant compound in treated samples, related to the possible degradation of unidentified PFASs precursors during the MBR treatment that was applied on-site to the landfill leachates.

Additionally, the high volume of consumer products and wastes disposed in landfill leachates in China resulted in more elevated levels of PFASs than in other countries, with concentrations ranging from 70 to 214,000 ng.L<sup>-1</sup> for PFCAs and 30 to 416,000 ng.L<sup>-1</sup> for PFSAs [43]. The volatile or semivolatile properties of PFAS precursors (some fluorotelomers such as FTOH, FASAs, FASEs, PAPs) facilitate the transport via atmosphere and subsequently the degradation into PFSAs and PFCAs [52]. The transport of these final degradation products proceeds mainly in water phase but also via gas-phase in the atmosphere, which can be deposited into soil and migrate until arriving to groundwater [25,32].

Furthermore, the consumption of AFFFs was also considered another significant source of PFASs pollution into groundwater and surface water near military sites. Investigations at AFFF-impacted sites revealed PFAS concentrations in the range of  $\mu\text{g.L}^{-1}$  up to  $\text{mg.L}^{-1}$  [25,29]. Filipovic et al. [44] reported concentrations of a mixture of PFAAs (PFOS, PFOA PFHxS and PFHxA) of 738 to 51,000  $\text{ng.L}^{-1}$  in groundwater and surface water at military airfield in Sweden, being PFOS the most predominant compound ( $<1$  to 42,000  $\text{ng.L}^{-1}$ ). Additionally, C6-C8 PFAAs were detected in groundwater ranging from 125-7,090  $\mu\text{g.L}^{-1}$  at two fire-training locations in the USA [29].

#### **1.4. Toxicity and legislative framework**

Humans are exposed to PFAS through commercial products, foods and primarily drinking water. The exceptional stability and bioaccumulative nature of PFASs led to increasing concern about their potential threat to human health [53]. The information on the toxicity of PFASs was focused on PFOS and PFOA due to their predominant presence in the environment. Moreover, the bioaccumulation potential has been observed predominantly in longer chain PFASs [54]. Most of the research comes from animal studies and information on adverse health effects in humans is limited to a small number of occupational studies [48,55]. PFASs were detected in human blood, serum, plasma and tissues [56]. Indeed, Calafat et al. [57] have reported that PFASs are detectable in the blood of more than 98% of the US population. The extent in the Spanish population showed that different PFASs were detected in over 85% of serum samples, with concentration ranged from 0.91 to 7.67  $\mu\text{g.L}^{-1}$  [26].

Recent research has found a negative association between combined serum levels of PFOA and PFOS and sperm count in young men [58], evidence of disruption of thyroid function by both PFOA and PFOS [59] and an association between PFOA levels and elevated cholesterol [60]. Additionally, Steenland et al. [61] published a review about epidemiological evidence on human health effects of PFOA. Exposure to PFOA was associated with alteration of the birth weight and size of newborns [62] and related to cholesterol metabolism [63]. The cancer incidence of kidney, bladder and urinary track organs was related to PFOS and PFOA exposure in worker-based populations in several studies [64]. However, studies within the general population (without occupational exposure to PFAS) did not reveal any direct correlation between PFOS/PFOA exposure and carcinogenicity [65].

Due to these possible effects on human health, national and international regulatory initiatives to restrict the production and use of PFASs have focused mainly on long-chain compounds, which have been shown to be more bioaccumulative than their short-chain analogues. Among the PFASs, perfluorooctanesulfonate (PFOS) and perfluorooctanoic acid (PFOA) are subjected to increasingly intense research. However, although there is a growing understanding of the properties of PFAS, it is clear that further information on their toxicology, persistence and bioaccumulation is required to define which specific PFAS compounds pose a potential for risk to human health and the environment.

In 2009, perfluorooctane sulfonic acid (PFOS) and related substances based on perfluorooctane sulfonyl fluoride (POSF) were included in the Stockholm Convention, a global treaty designed to protect the environment and human health from persistent organic pollutants (POPs) and their

usage is banned by the European Union for various applications [66]. PFOS is also listed as a priority substance in the field of European water policy according to Directive 2013/39/EU [67], which defined annual average environmental quality standards (EQS) of  $6.5 \cdot 10^{-4}$  and  $1.3 \cdot 10^{-4}$   $\mu\text{g}\cdot\text{L}^{-1}$  for inland surface waters and other surface waters, respectively.

PFOA is still produced and used. However, this compound and its salt ammonium pentadecafluorooctanoate (APFO), as well as long-chain PFCAs (C11-C14) have been listed in the Candidate List of substances of very high concern by the European Chemicals Agency (ECHA) since 2015 [68]. Particularly, since June 2017, the European Union has published measures to ban the production, use and placement on the market of PFOA, its salts and PFOA-related substances starting from 2020 [69]. Also, the United States Environmental Protection Agency has recently established health advisory levels for PFOA and PFOS in drinking water at  $0.07 \mu\text{g}/\text{L}$ , both individually and combined [70].

As a consequence of these regulations, the production of long-chain PFASs has shifted toward less regulated countries in Asia [71]. Also, the industry is moving towards the production of less toxic and bioaccumulative short-chain poly- and perfluorinated analogues [72].

### **1.5. Advanced technologies for PFASs treatments**

The scientific community is currently facing the challenge of developing clean technologies for the treatment of the emissions of PFASs and the remediation of existing water polluted sites. Among others, literature reports the use of membrane, adsorption and/or ion exchange processes, which seem to be effective for removal of long-chain PFASs but struggle to treat the shorter-chain PFAS compounds [73,74]. In addition, these

separation technologies involve the transfer of the contaminants to a second phase that needs to be further treated before its disposal in the receiving environment.

Conversely, destructive methods aim at the cleavage of the strong C-F bonds to complete the mineralization of PFASs. Common oxidative processes, such as photo-Fenton, can fail to degrade PFASs due to the strongly electronegative fluorine atoms that surround the carbon skeleton to protect it from the oxidative attack, particularly for perfluoroalkyl sulfonates [75,76].

However, over the last few decades, advanced oxidation processes (AOPs) have appeared as non-conventional techniques able to strengthen the oxidation ability for the degradation of recalcitrant compounds. AOPs are redox technologies with main characteristics of versatility, non-selectivity on the target useful to treat real wastewaters and the production of the highly reactive oxygen species (ROS), such as  $\cdot\text{OH}$ ,  $\text{O}_2\cdot^-$ ,  $\text{SO}_4\cdot^-$  or  $\text{CO}_3\cdot^-$  [77,78]. Among these group of technologies, electrochemical oxidation and photochemical technologies have become promising technologies for PFAS removal due to their capability to mineralize organic matter.

### 1.5.1. Electrochemical oxidation

Electrochemical oxidation processes generally involve the degradation of contaminants via two mechanisms (Figure 1.2): (1) indirect electrochemical oxidation, where contaminants are degraded via different strong reactive species (e.g.  $\cdot\text{OH}$  radicals) generated on the anode, and (2) direct anodic oxidation, by which contaminants are oxidized by electron transfer reaction after the interaction with the anode surface [78,79]. Many organic pollutants can undergo both electro-oxidative mechanisms [80,81].

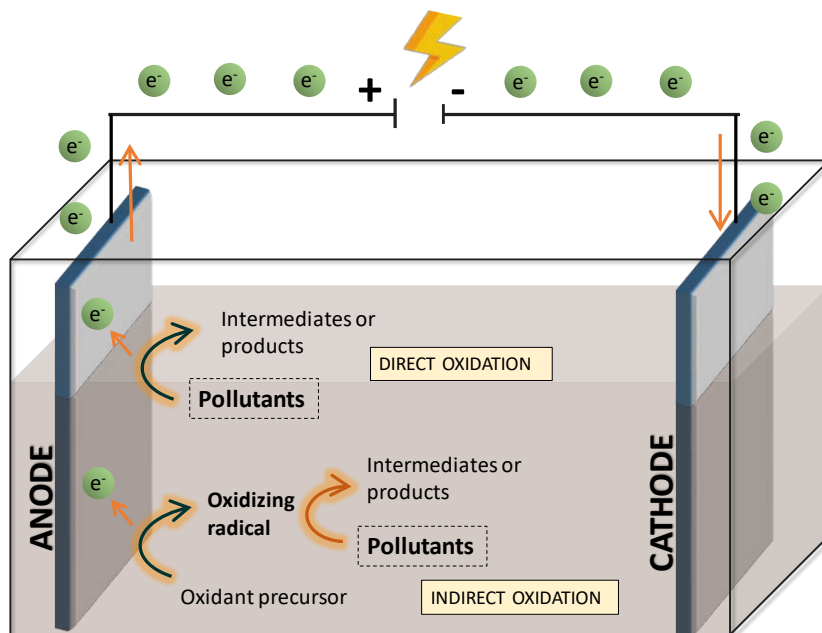


**Figure 1.2.** Scheme of direct and indirect electrolytic treatment of contaminants.

The main advantage of electrochemical processes is the environmental compatibility due to the fact that its main reagent, the electron, is a clean reagent [79,82]. It is well-known that the electrode material strongly influences both the selectivity and the efficiency of the process. Two types of electrode materials can be differentiated: “active” and “non-active” anodes. Active anodes provide high strong interaction between the electrode and the electro-generated species, such as  $\cdot\text{OH}$ , resulting in a high activity towards oxygen evolution (low  $\text{O}_2$  overvoltage) and low electrochemical performance for organics oxidation. Non-active anodes exhibit weak interactions between electro-generated species and the electrode material and possess higher electron transfer ability. As a result, these electrodes have a low electrochemical activity for the oxygen evolution reaction, leading to powerful oxidation conditions for the removal of organic compounds [82–84].

In particular, boron doped diamond (BDD) electrodes have gained attention for water treatment due to their unique properties compared to other electrode materials [83,85,86], such as superior chemical stability, long life span, low background currents and wider potential window for water decomposition reactions than other common non-active materials [87,88]. A major limitation of BDD anode application is the cost and difficulty of building BDD coatings compared with other electrode materials [89]. The efficiency of the electro-oxidation by BDD anodes has been already assessed for landfill leachates [90], and for mineralization purposes of other recalcitrant pollutants such as emerging contaminants contained in the secondary effluents of wastewaters treatment plants [84,91], polychlorinated dibenzo-p-dioxins and dibenzofurans [92], naphthenic acids [93] and organic pollutants in industrial wastewaters [94].

The ability of the electro-oxidation technology for PFASs degradation is now under research. The anodic material plays a key role in the effective degradation and mineralization of PFASs. PFASs can undergo direct oxidation by the electron transfer from the hydrophilic end group to the anode, but hydroxyl radicals formed from water molecule can also contribute to mineralize PFASs in the solution [80,95]. Therefore, the electrochemical performance of the electrode would depend on its electron transfer ability and its  $\cdot\text{OH}$  generation capacity. In this way, BDD have attracted interest for PFAS degradation, since it can provide high formation of  $\cdot\text{OH}$  at low background currents, and these  $\cdot\text{OH}$  are weakly absorbed to the BDD surface, avoiding the interference in the initial PFAS reaction with the electrode [78]. In contrast, “active” anodes, such as Pt, Ti/Ru-IrO<sub>2</sub>, and Ti/SnO<sub>2</sub>-Sb/MnO<sub>2</sub> presented poor electrochemical performance for PFOA degradation [96,97].

It has been demonstrated that PFBA, PFHxA, PFOA, PFDA, PFBS, PFHxS and PFOS could be effectively decomposed by a BDD anodes [98–102]. These previous studies dealt with model solution of single PFASs and the addition of electrolyte, using high initial concentration. However, it is worth pointing out that the observed removal rates of PFASs using BDD as anode material were very diverse among the literature [95,99,102–108]. While Carter and Farrel [99] observed a rate of  $7.8 \text{ h}^{-1}$  for PFOS removal when the applied current density ( $j$ ) was  $20 \text{ mA}\cdot\text{cm}^{-2}$ , Xiao et al. [103] obtained much lower kinetic rate ( $0.108 \text{ h}^{-1}$ ) for the PFOA electrooxidation, at the same current density. On the contrary, Ochiai et al. [104] obtained 8-fold higher kinetic constant ( $0.8 \text{ h}^{-1}$ ) for PFOA degradation than the work of Xiao and co-workers [103], regardless the applied current density was two orders of magnitude lower ( $0.15 \text{ mA}\cdot\text{cm}^{-2}$ ). Even though the experimental conditions were different in these studies, the chemical structure and morphology (boron doping concentration, roughness, grain size or  $\text{sp}^3/\text{sp}^2$  carbon ratio) of BDD surfaces could also play an important role on the electro-oxidation pathways of PFASs [109–114]. However, the relation of the BDD surface features with the PFAS removal response has not been studied yet.

Furthermore, the electro-oxidation pathways of PFASs on BDD anodes can occur along several steps involving both the hydroxyl radical attack and electron transfer to the anode. The mechanism widely proposed for PFCAs degradation would start with the electron transfer from the carboxyl group to the anode to generate the  $\text{C}_n\text{F}_{2n+1}\text{COO}\cdot$  radical (Eq. 1). Next, this highly unstable radical undergoes Kolbe decarboxylation to form a perfluoroalkyl radical ( $\text{C}_n\text{F}_{2n+1}\cdot$ ) (Eq. 2). The electrogenerated hydroxyl radical can react with the perfluoroalkyl radical to form a perfluoro alcohol  $\text{C}_n\text{F}_{2n+1}\text{OH}$  (Eq. 3), which is a thermally unstable species

that would undergo intramolecular rearrangement to form the perfluoro carbonyl fluoride and release fluoride anion (Eq. 4). Finally, the latter species hydrolyses to give the one-carbon-shorter-chain perfluorocarboxylic acid,  $C_{n-1}F_{2n-1}COO^-$  (Eq. 5) [95–97,115]. The  $C_{n-1}F_{2n-1}COO^-$  repeats the above steps and decomposes into shorter-chain perfluorocarboxylic acids by gradually losing a  $CF_2$  unit.



In the case of fluorotelomers, the electro-oxidation pathway consisted of an initial attack by  $\bullet OH$  radicals in the unfluorinated carbons, forming PFCA's which undergo the reactions previously described [115,116].

### 1.5.2. Photochemical technologies

Photochemical strategies are based on light-induced chemical reactions. The use of UV/Vis radiation and auxiliary chemicals or catalysts allow accelerating the degradation of contaminants. The wavelength range generally utilized lies between UV-C (200-280), UV-B (280-315) and UV-A (315-380) and visible light (380-850 nm). The photochemical processes are divided in three groups: (i) direct photolysis, (ii) photosensitized technique and (iii) photocatalysis; depending on the reagent or material that absorbs photons to form the consequent photochemical reactions.

Direct photolysis involves the transformation of the contaminant resulting from the direct photon absorption by the molecule. The photons from UV radiation are used to produce an electronically excited state of a molecule, which enables the cleavage of chemical bonds. Only one photon can cause a photochemical reaction, and each photon is absorbed by a single molecule to initiate the reaction. Most organic compounds show absorption bands at the UV-C region, which is a small percentage of solar radiation [117,118]. Some published direct photolytic degradation studies have demonstrated that PFASs can be photodegraded by light from deep UV-region to 220 nm [119]. Moreover, the presence of oxygen and acidic conditions could enhance the direct photodegradation [120].

Photosensitization consists of initiating a reaction through the use of an auxiliary photosensitizer capable of absorbing light producing reactive radicals or exchanging electrons with the pollutants. The combined action of sensitizer and UV radiation on aqueous pollutants can lead to faster and more efficient contaminant removal. Most photochemical processes employed have been based on UV and hydrogen peroxide and persulfate to generate  $\cdot\text{OH}$  and  $\text{SO}_4^{\cdot-}$  radicals with oxidation potential of 2.6 and 2.8 V, which play the main roles in removing organic molecules [121,122]. Accordingly, Hori et al. [123] observed slow PFOA degradation rates by means of  $\text{H}_2\text{O}_2$  under UV-Visible irradiation and  $\text{O}_2$  atmosphere. However, Yang et al. [124] observed nearly complete elimination of 6:2 FTSA and the intermediate perfluorocarboxylates formed during the UV- $\text{H}_2\text{O}_2$  treatment in air atmosphere. Qian et al. [125] and Yin et al. [126] demonstrated significant PFOA degradation in UV and heat activated-persulfate system, respectively, and under acidic conditions.

Among the photochemical techniques, new reductive strategies have been recently proposed as promising alternatives to form powerful reducing agents, such as hydrated electrons ( $e_{aq}^-$ , -2.9 V), which are able to degrade halogenated organic compounds [127]. Aqueous photolysis of different inorganic anions, such as dithionite [128], sulfite [129,130], potassium iodide [131], and ferrocyanide [132] have been previously used to produce the reducing species. The strong electronegativity of fluorine atoms can act as the reductive reaction center for defluorination by  $e_{aq}^-$ . Park et al. [133,134] dealt with this innovative photo-reductive technology for the treatment of PFOA and PFOS in aqueous iodide solution under UV irradiation, achieving higher degradation rates for perfluoroalkyl sulfonates. Additionally, Song et al. [135] reported the feasibility of using the UV-sulfite system to decompose PFOA under  $N_2$  atmosphere and alkaline conditions. Also, PFOS was successfully decomposed in 30 min using high-pressure mercury lamp at alkaline pH and 10 mM of sulfite [130].

Finally, photocatalysis consists of the acceleration of a chemical reaction by the presence of a catalyst which is capable of absorbing photons. The catalyst is usually a semiconductor which has an orbital with an electronic band structure. There are two bands describing the electronic structures of semiconducting materials, one is the conduction band ( $C_B$ ) with the lowest unoccupied molecular orbital and the valance band ( $V_B$ ) which is the highest occupied molecular orbital. The band-gap energy is the energy difference between these two bands. When a photon with an energy equal or greater than the band gap is absorbed, an electron ( $e^-$ ) from the  $V_B$  is promoted to the  $C_B$ , leaving at the same time a photogenerated hole ( $h^+$ ) in the  $V_B$ , generating an electron-hole pair ( $e^-/h^+$ ), as can be seen in Figure 1.3 for  $TiO_2$  catalyst. Then, the  $e^-/h^+$  pairs created can migrate to the surface of

the photocatalyst, they might further react with water or oxygen molecules forming mainly  $\cdot\text{OH}$  or superoxide anion radicals ( $\text{O}_2^{\cdot-}$ ), or they can recombine between themselves, liberating the previously absorbed energy as heat or light and avoiding the existence of redox reactions [136,137].

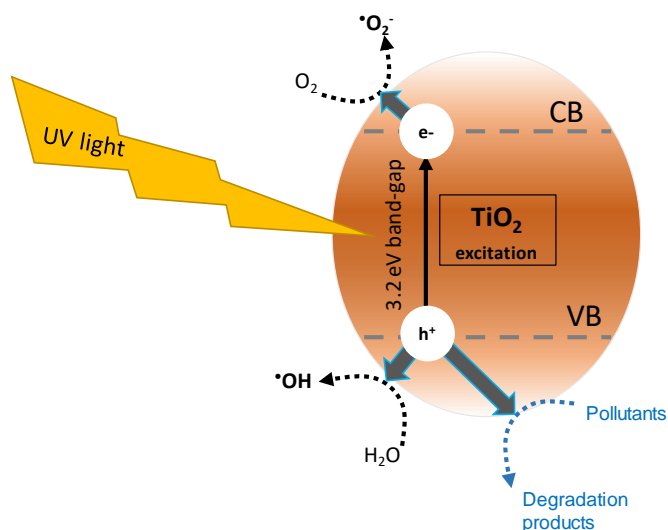


**Figure 1.3.** Photocatalytic mechanism of electron-hole pair formation in TiO<sub>2</sub> semiconductor in water and the consequent chemical reactions.

Several semiconductors have been used as photocatalysts, including bismuth (III) sulfide (Bi<sub>2</sub>S<sub>3</sub>), niobium pentoxide (Nb<sub>2</sub>O<sub>5</sub>), russellite (Bi<sub>2</sub>WO<sub>6</sub>), silver carbonate (Ag<sub>2</sub>CO<sub>3</sub>), titanium dioxide (TiO<sub>2</sub>), tungsten (VI) oxide (WO<sub>3</sub>), zinc oxide (ZnO), and zinc sulfide (ZnS), among others [138]. However, TiO<sub>2</sub> is the most commonly used catalyst for the treatment of organic matter, due to its non-toxicity, high efficiency at room temperature, easy availability, low cost, photo and chemical stability [139]. However, it is only activated under ultraviolet light, which represents 4% to 8% of the solar spectrum and the high recombination of the photogenerated electron-hole pairs reduces the production of ROS [140].

Sanchez et al. [141] have previously studied the photocatalysis of greywater from hotels with commercial  $\text{TiO}_2$  as photocatalyst. Furthermore, Dominguez et al. [142,143] evaluated the photocatalytic degradation of dodecylbenzenesulfonate by means of  $\text{TiO}_2$  with different light sources and photoreactor configurations.  $\text{TiO}_2$  catalyst also achieved the degradation of p-cresol under LED irradiation [144]. However, prior works have revealed the limited performance of  $\text{TiO}_2$ -mediated photocatalysis for PFAS elimination [145–147]. As a result, new strategies have been proposed to overcome the drawbacks of the  $\text{TiO}_2$  catalyst. The more promising alternatives are focused on the combination with transition or noble metals or carbon materials [145,148–151], which achieved an enhance photodegradation of PFOA synthetic solutions compared to the bare  $\text{TiO}_2$ .

## **1.6. Research approach and thesis structure**

This thesis has been performed in the Environmental and Bioprocess Technologies (EBT) Research Group at the Department of Chemical and Biomolecular Engineering of University of Cantabria. Based on the previous background, the main objective of this thesis is to develop advanced technologies for the treatment of PFASs in water. This main goal has been covered by the following technologies and materials:

- Electrochemical oxidation.

Firstly, the electrochemical degradation of PFOA model solutions was evaluated by means of different commercial BDD anodes. Additionally, the influence of the chemical composition and the morphology of the BDD surfaces on PFOA electrolysis was studied.

Secondly, the feasibility of electrochemical technology using BDD anodes in the degradation of a complex mixture of PFASs in a real industrial wastewater was investigated. Kinetic model of the electrocatalytic removal of contaminants has been performed.

- Heterogeneous photocatalysis.

Study of the photocatalytic degradation of PFOA by a prepared catalyst based on TiO<sub>2</sub> and reduced graphene oxide (rGO). The physical characterization of the TiO<sub>2</sub>-rGO composite and its photocatalytic performance were assessed. Comparison with direct photolysis and TiO<sub>2</sub>-mediated photocatalysis has been developed. The optimal TiO<sub>2</sub>-rGO catalyst dose has been reported. Kinetic model of PFOA and intermediate products has been studied.

- Homogeneous photocatalysis.

Application of reductive/oxidative photochemical technologies have been proposed to accomplish the degradation of a complex mixture of PFASs in AFFF-impacted water. Oxidative treatments consist of UV and sodium persulfate, whereas the innovative reductive process is based on UV and sulfite. Different combination of sequential oxidative/reductive treatments have been studied.

According to these specific goals and the current regulations of the University of Cantabria for thesis “as a compendium” of scientific publications (*Regulations of the academic management of Doctoral Studies regulated by the Royal Legislative Decree 99/2011*), this thesis document has been structured in four chapters (Figure 1.4).

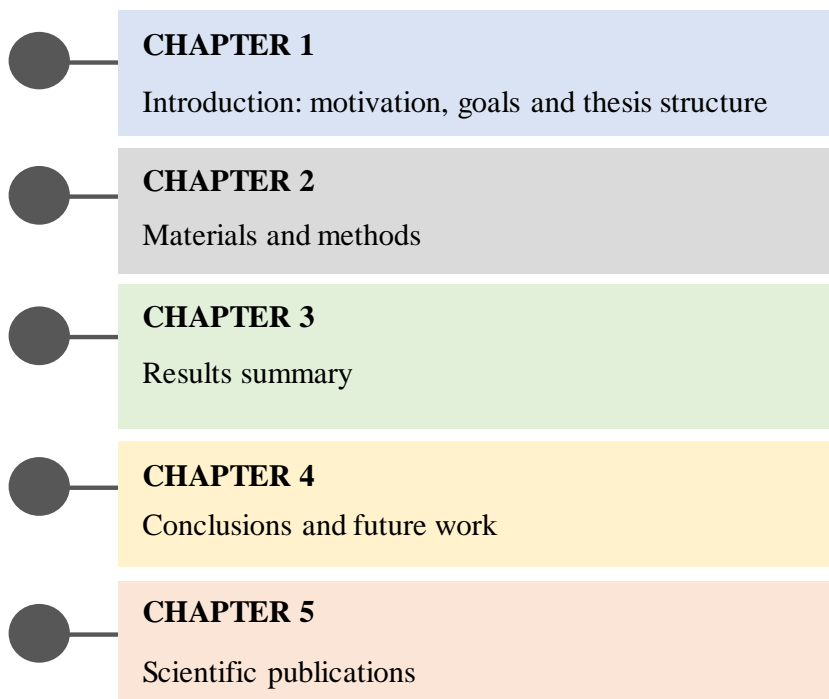


**Figure 1.4.** Thesis structure divided in 5 chapters.

**Chapter 1:** It contains the introduction of the thesis. In this point, an overview to PFASs, the fundamentals of the proposed water treatments and the goals of the thesis are described.

**Chapter 2:** This chapter describes the chemicals, experimental procedures and analytical methods used in the present thesis.

**Chapter 3:** It consists of a summary of the main results of the scientific publications done during the doctoral period.

This chapter includes initially the results of the electrochemical degradation of PFOA model solutions by means of different commercial BDDs anodes. Moreover, a comparative study of the chemical and

morphological features of the anode materials and their electrochemical performance was addressed. Scientific publication: “*Comparison of microcrystalline and ultrananocrystalline boron doped diamond anodes: Influence on perfluorooctanoic acid electrolysis*” (Sep. Purif. Technol. 208 (2019) 169-177).

The results of the feasibility of the microcrystalline BDD anode to treat a mixture of PFAS contained in real influents and effluents of a wastewater treatment facility was also reported. Scientific publications: “*Boron doped diamond electrooxidation of 6:2 fluorotelomers and perfluorocarboxylic acids. Application to industrial wastewaters treatment*” (J. Electroanal. Chem. 798 (2017) 51–57) and “*Efficient electrochemical degradation of poly- and perfluoroalkyl substances (PFASs) from the effluents of an industrial wastewater treatment plant*” (Chem. Eng. J. 322 (2017) 196-204).

On the other hand, the experimental findings obtained through the photo-assisted technologies were reported initially for the degradation of PFOA in model solutions by a prepared TiO<sub>2</sub>-rGO photocatalyst. Scientific publication: “*Photocatalytic degradation and mineralization of perfluorooctanoic acid (PFOA) using a composite TiO<sub>2</sub>-rGO catalyst*” (J. Hazard. Mater. 344 (2017) 950–957).

Finally, the results of the capability of sequential oxidative/reductive photochemical strategies to remediate PFASs contained in a AFFF formulation was also shown. Scientific publication: “*Degradation of poly- and perfluoroalkyl substances (PFASs) in Aqueous Film-Forming Foam by sequential UV oxidative/reductive treatments*”. This last work is under preparation to be submitted to a scientific journal.

**Chapter 4:** It comprises the final remarks of the thesis along with the future work.

**Chapter 5:** In this section the scientific publications during the doctoral period are included.

### 1.7. References

- [1] FAO, **2017**, 35.
- [2] UN WWAP, *Water* **2003**, 36.
- [3] V. Geissen, H. Mol, E. Klumpp, G. Umlauf, M. Nadal, M. van der Ploeg, S. E. A. T. M. van de Zee, C. J. Ritsema, *Int. Soil Water Conserv. Res.* **2015**, 3, 57.
- [4] I. Xagorarakis, D. Kuo, *Int. Encycl. Public Heal.* **2008**, 539.
- [5] E. Kissa, *Fluorinated Surfactants and Repellents*, Marcel Dekker, New York, **2001**.
- [6] R. C. Buck, J. Franklin, U. Berger, J. M. Conder, I. T. Cousins, P. De Voogt, A. A. Jensen, K. Kannan, S. A. Mabury, S. P. J. van Leeuwen, *Integr. Environ. Assess. Manag.* **2011**, 7, 513.
- [7] S. Fujii, C. Polprasert, S. Tanaka, N. P. H. Lien, Y. Qiu, *J. Water Supply Res. Technol. - AQUA* **2007**, 56, 313.
- [8] T. Pancras, G. Schrauwen, T. Held, K. Baker, I. Ross, H. Slenders, *Environmental Fate and Effects of Poly- and Perfluoroalkyl Substances (PFAS)*, **2016**.
- [9] S. Rayne, K. Forest, *J. Mol. Struct. THEOCHEM* **2010**, 949, 60.
- [10] L. Vierke, U. Berger, I. T. Cousins, *Environ. Sci. Technol.* **2013**, 47, 11032.
- [11] USEPA, *Fed. Regist.* 65 **2000**, 65, 62319.

- [12] M. M. Schultz, D. F. Barofsky, J. A. Field, *Environ. Eng. Sci.* **2003**, 20, 487.
- [13] J. C. D'Eon, M. D. Hurley, T. J. Wallington, S. A. Mabury, *Environ. Sci. Technol.* **2006**, 40, 1862.
- [14] B. J. Place, J. A. Field, *Environ. Sci. Technol.* **2012**, 46, 7120.
- [15] M. K. Moe, S. Huber, J. Svenson, A. Hagenaaars, M. Pabon, M. Trümper, U. Berger, D. Knapen, D. Herzke, *Chemosphere* **2012**, 89, 869.
- [16] L. A. D'Agostino, S. A. Mabury, *Environ. Sci. Technol.* **2014**, 48, 121.
- [17] K. A. Barzen-Hanson, S. C. Roberts, S. Choyke, K. Oetjen, A. McAlees, N. Riddell, R. McCrindle, P. L. Ferguson, C. P. Higgins, J. A. Field, *Environ. Sci. Technol.* **2017**, 51, 2047.
- [18] J. M. Jian, Y. Guo, L. Zeng, L. Liang-Ying, X. Lu, F. Wang, E. Y. Zeng, *Environ. Int.* **2017**, 108, 51.
- [19] C. M. Butt, D. C. G. Muir, S. A. Mabury, *Environ. Toxicol. Chem.* **2014**, 33, 243.
- [20] D. A. Ellis, J. W. Martin, A. O. De Silva, S. A. Mabury, M. D. Hurley, M. P. Sulbaek Andersen, T. J. Wallington, *Environ. Sci. Technol.* **2004**, 38, 3316.
- [21] L. A. D'Agostino, S. A. Mabury, *Environ. Toxicol. Chem.* **2017**, 36, 2012.
- [22] E. F. Houtz, C. P. Higgins, J. A. Field, D. L. Sedlak, *Environ. Sci. Technol.* **2013**, 47, 8187.
- [23] S. H. Prevedouros, Konstantinos; Cousins, Ian T.; Buck, Robert C., Korzeniowski, *Environ. Sci. Technol.* **2006**, 40, 32.
- [24] Z. Wang, I. T. Cousins, M. Scheringer, R. C. Buck, K. Hungerbühler, *Environ. Int.* **2014**, 70, 62.

- [25] L. Ahrens, *J. Environ. Monit.* **2011**, *13*, 20.
- [26] M. Bartolomé, A. Gallego-Picó, F. Cutanda, O. Huetos, M. Esteban, B. Pérez-Gómez, A. Castaño, *Sci. Total Environ.* **2017**, *603–604*, 352.
- [27] C. Bach, X. Dauchy, V. Boiteux, A. Colin, J. Hemard, V. Sagres, C. Rosin, J. F. Munoz, *Environ. Sci. Pollut. Res.* **2017**, *24*, 4916.
- [28] X. Dauchy, V. Boiteux, C. Bach, A. Colin, J. Hemard, C. Rosin, J. F. Munoz, *Sci. Total Environ.* **2017**, 576, 549.
- [29] C. A. Moody, J. A. Field, *Environ. Sci. Technol.* **2000**, *34*, 3864.
- [30] I. Fuertes, S. Gómez-Lavín, M. P. Elizalde, A. Urriaga, *Chemosphere* **2017**, *168*, 399.
- [31] C.-G. Pan, Y.-S. Liu, G.-G. Ying, *Water Res.* **2016**, *106*, 562.
- [32] N. Yamashita, K. Kannan, S. Taniyasu, Y. Horii, G. Petrick, T. Gamo, *Mar. Pollut. Bull.* **2005**, *51*, 658.
- [33] N. Saito, K. Harada, K. Inoue, K. Sasaki, T. Yoshinaga, A. Koizumi, *J. Occup. Health* **2004**, *46*, 49.
- [34] E. Sinclair, D. T. Mayack, K. Roblee, N. Yamashita, K. Kannan, *Arch. Environ. Contam. Toxicol.* **2006**, *50*, 398.
- [35] U. Berger, U. Järnberg, R. Kallenborn, *Organohalogen Compd.* **2004**, *66*, 4064.
- [36] M. K. So, S. Taniyasu, N. Yamashita, J. P. Giesy, J. Zheng, Z. Fang, S. H. Im, P. K. S. Lam, *Environ. Sci. Technol.* **2004**, *38*, 4056.
- [37] MDH, *Public Health Assessment on Perfluorochemical Contamination in Lake Elmo and Oakdale, Washington County, Minnesota*, **2008**.
- [38] E. Sinclair, K. Kannan, *Environ. Sci. Technol.* **2006**, *40*, 1408.
- [39] B. Gomez-Ruiz, S. Gómez-Lavín, N. Diban, V. Boiteux, A. Colin, X. Dauchy, A. Urriaga, *Chem. Eng. J.* **2017**, 322, 196.

- [40] B. Gomez-Ruiz, S. Gómez-Lavín, N. Diban, V. Boiteux, A. Colin, X. Dauchy, A. Urtiaga, *J. Electroanal. Chem.* **2017**, 798, 51.
- [41] X. Dauchy, V. Boiteux, C. Rosin, J. F. Munoz, *Bull. Environ. Contam. Toxicol.* **2012**, 89, 525.
- [42] H. Hamid, L. Y. Li, J. R. Grace, *Environ. Pollut.* **2018**, 235, 74.
- [43] H. Yan, I. T. Cousins, C. Zhang, Q. Zhou, *Sci. Total Environ.* **2015**, 524–525, 23.
- [44] M. Filipovic, A. Woldegiorgis, K. Norström, M. Bibi, M. Lindberg, A. H. Österås, *Chemosphere* **2015**, 129, 39.
- [45] J. Bräunig, C. Baduel, A. Heffernan, A. Rotander, E. Donaldson, J. F. Mueller, *Sci. Total Environ.* **2017**, 596–597, 360.
- [46] X. Dauchy, V. Boiteux, C. Bach, C. Rosin, J. F. Munoz, *Chemosphere* **2017**, 183, 53.
- [47] V. Boiteux, C. Bach, V. Sagres, J. Hemard, A. Colin, C. Rosin, J.-F. Munoz, X. Dauchy, *Int. J. Environ. Anal. Chem.* **2016**, 96, 705.
- [48] F. Suja, B. K. Pramanik, S. M. Zain, *Water Sci. Technol.* **2009**, 60, 1533.
- [49] A. Landsteiner, C. Huset, J. Johnson, A. Williams, *J. Environ. Health* **2014**, 77, 14.
- [50] M. M. Schultz, C. P. Higgins, C. A. Huset, R. G. Luthy, D. F. Barofsky, J. A. Field, *Environ. Sci. Technol.* **2006**, 40, 7350.
- [51] S.-K. Kim, J.-K. Im, Y.-M. Kang, S.-Y. Jung, Y. L. Kho, K.-D. Zoh, *J. Hazard. Mater.* **2012**, 201–202, 82.
- [52] C. J. Young, S. A. Mabury, *Atmospheric Perfluorinated Acid Precursors: Chemistry, Occurrence, and Impacts*, **2010**.
- [53] USEPA, *Contaminants of Emerging Concern (CECs) in Fish: Perfluorinated Compounds (PFCs)*, **2013**.
- [54] M. P. Krafft, J. G. Riess, *Curr. Opin. Colloid Interface Sci.* **2015**,

- 20, 192.
- [55] H. J. Lehmler, *Chemosphere* **2005**, 58, 1471.
- [56] L. Maestri, S. Negri, M. Ferrari, S. Ghittori, F. Fabris, P. Danesino, M. Imbriani, *Rapid Commun. mass Spectrom.* **2006**, 20, 2728.
- [57] A. M. Calafat, L. Y. Wong, Z. Kuklennyik, J. A. Reidy, L. L. Needham, *Environ. Health Perspect.* **2007**, 115, 1596.
- [58] U. N. Joensen, R. Bossi, H. Leffers, A. A. Jensen, N. E. Skakkebæk, N. Jørgensen, *Environ. Health Perspect.* **2009**, 117, 923.
- [59] S. S. Knox, T. Jackson, S. J. Frisbee, B. Javins, A. M. Ducatman, *J. Toxicol. Sci.* **2011**, 36, 403.
- [60] J. W. Nelson, E. E. Hatch, T. F. Webster, *Environ. Health Perspect.* **2010**, 118, 197.
- [61] K. Steenland, S. Tinker, A. Shankar, A. Ducatman, *Environ. Health Perspect.* **2010**, 118, 229.
- [62] T. Halldorson, D. Rytter, L. S. Haug, B. H. Bech, I. Danielsen, G. Becher, T. B. Henriksen, S. F. Olsen, *Environ. Health Perspect.* **2012**, 120, 668.
- [63] T. Fletcher, T. S. Galloway, D. Melzer, P. Holcroft, R. Cipelli, L. C. Pilling, D. Mondal, M. Luster, L. W. Harries, *Environ. Int.* **2013**, 57–58, 2.
- [64] F. D. Gilliland, J. S. Mandel, *J Occup Med* **1993**, 35, 950.
- [65] USEPA, *Health Effects Document for Perfluorooctane Sulfonate (PFOS)*, **2014**.
- [66] Secretary General of the United Nations, *The Stockholm Convention on Persistent Organic Pollutants*, **2009**.
- [67] The European Commission, *Directive 2013/39/EU of the European Parliament and of the Council, Amending Directives 2000/60/EC and 2008/105/EC as Regards Priority Substances in the Field of*

- Water Policy*, **2013**.
- [68] ECHA, *European Chemicals Agency. Candidate List of Substances of Very High Concern for Authorisation.*, **2015**.
- [69] The European Commission, *Commission Regulation (EU) 2017/1000 Concerning the Registration, Evaluation, Authorisation and Restriction of Chemicals as Regards Perfluorooctanoic Acid (PFOA), Its Salts and PFOA-Related Substances*, **2017**.
- [70] USEPA, *Drinking Water Health Advisory for Perfluorooctanoic Acid (PFOA)*, **2016**.
- [71] M. Land, C. A. de Wit, I. T. Cousins, D. Herzke, J. Johansson, J. W. Martin, *Environ. Evid.* **2015**, 4:3, 1.
- [72] Z. Wang, I. T. Cousins, M. Scheringer, K. Hungerbühler, *Environ. Int.* **2013**, 60, 242.
- [73] T. D. Appleman, C. P. Higgins, O. Quiñones, B. J. Vanderford, C. Kolstad, J. C. Zeigler-Holady, E. R. V Dickenson, *Water Res.* **2014**, 51, 246.
- [74] C. Flores, F. Ventura, J. Martin-Alonso, J. Caixach, *Sci. Total Environ.* **2013**, 461–462, 618.
- [75] S. Park, L. S. Lee, V. F. Medina, A. Zull, S. Waisner, *Chemosphere* **2016**, 145, 376.
- [76] H. F. Schröder, R. J. W. Meesters, *J. Chromatogr. A* **2005**, 1082, 110.
- [77] F. Méndez-Arriaga, R. A. Torres-Palma, C. Pétrier, S. Esplugas, J. Gimenez, C. Pulgarin, *Water Res.* **2009**, 43, 3984.
- [78] N. Merino, Y. Qu, R. A. Deeb, E. L. Hawley, M. R. Hoffmann, S. Mahendra, *Environ. Eng. Sci.* **2016**, 33, 615.
- [79] Á. Anglada, A. Urriaga, I. Ortiz, *J. Chem. Technol. Biotechnol.* **2009**, 84, 1747.

- [80] J. Carrillo-Abad, V. Pérez-Herranz, A. Urtiaga, *J. Appl. Electrochem.* **2018**, *48*, 589.
- [81] C. A. Martínez-Huitle, M. Panizza, *Curr. Opin. Electrochem.* **2018**, DOI <https://doi.org/10.1016/j.coelec.2018.07.010>.
- [82] I. Sirés, E. Brillas, M. A. Oturan, M. A. Rodrigo, M. Panizza, *Environ. Sci. Pollut. Res.* **2014**, *21*, 8336.
- [83] C. Di Dong, T. S. Chen, C. W. Chen, K. L. Huang, *Int. J. Electrochem. Sci.* **2016**, *11*, 5009.
- [84] A. M. Urtiaga, G. Pérez, R. Ibañez, I. Ortiz, *Desalination* **2013**, *331*, 26.
- [85] J. M. Peralta-Hernández, M. Méndez-Tovar, R. Guerra-Sánchez, C. A. Martínez-Huitle, J. L. Nava, *Int. J. Electrochem.* **2012**, *2012*, 1.
- [86] A. Fernandes, D. Santos, M. J. Pacheco, L. Ciríaco, A. Lopes, *Appl. Catal. B Environ.* **2014**, *148–149*, 288.
- [87] C. A. Martínez-Huitle, E. Brillas, *Appl. Catal. B Environ.* **2009**, *87*, 105.
- [88] X. Yu, M. Zhou, Y. Hu, K. Groenen Serrano, F. Yu, *Environ. Sci. Pollut. Res.* **2014**, *21*, 8417.
- [89] M. Panizza, G. Cerisola, *Chem. Rev.* **2009**, *109*, 6541.
- [90] Á. Anglada, A. M. Urtiaga, I. Ortiz, *J. Hazard. Mater.* **2010**, *181*, 729.
- [91] G. Pérez, P. Gómez, R. Ibañez, I. Ortiz, A. M. Urtiaga, *Water Sci. Technol.* **2010**, *62*, 892.
- [92] M. Vallejo, M. F. San Román, A. Irabien, I. Ortiz, *Chemosphere* **2013**, *90*, 132.
- [93] N. Diban, A. Urtiaga, *Environ. Sci. Pollut. Res.* **2018**, *1*.
- [94] A. Urtiaga, P. Fernandez-Castro, P. Gómez, I. Ortiz, *Chem. Eng. J.* **2014**, *239*, 341.

- [95] Q. Zhuo, S. Deng, B. Yang, J. Huang, B. Wang, T. Zhang, G. Yu, *Electrochim. Acta* **2012**, *77*, 17.
- [96] H. Lin, J. Niu, S. Ding, L. Zhang, *Water Res.* **2012**, *46*, 2281.
- [97] Q. Zhuo, S. Deng, B. Yang, J. Huang, G. Yu, *Environ. Sci. Technol.* **2011**, *45*, 2973.
- [98] A. Urriaga, C. Fernández-González, S. Gómez-Lavín, I. Ortiz, *Chemosphere* **2015**, *129*, 20.
- [99] K. E. Carter, J. Farrell, *Environ. Sci. Technol.* **2008**, *42*, 6111.
- [100] Q. Zhuo, S. Deng, B. Yang, J. Huang, B. Wang, T. Zhang, G. Yu, **2012**, *77*, 17.
- [101] T. Ochiai, Y. Iizuka, K. Nakata, T. Murakami, D. A. Tryk, A. Fujishima, Y. Koide, Y. Morito, *Diam. Relat. Mater.* **2011**, *20*, 64.
- [102] Z. Liao, J. Farrell, *J. Appl. Electrochem.* **2009**, *39*, 1993.
- [103] H. Xiao, B. Lv, G. Zhao, Y. Wang, M. Li, D. Li, *J. Phys. Chem. A* **2011**, *115*, 13836.
- [104] T. Ochiai, Y. Iizuka, K. Nakata, T. Murakami, D. A. Tryk, Y. Koide, Y. Morito, A. Fujishima, *Ind. Eng. Chem. Res.* **2011**, *50*, 10943.
- [105] H. Lin, J. Niu, J. Xu, H. Huang, D. Li, Z. Yue, C. Feng, *Environ. Sci. Technol.* **2013**, *47*, 13039.
- [106] Á. Soriano, D. Gorri, A. Urriaga, *Water Res.* **2017**, *112*, 147.
- [107] A. M. Trautmann, H. Schell, K. R. Schmidt, K. M. Mangold, A. Tiehm, *Water Sci. Technol.* **2015**, *71*, 1569.
- [108] C. E. Schaefer, C. Andaya, A. Burant, C. W. Condee, A. Urriaga, T. J. Strathmann, C. P. Higgins, *Chem. Eng. J.* **2017**, *317*, 424.
- [109] T. A. Ivandini, Y. Einaga, *Chem. Commun.* **2017**, *53*, 1338.
- [110] F. L. Souza, C. Saéz, M. R. V Lanza, P. Cañizares, M. A. Rodrigo, *Electrochim. Acta* **2016**, *187*, 119.

- [111] D. Medeiros De Araújo, P. Cañizares, C. A. Martínez-Huitle, M. A. Rodrigo, *Electrochem. commun.* **2014**, *47*, 37.
- [112] E. Guinea, F. Centellas, E. Brillas, P. Cañizares, C. Sáez, M. A. Rodrigo, *Appl. Catal. B Environ.* **2009**, *89*, 645.
- [113] S. Fierro, K. Abe, C. Comminellis, Y. Einaga, *J. Electrochem. Soc.* **2011**, *158*, F183.
- [114] S. Garcia-Segura, E. Vieira dos Santos, C. A. Martínez-Huitle, *Electrochem. commun.* **2015**, *59*, 52.
- [115] Q. Zhuo, X. Li, F. Yan, B. Yang, S. Deng, J. Huang, G. Yu, *J. Environ. Sci.* **2014**, *26*, 1733.
- [116] J. Niu, Y. Li, E. Shang, Z. Xu, J. Liu, *Chemosphere* **2016**, *146*, 526.
- [117] L. Yu, *Calgary* **2014**, DOI 10.1017/CBO9781107415324.004.
- [118] M. Gmurek, M. Olak-Kucharczyk, S. Ledakowicz, *Chem. Eng. J.* **2017**, *310*, 437.
- [119] R. Qu, J. Liu, C. Li, L. Wang, Z. Wang, J. Wu, *Water Res.* **2016**, *104*, 34.
- [120] R. R. Giri, H. Ozaki, T. Okada, S. Taniguchi, R. Takanami, *Chem. Eng. J.* **2012**, *180*, 197.
- [121] J. Saiena, M. Osalia, A. Soleymani, *Desalin. Water Treat.* **2015**, *56*, 3087.
- [122] H. D. Burrows, M. Canle L, J. A. Santaballa, S. Steenken, *J. Photochem. Photobiol. B Biol.* **2002**, *67*, 71.
- [123] H. Hori, E. Hayakawa, H. Einaga, S. Kutsuna, K. Koike, T. Ibusuki, H. Kiatagawa, R. Arakawa, *Environ. Sci. Technol.* **2004**, *38*, 6118.
- [124] X. Yang, J. Huang, K. Zhang, G. Yu, S. Deng, B. Wang, *Environ. Sci. Pollut. Res.* **2014**, *21*, 4634.
- [125] Y. Qian, X. Guo, Y. Zhang, Y. Peng, P. Sun, C. H. Huang, J. Niu, X. Zhou, J. C. Crittenden, *Environ. Sci. Technol.* **2016**, *50*, 772.

- [126] P. Yin, Z. Hu, X. Song, J. Liu, N. Lin, *Int. J. Environ. Res. Public Health* **2016**, *13*, 1.
- [127] B. P. Vellanki, A. Abdel-wahab, B. Batchelor, *Environ. Eng. Sci.* **2013**, *30*, 264.
- [128] P. Ohlsson, J. Blanck, K. Ruckpaul, *Eur. J. Biochem.* **1986**, *158*, 451.
- [129] X. Li, J. Fang, G. Liu, S. Zhang, B. Pan, J. Ma, *Water Res.* **2014**, *62*, 220.
- [130] Y. Gu, W. Dong, C. Luo, T. Liu, *Environ. Sci. Technol.* **2016**, *50*, 10554.
- [131] Y. Qu, C. Zhang, F. Li, J. Chen, Q. Zhou, *Water Res.* **2010**, *44*, 2939.
- [132] L. Huang, W. Dong, H. Hou, *Chem. Phys. Lett.* **2007**, *436*, 124.
- [133] H. Park, C. D. Vecitis, J. Cheng, N. F. Dalleska, B. T. Mader, M. R. Hoffmann, *Photochem. Photobiol. Sci.* **2011**, *10*, 1945.
- [134] H. Park, C. D. Vecitis, J. Cheng, W. Choi, B. T. Mader, M. R. Hoffmann, *J. Phys. Chem. A* **2009**, *113*, 690.
- [135] Z. Song, H. Tang, N. Wang, L. Zhu, *J. Hazard. Mater.* **2013**, *262*, 332.
- [136] K. Nakata, A. Fujishima, *J. Photochem. Photobiol. C Photochem. Rev.* **2012**, *13*, 169.
- [137] N. A. Ab Aziz, P. Palaniandy, H. A. Aziz, I. Dahlan, *J. Chem. Res.* **2016**, *40*, 704.
- [138] G. Boczkaj, A. Fernandes, *Chem. Eng. J.* **2017**, *320*, 608.
- [139] M. Pelaez, N. T. Nolan, S. C. Pillai, M. K. Seery, P. Falaras, A. G. Kontos, P. S. M. Dunlop, J. W. J. Hamilton, J. A. Byrne, K. O'Shea, M. H. Entezari, D. D. Dionysiou, *Appl. Catal. B Environ.* **2012**, *125*, 331.

- [140] D. Friedmann, C. Mendive, D. Bahnemann, *Appl. Catal. B Environ.* **2010**, *99*, 398.
- [141] M. Sanchez, M. J. Rivero, I. Ortiz, *Appl. Catal. B Environ.* **2011**, *101*, 515.
- [142] S. Dominguez, P. Ribao, M. J. Rivero, I. Ortiz, *Appl. Catal. B Environ.* **2014**, *178*, 165.
- [143] S. Dominguez, M. J. Rivero, P. Gomez, R. Ibañez, I. Ortiz, *J. Ind. Eng. Chem.* **2016**, *37*, 237.
- [144] C. J. Escudero, O. Iglesias, S. Dominguez, M. J. Rivero, I. Ortiz, *J. Environ. Manage.* **2017**, *195*, 117.
- [145] C. R. Estrellan, C. Salim, H. Hinode, *J. Hazard. Mater.* **2010**, *179*, 79.
- [146] Y. C. Chen, S. L. Lo, J. Kuo, *Water Res.* **2011**, *45*, 4131.
- [147] S. C. Panchangam, A. Y. C. Lin, K. L. Shaik, C. F. Lin, *Chemosphere* **2009**, *77*, 242.
- [148] M. J. Chen, S. L. Lo, Y. C. Lee, J. Kuo, C. H. Wu, *J. Hazard. Mater.* **2016**, *303*, 111.
- [149] M. Li, Z. Yu, Q. Liu, L. Sun, W. Huang, *Chem. Eng. J.* **2016**, *286*, 232.
- [150] P. Ribao, M. J. Rivero, I. Ortiz, *Environ. Sci. Pollut. Res.* **2016**, *24*, 1.
- [151] C. Song, P. Chen, C. Wang, L. Zhu, *Chemosphere* **2012**, *86*, 853.





# **MATERIALS AND METHODS**





This chapter includes the characteristics of the chemicals and solutions used in the experimental part of the present thesis, explains the procedures followed in the different treatments and describes the analytical methods.

## 2.1. Chemical reagents

The main reagents used in this thesis are detailed in Table 2.1. These chemicals were reagent grade or higher (purity > 98%). All solutions were prepared using ultrapure water (Q-POD Millipore).

**Table 2.1.** List of the chemicals used for the experimental work.

Reagent	Formula	Supplier	Use
Perfluorooctanoic acid	C <sub>7</sub> F <sub>15</sub> COOH	Sigma-Aldrich	Treatment and analysis
Perfluoroheptanoic acid	C <sub>6</sub> F <sub>13</sub> COOH	Sigma-Aldrich	Analysis
Perfluorohexanoic acid	C <sub>5</sub> F <sub>11</sub> COOH	Sigma-Aldrich	Analysis
Perfluoropentanoic acid	C <sub>4</sub> F <sub>9</sub> COOH	Sigma-Aldrich	Analysis
Perfluorobutanoic acid	C <sub>3</sub> F <sub>7</sub> COOH	Sigma-Aldrich	Analysis
Sodium sulfate	Na <sub>2</sub> SO <sub>4</sub>	Sigma-Aldrich	Electrolyte in treatments
Graphite powder	C	Acros Organics	Photocatalyst synthesis
Sulfuric Acid	H <sub>2</sub> SO <sub>4</sub>	Panreac	Photocatalyst synthesis
Chloride acid	HCl	Panreac	Photocatalyst synthesis
Potassium permanganate	KMnO <sub>4</sub>	Panreac	Photocatalyst synthesis
Sodium nitrate	NaNO <sub>3</sub>	Panreac	Photocatalyst synthesis
Titanium dioxide (TiO <sub>2</sub> ) P25 (20% rutile/80% anatase)	TiO <sub>2</sub>	Evonik Industries	Photocatalyst
Sodium sulfite	Na <sub>2</sub> SO <sub>3</sub>	Sigma-Aldrich	Photochemical Sensitizer
Sodium persulfate	Na <sub>2</sub> S <sub>2</sub> O <sub>8</sub>	Sigma-Aldrich	Photochemical Sensitizer
Sodium bicarbonate	NaHCO <sub>3</sub>	Macron, ACS Reagent	Buffer

## **2.2. Electrochemical oxidation treatment**

### **2.2.1. Contaminated water samples**

#### Synthetic solutions

The comparative study between different anodic materials was developed using PFOA model aqueous solutions with initial concentration  $0.24 \text{ mmol.L}^{-1}$ . Sodium sulfate ( $5 \text{ g.L}^{-1}$ ) was used as the electrolyte to provide the aqueous solution with the conductivity needed for electrochemical treatments ( $6.5 \text{ mS.cm}^{-1}$ ).

#### Real wastewater samples

Real industrial wastewaters were used as target contaminated water for electrochemical remediation studies. Specifically, grab samples (50 L) of the influent and effluent streams were obtained in one sampling campaign in 2015, from an industrial wastewater treatment utility (WWTP) located in France. The WWTP receives the sewage of several chemical industries, including a PFASs and fluoropolymer manufacturer. The different stages of the industrial WWTP consisted of a homogenization pool to neutralize the pH and a primary buffer tank. Next, the industrial wastewater enters an activated sludge aeration basin. The wastewater passes through a secondary clarifier to be treated by floatation. As a result, the effluent flows through sand filters before the discharge into the river [1]. Both influent and effluent samples were collected at the same day. Since the residence time in the WWTP is around nine days, the collected effluent sample did not correspond to the treatment of the influent sample.

Four manufacturing plants discharged in the WWTP, and only one of them produced side-chain-fluorinated polymers and fluorotelomer based products for fire-fighting foams and stain repellents which accounted for 3 to 17% of the overall influent flowrate. The characteristics of the industrial wastewaters are summarized in Table 2.2.

The main anions, chloride and sulfate, were present in similar concentration in both influent and effluent samples and provided the water samples with the conductivity required for the electrochemical treatment. The global organic pollution parameters, chemical oxygen demand (COD) and total organic carbon (TOC), were drastically higher in the influent stream. Therefore, the treatments applied in the WWTP led to a severe reduction of the total organic load background. The remaining content in the effluent is likely attributable to non-identified soluble organic compounds that are refractory to conventional treatments.

In addition, 10 individual PFASs were quantified in the raw and treated water samples, among the group of 29 PFASs included in the monitoring program (the full list of 29 PFASs is included in the supplementary material of the scientific publication, *Gomez-Ruiz et al. Chemical Engineering Journal*, 322 (2017), 196–204). The total concentration of PFASs reached  $1402 \mu\text{g}\cdot\text{L}^{-1}$  in the influent and  $1652 \mu\text{g}\cdot\text{L}^{-1}$  in the effluent. Particularly, the most abundant PFAS in the wastewaters was 6:2 FTAB which is a fluorosurfactant commonly used in some fire-fighting foams. 6:2 FTAB was relatively inert to the conventional water treatment since similar concentration values were found in both samples. The next prominent PFAS in the effluent was M4 and 6:2 FTSA. It has been observed that M4 is an intermediate transformation product of 6:2 FTAB and a raw material used for 6:2 FTAB synthesis [1,2]. 6:2 FTSA can be a

degradation product of fluorotelomer-based substances, such as fluorotelomer thioether amido, 6:2 FTAB and M4 [3].

**Table 2.2.** Main characteristics and initial concentration of PFASs (ng.L<sup>-1</sup>) in the influent and effluent samples of the industrial WWTP.

	Influent	Effluent
<i>Physico-chemical Parameters</i>		
Suspended Solids (mg.L <sup>-1</sup> )	125	55
Conductivity (mS.cm <sup>-1</sup> )	6.7	6.9
pH	8.4	7.6
<i>Organic Pollutants</i>		
COD (mg.L <sup>-1</sup> )	2,944	227
TOC (mg.L <sup>-1</sup> )	722	99
<i>Inorganic Compounds</i>		
Sulfate (mmol.L <sup>-1</sup> )	9	11.3
Chloride (mmol.L <sup>-1</sup> )	28.4	38
Ammonium (mmol.L <sup>-1</sup> )	5	<LOQ
Fluoride (mmol.L <sup>-1</sup> )	<LOQ	<LOQ
<i>PFASs</i>		
PFBA (ng.L <sup>-1</sup> )	496	7,544
PFPeA (ng.L <sup>-1</sup> )	3,154	52,500
PFHxA (ng.L <sup>-1</sup> )	5,291	24,827
PFHpA (ng.L <sup>-1</sup> )	2,793	37,847
PFOA (ng.L <sup>-1</sup> )	449	2,063
6:2 FTSA (ng.L <sup>-1</sup> )	242,496	382,200
8:2 FTSA (ng.L <sup>-1</sup> )	874	<LOQ
6:2 FTCA (ng.L <sup>-1</sup> )	328	<LOQ
6:2 FTAB (ng.L <sup>-1</sup> )	1,111,000	1,143,000
M4 (ng.L <sup>-1</sup> )	34,361	2,414

*The LOQ for fluoride was 0.002 mmol.L<sup>-1</sup>. The LOQs for 8:2 FTSA and 6:2 FTCA were 400 ng.L<sup>-1</sup> in the influent samples; and 2,000 and 5,000 ng.L<sup>-1</sup> in the effluent samples, respectively.*

As it can be shown in Table 2.2, M4 was partially removed after the WWTP treatments, whereas 6:2 FTSA concentration increased in the effluent sample likely due to the transformation of M4 or other precursors. Several PFCAs were also identified in the raw and treated sample: PFOA, PFHpA, PFHxA, PFPeA and PFBA. Mass flows of PFCAs notably increased after the activated sludge treatment due to the breakdown of precursors in the sample, such as fluorotelomers, as it has been previously reported [4–6]. Even though fluorotelomers are only manufactured as even-carbon chains, the degradation of these compounds can result in both even and odd PFCAs [7–9]. These results also indicated the large presence of unknown PFAS compounds in the raw sample which are transformed throughout the WWTP treatments.

### **2.2.2. Anodic materials and characterization**

Two commercial boron doped diamond (BDD) anodes were studied: a microcrystalline (MCD) BDD electrode supplied by Adamant Technologies (Switzerland) under the commercial reference Diacell 106, and an ultrananocrystalline (UNCD) BDD electrode that was purchased to Advanced Diamond Technologies (U.S.A.). The MCD anode was formed by a diamond coating of thickness 2–3  $\mu\text{m}$ , synthesized by hot filament chemical vapor deposition (CVD) on a monocrystalline p-Silicon circular substrate, with 70  $\text{cm}^2$  of geometrical area. The UNCD anode was made of a boron doped ultrananocrystalline diamond coating of 2  $\mu\text{m}$  film thickness and 3–5 nm average grain size, on a niobium substrate (42  $\text{cm}^2$  of geometrical area). Additionally, three commercial BDD electrodes were purchased from NeoCoat SA (Switzerland) for boron doping calibration (100, 2500 and 10000 ppm of boron, respectively). The latter electrodes were fabricated by hot filament CVD to give a polycrystalline diamond

film with 2-3  $\mu\text{m}$  thickness on a p-Silicon substrate, similarly to the MCD anode previously described.

The surface morphology of the BBD anodes was determined using field emission scanning electron microscopy (FESEM, JEOL JSM, 7000-F) at 10 kV. The Raman spectra were taken at room temperature under atmospheric pressure in backscattering geometry with a Horiba T64000 triple spectrometer using the 514.5 line of a Coherent Innova Spectrum 70C Ar<sup>+</sup>-Kr<sup>+</sup> laser and a nitrogen-cooled CCD detector (Jobin-Yvon Symphony) with a confocal microscope and a 100 $\times$  objective for detection. The power on the sample was kept below 4 mW to avoid laser-heating effects on the probed material and the concomitant softening of the observed Raman peaks. Lorentzian fitting of the Raman spectra was done using Origin 8 software. The relative sp<sup>3</sup>/sp<sup>2</sup> band ratios were determined by deconvolution of the spectra obtained from X-ray photoelectron spectroscopy (XPS), using an SPECS system (SPECS, Berlin, Germany) equipped with a Phoibos 150 1D-DLD analyser and monochromatic Al K $\alpha$  radiation (1486.6 eV). Data analysis was carried out using Casa XPS 2.3.16 Software to fit the signals to Gauss-Lorentzian curves, after removing the background (Shirley).

### **2.2.3. Experimental set-ups specifications**

The diagram of the experimental set-up used for the bench scale electro-oxidation experiments is shown in Figure 2.1. The configuration consists of an undivided flow-by cell with two parallel electrodes: boron doped diamond (BDD) anode and a cathode of either stainless steel or tungsten, depending on the system. The cell was connected to a power supply (Agilent 6654 A) and experiments were conducted in galvano-static

conditions. The feed solution was stored in a feed tank, pumped through the inter-electrode channel at a high linear velocity and recirculated to the feed reservoir. Every experiment was conducted in batch mode at constant temperature of  $293 \pm 2$  K. Treated samples were withdrawn from the feed tank at regular time intervals and preserved at  $4^\circ\text{C}$  until analysis.

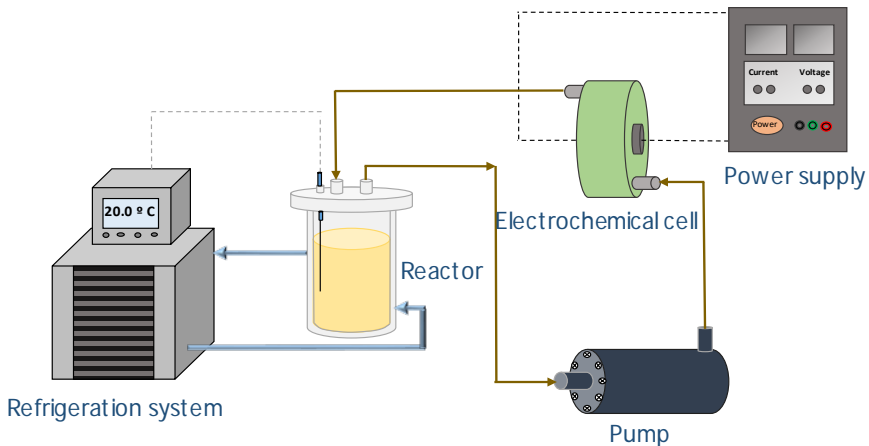


**Figure 2.1.** Electro-oxidation experimental system.

The different experimental procedures followed in this electrochemical technology for the study of: (a) comparative performance of BDD anodes, (b) treatment of industrial wastewaters; are shown below.

Initially, experimental work using two commercial BDD anodes (described in section 2.2.2) for the decomposition of PFOA from model solutions was carried out using two BDD electrochemical systems. Table 2.3 collects the details of experimental conditions applied for each electrochemical system. The feed volume was adapted to get similar anode area/volume ratios in both experimental systems. The mass transport coefficient ( $k_m$ ) in the liquid boundary layer created nearby the anode was calculated by Anglada et al. [10] and Urriaga et al. [11] being  $0.8 \cdot 10^{-5}$  and  $2.4 \cdot 10^{-5}$  m/s for the MCD

and UNCD electrolysis cells, respectively, taking into account the hydrodynamic conditions in each experimental system and the anode geometry.

The comparative experiments for MCD and UNCD anodes were conducted under galvanostatic conditions at a current density ( $j$ ) of  $5 \text{ mA}\cdot\text{cm}^{-2}$ . Moreover, different current densities were applied for MCD ( $j=1$  and  $2 \text{ mA}\cdot\text{cm}^{-2}$ ) and UNCD ( $j=10$  and  $20 \text{ mA}\cdot\text{cm}^{-2}$ ) to study the current density effect on the PFOA degradation from model solutions. The applied current densities were selected to allow appropriate evaluation of PFOA degradation kinetics during a 4-hour experiment accordingly to the dissimilar electrochemical responses observed for UNCD and MCD anodes, respectively.

**Table 2.3.** Description of the experimental conditions and anode geometry for the electro-oxidation experiments.

Characteristic	MCD system	UNCD system
Anode geometry	Circular	Rectangular
Anode surface area ( $\text{cm}^2$ )	70	42
Cathode	Stainless steel	Tungsten
Inter-electrode gap (mm)	5	8
Feed Volume (L)	1	0.5
Flow-rate ( $\text{m}^3\cdot\text{s}^{-1}$ )	$5\cdot 10^{-5}$	$1.1\cdot 10^{-4}$
Linear Velocity ( $\text{m}\cdot\text{s}^{-1}$ )	$0.11^{(1)}$	0.16
Anode substrate	Silicon	Niobium
Cathode	Stainless steel	Tungsten
Applied current density ( $\text{mA}\cdot\text{cm}^{-2}$ )	1,2,5	5,10,20
Cell voltage (V)	$5.6^{(2)}$	$4.9^{(2)}$

(1) Linear velocity was calculated at the central position of the circular electrode

(2) Cell voltage during the electro-oxidation experiments at  $5 \text{ mA}\cdot\text{cm}^{-2}$

Secondly, electro-oxidative tests of industrial wastewaters were performed in the microcrystalline BDD system. The experimental conditions used for raw (influent) and WWTP treated (effluent) wastewaters are listed in Table 2.4. The industrial wastewaters were filtered using 0.45  $\mu\text{m}$  nitrocellulose filters (Millipore). 2 L samples were used as feed in the experiments that were conducted in batch mode, under galvanostatic conditions at  $j=50 \text{ mA}\cdot\text{cm}^{-2}$ . In addition, different current densities (2, 5 and 10  $\text{mA}\cdot\text{cm}^{-2}$ ) were applied to assess their effect on the removal rate of PFASs and TOC from the effluent sample.

Gas phase sampling was not considered, even though it could contain small amounts of short-chain volatile PFCAs as final products of the electrochemical treatment. Each point of the kinetic data was obtained as a single electrochemical experiment, a procedure that allowed to keep the volume constant along the experimental time.

**Table 2.4.** Description of the experimental conditions for electrochemical treatment of the industrial wastewaters using BDD anode.

<b>Experimental conditions</b>	<b>Influent</b>	<b>Effluent</b>
BDD system	MCD	MCD
Feed Volume (L)	2	2
Applied current density ( $\text{mA}\cdot\text{cm}^{-2}$ )	1,2,5	5,10,20
Cell voltage (V)	11.7	13.9 – 15.3

(1) Cell voltage during the electro-oxidation experiments at  $50 \text{ mA}\cdot\text{cm}^{-2}$

## 2.3. Photocatalytic technology

### 2.3.1. PFOA model solutions

PFOA aqueous solutions  $0.24 \text{ mmol}\cdot\text{L}^{-1}$  were used as feed in all experiments. The  $\text{TiO}_2$ -rGO composite catalyst doses were 0.05, 0.1 and

0.5 g.L<sup>-1</sup>. Additionally, commercial P25 (Evonik) TiO<sub>2</sub> catalyst was also used for comparison.

### **2.3.2. Synthesis and characterization of the composite TiO<sub>2</sub>-rGO catalyst**

The first step consisted of the synthesis of graphene oxide (GO) following the modified Hummers method [12]. Thus, 70 mL of H<sub>2</sub>SO<sub>4</sub> were introduced into a jacketed reactor with the thermostatic bath set at 0 °C. After that, 3g of graphite powder, 1.5 g of NaNO<sub>3</sub> and 9g of KMnO<sub>4</sub> were added into the reactor under continuous stirring for 30 min at 35 °C, to obtain graphite oxidation. Specifically, Mn<sub>2</sub>O<sub>7</sub> formed through KMnO<sub>4</sub> and H<sub>2</sub>SO<sub>4</sub> reaction was the reactive species that oxidize the graphite. H<sub>2</sub>SO<sub>4</sub> and NaNO<sub>3</sub> were intercalary agents that enter between sheets to enhance the separation later. While the solution was cooling down, ultrapure water and H<sub>2</sub>O<sub>2</sub> was introduced to eliminate the KMnO<sub>4</sub> in excess. Additionally, the solution was centrifuged and washed with HCl to eliminate the NaNO<sub>3</sub> and H<sub>2</sub>SO<sub>4</sub> in excess. This cleaning processes was repeated with ultrapure water. The oxidized graphite was centrifuged (11,000 rpm) and washed with ultrapure water and with an aqueous HCl solution. Finally, the remaining solid graphite oxide (3D) was ultrasonicated (20 KHz, 20%, pulse 19) for 30 min to achieve exfoliated graphene oxide nanosheets (GO). After that, the sample was centrifuged and the supernatant was collected and dried in an oven at 50 °C overnight, obtaining GO as a solid.

The elaboration of the TiO<sub>2</sub>-rGO composite was performed by the hydrothermal method, following the procedure previously reported in the literature [13,14] (Figure 2.2). In this way, TiO<sub>2</sub> was added into 150 mL

GO dispersion in ultrapure water. The content of GO was controlled to be 5% wt. in the TiO<sub>2</sub>-rGO composites. After stirring for 2 h, the solution was placed in a 200 mL Teflon-lined stainless steel auto-clave and maintained at 120 °C for 3 h, to achieve simultaneously the reduction of GO and the loading of TiO<sub>2</sub> on the reduced GO sheets. The resulting composite was recovered by centrifugation, rinsed with ultrapure water, and fully dried at 50 °C overnight.

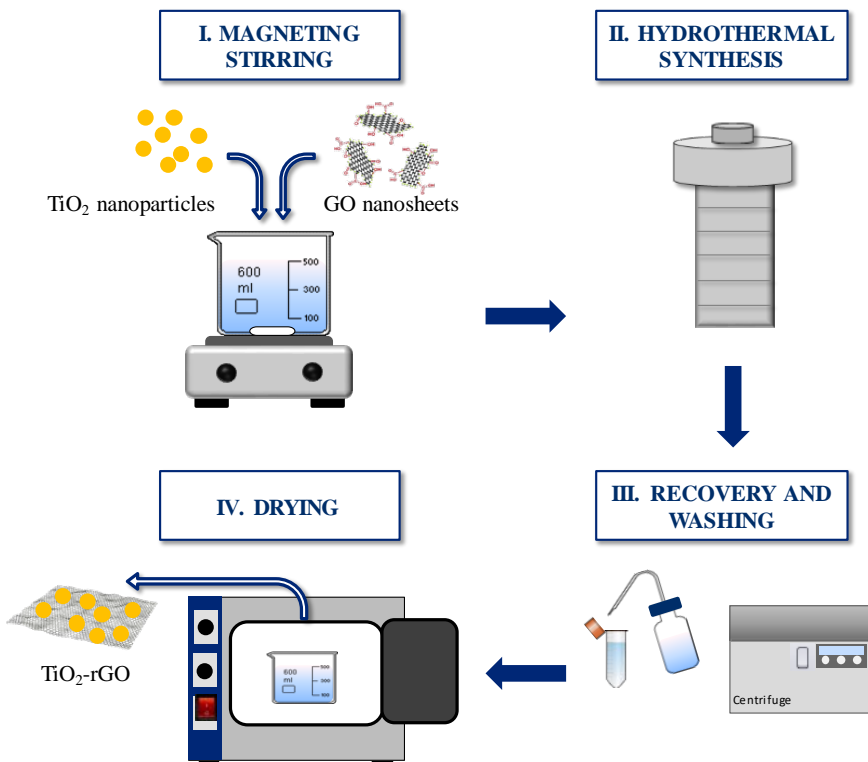


**Figure 2.2.** Methodology scheme for the synthesis of the TiO<sub>2</sub>-rGO composite.

### 2.3.3. Characterization of TiO<sub>2</sub>-rGO

The correct preparation of TiO<sub>2</sub>-rGO composite was examined by physical and chemical characterization. The TiO<sub>2</sub>-rGO morphology was analyzed by transmission electron microscopy (TEM) on a JEOL, JEM-2100 electron microscope. Attenuated Total Reflectance Fourier Transformed Infrared (ATR-FTIR) spectroscopy was also recorded on a Spectrum Two spectrometer (Perkin Elmer). The crystalline phases were obtained by X-ray diffraction (XRD) patterns that were recorded with a X-ray diffractometer (Bruker Kappa-APEX-II), equipped with a Molybdenum Rx tube operating at 50 Kv and 30 mA. X rays were obtained in a sealed tube of Molybdenum and processed by a monochromator of graphite ( $\lambda(K\alpha_1) = 0.71073\text{\AA}$ ). The specific surface area of the nanoparticles was calculated by the Brunauer-Emmett-Teller (BET) method from the nitrogen adsorption-desorption isotherm data employing the ASAP 2000 surface area analyzer (Micromeritics). Furthermore, the fluoride incorporation onto the TiO<sub>2</sub>-rGO surface was investigated by XPS, the characteristics of this technique have been detailed in section 2.2.2.

### **2.3.2. Experimental set-up specifications**

The photocatalytic system is illustrated in Figure 2.3. The experiments were performed in a 1L Heraeus Laboratory UV Reactor mounted on an Agimatic-S magnetic stirring plate (JP Selecta, Spain). A water/ethylene-glycol lamp cooling jacket (PolyScience Digital Temperature Controller) was used to keep the reactor temperature at 293-298 K. The light source consisted of a medium-pressure mercury lamp (Heraeus Noblelight TQ 150 W z1) which is placed inside a quartz sleeve in the centre of the reactor. The light emission spectrum of the lamp lies in UV and visible regions trying to simulate sun light (Figure 2.4). Samples were withdrawn from the

reactor at different time intervals and filter through 0.45 polypropylene filters to remove the catalyst particles before analysis.

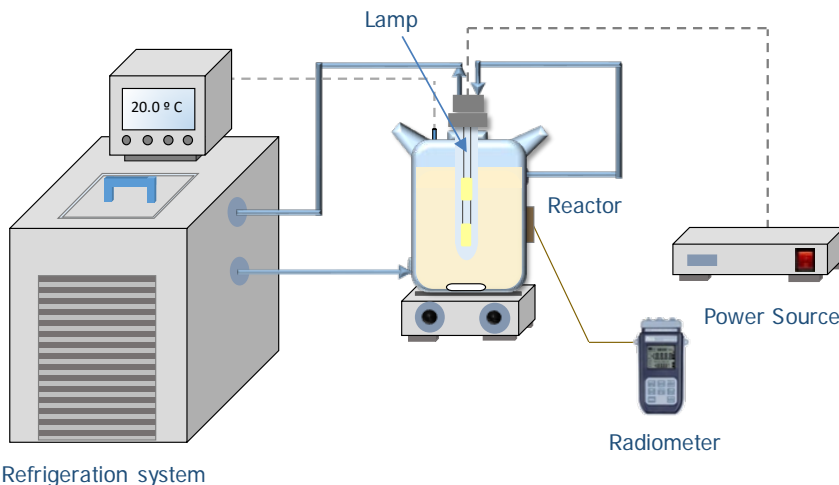


**Figure 2.3.** Schematic illustration of the photocatalytic system. The lamp was placed into a quartz sleeve, which was surrounded by a cooling jacket used to circulate a cooling fluid to maintain the temperature of the reacting media at 20 °C.

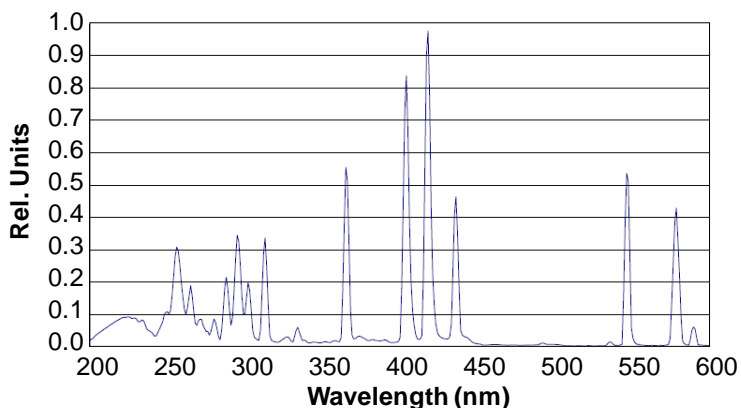


**Figure 2.4.** UV-Vis emission spectrum of the medium-pressure mercury lamp.

### 2.3.2. Irradiation measurement

A HD2102.1 photo/radiometer (Delta OHM) provided with VIS-NIR, UV-A, UV-B and UV-C detectors allowed measuring the light intensity received on the outer wall of the glass reactor (see Figure 2.3). The irradiation emitted by the medium-pressure mercury lamp for different ranges of the spectrum is reported in Table 2.5.

**Table 2.5.** Measurements of irradiation in UV and visible regions emitted by the medium-pressure mercury lamp on the outer wall of the reactor.

Spectrum Range	$\lambda$ (nm)	Irradiation ( $\text{W}\cdot\text{m}^{-2}$ )
UV-A	315-400	$145 \pm 41$
UV-B	280-315	$82 \pm 13$
UV-C	220-280	$1.7 \pm 0.1$
Visible	400-1050	$729 \pm 72$

## 2.4. Homogeneous photochemical techniques

### 2.4.1. AFFF contaminated water

A commercial AFFF mixture was obtained from CH2M (Englewood, Colorado). The AFFF mixture was spiked into laboratory water matrices as the target contaminated water. A 1-to- $10^6$  dilution of the AFFF formulation was prepared to simulate PFAS concentration ( $\mu\text{g}\cdot\text{L}^{-1}$  levels) typically found in real AFFF-impacted groundwater. Table 2.6 lists the composition of the resulting diluted AFFF solution, that was analyzed using the analytical method. As it is observed, AFFF contained a complex mixture of PFASs that is formed by: PFCAs, PFSAAs and FTs. PFOS was significantly the most abundant compound identified in the model AFFF-impacted water, as it has been observed in other AFFF formulations [15].

The total fluorine content the AFFF solution was  $0.0135 \text{ mg.L}^{-1}$  which was quantified by Fluorine-19 nuclear magnetic resonance spectroscopy ( $^{19}\text{F}$ -NMR). The F content calculated from the initial concentration of PFASs detected in the AFFF (Table 2.6) corresponded only to the  $30 \pm 5\%$  of the total fluorine obtained by  $^{19}\text{F}$ -NMR. This result revealed a high content of unknown PFASs or fluorinated precursors in the AFFF commercial formulation.

**Table 2.6.** Initial concentration of PFASs, total organic carbon (TOC) and F content in the 1-to- $10^6$  diluted AFFF solution.

PFASs	$C_0$ ( $\text{ng.L}^{-1}$ )
PFBA	$47 \pm 8$
PFPeA	$41 \pm 3$
PFH <sub>x</sub> A	$110 \pm 76$
PFHpA	$39 \pm 6$
PFOA	$86 \pm 24$
PFNA	$65 \pm 0$
PFPrS	$91 \pm 16$
PFBS	$17 \pm 3$
PFPeS	$124 \pm 16$
PFH <sub>x</sub> S	$725 \pm 91$
PFHpS	$104 \pm 17$
PFOS	$4,976 \pm 692$
PFNS	$51 \pm 3$
6:2 FTCA	$22 \pm 7$
6:2 FTSA	$67 \pm 29$
8:2 FTSA	$29 \pm 2$
6:2 FTUCA	$33 \pm 17$
TOC ( $\text{mg.L}^{-1}$ )	0.147
F ( $\text{mg.L}^{-1}$ )	0.0135

#### 2.4.2. Experimental set-ups specifications

The schematic of the experimental setup is shown in Figure 2.5. Batch

photochemical degradation experiments were conducted in an immersion well photoreactor (Ace Glass Inc.) mounted on a magnetic stirring plate (Isotemp, Fisher Scientific). A UV low-pressure mercury lamp (Ace Glass Inc., 18W) emitting at 254 nm, was placed in a quartz sleeve in the center of the reactor, as irradiation source. By flowing a cooling fluid through the outer cooling jacket that encases the lamp and the reactor, the temperature was maintained at  $20 \pm 1$  °C. Treated samples were withdrawn from the reactor at regular time intervals and preserved at 4°C until analysis. PFAS concentrations are shown as the average of duplicate experiments.

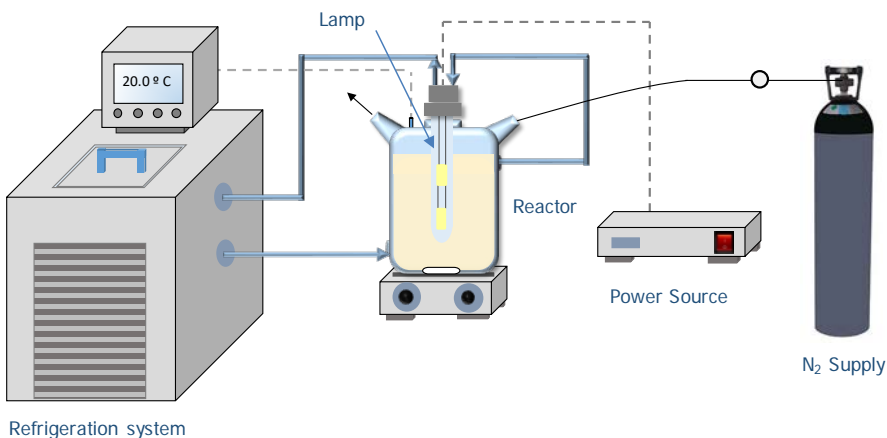


**Figure 2.5.** Photochemical experimental system formed by the UV reactor, refrigeration system, magnetic stirrer, UV low pressure mercury lamp and N<sub>2</sub> tank (for UV/sulfite experiments).

Two photochemical systems were studied: (O1) UV irradiation with persulfate (UV-S<sub>2</sub>O<sub>8</sub><sup>2-</sup>) and (R1) UV irradiation with sulfite (UV-SO<sub>3</sub><sup>2-</sup>). Table 2.7 summarizes the experimental conditions that were established based on the literature [16–24].

**Table 2.7.** Experimental conditions for each photolytic system: UV-S<sub>2</sub>O<sub>8</sub><sup>2-</sup> and UV-SO<sub>3</sub><sup>2-</sup>.

System	Reacting media	Atmosphere	Initial sensitizer concentration (mmol.L <sup>-1</sup> )	Initial AFFF concentration	Treatment time (h)
<b>O1:</b> UV-S <sub>2</sub> O <sub>8</sub> <sup>2-</sup>	Acidic pH <sub>0</sub> H <sub>2</sub> SO <sub>4</sub> + Na <sub>2</sub> SO <sub>4</sub>	Air	10 (Na <sub>2</sub> S <sub>2</sub> O <sub>8</sub> )	1-to-10 <sup>6</sup> dilution	34
<b>R1:</b> UV-SO <sub>3</sub> <sup>2-</sup>	Alkaline pH <sub>0</sub> NaOH + NaHCO <sub>3</sub>	Nitrogen	10 (Na <sub>2</sub> SO <sub>3</sub> )	1-to-10 <sup>6</sup> dilution	24

The same initial concentration of Na<sub>2</sub>S<sub>2</sub>O<sub>8</sub> and Na<sub>2</sub>SO<sub>3</sub> (10 mmol.L<sup>-1</sup>) was employed to allow the comparison of treatments efficiency. In each experiment, a volume of 575 mL of a 1-to-10<sup>6</sup> dilution of AFFF was irradiated. Oxidative treatment was carried out under atmospheric air, and the initial pH was adjusted to 3 with 0.5 mmol.L<sup>-1</sup> of H<sub>2</sub>SO<sub>4</sub> and 4 mmol.L<sup>-1</sup> Na<sub>2</sub>SO<sub>4</sub>, used for ionic strength adjustment. During AFFF impacted water treatments, additions of 10-12 mmol.L<sup>-1</sup> Na<sub>2</sub>S<sub>2</sub>O<sub>8</sub> aliquots to the reacting media were needed when the sensitizer concentrations dropped below 50% of their initial value. UV-sulfite tests were performed under N<sub>2</sub> gas and the initial pH was adjusted to 9.5 by NaOH and 5 mmol.L<sup>-1</sup> NaHCO<sub>3</sub> buffer. Before the test, the mixture was bubbled with N<sub>2</sub> for one hour to remove dissolved oxygen from solution before switching on the UV lamp. Individual experiments of each UV-system and sequences of UV oxidative/reductive treatments were performed as follows:

- 1) Control test: UV only
- 2) UV- Persulfate only
- 3) UV- Sulfite only
- 4) Sequence 1: UV- Persulfate followed by UV- Sulfite
- 5) Sequence 2: UV- Sulfite followed by UV- Persulfate

## 2.5. Analytical methods

### 2.5.1. Analysis of the poly- and perfluoroalkyl substances

The determination of PFASs in the aqueous solution was quantified via high performance liquid chromatography (HPLC). However, the protocol and characteristics of the detection techniques were different depending on the water matrix employed during the different works shown in this thesis.

Firstly, the concentration of PFOA in aqueous model solutions, and its degradation products PFHpA, PFHxA, PFPeA, were analysed using HPLC-DAD (Water 2695) system equipped with a X Bridge C18 column (5  $\mu\text{m}$ , 250 mm x 4.6 mm, Waters). The separation column was set in an oven at 40  $^{\circ}\text{C}$ . A mixture of methanol (65%) and di-hydrogen phosphate (35%) was used as mobile phase in isocratic mode with a flow rate of 0.5  $\text{mL}\cdot\text{min}^{-1}$ . The wavelength of the UV-Vis detector was set at 204 nm. Standard solutions were prepared by individual PFCAs obtained from Sigma Aldrich (Missouri, USA). The LOQ was 10  $\text{mg}\cdot\text{L}^{-1}$  for PFOA and 5  $\text{mg}\cdot\text{L}^{-1}$  for PFHpA, PFHxA and PFPeA. PFOA concentration in the electro-oxidation experiments by the microcrystalline BDD anode, was determined by HPLC-TQD mass spectrometry (Acquity, Waters), and the X-Bridge BEH C18 (2.5  $\mu\text{m}$ , 2.1 x 75 mm) column. The eluents were: (i) an aqueous solution containing ammonium acetate ( $\text{CH}_3\text{COONH}_4$ ) 2  $\text{mmol}\cdot\text{L}^{-1}$  and 5% of methanol, and (ii) pure methanol. The eluent flow rate was 0.15  $\text{mL}\cdot\text{min}^{-1}$ . The limit of quantification (LOQ) was 1  $\mu\text{g}\cdot\text{L}^{-1}$ . Certified standard solutions, containing PFCAs and PFSA, were purchased from Wellington Laboratories (Guelph, Ontario, Canada) [4].

The quantification of PFASs in industrial wastewater matrix was performed in the Laboratory of Hydrology of Nancy (Anses, France) following the

detailed protocol reported by Boiteux et al. [25]. Briefly, non-filtered water samples were diluted prior to extraction, purification and pre-concentration by a solid-phase extraction (SPE) procedure (Strata X-AW<sup>®</sup> (200 mg, 6 mL) cartridge (Phenomenex, Torrance, CA)). An ultra-high performance liquid chromatograph coupled to tandem mass spectrometer (UHPLC-MS/MS) in negative electrospray ionisation (ESI) mode was employed to separate and detect targeted compounds (Waters Xevo TQ-MS tandem mass spectrometer (Waters Corporation, Milford, MA, USA)). Twelve labelled internal standards (IS) were used to provide an adequate correction compensating for matrix effects. Due to initial dilutions, LOQs were between 2 to 5  $\mu\text{g}\cdot\text{L}^{-1}$  in water samples depending on the analytes.

Finally, the concentration of PFASs contained in the AFFF samples were analyzed on a SCIEX X500R QToF-MS system (Framingham, MA) using electrospray ionization in negative mode (ESI-) with SWATH<sup>®</sup> Data-Independent Acquisition for both TOFMS and MS/MS mode, which enables simultaneous tentative identification of >1500 PFASs in the suspect screening list, and including 44 analytes that are quantified against external reference standards. LOQs were analyte, matrix, and run dependent, but were generally 0.6–23 ng/L.

### **2.5.2. Determination of anions**

The determination of anions, such as fluoride, chloride, chlorate, perchlorate and sulfate, was carried out via ion chromatography. An ICS-1100 (Dionex 120 IC) ion chromatograph was used, provided with an AS9-HC column using a solution of  $\text{Na}_2\text{CO}_3$  (9  $\text{mmol}\cdot\text{L}^{-1}$ ) as the eluent at a flow rate of 1  $\text{mL}\cdot\text{min}^{-1}$  and a pressure of approximately 2000 psi, based on Standard Methods 4110B [26]. The equipment was provided with an

automatic sampler model AS 40 (Dionex) and the sample injection volume was 25  $\mu\text{L}$ . A conductivity cell (DS6 Heated Conductivity Cell) measured the electrical conductance of the sample ions and produced a signal based on a chemical or physical property of the analyte. Then, the signal was collected in the work station (software Peaknet) where it was translated to concentration units by pre-calibrating the different compounds identified.

In addition, free chlorine was monitored following the N,N-Diethyl-p-phenylene diamine (DPD) Ferrous Titrimetric Method according to Standard Methods 4500-Cl. Persulfate concentrations were quantified by colorimetric methods following the studies reported by Liang et al. [27]. A modified spectrophotometric method was applied to determine sulfite concentrations [28]. Briefly, sulfite reacts quantitatively with excess 5,5'-dithiobis(2-nitrobenzoic acid) (DTNB) in aqueous solutions buffered at pH 7.0 with  $\text{NaH}_2\text{PO}_4$  for 5 min before measuring absorbance at 412 nm. Fluoride determination by ion-selective electrode was unsuccessful due to the low concentrations present in the diluted AFFF mixture.

### **2.5.3. Total organic carbon (TOC)**

The mineralization of the organic pollutants was followed by means of the total organic carbon removal. TOC was determined using a TOC-V CPH (Shimadzu) analyzer. TOC was calculated from the subtraction of the inorganic carbon (IC) to the total carbon (TC) according to the Standard Methods 5310B [26]. For the analysis of the TC 50.0  $\mu\text{L}$  of the sample were introduced into the TC combustion tube, burned at 680  $^\circ\text{C}$  in a furnace and transformed to carbon dioxide ( $\text{CO}_2$ ). Then the sample was transported by means of a carrier gas with a flow rate of 150  $\text{mL min}^{-1}$  to an electronic dehumidifier where it was dried and, finally, it was transported to the cell

of a non-dispersive infrared (NDIR) gas analyzer, where the CO<sub>2</sub> formed was determined. The NDIR generated a signal and the software of the equipment registered a peak with a given area that was proportional to the amount of carbon present in the sample analyzed. In the case of the TIC analysis the sample was cooled down and acidified with phosphoric acid (25%), then the decomposition of the carbonates and bicarbonates of the sample generates CO<sub>2</sub> which was detected in the NDIR. Then, the procedure followed was the same that the one for TC.

#### **2.5.4. Chemical oxygen demand (COD)**

Chemical Oxygen Demand (COD) was measured following a closed reflux method according to Standard Methods 5220C [26]. The method consists of introducing the appropriate amount of sample into a vial containing a solution of potassium dichromate with mercuric sulphate and sulphuric acid. Then the mixture was incubated for 120 min at 150°C in a COD reactor. COD concentration was measured by titrimetric technique with FAS (Fe(NH<sub>4</sub>)<sub>2</sub>(SO<sub>4</sub>)<sub>2</sub>) and ferroin indicator.

#### **2.5.5. pH and conductivity**

Portable pH meter (Crison) was used for the monitoring of pH, and a HACH (Sesion) portable meter was employed to measure the conductivity and salinity of the samples.

### **2.6. References**

- [1] X. Dauchy, V. Boiteux, C. Bach, A. Colin, J. Hemard, C. Rosin, J. F. Munoz, *Sci. Total Environ.* **2017**, 576, 549.
- [2] M. K. Moe, S. Huber, J. Svenson, A. Hagensaaers, M. Pabon, M.

- Trümper, U. Berger, D. Knapen, D. Herzke, *Chemosphere* **2012**, 89, 869.
- [3] R. C. Buck, J. Franklin, U. Berger, J. M. Conder, I. T. Cousins, P. De Voogt, A. A. Jensen, K. Kannan, S. A. Mabury, S. P. J. van Leeuwen, *Integr. Environ. Assess. Manag.* **2011**, 7, 513.
- [4] I. Fuertes, S. Gómez-Lavín, M. P. Elizalde, A. Urtiaga, *Chemosphere* **2017**, 168, 399.
- [5] M. M. Schultz, C. P. Higgins, C. A. Huset, R. G. Luthy, D. F. Barofsky, J. A. Field, *Environ. Sci. Technol.* **2006**, 40, 7350.
- [6] S.-K. Kim, J.-K. Im, Y.-M. Kang, S.-Y. Jung, Y. L. Kho, K.-D. Zoh, *J. Hazard. Mater.* **2012**, 201–202, 82.
- [7] C. M. Butt, D. C. G. Muir, S. A. Mabury, *Environ. Toxicol. Chem.* **2014**, 33, 243.
- [8] N. Wang, J. Liu, R. C. Buck, S. H. Korzeniowski, B. W. Wolstenholme, P. W. Folsom, L. M. Sulecki, *Chemosphere* **2011**, 82, 853.
- [9] J. Liu, L. S. Lee, L. F. Nies, C. H. Nakatsu, R. F. Turco, *Environ. Sci. Technol.* **2007**, 41, 8024.
- [10] Á. Anglada, A. M. Urtiaga, I. Ortiz, *J. Hazard. Mater.* **2010**, 181, 729.
- [11] A. Urtiaga, C. Fernández-González, S. Gómez-Lavín, I. Ortiz, *Chemosphere* **2015**, 129, 20.
- [12] W. S. Hummers, R. E. Offeman, *J. Am. Chem. Soc.* **1958**, 80, 1339.
- [13] J. Li, S. L. Zhou, G. B. Hong, C. T. Chang, *Chem. Eng. J.* **2013**, 219, 486.
- [14] P. Ribao, M. J. Rivero, I. Ortiz, *Environ. Sci. Pollut. Res.* **2016**, 24, 1.
- [15] M. Filipovic, A. Woldegiorgis, K. Norström, M. Bibi, M. Lindberg,

- A. H. Österås, *Chemosphere* **2015**, 129, 39.
- [16] X. Yang, J. Huang, K. Zhang, G. Yu, S. Deng, B. Wang, *Environ. Sci. Pollut. Res.* **2014**, 21, 4634.
- [17] H. Hori, E. Hayakawa, H. Einaga, S. Kutsuna, K. Koike, T. Ibusuki, H. Kiatagawa, R. Arakawa, *Environ. Sci. Technol.* **2004**, 38, 6118.
- [18] Y. Qian, X. Guo, Y. Zhang, Y. Peng, P. Sun, C. H. Huang, J. Niu, X. Zhou, J. C. Crittenden, *Environ. Sci. Technol.* **2016**, 50, 772.
- [19] S. Yang, J. Cheng, J. Sun, Y. Hu, X. Liang, *PLoS One* **2013**, 8, 6.
- [20] P. Yin, Z. Hu, X. Song, J. Liu, N. Lin, *Int. J. Environ. Res. Public Health* **2016**, 13, 1.
- [21] Z. Song, H. Tang, N. Wang, L. Zhu, *J. Hazard. Mater.* **2013**, 262, 332.
- [22] Y. Gu, W. Dong, C. Luo, T. Liu, *Environ. Sci. Technol.* **2016**, 50, 10554.
- [23] H. Liu, T. A. Bruton, F. M. Doyle, D. L. Sedlak, *Environ. Sci. Technol.* **2014**, 48, 10330.
- [24] S. a Gauthier, S. a Mabury, *Environ. Toxicol. Chesistry* **2005**, 24, 1837.
- [25] V. Boiteux, C. Bach, V. Sagres, J. Hemard, A. Colin, C. Rosin, J.-F. Munoz, X. Dauchy, *Int. J. Environ. Anal. Chem.* **2016**, 96, 705.
- [26] APHA (American Public Health Association), *Standard Methods for the Examination of Water and Wastewater*, Washington DC, **1998**.
- [27] C. Liang, C. F. Huang, N. Mohanty, R. M. Kurakalva, *Chemosphere* **2008**, 73, 1540.
- [28] R. E. Humphrey, M. H. Ward, W. Hinze, *Anal. Chem.* **1970**, 42, 698.





# **RESULTS SUMMARY**



The work developed over this thesis aims to evaluate different materials and advanced technologies for the treatment of persistent poly- and perfluoroalkyl substances in water. The main findings presented in the scientific publications will be highlighted in this chapter.

### **3.1. Electrochemical oxidation**

Initially, the electrochemical oxidation by means of commercial BDD anodes, was studied. The research purpose was firstly focused on the evaluation and comparison of different commercial BDD materials for the anodic oxidation of PFOA from model solutions. Indeed, the influence of chemical and morphological features of BDD surfaces on the electrochemical process was analyzed. The two types of BDD electrodes consisted of: i) a microcrystalline (MCD) coating on silicon; and ii) an ultrananocrystalline (UNCD) coating on niobium. Furthermore, the applicability of the electro-oxidation technology using the microcrystalline BDD anode was investigated to degrade and mineralize a mixture of PFASs from real industrial wastewaters.

#### **3.1.1. PFOA electrolysis by BDD anodes**

Figure 3.1 reports the effect of the applied current density on the PFOA removal rate using MCD (Figure 3.1a) and UNCD (Figure 3.1b) anodes. Different electrochemical responses were observed for both materials. MCD anode allowed a sharp abatement of PFOA, which was almost completely degraded in only 4 hours, independently of the applied current density, within the studied range.

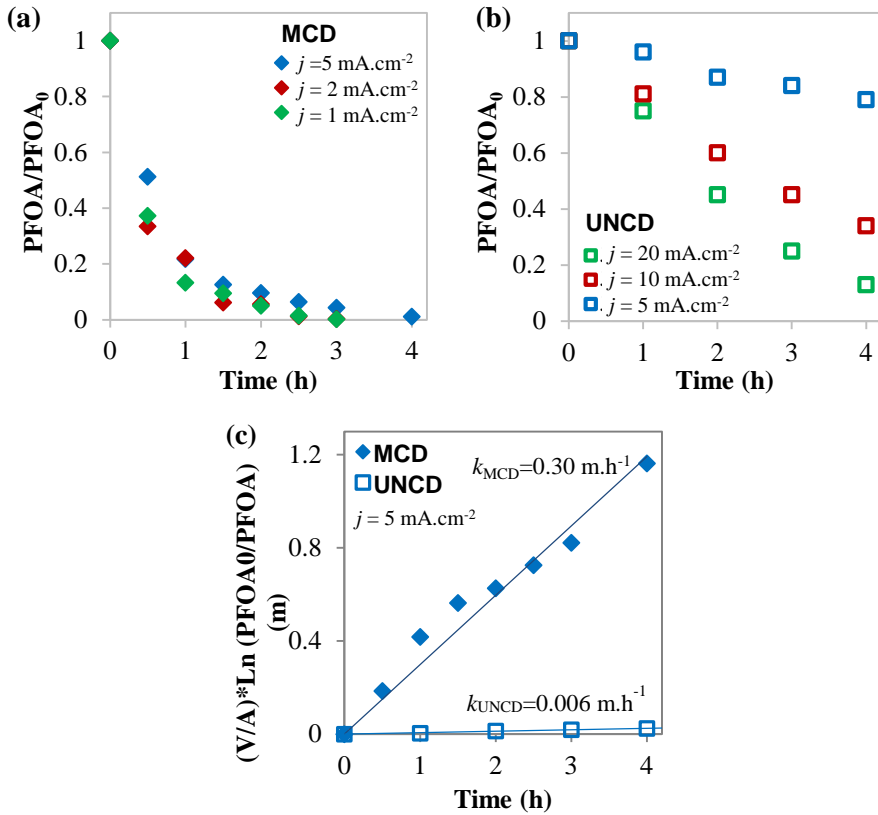


**Figure 3.1.** Influence of the applied current density on PFOA removal with the treatment time, using: (a) MCD ( $j=1, 2$  and  $5 \text{ mA.cm}^{-2}$ ) and (b) UNCD ( $j=5, 10$  and  $20 \text{ mA.cm}^{-2}$ ). (c) Fitting of the experimental data obtained at  $j=5 \text{ mA.cm}^{-2}$  to the kinetic model (Eq. 3.2) for both electrodes. The experimental standard deviation of MCD anode (a) was in the range of 10-15% and therefore the effect of  $j$  in the range 1–5  $\text{mA.cm}^{-2}$  had no significant difference. In the case of UNCD (b), the standard deviation of 3-7% demonstrated that the effect of the current density under the range 5-20  $\text{mA.cm}^{-2}$  on PFOA electro-oxidation was statistically significant.  $[\text{PFOA}]_0=0.24 \text{ mmol.L}^{-1}$

For the MCD anode, increasing  $j$  in the range 1-5  $\text{mA.cm}^{-2}$  involved the effect of increasing the specific energy consumption of the process. The energy consumption is defined as the amount of energy consumed per unit

of pollutant load removed. On the contrary, the UNCD anode provided significantly slower PFOA degradation kinetics. When using UNCD, 21, 66 and 87 % PFOA removals were achieved at 5, 10 and 20 mA.cm<sup>-2</sup>, respectively. It is worth mentioning that the enhancement of PFOA degradation by sodium sulfate electrolyte as a promoter of secondary oxidant species, was considered to be negligible at the low range of current densities applied in the present study [1,2]. Consequently, the remarkable lower PFOA removal ratios alongside the substantial effect of the applied current density observed for the UNCD film resulted in its less efficient electrochemical performance compared to the MCD anode.

The comparison of experimental systems for MCD and UNCD anodes was performed by means of the apparent kinetic rate. The PFOA mass balance in the electrochemical system is written as follows:

$$V \frac{\partial C}{\partial t} = -k A C \quad (\text{Eq.3.1})$$

where  $V$  is the volume of the treated solution (L),  $C$  is the PFOA concentration (mmol.L<sup>-1</sup>) in the feed tank,  $t$  is the electro-oxidation time (h),  $k$  is the apparent first order kinetic constant of PFOA degradation (m.h<sup>-1</sup>) and  $A$  is the electrode surface area (m<sup>2</sup>). The integration of Eq. 3.1 during the length of the experiment ( $t$ ) results in Eq. 3.2.

$$(V/A) \cdot \ln \left( \frac{C_0}{C} \right) = -k t \quad (\text{Eq.3.2})$$

PFOA removal data using MCD and UNCD electrodes, at the same applied current density  $j=5$  mA.cm<sup>-2</sup>, were fitted to Eq. 3.2 in Figure 3.1c. The definition of  $k$  in Eq. 3.2 allows removing the effect of the anode area and treated volume for comparison. Table 3.1 collects the values of  $k$  for MCD

and UNCD anodes at the different applied current densities that were tested. In the MCD system, the PFOA decays were fitted to first-order kinetics, and the values of the kinetic constants remained very similar when increasing the applied current densities.

**Table 3.1.** Apparent kinetic constants  $k$  ( $\text{m.h}^{-1}$ ) for the PFOA electro-oxidation on BDD anodes and the comparison with previous studies using similar electrodes. In reference [3], Soriano et al. studied the degradation of PFHxA instead of PFOA.

MCD/Si (this study)		UNCD/Nb (this study)		MCD/Si (bipolar) [3]		UNCD/Nb [4]	
$j$ ( $\text{mA.cm}^{-2}$ )	$k_{MCD}$ ( $\text{m.h}^{-1}$ )	$j$ ( $\text{mA.cm}^{-2}$ )	$k_{UNCD}$ ( $\text{m.h}^{-1}$ )	$j$ ( $\text{mA.cm}^{-2}$ )	$k$ ( $\text{m.h}^{-1}$ )	$j$ ( $\text{mA.cm}^{-2}$ )	$k$ ( $\text{m.h}^{-1}$ )
1	0.31	5	0.006	5	0.126	3	0.0054
2	0.36	10	0.027			15	0.026
5	0.30	20	0.048			50	0.086

This behavior has been previously described in the literature; the degradation of the perfluoroalkyl pollutant occurred through a fast series of reactions in which both direct electron transfer and indirect oxidation by electro-generated hydroxyl radicals took place, and the overall kinetics were controlled by the mass transport of PFOA from the liquid bulk to the anode surface [5,6]. On the other hand, the PFOA decomposition trend obtained by means of the UNCD anode at  $j=5 \text{ mA.cm}^{-2}$  could be described by either zero<sup>th</sup>-order or first-order kinetics. Moreover, the values of the kinetic constant were much lower compared to the ones obtained in the MCD system, and they gradually raised when increasing  $j$ . This electrochemical performance pointed out the limited availability of active sites on the surface of UNCD anode for direct electron transfer and hydroxyl radical production, which play the main roles in PFOA

electrochemical degradation [7,8].

The kinetic constants obtained in the present study for the UNCD anode are in agreement with the data reported by Schaefer et al. [4] for PFOA electrolysis using an UNCD electrode manufactured by the same provider (Table 3.1). Furthermore, Soriano et al. [3] studied the electrochemical removal of perfluorohexanoic acid (PFHxA), which contains two fluorinated carbons less than PFOA in the perfluoroalkyl chain, using an electrochemical cell that contained two parallel flow-by compartments made of a central bipolar BDD/Si electrode and two BDD/Si anode and cathode. In the latter case [3], the provider of the BDD electrodes was the same as the manufacturer of the MCD anode used in the present study. The reported kinetic constant for PFHxA ( $870 \text{ mg.L}^{-1}$ ) removal was  $0.13 \text{ m.h}^{-1}$  at  $j=5 \text{ mA.cm}^{-2}$ , that is moderately slower than the PFOA degradation constant using the MCD anode in the present work ( $0.30 \text{ m.h}^{-1}$ ), although  $k$  values were still within the same order of magnitude. The comparison of the kinetic constants of both MCD and UNCD anodes together with the results reported in the literature indicates that the PFOA degradation rates provided by UNCD/Nb electrodes were much slower than in case of using MCD/Si.

Additionally, shorter-chain perfluorocarboxylic acids formed as intermediate products during the electrochemical treatment of PFOA were monitored as indicator of the degradation. The degradation of PFOA by the UNCD anode did not produce enough quantity of shorter-chain PFCAs to be detected in the analytical procedure. However, the microcrystalline BDD was able to effectively degrade PFOA into the consecutive C<sub>7</sub>-C<sub>4</sub> PFCAs which were simultaneously formed and degraded into shorter-chain homologues in the well-known stepwise mechanism (Figure 3.2).

The reaction pathways of PFOA degradation will be detailed in the next section (3.1.3).

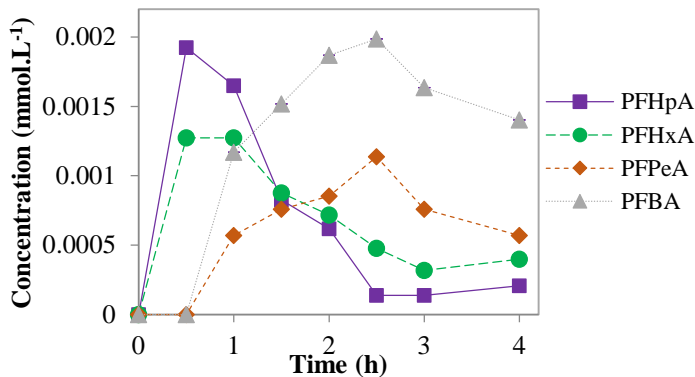


**Figure 3.2.** Evolution of intermediate products (PFHpA, PFHxA, PFPeA and PFBA) concentrations with the electrolysis time, using the MCD anode at  $j=5$  mA.cm<sup>-2</sup>.

In addition, PFOA mineralization was confirmed by the progress of TOC disappearance and the fluoride release (Figure 3.3). Similar to PFOA removal trends, the reduction of TOC was influenced by the type of anode (Figure 3.3a). At  $j=5$  mA.cm<sup>-2</sup> and  $t=4$  h, TOC was reduced by 89% using MCD, whereas only 13% TOC decrease was obtained using the UNCD anode. The effective cleavage of C-F bonds was verified by the release of fluoride in the solution (Figure 3.3b). The final F<sup>-</sup> concentration was 0.7 and 0.3 mmol.L<sup>-1</sup> for MCD and UNCD systems, respectively, after 4h of the treatment at  $j=5$  mA.cm<sup>-2</sup>. These results are in agreement with the faster PFOA decomposition rate on the MCD electrode.

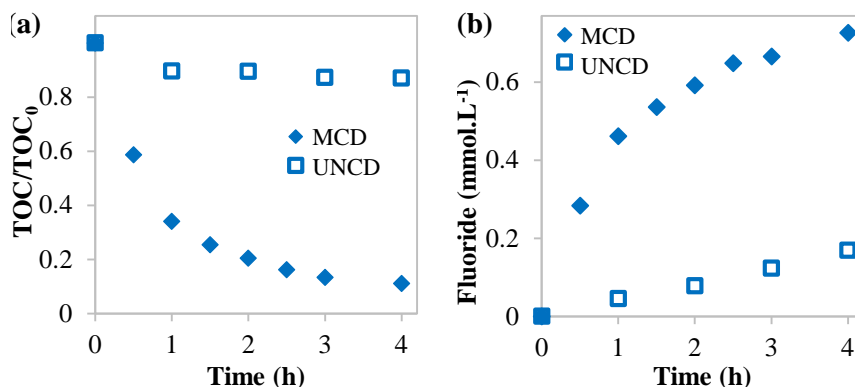


**Figure 3.3.** Evolution of: (a) TOC/TOC<sub>0</sub> and (b) fluoride concentration with the electrolysis time, using MCD and UNCD anodes at  $j=5 \text{ mA.cm}^{-2}$ .  $[\text{PFOA}]_0=0.24 \text{ mmol.L}^{-1}$

### 3.1.2. Characterization of the BDD electrodes and its influence on PFOA electrolysis

According to the literature [9–11], the anodic reactions on BDD electrodes could be influenced by (i) the boron doping level, (ii) the morphological features of the materials and (iii) the diamond carbon content, as it has been described for other organic compounds. Therefore, due to the different electrochemical responses of the two commercial BDD anodes, as well as the diverse results of PFAS removal rates reported in the literature (see Table S1 in the scientific publication), the surface chemical and morphological characterization of MCD and UNCD anodes was studied to elucidate its effect on PFOA electrolysis.

Figure 3.4 shows FESEM surface images of the MCD and UNCD anodes. The FESEM images confirm the information provided by the manufacturers. At  $\times 10000$  and  $\times 25000$  magnifications MCD shows the expected microcrystalline structure with crystal grains in the range of

approximately 1-3  $\mu\text{m}$  while at the same magnifications, the crystals cannot be appreciated in the UNCD anode. Nevertheless, at  $\times 100000$  magnification nanocrystal grains ranging approximately between 2-25 nm could be observed in the UNCD surface [12]. The surface images present well faceted microcrystalline diamond for MCD and line-granular ultrananocrystalline diamond for UNCD film [13]. Moreover, it is worth mentioning that the diamond grains were homogeneously distributed over the anode surface and no cracking defects were appreciated.

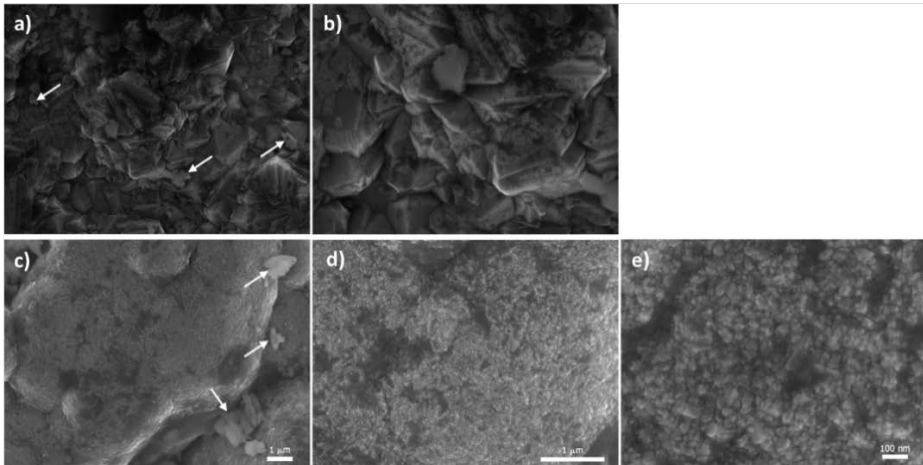


**Figure 3.4.** FESEM surface images of MCD at  $\times 10000$  (a) and  $\times 25000$  magnification (b), and UNCD at  $\times 10000$  (c),  $\times 25000$  (d) and  $\times 100000$  magnification (e). Scale bars indicated for each magnification. Arrows indicate dirtiness of salt deposits on the anode surface after the experiments.

Figure 3.5 presents Raman spectra obtained for MCD (Figure 3.5a) and UNCD (Figure 3.5b) anodes [13,14]. The values of the peaks were determined by deconvolution of Raman spectra using Lorentzian functions (green lines). MCD Raman spectra showed a sharp characteristic peak of microcrystals of diamond facet  $\{111\}$  at  $1329\text{ cm}^{-1}$  slightly shifted from

the typical  $1333\text{ cm}^{-1}$ , characteristic of pure diamond microcrystals. Indeed, its actual position depends on the boron concentration in the diamond lattice, and moves to lower wavenumbers with increasing boron concentration, as reported by [15,16]. The characteristic peaks at  $1350$  and  $1550\text{ cm}^{-1}$  of D ( $\text{sp}^2$  carbon impurities) and G (non-diamond  $\text{sp}^2$ -bonded carbon atoms in the grain boundaries, C-H bending bonds) bands respectively could be also observed (peaks at  $1387$  and  $1547\text{ cm}^{-1}$  in Figure 3.5a).

On the contrary, UNCD surface (Figure 3.5b) presents a wide peak at  $1327\text{ cm}^{-1}$  combining the  $\text{sp}^3$  diamond at  $1333\text{ cm}^{-1}$  and a more dominant D band ( $1310\text{--}1450\text{ cm}^{-1}$ ) coming from the presence of disordered carbon at the grain boundary [13,17]. Besides, the G band characteristic of  $\text{sp}^2$  carbon at  $1535\text{ cm}^{-1}$ , as well as the G' band at  $2515\text{ cm}^{-1}$  could be identified in UNCD anode. The peak at  $1175\text{ cm}^{-1}$  which was formerly [17] ascribed wrongly to transpolyacetylene (typically at  $1150\text{ cm}^{-1}$ ), has been demonstrated to actually correspond to  $\text{CH}_x$  bonds (with  $x \geq 2$ ) in the grain boundaries of nanocrystalline diamonds [18]. The UNCD spectrum in Figure 3.5b is a typical Raman spectrum of ultrananocrystalline diamonds using a laser excitation at  $514\text{ nm}$ . According to the literature [19], the small diamond grain size in the UNCD electrode produced a large presence of graphite in the boundary layers that scattered phonons to make the D peak intensity at  $1357\text{ cm}^{-1}$  being  $\sim 57$  times larger than the diamond peak at  $1333\text{ cm}^{-1}$ .

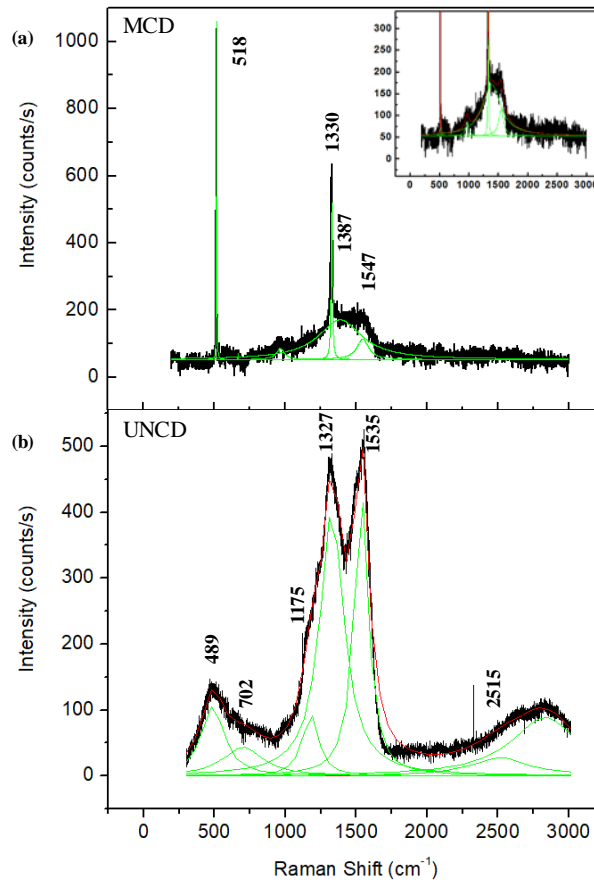


**Figure 3.5.** Raman spectra of (a) MCD and (b) UNCD electrodes. The values of the peaks were determined by deconvolution of Raman spectra using Lorentzian functions within the software Origin 8 (green lines).

Moreover, the displacement of the diamond peak to lower frequencies in microcrystalline BDD materials is proportional to the increase of boron content, according to May et al. [14]. This property has been applied in the present work to determine the concentration of boron in the diamond lattice of the MCD electrode. A calibration curve was built using 3 commercial microcrystalline BDD electrodes (NeoCoat, Switzerland) as standards with known boron concentrations of 100, 2500 and 10000 ppm, respectively.

Figure 3.6a shows the Raman spectra for each BDD standard and the displacement of the Raman shift of the diamond peak for each standard was determined.

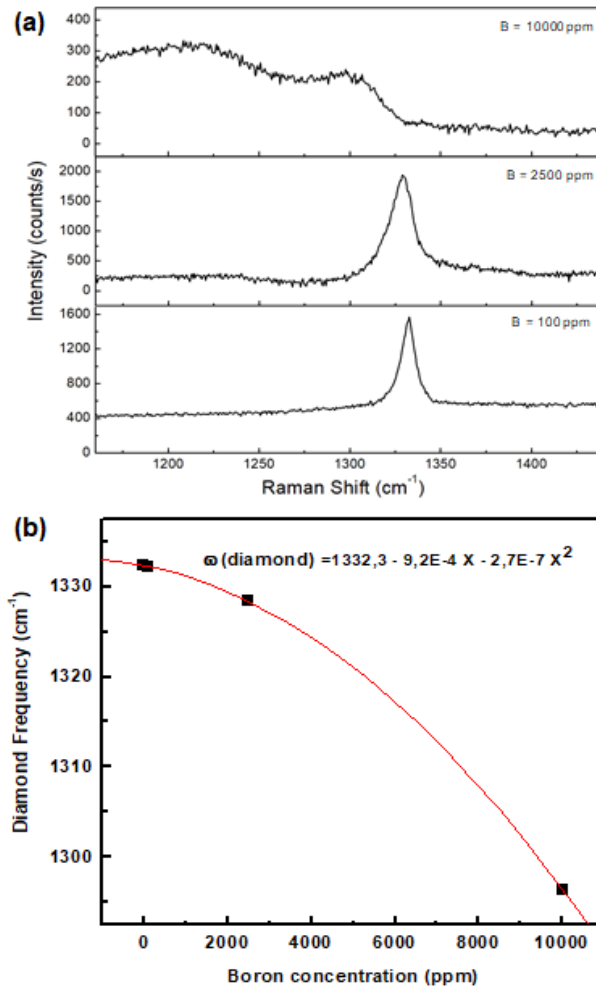


**Figure 3.6.** (a) Raman spectra of microcrystalline BDD standards with different boron concentration: 10000 ppm, 2500 ppm and 100 ppm. (b) Diamond frequency (cm<sup>-1</sup>) as a function of the boron concentration (ppm) in BDD standards obtained from Raman spectroscopy.

The pure diamond peak frequency was used as reference (0 boron concentration,  $1333\text{ cm}^{-1}$ ). The calibration curve that relates the boron concentration with the diamond Raman vibration frequency in  $\text{cm}^{-1}$  is represented in Figure 3.6b. From this calibration curve, the boron concentration for the MCD electrode was calculated as 1676 ppm. Similarly for boron doped ultrananocrystalline diamonds, it has been reported [13] that the D band peak shifted from  $1355\text{ cm}^{-1}$  at B/C ratios of 0 ppm towards  $1300\text{ cm}^{-1}$  at B/C ratios of 6000 ppm. A comparison between the Raman spectrum of the UNCD anode and the Raman spectra of ultrananocrystalline BDDs at different boron doping levels reported by Zeng et al. [13] indicated that our UNCD anode would have a boron content of approximately 3000 ppm.

For further surface characterization, Figure 3.7 depicts the XPS C-1s spectra of the MCD and UNCD anodes. The peak at  $284.5 \pm 0.1\text{ eV}$  was labelled as C-C<sub>1</sub> and the component C-C<sub>2</sub> was shifted +0.9 eV. These peaks were attributed to hydrogenated and non-hydrogenated carbon diamond, respectively [20,21]. The peak at  $283.4 \pm 0.3\text{ eV}$  was ascribed to C=C sp<sup>2</sup> carbon or graphitic defects at the diamond surface and oxygenated carbon species were detected at higher binding energies: 286.5, 287.5 and 289.3 eV for single oxidized components (C-O), such as i.e. -C-OH and -C-O-C- bonds, and further oxidized groups as -C=O or -COOH [20]. The oxidized carbon species typically appear after usage as a result of anode ageing. The B-C peak of boron doped diamonds that should appear at approximately 282.6 eV is not usually observed in these materials due to the presence of surface defects that affect the surface Fermi level [21]. It can be seen that the major component of the MCD surface is C-C<sub>2</sub> or sp<sup>3</sup> crystal diamond carbon (56.0%), the contribution of C-C<sub>1</sub> or hydrogenated

diamond was 16.1%, the total oxygenated species were 23.3% and graphitic defects counted up to 4.6% of the total carbon of the MCD anode.

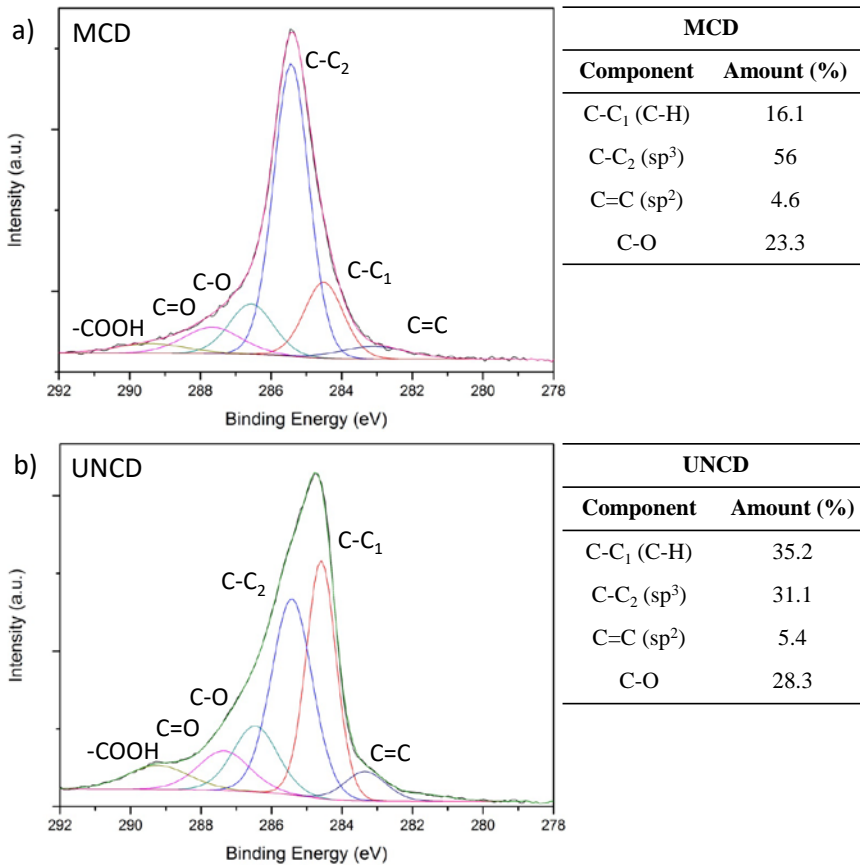


**Figure 3.7.** XPS C1s spectra of (a) MDC and (b) UNCD electrodes. -COOH, C=O and C-O were assigned to oxygenated carbon species. C-C<sub>1</sub> and C-C<sub>2</sub> corresponded to hydrogenated and non-hydrogenated carbon diamond, respectively, and C=C sp<sup>2</sup> refers to the graphitic defects in the diamond surface. Peaks were fitted to the spectra using Gauss-Lorentzian functions.

On the other hand, the major component of the UNCD anode is hydrogenated diamond carbon (C-C<sub>1</sub>) with 35.2%, non-hydrogenated diamond (C-C<sub>2</sub>) accounted for 31.1%, the graphitic carbon was 5.4% and oxidized species were 28.3% of the total carbon. Hydrogen-terminated diamond (C-C<sub>1</sub>) is produced during the BDD synthesis under H<sub>2</sub>-rich conditions to avoid the formation of graphitic carbon at grain boundaries [19]. The higher content of (C-C<sub>1</sub>) of the UNCD is related to the smaller (ultrananano) grain size and consequently higher grain boundary density [21]. The amount of oxygenated species on both diamond films was comparable (23.3 vs 28.3% for the MCD and UNCD anodes, respectively), which is related to the formation of hydroxyl radicals during the use of the materials for anodic oxidation [22].

Overall the following remarkable differences about BDD films characterization can be highlighted: i) the sp<sup>3</sup> diamond relative carbon abundance on the MCD surface is 1.8 times higher than on the UNCD surface, ii) lower boron doping level was found in MCD material compared to UNCD anode, and iii) the hydrogen-terminated diamond on MCD is 2.2 times lower than in UNCD.

Thus, some studies have demonstrated that higher content of sp<sup>3</sup> carbon resulted in more rapid and efficient contaminant decay by electrochemical oxidation [10,11,23]. Assuming that the sp<sup>3</sup> diamond is the direct responsible of the formation of hydroxyl radicals on the anode surface for electrooxidation applications, a lower abundance of sp<sup>3</sup> diamond carbon might imply lower hydroxyl radical generation per unit anode surface area [11,23]. The sp<sup>2</sup> or graphitic carbon content is very similar in both anodes (MCD = 4.6% and UNCD = 5.4%) and thus, the lower PFOA degradation efficiency of UNCD anode encountered in the present work cannot be

justified by differences in the grain boundary graphitic defects. The introduction of boron atoms into the diamond lattice is the main mechanism responsible for the conductivity and the density of active sites on the surface [24]. The anodic materials herein compared present a boron doping level of 1600 (MCD) and 3000 ppm (UNCD). However, despite the higher boron doping level of UNCD anode, the PFOA degradation efficiency was not improved, possibly related to the distortions or defects added into the lattice hindering the electrochemical activity [25,26]. The presence of H-terminated carbon also favors the p-type electrical conductivity on the conductive diamond film surface and enhances the surface hydrophobicity, electron affinity and conductivity [27]. However, the superficial hydrogen content can be progressively changed to O-terminated surface during the electro-oxidation treatments, which would cause the anode surface oxidation and its consequent passivation.

According to the XPS and Raman analysis, UNCD possessed higher boron doping and more H-terminated superficial carbon content than the MCD material, a sum of characteristics that could improve the UNCD p-type superficial conductivity [24,28]. This assumption was verified by the cyclic voltammetry (CV) of PFOA solution using sodium sulfate electrolyte, of both BDD anodes. Figure 3.8 shows that higher current densities were recorded for the UNCD electrode (Figure 3.8b), because of its more elevated electrical conductivity. Moreover, a distinctive feature is observed for the MCD anode, as its cyclic voltammogram (Figure 3.8a) shows the PFOA direct oxidation peak at a potential close to 2.6 V, which is neither observed in the CV with the single  $\text{Na}_2\text{SO}_4$  electrolyte solution, nor in the case of UNCD anode.

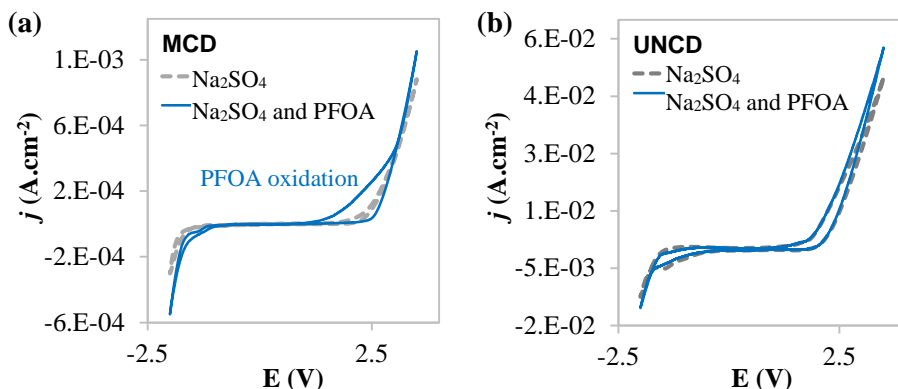


**Figure 3.8.** Cyclic voltammogram of  $0.24 \text{ mmol.L}^{-1}$  of PFOA (blue lines) in  $5 \text{ g.L}^{-1}$   $\text{Na}_2\text{SO}_4$  solutions for (a) MCD and (b) UNCD anodes, obtained at a scan rate of  $100 \text{ mV.s}^{-1}$ . Cyclic voltammograms of single  $\text{Na}_2\text{SO}_4$  (dotted lines) are included for comparison.

Overall, the higher  $\text{sp}^3$  carbon content, lower hydrogen terminated carbon and lower conductivity of the MCD film seem to favor the faster and more efficient PFOA degradation. On the contrary, the surface features, such as extremely small grain size, lower  $\text{sp}^3$  carbon abundance and higher conductivity, of the UNCD electrode provided a limited electrochemical activity for the PFOA removal.

Finally, the practical feasibility of the electrochemical technology is often linked to the energy consumption. The energy consumption ( $W$ ,  $\text{kWh.m}^{-3}$ ) is directly related to the specific electrical charge ( $Q$ ,  $\text{kAh.m}^{-3}$ ) and the cell potential ( $v$ ) [29]. Due to the different electrochemical behavior exhibited by the MCD and UNCD anodes, the energy consumption has been calculated for the maximum PFOA degradation rate obtained in each system, which was 99% and 87% after 4h of treatment, respectively. In this way, the energy consumption estimated for PFOA removal using MCD was only  $1.4 \text{ kWh.m}^{-3}$  ( $j=1 \text{ mA.cm}^{-2}$ ). On the contrary, using UNCD anode

would imply shifting to a higher current density ( $j=20 \text{ mA}\cdot\text{cm}^{-2}$ ) that implies an estimated consumption of  $52.4 \text{ kWh}\cdot\text{m}^{-3}$ . These results confirmed that the differences on BDD surface features can influence on the reaction time and the current density needed for the contaminant removal which impacts directly on the energy costs of the electrochemical process.

Additionally, to determine the efficacy of the electro-oxidation process, the decrease in pollutant concentration during electrolysis can be plotted as a function of the specific electrical charge passed ( $Q$ ).

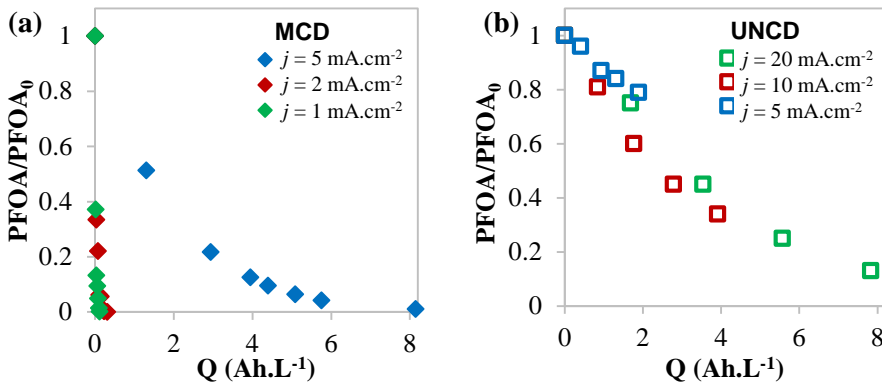


**Figure 3.9.** PFOA evolution as a function of specific electrical charge ( $Q$ ) using: (a) MCD anode ( $j=1, 2$  and  $5 \text{ mA}\cdot\text{cm}^{-2}$ ) and (b) UNCD anode ( $j=5, 10$  and  $20 \text{ mA}\cdot\text{cm}^{-2}$ ).  $[\text{PFOA}]_0 = 0.24 \text{ mmol}\cdot\text{L}^{-1}$

To illustrate this point, the variation of PFOA degradation with  $Q$  was plotted in Figure 3.9. It can be seen that for the MCD system, the increase in current density from  $2 \text{ mA}\cdot\text{cm}^{-2}$  to  $5 \text{ mA}\cdot\text{cm}^{-2}$  significantly decreased the oxidation efficacy (Figure 3.9a). Therefore, current densities higher than  $5 \text{ mA}\cdot\text{cm}^{-2}$  only lead to a massive loss of current efficiency in this process. During PFOA electrolysis by the UNCD anode (Figure 3.9b), the

concentration decreased with the increase of specific electrical charge passed with similar trends for all the applied current densities from 5 to 20 mA.cm<sup>-2</sup>. In conclusion, to achieve satisfactory PFOA removal rates, e.g.: 90% removal, the specific electrical charge passed was two orders of magnitude larger for UNCD anode than MCD electrode.

### **3.1.3. Industrial wastewaters treatment**

In this section, the target streams were the influent and effluent streams of an industrial wastewater treatment utility that receives the sewage of a manufacturer of fluorinated compounds. The effect of the complex matrix composition and the organic load background on PFASs degradation was also studied.

The physical-chemical characterization of the wastewaters showed that the influent exhibited 7-fold higher content of total organic matter than the effluent, whereas the initial content of inorganic anions was very similar between both samples. The TOC content in the effluent can be attributed to organic compounds that are recalcitrant to the conventional water treatments applied in the WWTP. Additionally, the identification and quantification of PFASs in the samples revealed that 10 individual PFAS were found over the limit of quantification (LOQ) of the analytical method, among the group of 29 PFASs included in the monitoring program. The total concentration of PFASs reached 1402 µg.L<sup>-1</sup> in the influent and 1652 µg.L<sup>-1</sup> in the effluent. According to the products manufactured in the industrial facilities above mentioned, 6:2 FTAB, M4 and 6:2 FTAS were the predominant components. Moreover, it is remarkable that the total content of PFCAs increased by one order of magnitude in the effluent after the WWTP treatments. The possible transformation of unknown PFAS

precursors in the conventional water treatments can generate perfluorocarboxylic acids.

The superior electrochemical performance of BDD anodes (microcrystalline BDD in this study) was evaluated by the degradation of PFASs along with the reduction of the major organic pollution parameter, total organic carbon, and inorganic anions in both wastewater samples. The influence of the matrix composition contained in each sample and the applied current density on PFASs electrolysis were also studied.

#### Poly- and perfluoroalkyl substances

The electrochemical treatment by BDD anode was initially studied for the influent sample of the industrial WWTP. The experiments showed that the total content of PFASs was reduced by 97.1% after 8h of electro-oxidation time, under  $50 \text{ mA}\cdot\text{cm}^{-2}$ . More specifically, the progress of the major fluorotelomers, 6:2 FTAB, M4 and 6:2 FTSA, in the influent at  $50 \text{ mA}\cdot\text{cm}^{-2}$  is depicted in Figure 3.10. Due to the use of a specific calibration method, which is costly and time-consuming (standard addition, details are described by Boiteux et al. [30]), 6:2 FTAB and M4 were only determined in three samples of the experiment. The electrochemical treatment allowed a fast decrease of these compounds. Moreover, the concentration data shown in Figure 3.10c were fitted to a first-order kinetic model,  $C=C_0e^{-kt}$ , where  $C$  is the concentration of the compound at a given time  $t$ ,  $C_0$  is the initial concentration and  $k$  is the apparent kinetic constant. The removal of both 6:2 FTAB and 6:2 FTSA followed first-order kinetic trends, typically observed in BDD electro-oxidation processes that are governed by mass transfer limitations. The first-order kinetic constant for 6:2 FTAB removal

was  $1.22 \text{ h}^{-1}$ , whereas the kinetic constant for 6:2 FTSA was significantly lower,  $0.35 \text{ h}^{-1}$ .

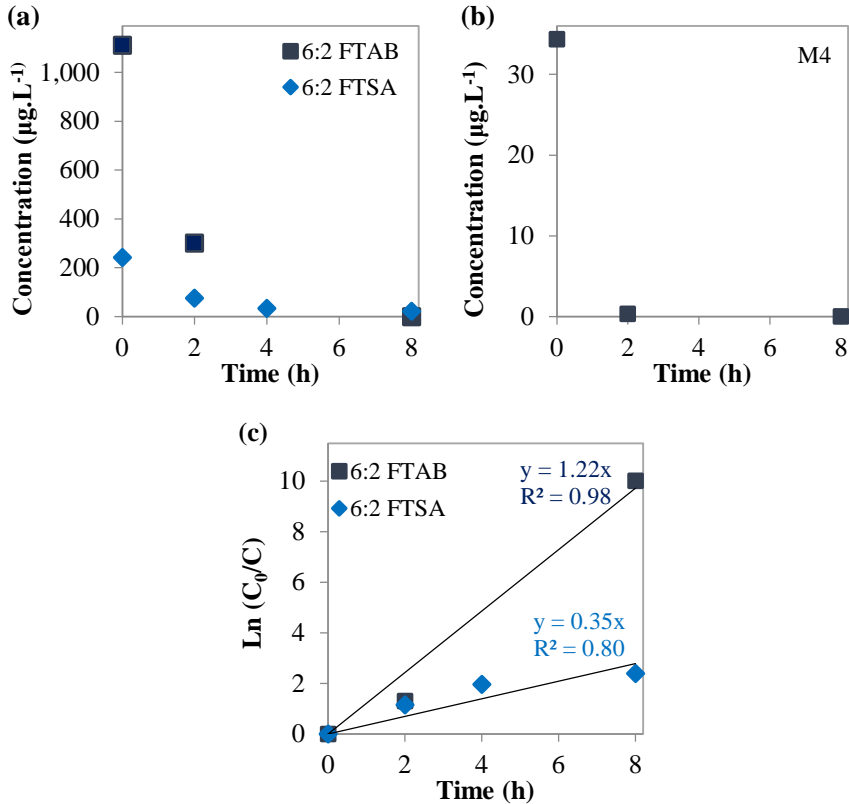


**Figure 3.10.** Change with the treatment time of the main fluorotelomers contained in the influent sample: a) 6:2 FTAB and 6:2 FTSA, b) M4 and c) fitting of 6:2 FTAB and 6:2 FTSA removal data to a first-order kinetic model.

$$j=50 \text{ mA.cm}^{-2}.$$

Similarly, the progress of the major fluorotelomers (6:2 FTAB and 6:2 FTSA) during the electrochemical treatment of the effluent wastewater sample at  $50 \text{ mA.cm}^{-2}$ , is depicted in Figure 3.11. The fitting of these data to first-order kinetics gave rise to kinetic constants of  $0.92$  and  $0.47 \text{ h}^{-1}$ , for

6:2 FTAB and 6:2 FTSA removals, respectively. M4 was reduced to below LOQ after 2 h of treatment (data not shown).

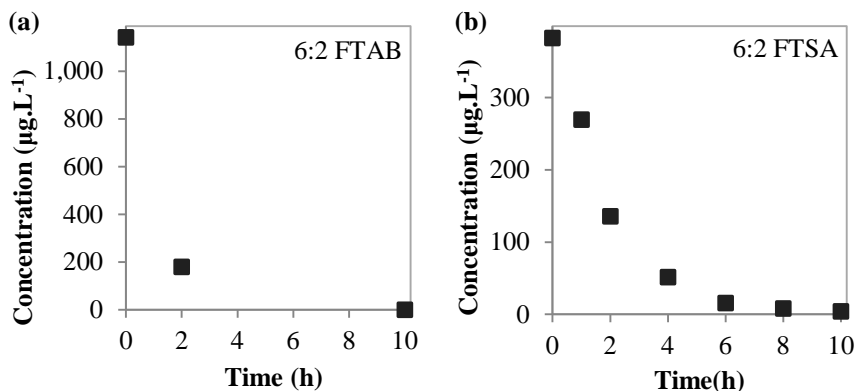


**Figure 3.11.** Evolution of the main fluorotelomers a) 6:2 FTAB and b) 6:2 FTSA with electro-oxidation time,  $j=50 \text{ mA.cm}^{-2}$ , of effluent sample.

Although the initial organic load was drastically higher in the influent wastewater, the electrochemical technology by BDD achieved similar degradation kinetics for the predominant fluorotelomers in both wastewater samples (see Figure 3.12). It is important to note the inaccurate estimation of the kinetic constant for 6:2 FTAB by three measurements.

Based on these results and the molecular structure of 6:2 FTAB, M4 and 6:2 FTSA (see Table 1.1 in Chapter 1), it is possible to foresee that 6:2 FTAB and M4 were partially degraded into 6:2 FTSA. In addition, the lower kinetic constant of 6:2 FTSA disappearance can support the assumption of 6:2 FTAB being progressively degraded into 6:2 FTSA, which was simultaneously generated and broken under these conditions. The formation of 6:2 FTSA as a degradation product of 6:2 FTAB in abiotic conditions has been recently reported. D'Agostino et al. [31] postulated a degradation pathway that involved the activation of molecular

oxygen by Fe (II) ions contained in the aqueous solutions to form reactive oxygen species.

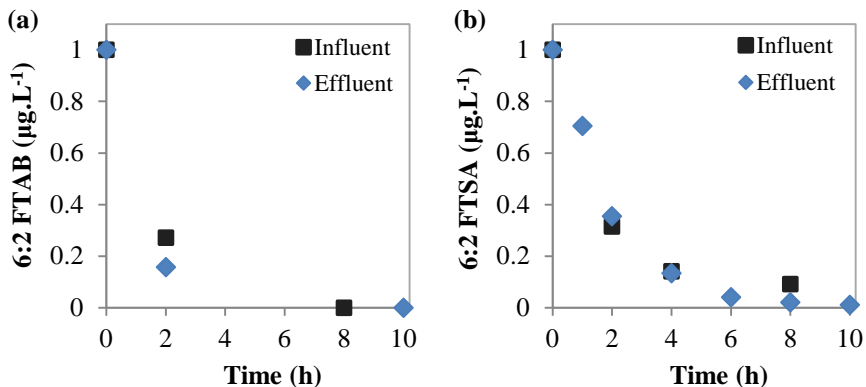


**Figure 3.12.** Evolution of the dimensionless concentration of a) 6:2 FTAB and b) 6:2 FTSA with electro-oxidation time,  $j=50 \text{ mA.cm}^{-2}$ , of influent and effluent wastewater samples.

Perfluorocarboxylic acids were the next important group of PFASs in the industrial wastewaters ( $\Sigma[\text{PFCA}]_0=12.18 \text{ μg.L}^{-1}$ ). Figure 3.13 shows the change of PFCAs in the electrochemical treatment of the influent wastewater sample, at  $50 \text{ mA.cm}^{-2}$ . PFOA present the lowest initial concentration in the raw wastewater (Figure 3.13a) among the group of PFCAs. However, the concentration of PFOA slightly increased during the electrolysis treatment, likely due to the decomposition of 8:2 FTSA that is present in the feed sample ( $[\text{8:2 FTSA}]_0=874 \text{ ng.L}^{-1}$ , Table 2.2 in Chapter 2) [32]. PFHxA was the compound that reached the highest concentration, as it is observed in Figure 3.13c. Its concentration gradually increased during the first 6 h that coincided with the complete depletion of 6:2 FTSA and 6:2 FTAB. In contrast, the concentration of PFHpA (Figure 3.13b) only raised during the initial 2 h. These results revealed that the oxidation

of 6:2 fluorotelomers led to the generation of C<sub>6</sub> PFCAs as the main product, and that C<sub>7</sub> PFCA is a minor by-product.

These experimental results in real industrial wastewaters seems to be in accordance with the mechanisms for 6:2 FTSA splitting reported by Park et al. [33], who found a 25/75 formation ratio of PFHpA/PFHxA upon 6:2 FTSA degradation using heat activated persulfate oxidation. Similarly, the UV-activated hydrogen peroxide oxidation of 6:2 FTSA resulted in a 2-fold formation of PFHxA over PFHpA generation, as reported by Yang et al. [34]. Figure 3.13d and 3.13e report the trends of the shorter-chain PFCAs (PFPeA and PFBA) in the sample. The content of these compounds progressively increased up to 6 hours of treatment, in coincidence with the trend of PFHxA. After that, their concentration decreased below 3 µg.L<sup>-1</sup> after 8h of treatment.

The PFCAs evolution trends in Figure 3.13 indicate that shorter-chain PFCAs were simultaneously formed and degraded, following the stepwise degradation pathways of longer-chain homologues in the sample. Further degradation of PFBA into shorter PFCAs or transfer to the gas phase of volatile PFPrA and trifluoroacetic acid are expected to have occurred too.

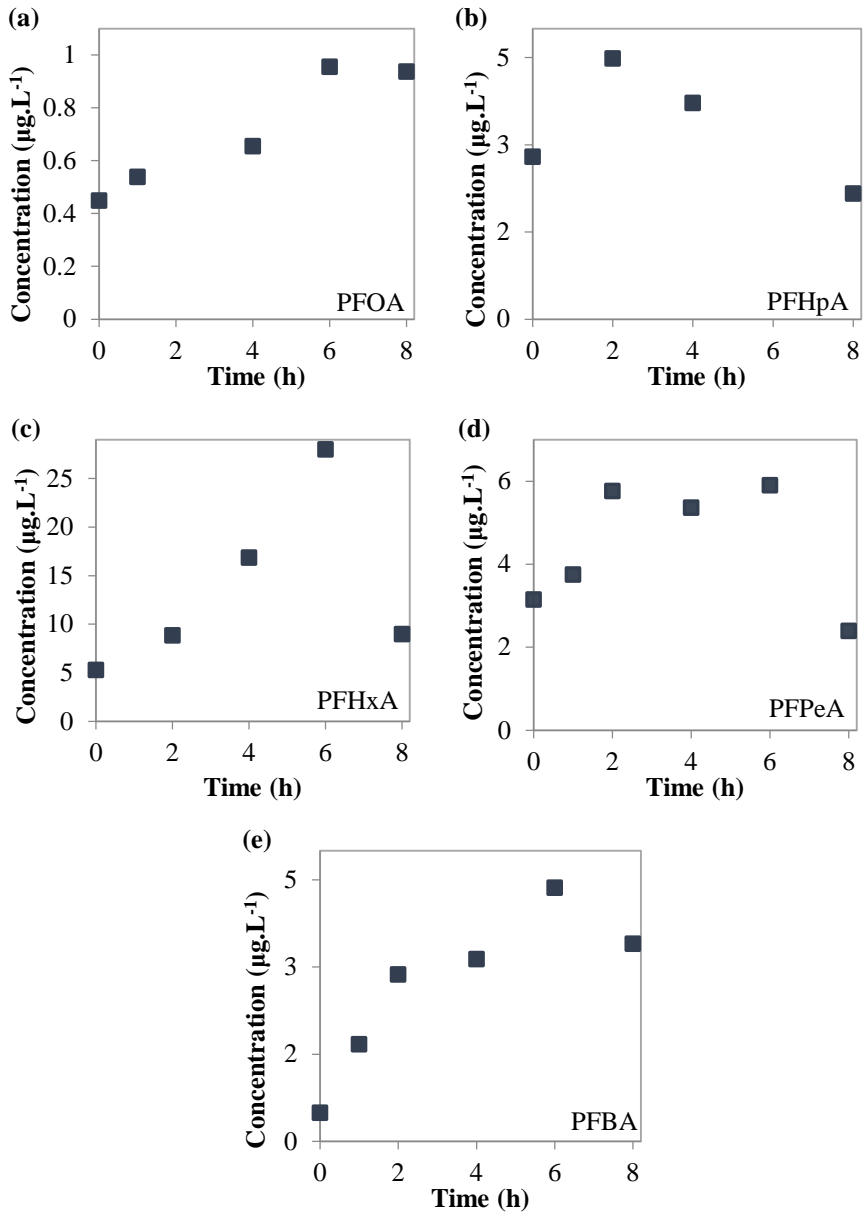


**Figure 3.13.** Evolution with the treatment time of: a) PFOA, b) PFHpA, c) PFHxA, d) PFPeA and e) PFBA concentration, during the electrochemical treatment of the influent wastewater at  $j=50 \text{ mA}\cdot\text{cm}^{-2}$ .

The progress of the PFCAs concentrations during the treatment of the effluent wastewater is depicted in Figure 3.14. The most abundant PFCAs in the effluent were PFHpA ( $C_0=37.85 \mu\text{g.L}^{-1}$ ), PFHxA ( $C_0=24.83 \mu\text{g.L}^{-1}$ ), PFPeA ( $C_0=52.50 \mu\text{g.L}^{-1}$ ) and PFBA ( $C_0=7.54 \mu\text{g.L}^{-1}$ ). The total concentration of PFCAs ( $\Sigma[\text{PFCA}]_0=124.78 \mu\text{g.L}^{-1}$ ) in the effluent was one order of magnitude higher compared to the total initial content in the raw wastewater, due to the degradation of polyfluorinated compounds after the WWTP treatments. The low initial concentration of PFOA ( $C_0=2.06 \mu\text{g.L}^{-1}$ ) could be related to the low concentration of 8:2 fluorotelomers and other PFOA precursors in the WWTP influent. Additionally, the progresses of PFCAs concentrations were studied under different current densities. In Figure 3.14 the change of PFCAs concentrations varied according to the applied current density. Initially, electrochemical experiments were performed at 5 and 10  $\text{mA.cm}^{-2}$ , and for shorter degradation times, up to 2 h. For the lowest value of  $j$ , 5  $\text{mA.cm}^{-2}$ , the progress of all PFCAs showed a gradual increase of concentration with time, a behavior that was assigned to the faster rate of formation compared to their degradation rate. When the applied current density was increased to 10  $\text{mA.cm}^{-2}$ , the peak of maximum PFCAs concentrations was reduced, as a result of accelerating the degradation rates. It should be reminded, that additionally to the PFASs content, electro-oxidation is also acting on other recalcitrant organic pollutants that are consuming most of the applied current for their degradation and mineralization. During the electrochemical treatment at 50  $\text{mA.cm}^{-2}$ , the progress of PFHpA and PFPeA progressively decreased, whereas increases of PFHxA and PFBA were observed at the initial stages of the electrochemical treatment with BDD anodes.

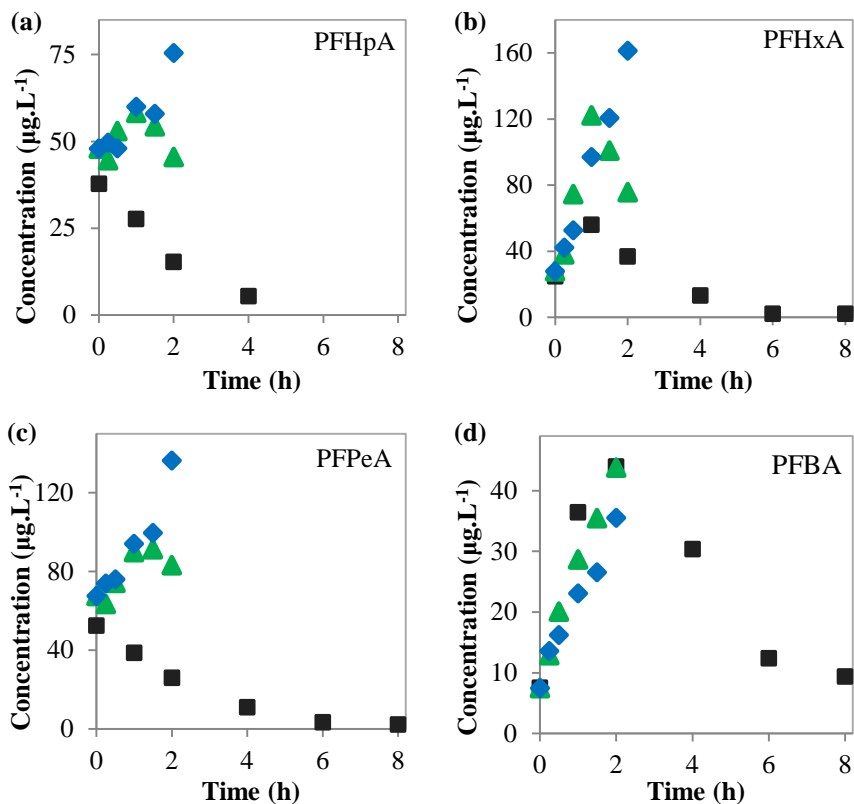


**Figure 3.14.** Evolution with the treatment time of: a) PFHpA, b) PFHxA, c) PFPeA and d) PFBA concentration, during the electrochemical treatment of the effluent wastewater, under different applied current densities: (■)  $j=50 \text{ mA.cm}^{-2}$  (cell voltage= $14.6 \pm 0.5 \text{ V}$ ), (▲)  $j=10 \text{ mA.cm}^{-2}$  (cell voltage= $5.4 \pm 0.02 \text{ V}$ ), (◆)  $j=5 \text{ mA.cm}^{-2}$  (cell voltage= $4.5 \pm 0.07 \text{ V}$ ).

These trends reinforced the idea that PFHxA was the main degradation product of 6:2 fluorotelomers. Among the measured compounds, PFBA is at the end of the degradation pathway of longer chain homologues, and it tends to accumulate at all the applied current conditions under study. However, after 2 h of treatment all these perfluorocarboxylates started to disappear in contrast with the delay observed in the raw influent

wastewater. Therefore, the lower content of the organic load in the effluent allowed a more rapid degradation of most PFASs, compared to the influent treatment, as a consequence of the lower consumption of electrogenerated radicals to degrade the background organic pollutants.

As a result, the evolution of the PFASs analyzed in this work can be described by the degradation pathways gathered in Figure 3.15.

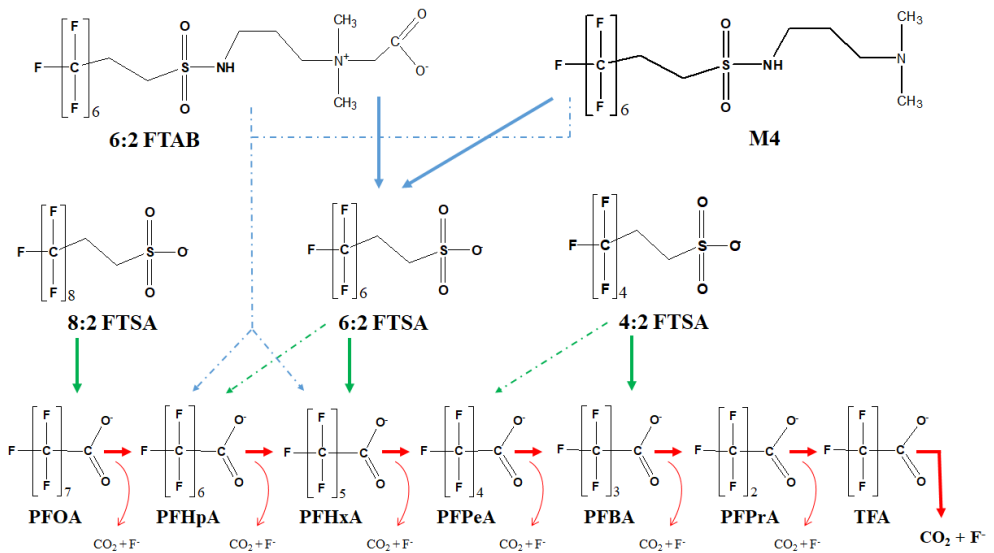
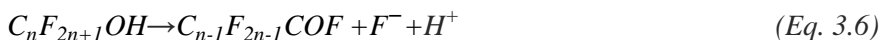


**Figure 3.15.** Electrochemical degradation pathway of the group of PFASs observed in the industrial wastewater case of study. Solid lines represent the main degradation pathways, whereas dotted lines show alternative pathways that may also take place.

By inspection of the chemical structures of 6:2 FTAB and M4, the cleavage of the S-N bond by the electrogenerated oxidants would promote the partial conversion of these fluorotelomer sulfonamides into 6:2 FTSA, which in these conditions would be simultaneously generated and broken. Moreover, fluorotelomer sulfonates present a CH<sub>2</sub>-CH<sub>2</sub> unit between the

perfluoroalkyl chain and the sulfonate end group, which makes fluorotelomers much more susceptible to oxidation than PFCAs. Therefore, 6:2 FTSA degradation would start with the attack of electrogenerated  $\cdot\text{OH}$  radicals to the C-C and C-H bonds of the two unfluorinated carbons, causing the desulfonation and forming  $\text{C}_6\text{F}_{13}\text{COO}^-$  and  $\text{C}_5\text{F}_{11}\text{COO}^-$  [34,35]. The degradation of 8:2 FTSA was expected to follow a similar pathway to form PFOA as main secondary product.

Once the PFCAs have been formed, the following degradation steps would start with the electron transfer from the carboxyl group to the anode to generate the  $\text{C}_n\text{F}_{2n+1}\text{COO}^\bullet$  radical (Eq. 3.3). Next, this highly unstable radical would undergo Kolbe decarboxylation to form a perfluoroalkyl radical ( $\text{C}_n\text{F}_{2n+1}^\bullet$ ) (Eq. 3.4). Then, the electrogenerated hydroxyl radical reacts with the perfluoroalkyl radical to form a perfluoroalcohol  $\text{C}_n\text{F}_{2n+1}\text{OH}$  (Eq. 3.5), which is a thermally unstable species that would undergo intramolecular rearrangement to form the perfluorocarbonyl fluoride and release one fluoride anion (Eq. 3.6). Finally, the latter species hydrolyses to give the one-carbon-shorter-chain perfluorocarboxylic acid,  $\text{C}_{n-1}\text{F}_{2n-1}\text{COO}^-$  (Eq. 3.7) [7,35–37].



The  $C_{n-1}F_{2n-1}COO^-$  repeats the aforementioned steps and decomposes into shorter-chain PFCAs by gradually losing a  $CF_2$  unit. Nevertheless, more studies using model solutions of single fluorinated compounds would be needed to completely assess the proposed degradation pathway.

#### Total organic load and inorganic anions

The electrochemical performance of the BDD anode was also evaluated through the mineralization of the organic pollutant load, using TOC as the global parameter, and the release of fluoride as individual indicator of PFASs mineralization.

In this way, the progress of TOC concentration during the electrochemical treatment of the raw wastewater at  $50 \text{ mA}\cdot\text{cm}^{-2}$ , is shown in Figure 3.16a. The high TOC content of this wastewater ( $722 \text{ mg}\cdot\text{L}^{-1}$ , Table 2.2 in Chapter 2) revealed that the analyzed PFASs contributed with  $<0.1\%$  to the total organic load. Nevertheless, the electrochemical treatment successfully removed 80% of TOC after 8 h, which demonstrated the effectiveness of BDD anodic oxidation for the removal of recalcitrant organic compounds regardless the variety of chemical composition. Moreover, the TOC removal of the industrial WWTP effluent is given in Figure 3.16b. The TOC concentration was effectively reduced by 91% from the WWTP effluent sample under  $50 \text{ mA}\cdot\text{cm}^{-2}$ , after 10h of treatment. In order to compare the elimination of TOC between both types of wastewaters, the TOC results were fitted to a first-order kinetic model. As a result, it was observed that the TOC removal kinetics was slightly faster in the effluent sample ( $k_{TOC,effluent}=0.37 \text{ h}^{-1}$ ) compared to the influent ( $k_{TOC,influent}=0.27 \text{ h}^{-1}$ ). Additional experiments were developed under 2, 5, 10  $\text{mA}\cdot\text{cm}^{-2}$ , to study the effect of  $j$  on the TOC reduction in the effluent sample. At the low

current regime ( $2 \text{ mA}\cdot\text{cm}^{-2}$ ) the TOC removal was slow, and showed zero-order kinetics, typically obtained when electrolysis is under current control. Using higher values of  $j$  (5 and  $10 \text{ mA}\cdot\text{cm}^{-2}$ ), a transient behavior of the trends of TOC removal was observed, to finally observed a first-order trend under  $50 \text{ mA}\cdot\text{cm}^{-2}$ , which the electrolysis is conducted under mass transport control [38,39].

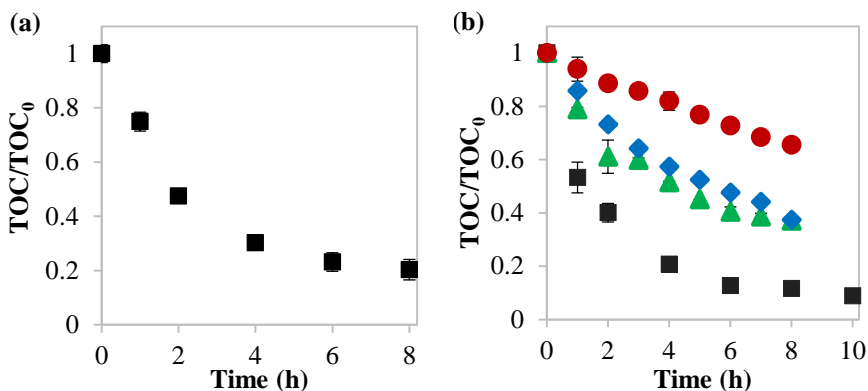


**Figure 3.16.** Evolution of TOC/TOC<sub>0</sub> ratios during the electrochemical oxidation of the (a) influent, and (b) effluent wastewaters, where TOC<sub>0</sub> is 722 and 99 mg.L<sup>-1</sup>, respectively. (■)  $j=50 \text{ mA}\cdot\text{cm}^{-2}$ , (▲)  $j=10 \text{ mA}\cdot\text{cm}^{-2}$ , (◆)  $j=5 \text{ mA}\cdot\text{cm}^{-2}$ , (●)  $j=2 \text{ mA}\cdot\text{cm}^{-2}$ . Data shown as the average of duplicate experiments.

The data about the release of fluoride anions are given in Figure 3.17. The electro-oxidation of the influent sample generated F<sup>-</sup> concentration above the LOQ of the analytical method after 4h of treatment, as a result of the fluoride release during the PFASs degradation (Figure 3.17a). However, after 8 h of electrochemical treatment, fluoride increased to 0.012 mmol.L<sup>-1</sup>, a value that is significantly below the initial fluoride contained in the analyzed PFASs, 0.034 mmol.L<sup>-1</sup>. This difference could be explained by the formation of other shorter-chain PFASs not included as target species in the analytical survey or due to the possible fluoride adsorption on the

BDD electrode during the mineralization of PFASs, as it has been previously reported when PFOA was electrochemically degraded on BDD [40,41]. The monitoring of the fluoride released during the electrochemical treatment of the effluent is shown in Figure 3.17b. The  $F^-$  concentration in the solution progressively increased during the process, reaching higher values than the defluorination data of the raw wastewater sample. After 10 h of electrochemical treatment, the generation of fluoride was  $0.053 \text{ mmol.L}^{-1}$ . This result was higher than the initial  $F^-$  content in the PFAS detected in the sample ( $0.042 \text{ mmol.L}^{-1}$ ) pointing out that unknown PFAS precursors were also degraded during electrochemical oxidation of the effluent. Similarly, previous works highlighted the presence of unidentified perfluorinated compounds in various types of samples by the determination of total fluorine and total oxidizable precursors [42–45].

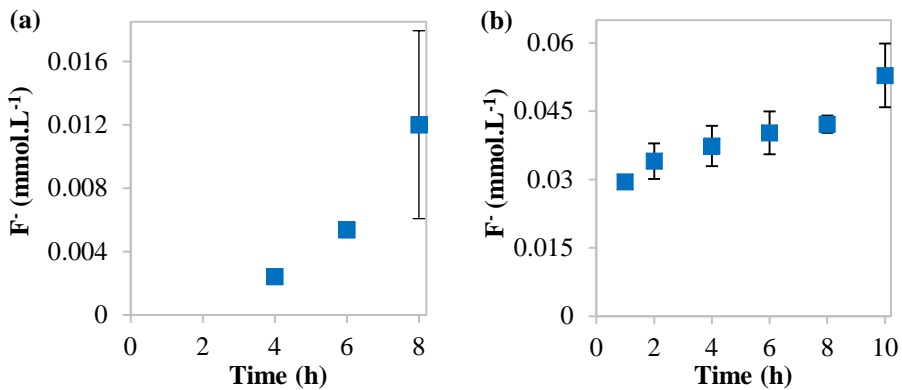


**Figure 3.17.** Evolution of fluoride concentration in solution during the electrochemical oxidation of (a) influent and (b) effluent wastewaters, under  $j=50 \text{ mA.cm}^{-2}$  of applied current density. Average values of duplicate experiments are shown.

Regarding other inorganic anions, chloride is the most abundant ion in both industrial wastewater samples. Figure 3.18 displays the evolution of

chlorine species during the electro-oxidation time. The electrochemical treatment of the influent sample resulted in a slow reduction of the chloride content along the process (Figure 3.18a). Firstly, the depletion of chloride as a result of its anodic oxidation generated the increase of free chlorine. During the formation of free chlorine, the bulk pH was around 7, therefore, hypochlorous acid (HOCl) was the most abundant chlorine species in solution. Chloride and free chlorine are not expected to promote the degradation of PFASs, e.g.: Schaefer et al. [46] showed that the presence of chloride had a minimal effect on the observed rates of PFOA removal from impacted groundwaters, by means of BDD electrolysis, compared to the absence of chloride. After 4 h of treatment, free chloride started to decrease, in coincidence with the depletion of its chloride precursor to proceed with the formation of more oxidized chlorine species, such as chlorate and perchlorate. However, the operating conditions of the electrochemical treatment must be carefully selected in order to avoid the formation of undesirable perchlorate [47,48]. It is important to note that in the present study the oxidation of chlorate to perchlorate was significantly delayed and started after 6 h of electrochemical treatment, a behavior that can be explained by the preferential consumption of the electrogenerated hydroxyl radicals for the oxidation of organic compounds. Only after the oxidation of most of the organic load and when the chloride content was low enough, hydroxyl radicals are available for perchlorate formation [49,50]. As a result, the formation of undesirable perchlorate was avoided in the period in which >91% of the initial PFASs content had been degraded from the influent sample.

In addition, Figure 3.18b reports the progress of the chlorine species during the electro-oxidative treatment of the effluent wastewater. The progress of chlorine species shows similarities with the results obtained for the influent

sample. However, in contrast to the raw sample (Figure 3.17a), the chloride removal rate was accelerated, which involved higher formation and degradation of HOCl. After 4h of treatment, the concentration of chloride and HOCl was highly reduced that gave rise to the consequent generation of perchlorate. Nevertheless, it is also important to note that before the perchlorate formation, most of the PFASs in the sample were degraded. Additionally, the total concentration of all chlorine species at 10 h ( $42.4 \pm 0.9 \text{ mmol.L}^{-1}$ ) was quite similar to the value at the beginning of the experiment ( $38.2 \pm 1.6 \text{ mmol.L}^{-1}$ ), and the small increase could be assigned both to the experimental error or to the release of chloride upon oxidation of organochlorinated compounds [51].

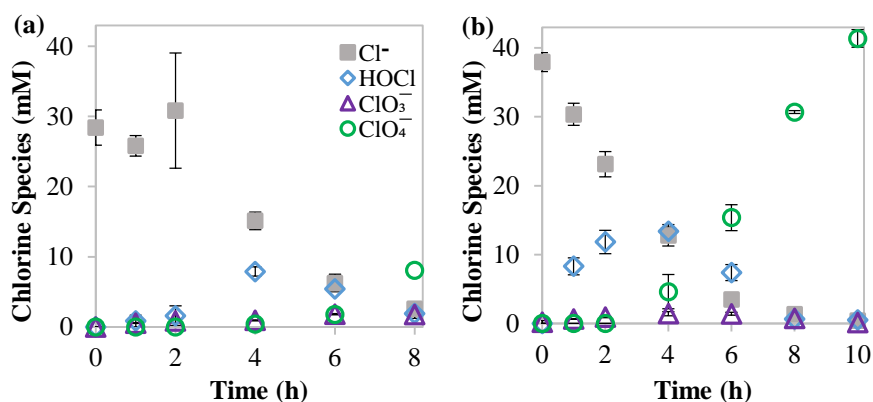


**Figure 3.18.** Evolution of inorganic chlorine species (chloride, free chlorine, chlorate and perchlorate) during the electrochemical oxidation of (a) influent and (b) effluent wastewaters, at  $j=50 \text{ mA.cm}^{-2}$ . Average values of duplicate experiments are shown.

Nitrate and sulfate ions were also monitored during the electrochemical treatment of industrial wastewater samples (data not included in this summary). For the raw wastewater, nitrate and sulfate concentrations initially increased, and then, remained constant. Nitrate formation can be

attributed to the transformation of the initial content of ammonium, which was partially converted into gaseous nitrogen, as it typically occurs in the BDD electrochemical removal of ammonium from wastewaters that also contain organic pollutants and chloride [39,50,52]. Similarly, there was a net formation of sulfate that was attributed to the oxidation of unknown sulfur compounds contained in the industrial wastewater. Nevertheless, the nitrogen and sulfur content of 6:2 FTSA, 6:2 FTAB and M4 only contributed to a maximum of 0.1-0.15% of the change in nitrate and sulfate concentration. Therefore, nitrate and sulfate formation due to the degradation of polyfluorinated sulfonamides and sulfonated fluorotelomers contained in the industrial wastewater was observed to be negligible. On the other hand, the nitrate and sulfate concentration stayed nearly constant in the effluent sample during the electrochemical treatment.

Therefore, the results herein reported showed that PFAS compounds were efficiently removed by BDD anodes in both industrial wastewater samples. However, it is noted that the lower organic load of the WWTP effluent sample allowed to enhance the degradation rates of the total organic load (TOC), most PFASs and the unknown PFAS precursors in the sample, which also led to higher  $F^-$  release in the solution. Moreover, the applied current density should be high enough ( $50 \text{ mA}\cdot\text{cm}^{-2}$ ) to reach higher degradation ratios of all of the PFASs contained in the wastewater.

### **3.2. Heterogeneous photocatalysis**

In this research approach, the photocatalytic removal of PFOA from model solutions was studied using a prepared composite catalyst, based on  $\text{TiO}_2$  and reduced graphene oxide (rGO). This strategy aims at exploring an

alternative to overcome the limited photoactivity of the conventional  $\text{TiO}_2$  catalyst for PFAS degradation [53].

### 3.2.1. Characterization of the prepared $\text{TiO}_2$ -rGO catalyst

Firstly, the prepared  $\text{TiO}_2$ -rGO composite (95  $\text{TiO}_2$  /5 rGO, wt.%) was characterized by attenuated total reflectance - Fourier transform infrared (ATR-FTIR; Spectrum Two spectrometer, Perkin Elmer) Additionally, ATR-FTIR spectra of the GO and commercial  $\text{TiO}_2$  materials were performed for comparison (Figure 3.19).

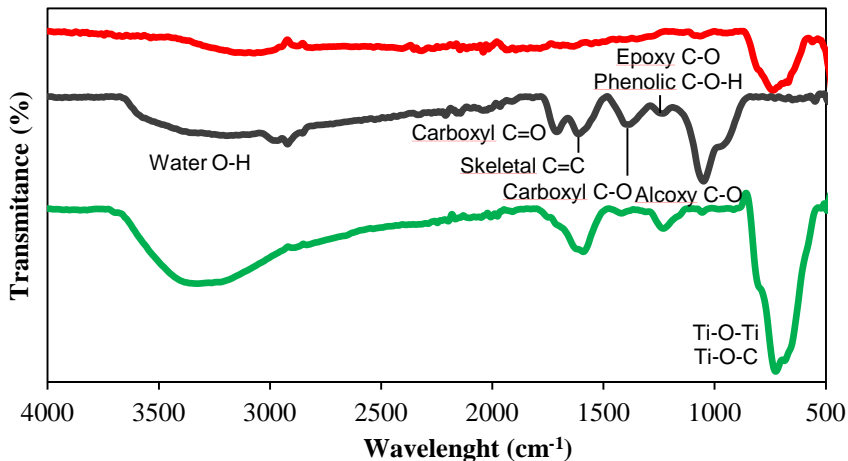


**Figure 3.19.** FTIR spectra of  $\text{TiO}_2$  (—), GO (—) and  $\text{TiO}_2$ -rGO (—).

GO spectrum displayed strong absorption peaks that correspond to different oxygenated functional groups. The peaks at  $3400\text{ cm}^{-1}$  and  $1620\text{ cm}^{-1}$  are ascribed to the stretching vibration of water hydroxyl groups and the skeletal vibration of  $\text{C}=\text{C}$ , respectively. The peaks at  $1732$ ,  $1380$ ,  $1220$  and  $1055\text{ cm}^{-1}$  are attributed to carboxylates  $\text{C}=\text{O}$  stretching, carboxyl  $\text{C}-\text{O}$ , epoxide  $\text{C}-\text{O}-\text{C}$  or phenolic  $\text{C}-\text{O}-\text{H}$  and alkoxy  $\text{C}-\text{O}$ , respectively. Moreover,  $\text{TiO}_2$ -rGO samples still show skeletal vibration peak of  $\text{C}=\text{C}$ ;

however, there is no presence of peaks associated to carboxyl and alkoxy functional groups. This fact implies that GO was partially reduced during the hydrothermal synthesis of the composite catalyst. Moreover, the important intensity increase of the band range between 500-900  $\text{cm}^{-1}$  in the spectrum of  $\text{TiO}_2$ -rGO in comparison to the  $\text{TiO}_2$  spectrum could be related to the possible formation of Ti-O-C bonds additional to the Ti-O-Ti bonds typically occurring in  $\text{TiO}_2$ .

Figure 3.20a shows transmission electron microscopy (TEM; JEOL, JEM-2100 electron microscope) images of the prepared  $\text{TiO}_2$ -rGO composites. It is observed that  $\text{TiO}_2$  nanoparticles were well loaded on the graphene plane, which presents a flake-like structure with some wrinkles. Figure 3.20b and 3.20c present the energy dispersive X-ray (EDX) spectrum collected from Si1 and Si2 areas in Figure 3.20a. The composition of the GO sheets (Si1) was mainly carbon. The EDX spectrum of Si2 area shows a composition based on titanium and oxygen, evidencing the presence of  $\text{TiO}_2$  on the graphene oxide nanosheets. Copper signal is attributed to the sample holder. Therefore, results indicated that  $\text{TiO}_2$  nanoparticles were well loaded on the graphene plane where GO was reduced during the bonding with  $\text{TiO}_2$ .

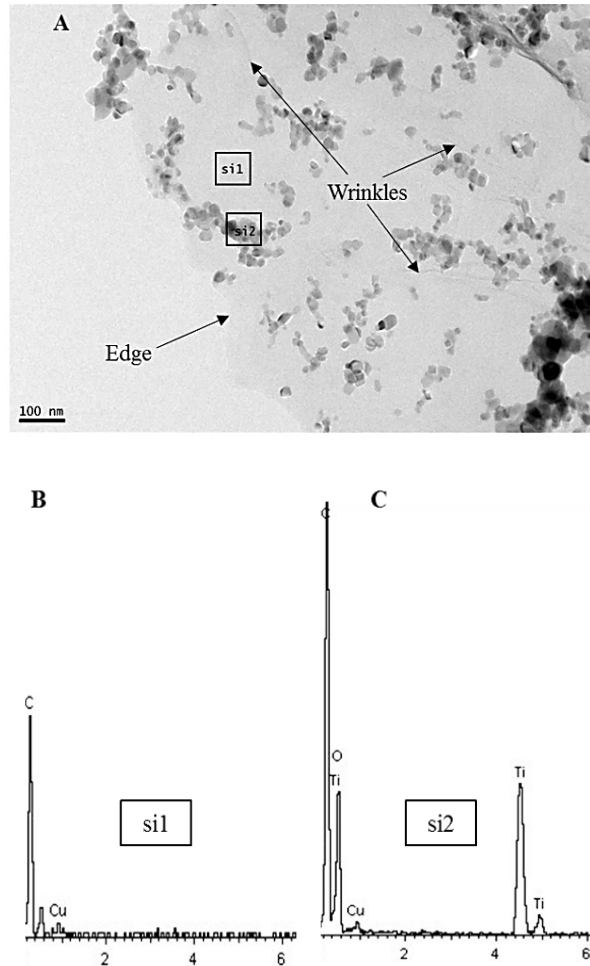


**Figure 3.20.** TEM image of the composite TiO<sub>2</sub>-rGO (A) and EDX scan of zones Si1 (B) and Si2 (C) in the image.

### 3.2.2. Photocatalytic decomposition of PFOA

The photocatalytic degradation of PFOA using the TiO<sub>2</sub>-rGO composite and commercial TiO<sub>2</sub> was studied. Moreover, the removal of PFOA by direct photolysis under UV irradiation was also studied for comparison. The adsorption of PFOA in the experimental system was negligible (less

than 1%) after 12 h of contact of the feed solution inside the glass reactor. The amount of PFOA adsorbed on the  $\text{TiO}_2$  and  $\text{TiO}_2$ -rGO ( $0.5 \text{ g.L}^{-1}$ ) were found to be  $6.4 \pm 0.6\%$  and  $8.4 \pm 0.4\%$ , respectively, after 12 h of contact under stirring in dark conditions. These values of adsorption could be explained by the higher BET specific surface area of  $\text{TiO}_2$ -rGO,  $S_{\text{TiO}_2\text{-rGO}} = 62.2 \text{ m}^2.\text{g}^{-1}$ , compared to  $\text{TiO}_2$ ,  $S_{\text{TiO}_2} = 50 \text{ m}^2.\text{g}^{-1}$  [54]. Similar values of PFOA adsorption on  $\text{TiO}_2$  and metal-modified  $\text{TiO}_2$  have been reported [55]. The electrostatic attraction between the negatively charged perfluorooctanoate anion and the positively charged surface of  $\text{TiO}_2$  particles in acidic solution could have favored the adsorption [56,57], that nevertheless reached only a minor fraction of the initial content.

Next, the influence of the photocatalytic media was assessed. Figure 3.21 allows the comparison of the disappearance of PFOA with time by means of direct photolysis (without catalyst) and when using  $\text{TiO}_2$  and  $\text{TiO}_2$ -rGO as photocatalysts. In every experiment, a volume of 0.8 L of an aqueous PFOA solution ( $0.24 \text{ mmol.L}^{-1}$ ) was irradiated. It is observed that the application of UV light in the absence of any catalyst produced a significant PFOA degradation that reached  $58 \pm 9\%$  removal after 12 h of irradiation. These results are in agreement with available data reported elsewhere [58,59]. PFOA molecule strongly absorbs light with wavelengths from deep UV-region to 220 nm, and presents weak absorption in the 220-270 nm range of light wavelengths [60]. In line with these properties, some authors reported high PFOA photoabatement using a vacuum UV lamp with a monochromatic emission at 185 nm, although the kinetics of PFOA removal were significantly reduced when using the more common emission at 254 nm [61,62]. However, the comparison of literature data about the direct photolysis of PFOA is hindered by the diversity of the applied experimental conditions, range of UV emission

wavelength and power of the UV lamp [58]. In line with the previous discussion, it was concluded that the medium-pressure mercury lamp used in the present study promoted PFOA degradation by means of the deep UV-region of its emission spectrum.

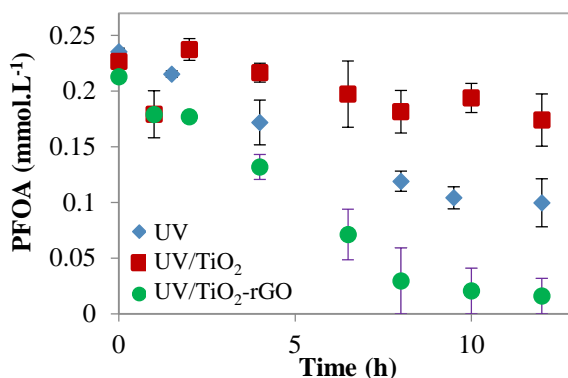


**Figure 3.21.** Evolution of PFOA concentration ( $\text{mmol.L}^{-1}$ ) with irradiation time by photolysis and photocatalysis using  $\text{TiO}_2$  and  $\text{TiO}_2\text{-rGO}$ ; photocatalyst concentration:  $0.1 \text{ g.L}^{-1}$ .

The addition of the  $\text{TiO}_2$  catalyst (Figure 3.21, UV- $\text{TiO}_2$ ) had the effect of decreasing the PFOA removal to only  $24 \pm 11\%$ , after 12 h of irradiation. Although PFOA could have been partially adsorbed on the  $\text{TiO}_2$  surface (6.4% adsorption was observed in the dark experiment), the little release of fluoride ( $0.14 \text{ mmol.L}^{-1}$ ) and the detection of a small amount of PFHpA ( $0.023 \text{ mmol.L}^{-1}$ ) confirmed that PFOA had been degraded in a small extent, into shorter-chain perfluorocarboxylic acids. The lower degradation rate of PFOA observed upon the addition of  $\text{TiO}_2$  can be assigned to a light screening effect by the  $\text{TiO}_2$  particles, that would have significantly reduced the penetration of the UV light into the reaction medium [63]. In contrast, the use of the  $\text{TiO}_2\text{-rGO}$  composite (Figure 3.21, UV- $\text{TiO}_2\text{-rGO}$ ) enhanced PFOA degradation compared to direct photolysis and  $\text{TiO}_2\text{-}$

mediated photocatalysis.  $93 \pm 7\%$  of the initial PFOA was removed after 12 h of irradiation, 4-fold higher than in  $\text{TiO}_2$ -mediated photocatalysis for the same reaction time. This high degradation has been previously demonstrated in the literature using  $\text{TiO}_2$  catalysts modified with metals such as Pb [64]. Moreover, a control experiment using GO nanoplatelets as photocatalyst showed that graphene oxide particles did not produce a significant variation of PFOA concentration, at the same time no degradation products were detected in solution. This result pointed out a synergistic effect between the reduced graphene oxide (rGO) layers and  $\text{TiO}_2$  nanoparticles during the photocatalytic degradation of PFOA. The effect can be ascribed to the good transparency of one-atom thickness rGO sheets towards the UV-visible spectrum, that can decrease the light screening phenomena caused by  $\text{TiO}_2$  particles, and therefore, facilitate a more efficient utilization of light and avoid the electron-hole recombination [65,66].

The irradiance received on the outer wall of the reactor was measured to get an indirect evaluation of the light screening phenomena. The results are displayed in Figure 3.22, using a background PFOA ( $0.24 \text{ mmol.L}^{-1}$ ) aqueous solution in all cases. The radiation received when using  $\text{TiO}_2$  suspensions was significantly lower than through  $\text{TiO}_2$ -rGO suspensions, for every ultraviolet light range tested and for each catalyst concentration. If we focus on the UV-A range (315-400 nm) and  $0.1 \text{ g.L}^{-1}$  catalyst dose, where the  $\text{TiO}_2$  catalyst can absorb photons to generate the electron/hole pairs, the irradiance through  $\text{TiO}_2$  suspensions was approximately one-tenth of the irradiance received through the  $\text{TiO}_2$ -rGO solution. These results confirm that  $\text{TiO}_2$  particles were promoting the UV light screening and hindered UV-A light penetration through the PFOA solution. While the  $\text{TiO}_2$ -rGO composite ( $0.1 \text{ g.L}^{-1}$ ) still reduced the light transmission

compared to the absence of catalyst, the suitable photocatalytic properties of the prepared TiO<sub>2</sub>-rGO composite overcame the UV light screening, as the achieved PFOA degradation yield (93%) was much higher than the degradation percentage obtained under direct photolysis conditions (58%), as it was reported in Figure 3.21.

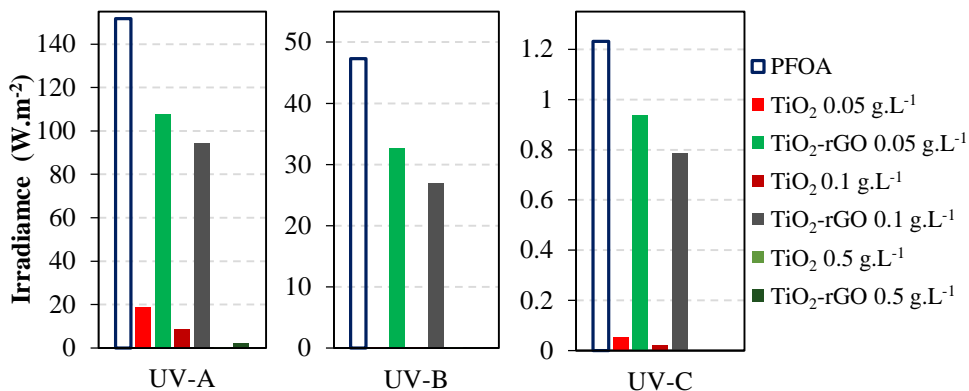


**Figure 3.22.** Irradiance measurements ( $\text{W}\cdot\text{m}^{-2}$ ) on the outer wall of the reactor using TiO<sub>2</sub> (0.05, 0.1 and 0.5  $\text{g}\cdot\text{L}^{-1}$ , red bars) and TiO<sub>2</sub>-rGO suspensions (0.05, 0.1 and 0.5  $\text{g}\cdot\text{L}^{-1}$ , green bars) in a PFOA (0.24  $\text{mmol}\cdot\text{L}^{-1}$ ) aqueous solution, in the regions: UV-A (315-400 nm), UV-B (280-315 nm) and UV-C (110-280 nm).

Some studies have already shown that the combination of TiO<sub>2</sub> with rGO leads to a reduction in the band gap energy to 2.72 eV [48], a feature that would provide the composite TiO<sub>2</sub>-rGO with the ability of visible light adsorption, and a more efficient utilization of light than TiO<sub>2</sub> (band gap 3.2 eV). On the other hand, Kamat and co-workers [67,68] have shown that photo-electrons generated by TiO<sub>2</sub> under UV irradiation can be transferred to rGO due to the excellent electrical conductivity of graphene materials, thus avoiding the electron/hole recombination [69,70]. Therefore, rGO sheets would act as an electron-trap similar to the reported behavior of the metallic nanoparticles in metal-modified TiO<sub>2</sub> photocatalysts [55,71]. The

electron conduction throughout the TiO<sub>2</sub>-rGO photocatalyst may allow further generation of superoxide and hydroxyl radicals [71,72], which in turn will enhance the oxidation of PFOA molecules. In addition, the excellent electron mobility of rGO could promote the electron transfer from PFOA molecule that favors the initial degradation steps, similar to Eq. 3.3.

The structure and morphology of TiO<sub>2</sub>-rGO could also have a significant role in the photocatalytic process. It is well known that the spherical-like TiO<sub>2</sub> nanoparticles aggregate to form larger particles [72,73]. Sun et al. [74] demonstrated that UV irradiation of TiO<sub>2</sub> nanoparticles suspended in water accelerated particle aggregation, that hindered the TiO<sub>2</sub> photocatalytic degradation of Rhodamine B. However, the TiO<sub>2</sub>-rGO composite prepared in the present study presented a homogeneous distribution of TiO<sub>2</sub> nanoparticles spread on the platform of a graphene oxide nano-sheet (Figure 3.20). This structure may have limited TiO<sub>2</sub> particles agglomeration with the benefit of a more efficient use of the UV light by the composite particles.

Results for experiments performed at different TiO<sub>2</sub>-rGO catalyst concentrations are provided in Figure 3.23. The concentration of the catalyst was first increased from 0.1 g.L<sup>-1</sup> to 0.5 g.L<sup>-1</sup>, as the latter value is a common dose in TiO<sub>2</sub> photocatalytic experiments, according to the literature survey (Table S1 in the scientific publication). However, increasing the catalyst dose had the effect of reducing significantly the rate of PFOA removal. Considering that TiO<sub>2</sub> is the major component (95% wt.) of the composite catalyst, the higher concentration of TiO<sub>2</sub> at the highest catalyst dose may have facilitated the UV light screening, as it can be seen in Figure 3.22. In contrast, the reduction of the catalyst dose to 0.05

$\text{g.L}^{-1}$  had a minimal effect on PFOA removal in comparison to  $0.1 \text{ g.L}^{-1}$  catalyst concentration, in agreement with the similar values of light transmission for  $0.05 \text{ g.L}^{-1}$  and  $0.1 \text{ g.L}^{-1}$   $\text{TiO}_2\text{-rGO}$  concentrations (Figure 3.22).

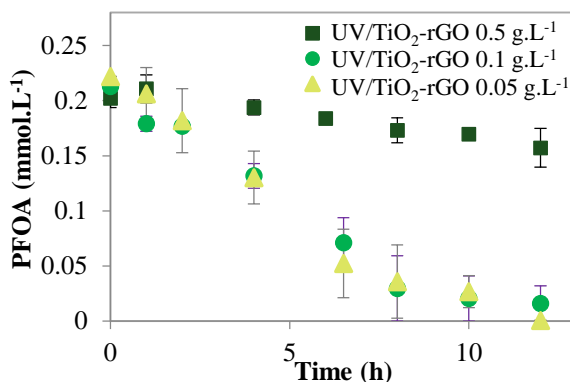


**Figure 3.23.** Influence of the  $\text{TiO}_2\text{-rGO}$  loading on the PFOA concentration ( $\text{mmol.L}^{-1}$ ) with the irradiance time.  $\text{TiO}_2\text{-rGO}$  concentrations were 0.05, 0.1 and  $0.5 \text{ g.L}^{-1}$ .

### 3.2.3. PFOA Mineralization and intermediate degradation products

Generation of shorter chain PFCAs that were formed as intermediates from PFOA degradation is presented in Figure 3.24a, working with a catalyst concentration of  $0.1 \text{ g.L}^{-1}$ . The corresponding fluoride generation for the same experiment is shown in Figure 3.24b, that also presents the total fluorine in the reactor calculated as the sum of fluoride anions in solution and the fluorine contained as part of the quantified PFCAs. Finally, Figure 3.24c presents the reduction of TOC together with the TOC calculated from the organic compounds that were found in the analytical survey. Lines plotted in Figures 3.24a and 3.24c correspond to simulated values

that were obtained using the model and kinetic parameters that will be described next in this section.

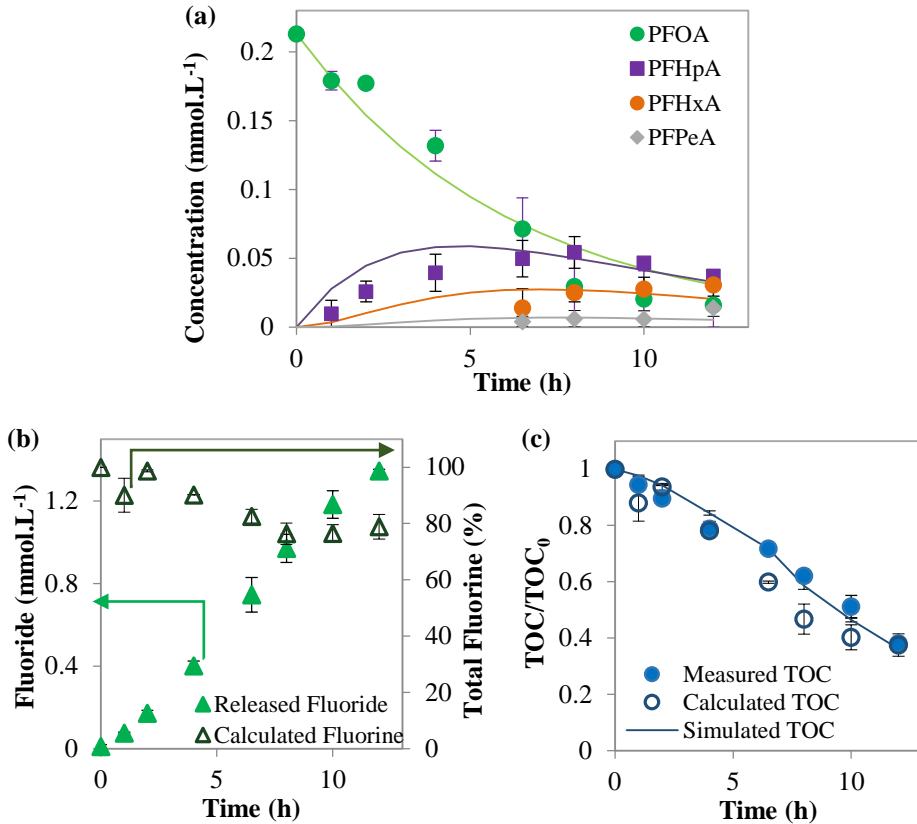


**Figure 3.24.** Evolution of (a) PFOA, PFHpA, PFHxA and PFPeA (mmol.L<sup>-1</sup>), and their simulated concentrations using the pseudo-first order estimated kinetic parameters (solid line); (b) fluoride (mmol.L<sup>-1</sup>) in solution and calculated total fluorine (%), and (c) measured TOC/TOC<sub>0</sub>, calculated TOC/TOC<sub>0</sub> from the analyzed PFCAs, and simulated TOC/TOC<sub>0</sub> using the simulated PFCAs concentrations. Experimental data obtained using 0.1 g.L<sup>-1</sup> of TiO<sub>2</sub>-rGO. TOC<sub>0</sub> was the initial value in each experiment.

PFOA removal can be described by a first order rate kinetic law. The order of appearance of shorter-chain of PFCAs as intermediates (Figure 3.24a) were consistent with the well-known stepwise degradation mechanism [75] in which PFOA would have lose one  $-CF_2$  group to give PFHpA, and consecutively PFHxA and PFPeA. The next molecule in the degradation pathway would be PFBA that was detected although at concentrations below the LOD (Limit of Detection) of the analytical technique.

TOC was reduced by 62% during the photocatalytic decomposition of PFOA (Figure 3.24c). The difference between PFOA reduction (93%) and TOC decrease can be ascribed to the presence of intermediate degradation products. It is worth mentioning the good match between the analyzed TOC and the TOC calculated from the quantified concentrations of PFOA, PFHpA, PFHxA, and PFPeA. The coincident trends prove the step-by-step PFOA degradation pathway in which shorter-chain perfluorocarboxylates are the intermediate products.

The gradual increase of fluoride in the aqueous solution demonstrated that the cleavage of the C-F bonds was effective during PFCAs degradation (Figure 3.24b). Total fluorine measurements showed a net loss of fluorine of 20 % after 12 h of photocatalytic treatment. The loss of fluorine may be attributed to two factors: i) fluoride adsorption on the surface of the  $TiO_2$  fraction of the composite catalysts, which is positively charged in acidic conditions [76–78], and ii) the volatilization of the shortest PFCAs obtained as end products of the PFOA degradation chain [79].

In order to verify the possible fluoride incorporation onto the photocatalyst surface, XPS analysis of the  $TiO_2$ -rGO particles surface was performed, using used samples of the photocatalytic material. Figure 3.25 shows the

section of the high resolution XPS spectrum of used  $\text{TiO}_2$ -rGO particles, where the F-1s region has been magnified. Three deconvoluted peaks at 684.2 (A), 688.8 (B) and 691.0 eV (C) can be observed: the first peak was related to negatively charged monovalent fluorine ( $\text{F}^-$ ); and the signals around 688-691 eV could be assigned to fluorine bonded to carbon, as it happens in the C-F bonds of PFOA and its perfluorinated degradation intermediates that may have been absorbed on the catalyst surface [77,78].

Based on the above results, part of the fluoride anions that were released during PFOA abatement were absorbed onto the  $\text{TiO}_2$ -rGO photocatalyst, to account for 6.8% of the total mass of the catalyst sample used in the XPS analyses. As this adsorption rate did not represent the total fluorine loss, volatile or undetected shorter PFCAs not determined by the analytical technique could also contributed to the 20% of fluorine loss observed in Figure 3.24b.

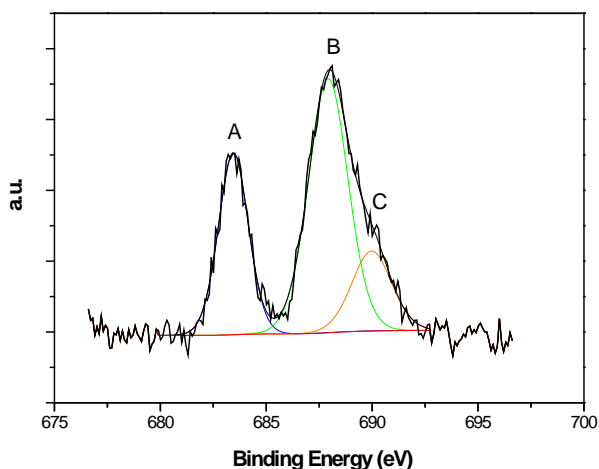


**Figure 3.25.** XPS spectrum in the F-1s region of  $\text{TiO}_2$ -rGO surface after PFOA photocatalytic degradation. A peak is attributed to inorganic fluorinated species.

B and C peaks are assigned to organic fluorinated compounds.

Figure 3.26 presents the proposed mechanism and pathway of PFOA decomposition in the TiO<sub>2</sub>-rGO mediated photocatalysis and the role of rGO in the mechanism. Previous studies considered different possibilities for the initiation of the PFOA molecule degradation: i) direct reaction of PFOA with the photogenerated holes of the photocatalyst surface [55,57,78,80], ii) indirect reaction with hydroxyl radicals [58,64,75,81,82] or iii) combination of both mechanisms. Thereby, the degradation of PFOA could start from terminal carboxylic end, where the photogenerated hydroxyl radicals can attack the first alkyl C atom adjacent to the -COOH group, leading to the cleavage of C-C bond between the perfluorinated alkyl chain -C<sub>7</sub>F<sub>15</sub> and -COOH by the formation of perfluorinated alkyl radicals, which can then react with water or hydroxyl radicals to produce the unstable perfluorinated alcohol C<sub>7</sub>F<sub>15</sub>OH (similar to the equation 3.3-3.5 previously reported). After that, C<sub>7</sub>F<sub>15</sub>OH would eliminate HF to form C<sub>6</sub>F<sub>13</sub>COF (Eq. 3.6). The active C<sub>6</sub>F<sub>13</sub>COF undergoes hydrolysis in the solution, resulting in the formation of PFHpA with the release of CF<sub>2</sub> unit (Eq. 3.7). On the other hand, other possible initiations of PFOA degradation could be the direct reaction of C<sub>7</sub>F<sub>15</sub>COO<sup>-</sup> with the holes. This step would involve the electron transfer from the dissociated PFOA to the valence band of the photocatalyst, generating the C<sub>7</sub>F<sub>15</sub>COO<sup>•</sup> radical that subsequently would undergo Kolbe decarboxylation, to give perfluoroalkyl radical C<sub>7</sub>F<sub>15</sub><sup>•</sup> and CO<sub>2</sub> [80]. The next degradation pathways would be similar to equations 3.5 to 3.7. Correspondingly, the intermediates will be decomposed stepwisely into shorter-chain PFCAs, and eventually to CO<sub>2</sub> and F<sup>-</sup>. Although the reaction mechanism seems to be mostly driven by <sup>•</sup>OH radical attack, the formation of the reactive species such as radical superoxide anion (O<sub>2</sub><sup>•-</sup>) and perhydroxyl radical (HO<sub>2</sub><sup>•</sup>), and may also be associated with the PFOA degradation [83].

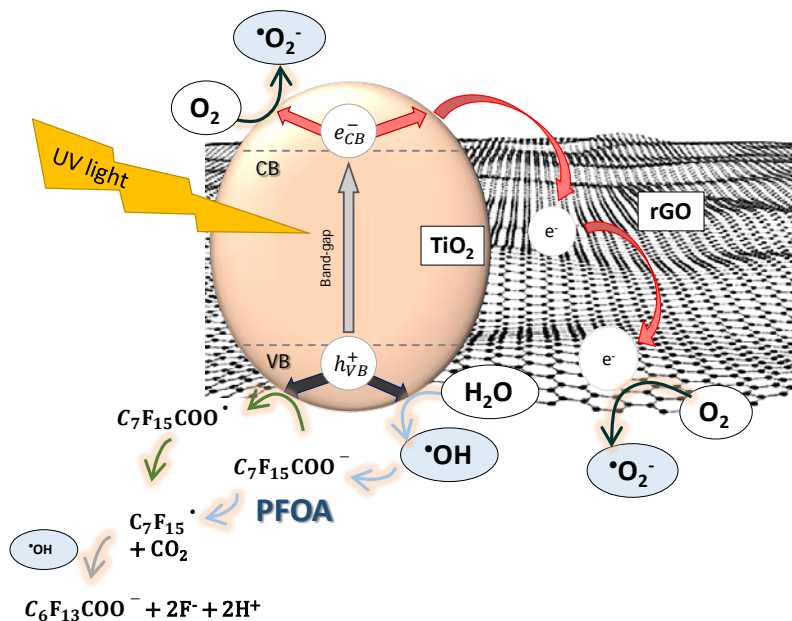


**Figure 3.26.** Photocatalytic pathways of PFOA decomposition using the TiO<sub>2</sub>-rGO catalyst.

Although all the semiconductor-based photocatalysis is initiated by the photogenerated electron/hole pairs, the reaction pathways and the activity of the electron and the hole would be strongly dependent on the type of photocatalyst. It is well-known that TiO<sub>2</sub> tends to oxidize organic compounds by hydroxyl radicals which present limited activity for PFOA degradation [79]. However, the prepared TiO<sub>2</sub>-rGO provided an enhanced elimination of this contaminant likely due to the combination of hole and hydroxyl radicals mechanisms [84,85].

### 3.2.4. Kinetic model for PFOA and its degradation products

In a first attempt to quantify the kinetics of PFOA photocatalytic degradation by the TiO<sub>2</sub>-rGO composite catalyst, the concentrations of

PFOA and intermediate products were fitted to the following first-order rate equation [57,75,77–79,86]:

$$\frac{d[C_n]}{dt} = k_{n+1} [C_{n+1}] - k_n [C_n] \quad (\text{Eq. 3.8})$$

where  $n$  is the carbon atoms number in each PFCA molecule,  $C$  is the concentration in the solution ( $\text{mmol.L}^{-1}$ ),  $t$  is the time (h),  $k$  the observed degradation rate constant ( $\text{h}^{-1}$ ) of each PFCA. Concentration data shown in Figure 3.24a ( $0.1 \text{ g.L}^{-1}$   $\text{TiO}_2\text{-rGO}$ ) were used for the estimation of kinetic parameters. The obtained values of the apparent kinetic constants can be ordered as  $k_{\text{PFPeA}} > k_{\text{PFHxA}} > k_{\text{PFHpA}} > k_{\text{PFOA}}$ , with values of 2.14, 0.54, 0.27 and  $0.163 \text{ h}^{-1}$ , respectively. These results point to a clear influence of the length of the perfluoroalkyl chain on the degradation rate. Similarly to our process, Qian et al. [87] reported that the rate constant of PFCAs UV-persulfate decomposition distinctly increased when the carbon-chain of the PFCAs was shorter.

Eq. 3.8 and the reported  $k$  values were used to simulate the concentration of PFCAs, as depicted by the solid lines included in Figure 3.24a. Similarly, simulated PFCAs concentrations were employed to calculate TOC evolution, which is also shown as solid line in Figure 3.24c. The good agreement between measured and simulated TOC supports the validity of the kinetic constants obtained from the fitting of the experimental results.

### 3.3. Homogeneous photocatalysis

Homogenous photocatalytic strategies present several advantages, in terms of avoiding catalyst recovery and overcoming the diffusion limitations. This section aims at investigating the performance of different

photochemical treatments to remediate a complex mixture of PFASs contained in Aqueous Film-Forming Foam (AFFF) formulation. The large volume of AFFF used for decades for firefighting has resulted in a high number of AFFF-impacted sites that need to be assessed and remediated [88,89]. As the efficacy of reduction and oxidation processes seems to be affected by the molecular structure of PFASs, individual and sequential UV reductive/oxidative systems were applied to gain insights into the effect of different conditions on the removal trends of each group of PFASs.

The AFFF present a PFAS profile defined by perfluorocarboxylates, perfluorosulfonates, fluorotelomer carboxylates and fluorotelomer sulfonates. A 1-to- $10^6$  dilution of the AFFF formulation supplied by CH2M (see section 2.4.1 of Chapter 2) was prepared as the target contaminated stream, mimicking PFASs concentration found in real AFFF-impacted groundwater. PFOS was the most abundant compound in the model AFFF-impacted water ( $\sim 4 \mu\text{g}\cdot\text{L}^{-1}$ ). The oxidative treatment consisted of UV irradiation of sodium persulfate solution to generate sulfate radicals ( $\text{SO}_4^{\cdot-}$ ,  $E=+2.5\text{-}3.1 \text{ V}$ ). The reductive approach was accomplished by UV irradiation of sulfite to promote the generation of hydrated electrons ( $e_{\text{aq}}^-$ ,  $E=-2.9 \text{ V}$ ). The light source consisted of a low-pressure mercury lamp for every treatment.

### **3.3.1. Direct photolysis**

Prior to AFFF experiments, the effect of UV irradiation on AFFF degradation (in the absence of any sensitizer) was also studied in a sequence formed by a first stage in acidic matrix (Figure 3.27, red colored background) and the second alkaline stage (Figure 3.27, blue colored

background). The value of the pH remained nearly constant during the treatments.

As it can be observed in Figure 3.27a, the content of PFCAs highly increased during the first 15 h of experiment, particularly PFNA, PFOA and PFHxA. Possible direct photolysis of fluorotelomers or unknown precursors promoted the generation of PFCAs [31,43,90,91]. However, after 34 h of UV irradiation, the concentrations of longer-chain PFCAs (PFNA and PFOA) decreased likely due to their moderate photolysis [61,62,92]. PFOA molecule absorbs photons from deep UV-region to 220 nm, and presents weak absorption in the 220–270 nm range of light wavelengths [60]. Qu et al. [59] also observed that the C-C bond strength between carboxylic carbon and the adjacent carbon increases with the shortened carbon chains of PFCAs, revealing that photolysis rate gradually increases with the alkyl chain length. Additionally, other components in AFFF solution possibly absorb UV light (254 nm) which can generate small concentrations of reactive species.

In contrast, PFSAs seemed to be relatively inert to direct photolysis (Figure 3.27b). Only a slow degradation of PFOS ( $14 \pm 10\%$ ) could be observed after 34 h of UV irradiation and acidic conditions. Direct photolysis of PFOS has been previously investigated using a low pressure mercury lamp by Yamamoto et al. [93], who reported that PFOS was slowly photodecomposed by 8 and 68% after 1 and 10 days, respectively. Moreover, this result can be related to the elimination of branched PFOS isomers in the sample, which are more susceptible to degradation due to the presence of one or two  $-\text{CF}_3$  groups branching from the perfluorinated alkyl chain [94,95]. The AFFF sample used in the present work typically contains a ratio of  $\sim 70/30$  of linear/branched PFOS. The concentrations of

FTs were depicted in Figure 3.27c. Overall, the content of FTs increased dramatically during the first 15 h of treatment, particularly 6:2 FTCA. After 34 h of irradiation, 6:2 FTCA achieved its maximum concentration of 26,000 ng.L<sup>-1</sup>, whereas the concentrations of 6:2 FTSA, 8:2 FTSA and 6:2 FTUCA were photodegraded by 67, 60 and 41%, respectively. It can be suggested that 6:2 FTCA was the main PFAS component in the sample. Therefore, AFFF mixture contains high content of unknown precursors which may firstly form fluorotelomers, and subsequently, PFNA, PFOA and PFHxA under photolytic conditions [91,96,97]. However, this last assumption will be discussed in the section 3.3.4.

Before the second stage of this control sequence, the experimental conditions of the AFFF sample were adjusted to alkaline conditions (see Table 2.7 of Chapter 2), to mimic conditions used for UV-SO<sub>3</sub><sup>2-</sup>. Then, during this second UV-only treatment (Figure 3.27, 34-58 h), no further photodecomposition of the different groups of PFASs was observed. Only minor eliminations of PFNA, PFOA and PFOS during the first 10 h of treatment (34-44 h in the overall experimental cycle) could be detected. Longer-chain PFCAs may be more sensitive to UV irradiation than shorter-chain PFCAs [59]. Nevertheless, the bicarbonate presence in the alkaline matrix may have interfered with PFASs photodegradation, as it has been observed by Giri et al. [98].

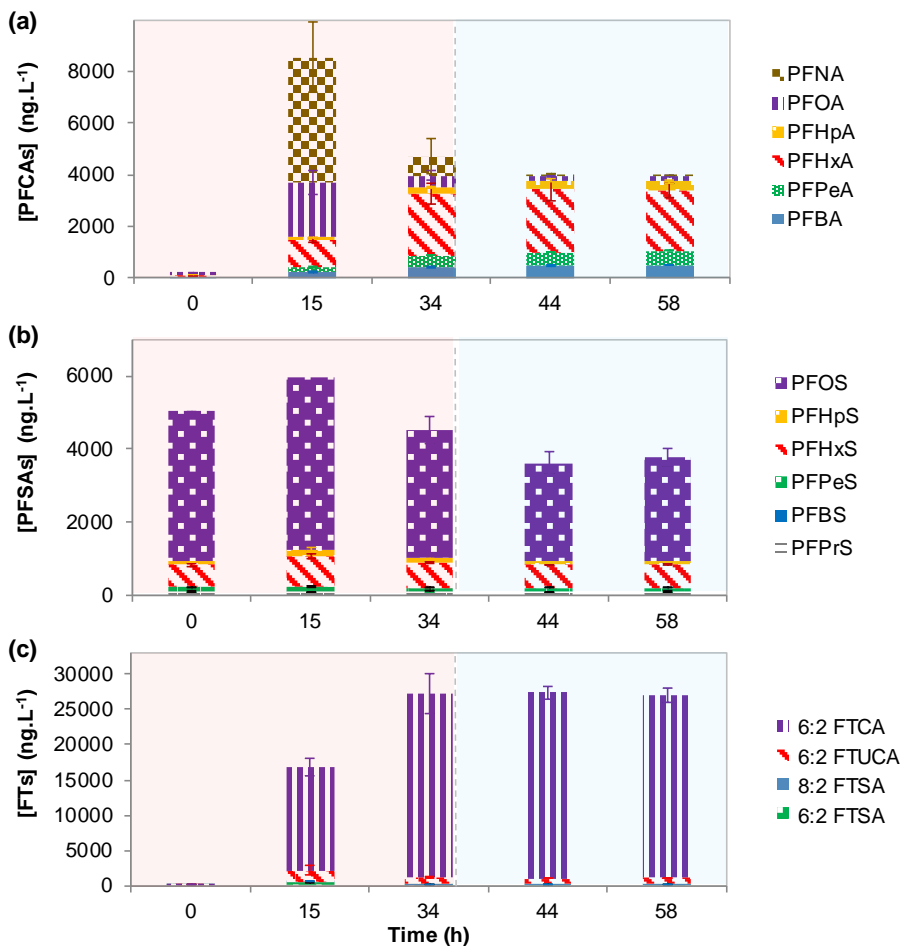


**Figure 3.27.** Concentration of (a) PFCAs, (b) PFSAs and (c) FTs during the photolytic treatment in absence of sensitizers. The first stage (0-34 h) developed under acidic matrix and air is shown in red colored background, whereas the second stage (34-58 h) in alkaline matrix and N<sub>2</sub> is shown in blue colored background. 1-to-10<sup>6</sup> dilution of AFFF. Error bars represent standard deviation derived from duplicated experiments.

### 3.3.2. Individual photochemical treatment

In this section, the progress of PFASs concentration after the application of each individual treatment (UV- Persulfate and UV- Sulfite) will be explained. Each individual UV system correspond to the first stage of the sequence of treatments proposed. However, the results of PFASs concentrations of the second stage in each sequence will be reported in the next section.

#### UV – Persulfate

The AFFF degradation by UV activated-persulfate is depicted in Figure 3.28 (0-34 h, red colored background). Figure 3.28a presents the monitoring of persulfate concentration with time. The results showed the concentration before and after the persulfate spikes into the reacting media. The rate of persulfate decomposition by UV light became gradually slower during the test (Figure 3.28a). Some species formed during the treatment of AFFF impacted water may hinder the photoreaction between persulfate and UV light. As a result, the experiments were carried out during 34 h, to completely eliminate the residual persulfate at the end of the treatment.

Persulfate salts dissociate in water to persulfate anion ( $S_2O_8^{2-}$ ) which can be activated photo-chemically or thermally to form two free sulfate radicals ( $SO_4^{\bullet-}$ , standard reduction potential = 2.5-3.1 V [99]) with quantum efficiency of unity (Eq. 3.9) [100].



$SO_4^{\bullet-}$  is an oxidizing radical that reacts by direct one-electron transfer to form sulfate ion. Sulfate radicals may react with water to form bisulfate

and hydroxyl radicals (Eq. 3.10). Moreover, bisulfate can release protons to the solution due to its low  $pK_a$  (Eq. 3.11) [101]. This is the main mechanism that caused the pH drop from 3 to 1.4 at the end of persulfate experiment. The  $H^+$  released from the decomposition of some PFASs was considered negligible because of their lower concentration compared to persulfate. Therefore, under acidic conditions,  $SO_4^{\bullet-}$  is the predominant oxidizing species for PFASs degradation reactions during the persulfate process [87,102].



Figure 3.28b shows the concentrations of PFCAs during the UV-persulfate process. PFCAs progressively increased during the first 10 h of irradiation. Particularly, the concentrations of shorter-chain PFCAs (PFPeA and PFBA) increased in  $1,000 \text{ ng}\cdot\text{L}^{-1}$  during this period, a significantly higher rate than the results obtained in direct photolysis. These results may indicate that longer PFCAs were simultaneously formed and decomposed step-by-step by  $SO_4^{\bullet-}$  radicals into shorter-chain PFCAs, as it has been previously reported [33,87,102,103]. After that, PFCAs concentrations partially decreased after 34 h of irradiation time, more noticeable for longer chain PFCAs by the role of sulfate radicals (see Table 3.2).

In the case of PFASs (Figure 3.28c), a high 79% PFOS removal ratio was obtained after 34 h of treatment. Even though a possible PFOS sorption to the reactor walls or other physical phenomenon related to AFFF components can take place [104], the progressive decay with time elucidated its degradation under the applied experimental conditions. This finding revealed a higher removal of PFOS by UV-activated persulfate

than heat-activated persulfate previously reported [33,104]. It may be related to the high energy introduced by UV photons into the molecular entity that could promote electronically excited states of molecules, giving products probably different from the products of chemical/thermal reactions [105]. Alternatively, intermediates between persulfate or sulfate radicals and other components of AFFF may promote formation of unidentified PFOS-reactive species. Moreover, concentrations of PFHpS, PFHxS and PFPeS also decreased by 43, 28 and 34%, respectively. On the contrary, shorter-chain PFSAs exhibited poorer reactivity during the oxidative treatment.

The progresses of FT carboxylates and FT sulfonates are shown in Figure 3.28d. 6:2 FTCA notably increased during the first 10 h of treatment (1,800 ng.L<sup>-1</sup>), and then, its concentration only slightly decreased after 34 h. However, these levels of 6:2 FTCA were lower than those obtained by photolysis. This result points out that 6:2 FTCA was formed and simultaneously degraded by the strong reactive capacity of SO<sub>4</sub><sup>•-</sup> radicals with this compound. Additionally, n:2 FTSA and 6:2 FTUCA were completely decomposed, likely to form PFCAs by UV-activated persulfate [33].

After 34 h of UV activated-persulfate treatment, the total concentration of PFASs (listed in Table 3.2) decreased by 17%. Even though SO<sub>4</sub><sup>•-</sup> radicals were strong oxidizing species for PFASs degradation, the final concentration was still high, likely due to the formation of PFCAs and FTs as degradation products of PFAS precursors in the AFFF sample.

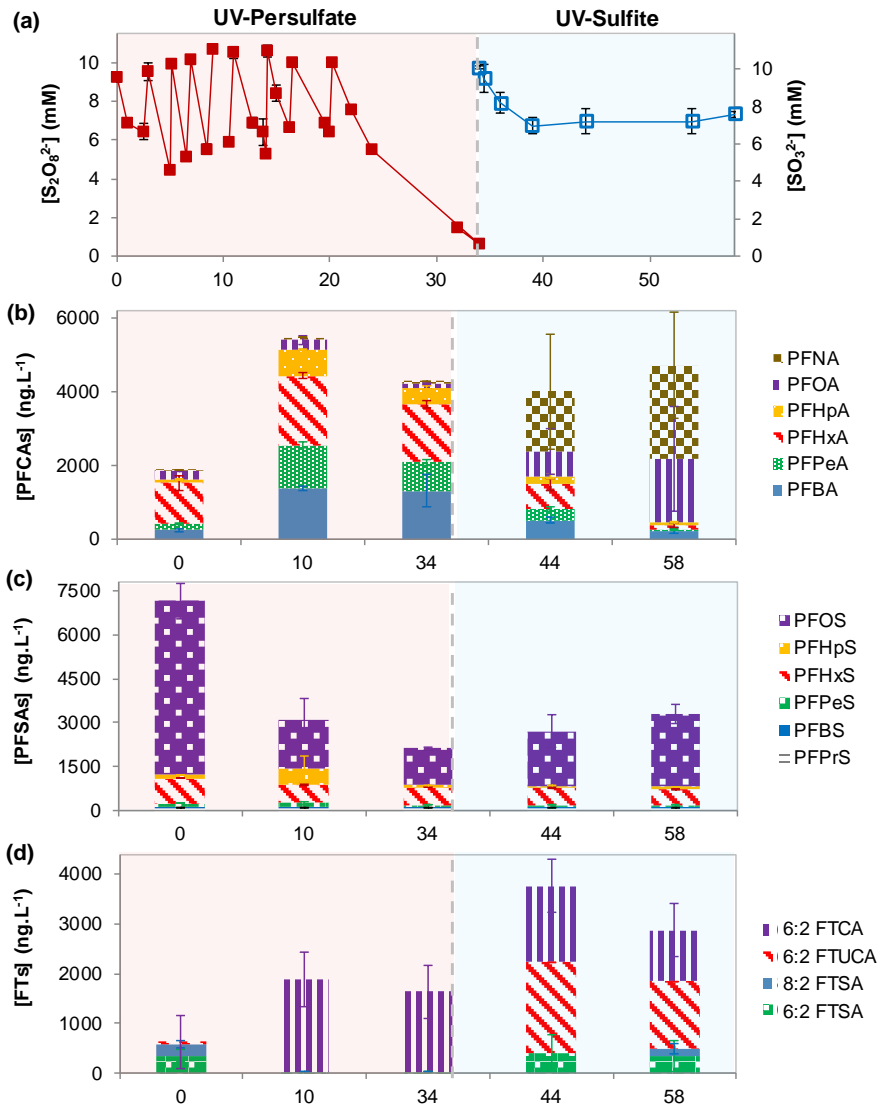


**Figure 3.28.** Concentration of (a) sensitizers persulfate and sulfite, (b) PFCAs, (c) PFASs, and (d) FTs during the sequence 2, formed by the first stage of UV- $S_2O_8^{2-}$  (0-34 h, red background) and the second treatment of UV- $SO_3^{2-}$  (34-58 h, blue background). 1-to- $10^6$  dilution of AFFF. Error bars represent standard deviation derived from duplicated experiments.

Moreover, it is important to note that the high presence of unknown fluorinated precursors in AFFF were highlighted previously, when the total fluorine content in the detected PFASs in the AFFF solution only corresponded to the 30% of the total fluorine content of AFFF obtained by  $^{19}\text{F}$ -NMR.

**Table 3.2.** Initial concentration ( $C_{\text{initial}}$ ) and the variation of each PFAS concentration ( $\Delta C = C_{\text{final}} - C_{\text{initial}}$ ) after individual UV- $\text{S}_2\text{O}_8^{2-}$  treatment and sequence of UV- $\text{S}_2\text{O}_8^{2-}$  and UV- $\text{SO}_3^{2-}$  systems.

	$C_{\text{initial}}$ (ng.L $^{-1}$ )	$\Delta C$ (ng.L $^{-1}$ ) UV- $\text{S}_2\text{O}_8^{2-}$	$\Delta C$ (ng.L $^{-1}$ ) UV- $\text{S}_2\text{O}_8^{2-}$ + UV- $\text{SO}_3^{2-}$
<b>PFBA</b>	244 ± 44	1068 ± 406	-2 ± 39
<b>PFPeA</b>	178 ± 38	601 ± 40	-151 ± 21
<b>PFHxA</b>	1103 ± 196	462 ± 88	-984 ± 133
<b>PFHpA</b>	100 ± 6	359 ± 41	-30 ± 6
<b>PFOA</b>	220 ± 15	-112 ± 8	1512 ± 1406
<b>PFNA</b>	39 ± 2	24 ± 1	2482 ± 1429
<b>PFPrS</b>	100 ± 1	-3 ± 0*	-5 ± 4
<b>PFBS</b>	19 ± 0	0 ± 0*	2 ± 0
<b>PFPeS</b>	128 ± 3	-43 ± 2	-50 ± 3
<b>PFHxS</b>	844 ± 3	-239 ± 5	-307 ± 13
<b>PFHpS</b>	131 ± 3	-56 ± 1	-41 ± 2
<b>PFOS</b>	5929 ± 587	-4686 ± 551	-3436 ± 259
<b>6:2 FTCA</b>		1611 ± 154	1028 ± 6
<b>6:2 FTSA</b>	357 ± 119	-333 ± 117	2 ± 192
<b>8:2 FTSA</b>	230 ± 76	-230 ± 76	-94 ± 32
<b>6:2 FTUCA</b>	50 ± 0	-50 ± 0	1303 ± 0
<b>ΣPFASs</b>	9672 ± 1094	-1628 ± 197	1228 ± 2720

\*The drop of PFAS concentration associated with the effect of adding extra volume by  $\text{Na}_2\text{S}_2\text{O}_8$  spikes (10mM) into the reacting media, which represented a removal ratio ~6 %.

### UV - Sulfite

The reductive method was developed by UV photolysis of sulfite which involves hydrated electrons ( $e_{aq}^-$ ) generation (Eq. 3.12), in an alkaline matrix and  $N_2$  atmosphere, in order to avoid the high reactivity of  $e_{aq}^-$  with  $H^+$  and oxygen.



Sulfite decay with UV irradiation time was depicted in Figure 3.29a (0-24 h, blue colored background). The sulfite concentration remained at ~4mM after 24 h, without any further addition of sensitizer. Increasing the initial sulfite concentration could hinder AFFF degradation due to the formation of  $SO_3^{\bullet-}$  which could react with other  $SO_3^{\bullet-}$  radicals to give  $S_2O_6^{2-}$ , an  $e_{aq}^-$  quencher (Eq. 3.13 and 3.14) [106–108].



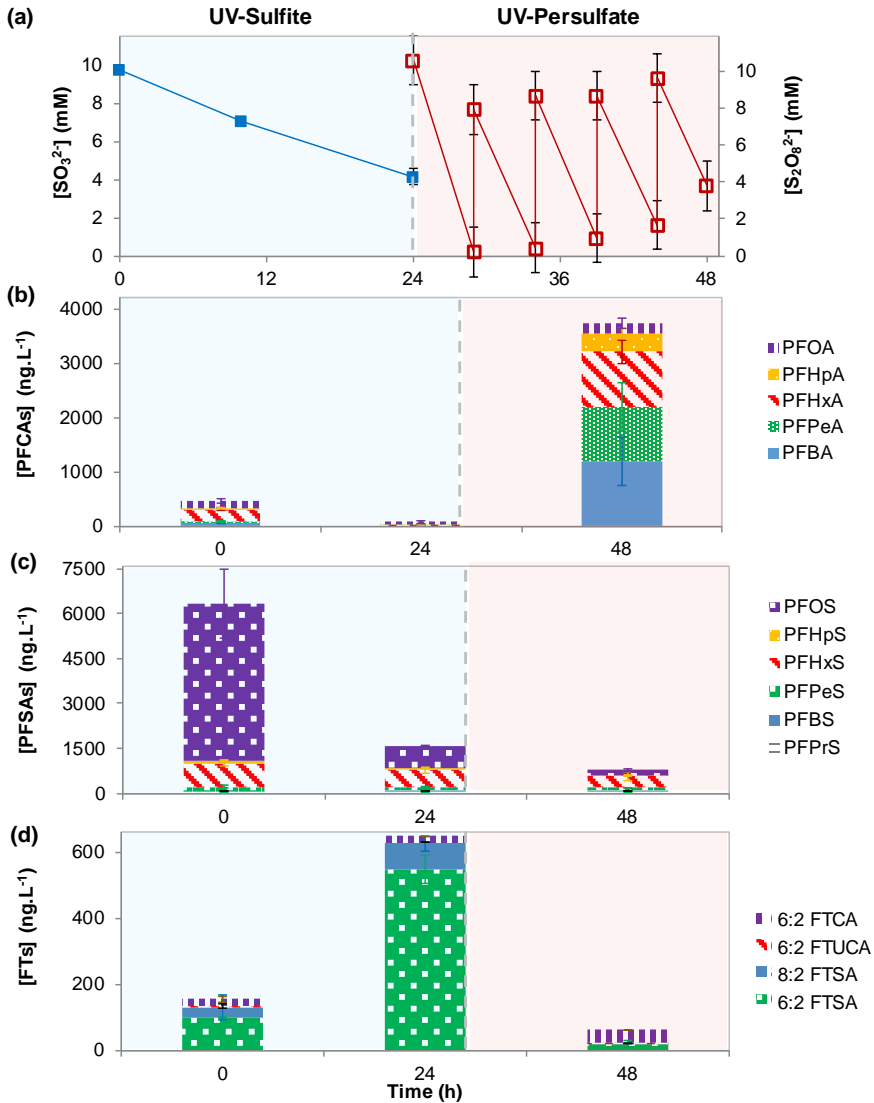
The solution pH increased from 9.6 to 10.3 at the end of the experiment without pH adjustment. The pH increase could be assigned to the minor reaction of  $e_{aq}^-$  with water, which produce  $OH^-$  and  $H^+$ , since this later compound can react with other components of AFFF solution (Eq. 3.15) [109].



Figure 3.29 (0-24 h, blue colored background) shows the concentrations of PFCAs (b), PFSA (c) and FTs (d) during the reductive treatment. In contrast to the oxidative technique,  $e_{aq}^-$ -mediated experiments efficiently

allowed higher removal rates of all PFCAs initially contained in the AFFF solution (Figure 3.29b). After 24h, PFHxA and PFPeA almost disappeared, whereas PFOA, PFHpA and PFBA exhibited 69, 45 and 75% of degradation, respectively. It must be noted that the overall initial concentration of PFCAs was notably lower than in the initial sample of experiments shown in Figure 3.29, an indicative of the uncertainty of the composition of the AFFF formulation. In addition, PFCAs concentration did not increase during the treatment time of UV-sulfite system. Although unknown PFASs precursors were degraded into PFCAs over the treatment, the degradation rates of PFCAs were higher than the formation kinetics from the precursors transformation. This behavior contrast with the results obtained in the UV activated persulfate treatment, pointing to differences in the degradation mechanisms by the oxidative and reductive treatments.

The concentrations of PFASs in the treatment are shown in Figure 3.29c. As it is observed, this reductive test achieved the highest elimination of PFOS (86%) from the AFFF mixture after 24 h. PFHpS, PFHxS and PFPeS, decreased by 42, 26 and 25%, respectively, whereas shorter-chain PFASs remained inert to  $e_{aq}^-$  species formed during the treatment. Figure 3.29d shows that the concentration of FT carboxylates (6:2 FTCA and 6:2 FTUCA) remained nearly constant, however, the levels of FT sulfonates increased considerably after 24h of irradiation, likely due to the reduction of unknown sulfonamide-based precursors. In addition, control reductive experiments revealed that individual PFOA and PFOS solutions exhibited similar degradation rates compared to those obtained over AFFF treatment. Therefore, although unknown precursors were degraded over the UV-sulfite treatment, the degradation rates of PFCAs and PFASs by hydrated electrons were notably higher than the formation kinetics from the precursors or fluorotelomers transformation.



**Figure 3.29.** Concentration of (a) sensitizers sulfite and persulfate, (b) PFCAs, (c) PFSAAs, and (d) FTs during the sequence 3, formed by the first stage of UV-SO<sub>3</sub><sup>2-</sup> (0-24 h, blue background) and the second treatment of UV-S<sub>2</sub>O<sub>8</sub><sup>2-</sup> (24-48 h, red background). 1-to-10<sup>6</sup> dilution of AFFF. Error bars represent standard deviation derived from duplicated experiments.

According to the results shown above, it could be highlighted that hydrated electrons reacted more rapidly with perfluorinated compounds (PFCAs and PFASs) than with the fluorotelomers or unknown precursors that contained unfluorinated carbons in their molecules. After 24h of the reductive process, the  $\Sigma$ PFAS concentrations in the AFFF mixture was decreased to 2,281 ng.L<sup>-1</sup> (Table 3.3), which represented a significantly improved overall removal compared to UV-S<sub>2</sub>O<sub>8</sub><sup>2-</sup> treatment.

**Table 3.3.** Initial concentration (C<sub>initial</sub>) and the variation of each PFAS concentration ( $\Delta C = C_{\text{final}} - C_{\text{initial}}$ ) after individual UV-SO<sub>3</sub><sup>2-</sup> treatment and sequence of UV-SO<sub>3</sub><sup>2-</sup> and UV-S<sub>2</sub>O<sub>8</sub><sup>2-</sup> systems.

	<i>C<sub>initial</sub></i> (ng.L <sup>-1</sup> )	$\Delta C$ (ng.L <sup>-1</sup> ) UV-SO <sub>3</sub> <sup>2-</sup>	$\Delta C$ (ng.L <sup>-1</sup> ) UV-SO <sub>3</sub> <sup>2-</sup> + UV-S <sub>2</sub> O <sub>8</sub> <sup>2-</sup>
<b>PFBA</b>	58 ± 19	-43 ± 6	1137 ± 426
<b>PFPeA</b>	31 ± 14	-29 ± 14	959 ± 435
<b>PFHxA</b>	217 ± 27	-213 ± 27	818 ± 185
<b>PFHpA</b>	30 ± 10	-13 ± 4	299 ± 81
<b>PFOA</b>	119 ± 45	-82 ± 15	77 ± 50
<b>PFNA</b>			
<b>PFPrS</b>	63 ± 27	20 ± 2	8 ± 6*
<b>PFBS</b>	13 ± 5	7 ± 0	9 ± 0*
<b>PFPeS</b>	149 ± 39	-38 ± 26	-54 ± 27
<b>PFHxS</b>	777 ± 95	-200 ± 2	-388 ± 41
<b>PFHpS</b>	84 ± 15	-35 ± 12	-54 ± 6
<b>PFOS</b>	5269 ± 1151	-4547 ± 1126	-5096 ± 1092
<b>6:2 FTCA</b>	22 ± 7	-3 ± 7	19 ± 7
<b>6:2 FTSA</b>	99 ± 4	447 ± 39	-80 ± 8
<b>8:2 FTSA</b>	31 ± 37	48 ± 16	-30 ± 37
<b>6:2 FTUCA</b>	3 ± 0	1 ± 0	-1 ± 0
<b><math>\Sigma</math>PFASs</b>	6964 ± 1497	-4683 ± 1182	-2379 ± 61

\*The drop of PFAS concentration associated with the effect of adding extra volume by Na<sub>2</sub>S<sub>2</sub>O<sub>8</sub> spikes (10mM) into the reacting media, which represented a removal ratio ~6 %.

### 3.3.3. Sequential oxidative/reductive treatments of AFFF

#### Sequence 1: UV- Persulfate followed by UV- Sulfite

The AFFF sample treated firstly by UV-activated persulfate was adjusted to the experimental conditions needed for UV-sulfite system (see Table 2.7 of Chapter 2). The sulfite concentration represented in Figure 3.28a (34-58 h, blue colored background) stayed nearly constant after 4 h of the treatment, which could involve lower formation of  $e_{aq}^-$  during that period.

Figure 3.28b shows that the high content of C<sub>4</sub>-C<sub>7</sub> PFCAs after the first UV-S<sub>2</sub>O<sub>8</sub><sup>2-</sup> oxidative stage were progressively removed by  $e_{aq}^-$ , and decreased by 80-90% at the end of this second treatment. However, PFOA and PFNA were significantly formed over the reductive treatment, up to levels of 1,700-2,500 ng.L<sup>-1</sup>. It is thought that 8:2 precursors may be inert to  $e_{aq}^-$  during the first sulfite treatment, whereas these contaminants can be degraded by oxidizing species producing PFOA and PFNA in this second stage.

Figure 3.28c shows the evolution of PFSAs with the irradiation time. PFOS concentration slightly increased during the reductive treatment. However, an overall 60% PFOS removal resulted from this sequence of treatments. In contrast, shorter-chain PFSAs did not exhibit high interaction with  $e_{aq}^-$  species formed in this second treatment. Figure 3.28d displays the change of FTs concentrations with time. 6:2 FTCA and 6:2 FTUCA initially increased during the first part of the treatment, and then, slightly decreased after 24 h of treatment. n:2 FTSA compounds seemed to be formed and degraded simultaneously during the treatment. These results pointed out the presence of unknown 8:2 sulfonamide-based or fluorotelomer precursors in the second stage, producing mainly PFOS, PFOA and PFNA

during the reductive treatment [110,111]. Moreover, previous experiments in the research group revealed the formation of PFOA, PFOS and perfluorooctane sulfonamide as degradation product of the reductive treatment of perfluorooctane sulfonamidoacetic acid (data not shown). These possible mechanisms are reported in Figure 3.30.

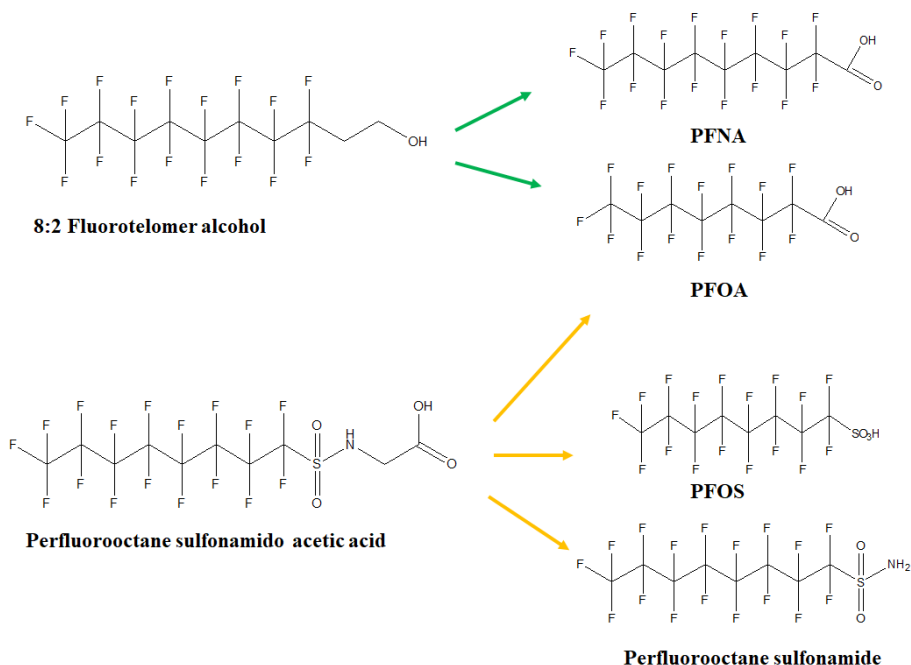


**Figure 3.30.** Degradation pathways of possible precursors of PFOS, PFOA, PFNA.

Additionally, the lower formation of n:2 FTSA in this second stage than in the UV-sulfite treatment (Figure 3.29d), revealed the partial removal of 6:2 unknown precursors at the first persulfate treatment.

The results of this reductive treatment differed with the individual UV-sulfite treatment applied as the first treatment in the sequence (Fig 3.29 0-24 h), particularly for long-chain PFCAs and PFSA trends. This response

may be attributed to the limited formation of  $e_{aq}^-$  after 4-5 h of this treatment, since the sulfite concentration stayed constant. Moreover, it is important to note that the AFFF sample contained high sulfate ion concentration ( $\sim 180 \text{ mmol.L}^{-1}$ ) due to the persulfate spikes over the first stage, which may interfere in the reactions scenario in this second reductive treatment.

Even though the total concentration of PFASs slightly decreased during the first UV- $\text{S}_2\text{O}_8^{2-}$  stage (Table 3.2), the transformation of unknown components into the identified PFASs which were also degraded resulted in a similar total content of PFAS at the end of this sequence of oxidative and reductive treatments.

#### Sequence 2: UV- Sulfite followed by UV- Persulfate

The background of the AFFF sample, treated initially by the reductive UV-sulfite treatment, was modified according to the needs of the UV- $\text{S}_2\text{O}_8^{2-}$  process (see Table 2.7 of the Chapter 2). It is noteworthy that residual sulfite was totally quenched by an equimolar amount of  $\text{H}_2\text{O}_2$  without UV irradiation in 5 min (data not shown) [112], to avoid any interference in the generation of  $\text{SO}_4^{\cdot-}$ , since  $e_{aq}^-$  can also rapidly react with  $\text{S}_2\text{O}_8^{2-}$ . The monitoring of persulfate concentration during the treatment is depicted in Figure 3.29a (24-48 h, red colored background).

Figure 3.29b (24-48 h) shows that the total concentrations of PFCAs highly increased, particularly  $\text{C}_4\text{-C}_6$  PFCAs, as it was observed in the individual UV- $\text{S}_2\text{O}_8^{2-}$  treatment. Regarding the progress of the PFASs with time (Figure 3.29c), the concentrations of longer-chain PFASs progressively decreased during this second treatment, in agreement with the results of UV- $\text{S}_2\text{O}_8^{2-}$  treatment that were shown in Figure 3.28b. Additionally, this

sequence of UV-sulfite plus UV-persulfate treatments, achieved the highest total removal ratios of 96, 65, 50 and 36 %, for PFOS, PFHpS, PFHxS and PFPeS, respectively, after 48 h of irradiation. The change of FTs concentrations with time is displayed in Figure 3.29d. Whereas 6:2 FTCA partially increased during the treatment,  $\text{SO}_4^{\cdot-}$  radicals can efficiently remove 6:2 FTSA, 8:2 FTSA and 6:2 FTUCA from the AFFF solution, similarly to the effect of the UV-  $\text{S}_2\text{O}_8^{2-}$  displayed in Figure 3.28d.

In summary, during the first reductive stage, the  $\Sigma$ PFASs content decreased to 2,281  $\text{ng}\cdot\text{L}^{-1}$  after 24h of irradiation time. However, this total concentration of PFASs increased again to 4585  $\text{ng}\cdot\text{L}^{-1}$  after the second persulfate stage of this sequence (Table 3.3), due to the degradation of unidentified precursors by sulfate radicals.

### **3.3.4. Overview of AFFF composition and treatments**

Since AFFF compositions are proprietary, some possible PFASs precursors in the AFFF formulation used in the present work were proposed, based on the trends of PFASs during the treatments and data from literature.

#### Fluorotelomers

Firstly, the initial content of the fluorotelomer carboxylates and fluorotelomer sulfonates on the target screening list studied in the sample was minor among the total PFASs content. However, the important formation of 6:2 fluorotelomer carboxylate during the oxidative treatment, revealed that unknown fluorotelomer-based precursors could be considered the most abundant component in the AFFF sample. The formation of FT carboxylates has been previously related to the photolytic

degradation of fluorotelomer alcohols which can exist as both primary contaminants and intermediates. In this way,  $C_n$  fluorotelomer alcohols were degraded into  $C_n$  fluorotelomer carboxylates and PFCAs under UV oxidations [113–116]. Moreover, 6:2 FTCA, FTUCA and 5:3 FTCA were also detected as semi-stable intermediates by abiotic and biotic 6:2 FTOH degradation [117], which can also explain the generation of FTUCA as a by-product in the present work. On the other hand, the formation of fluorotelomer sulfonates, particularly 6:2 FTSA, can be associated with the presence of fluorotelomer sulfonamide-based compounds in AFFF, such as fluorotelomer sulfonamide alkylbetaine (FTAB). FTAB, fluorotelomer thioether amido sulfonate (FtTAoS) and fluorotelomer sulfoxide amido sulfonate (FTSAS-sulfoxide) have been recently identified as alternatives to replace PFOS in AFFF formulations [104,118–120]. These PFASs precursors and fluorotelomers are more susceptible to oxidative degradation since they contain unfluorinated carbons (i.e.,  $-\text{CH}_2-\text{CF}_2-$  into  $-\text{CH}=\text{CF}-$ ) or individual chemical moieties within their molecular structures [2]. D'Agostino et al. [31] reported the biodegradation 6:2 FTAB produces FTOH, FTCA, FTUCA, 5:3 FTCA and PFHxA and PFPeA. Direct photolysis of 6:2 FTAB gave rise to the generation of 6:2 fluorotelomer sulfonamide (6:2 FTSA<sub>m</sub>), 6:2 fluorotelomer sulfonamide alkylamine (6:2 FTAA), 6:2 FTOH and 6:2 FTUCA and PFHpA, PFHxA and PFPeA, whereas the BDD electrochemical oxidation of industrial effluents that contain 6:2 FTAB produced 6:2 FTSA and PFCAs ( $C_7$ - $C_4$ ) [97,121]. Bruton et al. [104] observed the transformation of 6:2 FtTAoS in mainly PFHxA, and also PFHpA, PFPeA and PFBA, by heat activated-persulfate. Overall, it has been reported that  $C_n$  sulfonamide-containing compounds can be transformed to equimolar quantities of the corresponding  $C_n$  fluorotelomers or PFCAs [97,104], whereas  $C_n$

fluorotelomers are transformed to a mixture of PFCAs of varying carbon chain length [33–35,104,116]. Furthermore, based on the literature and the fluorotelomer trends in the different treatments herein shown, it could be pointed out that high content of an unknown 6:2 sulfonamide-based precursor (such as 6:2 FTAB [122]) in the AFFF formulation could give rise to 6:2 FTCA in the oxidative treatment, whereas 6:2 FTSA and 6:2 FTUCA can be formed as by-product during the reductive treatment. This idea is supported by the low generation of 6:2 FTCA during the UV-persulfate treatment used as the second stage (Fig. 3.29d), when its precursors seems to be eliminated in the first reductive stage. However, future research will be focus on the identification of these kind of sulfonamide precursors in the initial AFFF sample.

#### Perfluoroalkyl sulfonates

Within this group of PFASs, PFOS was initially the most abundant component in the AFFF mixture used in this work. On the one hand, PFOS initially increased during the second reductive stage in sequence 1, and then decreased by means of  $e_{aq}^-$  species. This indicates that AFFF also contains perfluoroalkyl sulfonamide-based precursors, such as perfluorooctane sulfonamide (FOSA) which has been found in AFFF-impacted groundwater [123,124]. This type of precursors can be also transformed into PFCAs (PFOA in this case) and the corresponding perfluoroalkyl sulfonamide as well [91].

On the other hand, based on the results, it is concluded that both sulfate radicals and hydrated electrons could decompose long-chain PFASs in the UV-persulfate and UV-sulfite treatments. The oxidative degradation pathways of PFOS initiated by  $SO_4^{\cdot-}$  radicals are not clear at present.

However, it has been reported that the first oxidative attack of PFOS may occur at the C-S bond, to form  $C_8F_{17}\cdot$  [53,93,125,126]. Yamamoto et al. [93] demonstrated that PFOS can undergo two major degradation pathways, via  $C_8HF_{17}$  and  $C_8F_{17}OH$ , under UV irradiation and alkaline 2-propanol. As a result, short-chain fluorinated compounds such as  $C_7HF_{15}$  and  $C_7F_{15}OH$  by stepwise removal of  $CF_2$  were produced, to result in the formation of PFCAs. On the other hand, the reductive route of PFOS by  $e_{aq}^-$  species could initially start with the formation of  $PFOS^{2-}$  ( $C_nF_{2n+1}SO_3^{2-}$ ) which would further dissociate and produce different fragments [127,128].  $C_nF_{2n+1}^-$  was the most likely produced species which may be transformed to PFOA through defluorination and hydrolysis reactions.

#### Perfluoroalkyl carboxylates

The initial content of PFCAs ( $C_4$ - $C_9$ ) in the AFFF formulation was relatively low. Two different PFCAs trends were observed over the treatments: (i) formation and degradation of PFCAs in the oxidative system, and (ii) only degradation of PFCAs was obtained by UV-sulfite treatment.

The formation of PFCAs was the last step in the degradation of fluorotelomers or unknown sulfonamide- and fluorotelomer-based precursors in the UV-persulfate treatment. Houtz et al. [89] also observed the presence of perfluorohexane sulfonamide amine (PFHxSA<sub>m</sub>) and perfluorohexane sulfonamide amino carboxylate responsible for PFHxA production in 3M AFFF. Once PFCAs have been formed, the content of PFCAs subsequently decreased with the reaction with  $SO_4^{\cdot-}$  by the well-

known sequential chain-shortening mechanism forming shorter-chain PFCAs,  $F^-$  and  $CO_2$  [33,87,102,103].

On the other hand,  $e_{aq}^-$  generated during the UV-sulfite treatment were more reactive with fully fluorinated compounds (PFCAs and PFSAs) than with compounds that contained unfluorinated carbons. Qu et al. [129] and Song et al. [106] proposed reductive degradation routes in which PFOA could initially react with  $e_{aq}^-$  releasing fluorine to form  $C_7F_{14}HCOOH$  and  $C_7F_{13}H_2COOH$ . Afterward,  $C_6F_{13}^*$ ,  $^*COOH$  radicals and  $CH_2$  carbene were generated from  $C_7F_{13}-H_2COOH$  under irradiation. The reaction between  $C_6F_{13}^*$  and  $^*COOH$  radicals may occur to form shorter chain perfluoroalkyl carboxylate,  $C_6F_{13}COOH$ , which is further degraded in the same manner. Similarly,  $C_6F_{13}^*$  radical can undergo hydrolysis and HF loss to yield perfluoroalkyl carboxylates, which would be further decomposed by the same mechanism.

### **3.4. Assessment of the energy consumption**

Both electrochemical and photochemical treatments need of an energy supply, either as electricity power or photoirradiation, to activate the advanced oxidation/reduction processes. Then, the main operation cost of these technologies in lab-scale arises predominantly from the energy consumption. Therefore, this section is aimed at assessing the energy demands of the technologies that have been studied in the present research, with the purpose of analyzing their viability from the economic point of view.

The electrical energy per order ( $E_{EO}$ ) is a useful standard parameter that allows to compare the energy intake of diverse water treatment processes.

This concept was introduced by Bolton et al. [130] in a IUPAC technical report.  $E_{EO}$  ( $\text{kWh}\cdot\text{m}^{-3}\cdot\text{order}^{-1}$ ) represents the electrical energy necessary to degrade a contaminant with low initial concentration by one order of magnitude in a fixed volume of wastewater (Eq. 3.16).

$$E_{EO} = \frac{P_e \cdot t}{V \lg\left(\frac{C_0}{C_f}\right)} \quad (\text{Eq. 3.16})$$

where  $P_e$  is the electric power (kW),  $t$  represents the time (h),  $V$  symbolizes the reaction volume of PFASs contaminated water ( $\text{m}^3$ ),  $\lg$  denotes the decadic logarithm, and  $C_0$  and  $C_f$  are the initial and the final contaminant concentrations ( $\text{mg}\cdot\text{L}^{-1}$ ).

Since the initial PFASs concentrations and water matrixes were diverse over the work of this thesis, the estimation of  $E_{EO}$  was calculated as the electrical energy needed to degrade either PFOA from model solutions or the total content of PFASs in real wastewater samples. In addition, the TOC removal was also considered in this section as a global parameter related to the mineralization of the organic pollutants.

The removal rates of PFASs and TOC obtained in the experimental systems can be described by a first-order kinetic expression. Therefore, substituting the first-order kinetic constant into Eq. 3.16, Eq. 3.17 was obtained.

$$E_{EO} = \frac{P_e}{V \cdot k} \quad (\text{Eq. 3.17})$$

where  $P_e$  is the electric power (kW),  $V$  symbolizes the reaction volume of PFASs contaminated water ( $\text{m}^3$ ) and  $k$  denotes the first-order kinetic constant related to the contaminants removal rates ( $\text{h}^{-1}$ ).

The kinetic parameters of PFASs and TOC removals, following the first-order kinetic model, are listed in Tables 3.4 and 3.5.

**Table 3.4.** Kinetic data of PFASs degradation rates under electrochemical and photochemical systems studied.

Water treatment	Water source	Initial PFASs concentration	$k_{PFASs}$ ( $\text{h}^{-1}$ )	$R^2$
Electro-oxidation 1	Model solution	[PFOA] <sub>0</sub> =100 $\text{mg.L}^{-1}$	1.82	0.952
Electro-oxidation 2	WWTP influent	[PFASs] <sub>0</sub> =1.40 $\text{mg.L}^{-1}$	0.45	0.980
Electro-oxidation 3	WWTP effluent	[PFASs] <sub>0</sub> =1.65 $\text{mg.L}^{-1}$	0.58	0.993
Photocatalysis	Model solution	[PFOA] <sub>0</sub> =100 $\text{mg.L}^{-1}$	0.16	0.949

**Table 3.5.** Kinetic data of TOC degradation rates under electrochemical and photochemical systems studied.

Water treatment	Water source	Initial TOC concentration	$k_{TOC}$ ( $\text{h}^{-1}$ )	$R^2$
Electro-oxidation 1	Model solution	22 $\text{mg.L}^{-1}$	0.80	0.944
Electro-oxidation 2	WWTP influent	722 $\text{mg.L}^{-1}$	0.27	0.945
Electro-oxidation 3	WWTP effluent	99 $\text{mg.L}^{-1}$	0.37	0.949
Photocatalysis	Model solution	25 $\text{mg.L}^{-1}$	0.069	0.948

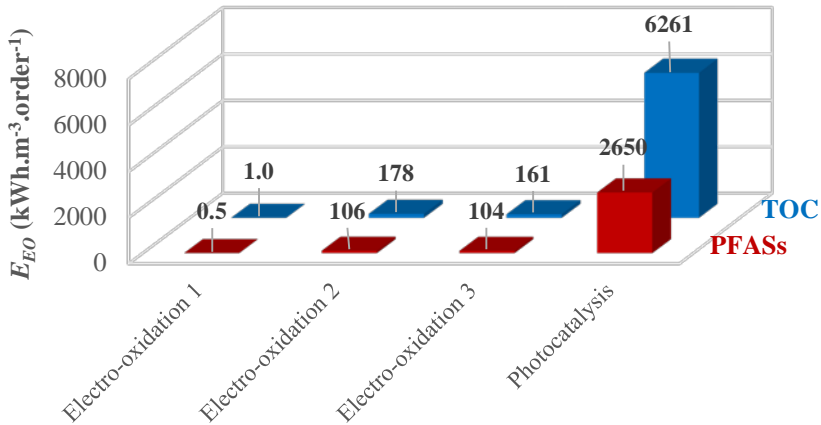


**Figure 3.31.**  $E_{EO}$  calculated for PFASs and TOC removals via electro-oxidation by BDD anode and photocatalysis using  $TiO_2$ -rGO.

The  $E_{EO}$  results obtained for the treatments studied in this thesis are shown in Figure 3.31. In the case of electro-oxidation technology using the microcrystalline BDD anode, the energy consumption was estimated for the three types of target waters used: PFOA model solution (electro-oxidation 1), WWTP influent (electro-oxidation 2) and effluent wastewaters (electro-oxidation 3). It can be observed that the initial concentration of the contaminants and the type of background water composition highly impacted on the values of the kinetic parameter, and consequently, on the energy requirements. Whereas PFOA in the model solution ( $100 \text{ mg.L}^{-1}$ ) was removed by 90% after 1.5 h at  $1 \text{ mA.cm}^{-2}$ , the concentration of  $\Sigma$ PFASs in industrial wastewaters ( $\sim 1.5 \text{ mg.L}^{-1}$ ) only decreased at adequate rates when a much higher current density of  $50 \text{ mA.cm}^{-2}$  was applied at longer treatment times. As a result, the  $E_{EO}$  required for PFASs removal in the industrial wastewater was  $\sim 100 \text{ kWh.m}^{-3}.\text{order}^{-1}$ , 200 times higher than for the PFOA solution prepared in the laboratory, which needed  $0.5 \text{ kWh.m}^{-3}.\text{order}^{-1}$  for the same degree of

treatment. It is important to note that the energy consumption was similar between the two types of industrial wastewaters, regardless their dissimilar background organic loads, that was significantly higher in the influent stream. Therefore, PFASs degradation kinetics were not strongly affected by the concentration of the other organic contaminants of the samples, at least in the range of TOC concentrations studied (99-722 mg.L<sup>-1</sup>).

The results of  $E_{EO}$  estimated for TOC degradation are also shown in Figure 3.31. In every water sample, and for the three electrochemical treatments, higher  $E_{EO}$  values for TOC removal compared to those obtained for PFASs degradation were observed, as a result of the slower TOC removal kinetics (Tables 3.4 and 3.5). The TOC content of the model solution was uniquely assigned to PFOA concentration, therefore, the slower TOC removal kinetics ( $k_{TOC} < k_{PFOA}$ ) was due to the formation of intermediate degradation PFOA products until its complete mineralization.

However, the TOC content of industrial wastewater samples corresponds to a variety of unknown organic compounds, and the contribution of PFASs in the samples is lower than 1.5% of the total TOC. Therefore, PFASs content was not expected to bring a strong influence on TOC removal rates. Overall, TOC removal rates and energy consumptions were very similar in both the influent and the effluent streams of the WWTP.

The photocatalytic treatment using TiO<sub>2</sub>-rGO catalyst led to an energy consumption of 2,650 kWh.m<sup>-3</sup>.order<sup>-1</sup> for PFOA degradation in the synthetic solution (Figure 3.31), drastically higher than the  $E_{EO}$  needed for the BDD anodic oxidation (electro-oxidation 1) of the same solution, 0.5 kWh.m<sup>-3</sup>. The medium-pressure mercury lamp (150W) that demands a high power supply and longer times in photocatalysis significantly

increased the energy consumption. Furthermore, as TOC removal presented slower kinetics than PFOA removal, the  $E_{EO}$  obtained for TOC degradation increased up to  $6,261 \text{ kWh}\cdot\text{m}^{-3}\cdot\text{order}^{-1}$ . Our results are in good agreement with previous data reported by Dominguez et al. [131], who estimated  $E_{EO}$  values around  $600 \text{ kWh}\cdot\text{m}^{-3}\cdot\text{order}^{-1}$ , for 90% degradation of sodium dodecylbenzenesulfonate (SDBS,  $C_0=50 \text{ mg}\cdot\text{L}^{-1}$ ) using  $\text{TiO}_2$  photocatalysis in the same photocatalytic reactor. The lower energy demand reported in [131] is associated to the faster degradation kinetics of SDBS, compared to PFOA photocatalytic removal by  $\text{TiO}_2$ -rGO obtained in the present research, as a result of the extreme recalcitrant behavior of PFOA.

On the other hand, the energy consumption of the UV oxidative/reductive treatments applied to degrade PFASs ( $\Sigma\text{PFAS}_0\sim 0.007 \text{ mg}\cdot\text{L}^{-1}$ ) in model AFFF-impacted groundwater was estimated for the sequence 2 consisting of using persulfate sensitizer in the oxidative step, followed by adding sulfite as sensitizer in the reduction step. Sequence 2 enabled 34% removal of the detected  $\Sigma\text{PFASs}$ , although the experimental data did not allow to obtain the kinetic parameters for PFASs removals. The sequence of treatments was carried out for 48 h of irradiation by a low-pressure mercury lamp (18 W), which implied an energy input of  $1,503 \text{ kWh}\cdot\text{m}^{-3}$ . The energy consumption was also elevated due to the long time needed for PFASs degradation.

These results point out that electrochemical oxidation by means of microcrystalline BDD anodes is the most promising technology for real wastewater treatment, achieving high rates of PFAS removal and lower energy consumptions than the photochemical strategies studied in this work.

### 3.5. References

- [1] A. Urtiaga, C. Fernández-González, S. Gómez-Lavín, I. Ortiz, *Chemosphere* **2015**, 129, 20.
- [2] A. Urtiaga, A. Soriano, J. Carrillo-Abad, *Chemosphere* **2018**, 201, 571.
- [3] Á. Soriano, D. Gorri, A. Urtiaga, *Water Res.* **2017**, 112, 147.
- [4] C. E. Schaefer, C. Andaya, A. Burant, C. W. Condee, A. Urtiaga, T. J. Strathmann, C. P. Higgins, *Chem. Eng. J.* **2017**, 317, 424.
- [5] M. Mascia, A. Vacca, S. Palmas, A. M. Polcaro, *J. Appl. Electrochem.* **2007**, 37, 71.
- [6] M. Panizza, G. Siné, I. Duo, L. Ouattara, C. Comninellis, *Electrochem. Solid-State Lett.* **2003**, 6, D17.
- [7] Q. Zhuo, S. Deng, B. Yang, J. Huang, B. Wang, T. Zhang, G. Yu, *Electrochim. Acta* **2012**, 77, 17.
- [8] Z. Liao, J. Farrell, *J. Appl. Electrochem.* **2009**, 39, 1993.
- [9] P. Cañizares, C. Sáez, A. Sánchez-Carretero, M. A. Rodrigo, *Electrochem. commun.* **2008**, 10, 602.
- [10] F. L. Souza, C. Saéz, M. R. V Lanza, P. Cañizares, M. A. Rodrigo, *Electrochim. Acta* **2016**, 187, 119.
- [11] E. Guinea, F. Centellas, E. Brillas, P. Cañizares, C. Sáez, M. A. Rodrigo, *Appl. Catal. B Environ.* **2009**, 89, 645.
- [12] “Advanced Diamond Technologies,” can be found under <http://www.thindiamond.com/uncd-technology/what-is-uncd/>, **2016**.
- [13] H. Zeng, A. R. Konicek, N. Moldovan, F. Mangolini, T. Jacobs, I. Wylie, P. U. Arumugam, S. Siddiqui, R. W. Carpick, J. A. Carlisle, *Carbon N. Y.* **2015**, 84, 103.
- [14] P. W. May, W. J. Ludlow, M. Hannaway, P. J. Heard, J. A. Smith,

- K. N. Rosser, *Diam. Relat. Mater.* **2008**, *17*, 105.
- [15] P. Szirmai, T. Pichler, O. A. Williams, S. Mandal, C. Bäuerle, F. Simon, *Phys. status solidi* **2012**, *249*, 2656.
- [16] W. Gajewski, P. Achatz, O. A. Williams, K. Haenen, E. Bustarret, M. Stutzmann, J. A. Garrido, *Phys. Rev. B - Condens. Matter Mater. Phys.* **2009**, *79*, 1.
- [17] H. Kuzmany, R. Pfeiffer, N. Salk, B. Günther, *Carbon N. Y.* **2004**, *42*, 911.
- [18] V. Mortet, L. Zhang, M. Eckert, J. D'Haen, A. Soltani, M. Moreau, D. Troadec, E. Neyts, J. C. De Jaeger, J. Verbeeck, A. Bogaerts, G. Van Tendeloo, K. Haenen, P. Wagner, *Phys. Status Solidi Appl. Mater. Sci.* **2012**, *209*, 1675.
- [19] J. H. T. Luong, B. Male, J. D. Glennon, K. B. Male, J. D. Glennon, *Analyst* **2009**, *134*, 1965.
- [20] M. Wang, N. Simon, G. Charrier, M. Bouttemy, A. Etcheberry, M. Li, R. Boukherroub, S. Szunerits, *Electrochem. commun.* **2010**, *12*, 351.
- [21] D. Ballutaud, N. Simon, H. Girard, E. Rzepka, B. Bouchet-Fabre, *Diam. Relat. Mater.* **2006**, *15*, 716.
- [22] T. A. Ivandini, Y. Einaga, *Chem. Commun.* **2017**, *53*, 1338.
- [23] D. Medeiros De Araújo, P. Cañizares, C. A. Martínez-Huitle, M. A. Rodrigo, *Electrochem. commun.* **2014**, *47*, 37.
- [24] R. Bogdanowicz, A. Fabiańska, L. Golunski, M. Sobaszek, M. Gnyba, J. Ryl, K. Darowicki, T. Ossowski, S. D. Janssens, K. Haenen, E. M. Siedlecka, *Diam. Relat. Mater.* **2013**, *39*, 122.
- [25] S. C. Ramos, A. F. Azevedo, M. R. Baldan, N. G. Ferreira, *J. Vac. Sci. & Technol. A-vacuum Surfaces Film.* **2010**, *28*, 27.
- [26] Y. Feng, J. Lv, J. Liu, N. Gao, H. Peng, Y. Chen, *Appl. Surf. Sci.*

- 2011**, 257, 3433.
- [27] O. Andrade, L. S., Salazar-Banda, G. R., Rocha-Filho, R. C. and Fatibello-Filho, in *Synth. Diam. Film. Prep. Electrochem. Charact. Appl.* (Eds.: E. Brillas, C.A. Martínez-Huitle), John Wiley & Sons, Inc., Hoboken, NJ, USA, **2011**.
- [28] G. R. Salazar-Banda, L. S. Andrade, P. A. P. Nascente, P. S. Pizani, R. C. Rocha-Filho, L. A. Avaca, *Electrochim. Acta* **2006**, 51, 4612.
- [29] Á. Anglada, A. Urtiaga, I. Ortiz, *J. Chem. Technol. Biotechnol.* **2009**, 84, 1747.
- [30] V. Boiteux, C. Bach, V. Sagres, J. Hemard, A. Colin, C. Rosin, J.-F. Munoz, X. Dauchy, *Int. J. Environ. Anal. Chem.* **2016**, 96, 705.
- [31] L. A. D'Agostino, S. A. Mabury, *Environ. Toxicol. Chem.* **2017**, 36, 2012.
- [32] C. Fang, M. Megharaj, R. Naidu, *Environ. Toxicol. Chem.* **2015**, 34, 2625.
- [33] S. Park, L. S. Lee, V. F. Medina, A. Zull, S. Waisner, *Chemosphere* **2016**, 145, 376.
- [34] X. Yang, J. Huang, K. Zhang, G. Yu, S. Deng, B. Wang, *Environ. Sci. Pollut. Res.* **2014**, 21, 4634.
- [35] Q. Zhuo, X. Li, F. Yan, B. Yang, S. Deng, J. Huang, G. Yu, *J. Environ. Sci.* **2014**, 26, 1733.
- [36] H. Lin, J. Niu, S. Ding, L. Zhang, *Water Res.* **2012**, 46, 2281.
- [37] Q. Zhuo, S. Deng, B. Yang, J. Huang, G. Yu, *Environ. Sci. Technol.* **2011**, 45, 2973.
- [38] M. Panizza, P. A. Michaud, G. Cerisola, C. Comninellis, *J. Electroanal. Chem.* **2001**, 507, 206.
- [39] A. Urtiaga, I. Ortiz, A. Anglada, D. Mantzavinos, E. Diamadopoulos, *J. Appl. Electrochem.* **2012**, 42, 779.

- [40] T. Ochiai, Y. Iizuka, K. Nakata, T. Murakami, D. A. Tryk, A. Fujishima, Y. Koide, Y. Morito, *Diam. Relat. Mater.* **2011**, *20*, 64.
- [41] B. Guan, J. Zhi, X. Zhang, T. Murakami, A. Fujishima, *Electrochem. commun.* **2007**, *9*, 2817.
- [42] X. Dauchy, V. Boiteux, C. Bach, A. Colin, J. Hemard, C. Rosin, J. F. Munoz, *Sci. Total Environ.* **2017**, *576*, 549.
- [43] E. F. Houtz, D. L. Sedlak, *Environ. Sci. Technol.* **2012**, *46*, 9342.
- [44] L. W. Y. Yeung, E. I. H. Loi, V. Y. Y. Wong, K. S. Guruge, N. Yamanaka, N. Tanimura, J. Hasegawa, N. Yamashita, S. Miyazaki, P. K. S. Lam, *Arch. Environ. Contam. Toxicol.* **2009**, *57*, 377.
- [45] Y. Miyake, N. Yamashita, P. Rostkowski, M. K. So, S. Taniyasu, P. K. S. Lam, K. Kannan, *J. Chromatogr. A* **2007**, *1143*, 98.
- [46] C. E. Schaefer, C. Andaya, A. Burant, C. W. Condee, A. Urriaga, T. J. Strathmann, C. P. Higgins, *Chem. Eng. J.* **2017**, *317*, 424.
- [47] A. M. Polcaro, A. Vacca, M. Mascia, S. Palmas, J. Rodriguez Ruiz, *J. Appl. Electrochem.* **2009**, *39*, 2083.
- [48] M. E. H. Bergmann, T. Iourtchouk, W. Schmidt, J. Hartmann, M. Fischer, G. Nüsse, D. Gerngroß, *J. Appl. Electrochem.* **2015**, *45*, 765.
- [49] B. P. Chaplin, D. K. Hubler, J. Farrell, *Electrochim. Acta* **2013**, *89*, 122.
- [50] G. Pérez, J. Saiz, R. Ibañez, A. M. Urriaga, I. Ortiz, *Water Res.* **2012**, *46*, 2579.
- [51] Á. Anglada, A. Urriaga, I. Ortiz, D. Mantzavinos, E. Diamadopoulos, *Water Res.* **2011**, *45*, 828.
- [52] A. Kapalka, L. Joss, A. Anglada, C. Comninellis, K. M. Udert, *Electrochem. commun.* **2010**, *12*, 1714.
- [53] S. Wang, Q. Yang, F. Chen, J. Sun, K. Luo, F. Yao, X. Wang, D.

- Wang, X. Li, G. Zeng, *Chem. Eng. J.* **2017**, *328*, 927.
- [54] J. Li, S. L. Zhou, G. B. Hong, C. T. Chang, *Chem. Eng. J.* **2013**, *219*, 486.
- [55] M. Li, Z. Yu, Q. Liu, L. Sun, W. Huang, *Chem. Eng. J.* **2016**, *286*, 232.
- [56] C. R. Estrellan, C. Salim, H. Hinode, *J. Hazard. Mater.* **2010**, *179*, 79.
- [57] S. C. Panchangam, A. Y. C. Lin, K. L. Shaik, C. F. Lin, *Chemosphere* **2009**, *77*, 242.
- [58] Y. C. Chen, S. L. Lo, J. Kuo, *Water Res.* **2011**, *45*, 4131.
- [59] R. Qu, J. Liu, C. Li, L. Wang, Z. Wang, J. Wu, *Water Res.* **2016**, *104*, 34.
- [60] H. Hori, E. Hayakawa, H. Einaga, S. Kutsuna, K. Koike, T. Ibusuki, H. Kiatagawa, R. Arakawa, *Environ. Sci. Technol.* **2004**, *38*, 6118.
- [61] J. Chen, P. Zhang, J. Liu, *J. Environ. Sci.* **2007**, *19*, 387.
- [62] R. R. Giri, H. Ozaki, T. Morigaki, S. Taniguchi, R. Takanami, *Water Sci. Technol.* **2011**, *63*, 276.
- [63] N. A. Ab Aziz, P. Palaniandy, H. A. Aziz, I. Dahlan, *J. Chem. Res.* **2016**, *40*, 704.
- [64] M. J. Chen, S. L. Lo, Y. C. Lee, J. Kuo, C. H. Wu, *J. Hazard. Mater.* **2016**, *303*, 111.
- [65] H. A. Becerril, J. Mao, Z. Liu, R. M. Stoltenberg, Z. Bao, Y. Chen, *ACS Nano* **2008**, *2*, 463.
- [66] H. Zhang, X. Lv, Y. Li, Y. Wang, J. Li, *ACS Nano* **2009**, *4*, 380.
- [67] G. Williams, B. Seger, P. V. Kamat, *ACS Nano* **2008**, *2*, 1487.
- [68] I. V. Lightcap, T. H. Kosel, P. V. Kamat, *Nano Lett.* **2010**, *10*, 577.
- [69] P. Wang, J. Wang, X. Wang, H. Yu, J. Yu, M. Lei, Y. Wang, *Appl. Catal. B Environ.* **2013**, *132–133*, 452.

- [70] H. Mahmood, A. Habib, M. Mujahid, M. Tanveer, S. Javed, A. Jamil, *Mater. Sci. Semicond. Process.* **2014**, *24*, 193.
- [71] P. Ribao, M. J. Rivero, I. Ortiz, *Environ. Sci. Pollut. Res.* **2016**, *24*, 1.
- [72] M. J. Sampaio, C. G. Silva, A. M. T. Silva, L. M. Pastrana-Martínez, C. Han, S. Morales-Torres, J. L. Figueiredo, D. D. Dionysiou, J. L. Faria, *Appl. Catal. B Environ.* **2015**, *170–171*, 74.
- [73] L. M. Pastrana-Martínez, S. Morales-Torres, V. Likodimos, J. L. Figueiredo, J. L. Faria, P. Falaras, A. M. T. Silva, *Appl. Catal. B Environ.* **2012**, *123–124*, 241.
- [74] J. Sun, L.-H. Guo, H. Zhang, L. Zhao, *Environ. Sci. Technol.* **2014**, *48*, 11962.
- [75] M. J. Chen, S. L. Lo, Y. C. Lee, C. C. Huang, *J. Hazard. Mater.* **2015**, *288*, 168.
- [76] M. S. Vohra, S. Kim, W. Choi, *J. Photochem. Photobiol. A Chem.* **2003**, *160*, 55.
- [77] M. Sansotera, F. Persico, C. Pirola, W. Navarrini, A. Di Michele, C. L. Bianchi, *Appl. Catal. B Environ.* **2014**, *148–149*, 29.
- [78] S. Gatto, M. Sansotera, F. Persico, M. Gola, C. Pirola, W. Panzeri, W. Navarrini, C. L. Bianchi, *Catal. Today* **2015**, *241*, 8.
- [79] X. Li, P. Zhang, L. Jin, T. Shao, Z. Li, J. Cao, *Environ. Sci. Technol.* **2012**, *46*, 5528.
- [80] M. Sansotera, F. Persico, V. Rizzi, W. Panzeri, C. Pirola, C. L. Bianchi, A. Mele, W. Navarrini, *J. Fluor. Chem.* **2015**, *179*, 159.
- [81] C. Song, P. Chen, C. Wang, L. Zhu, *Chemosphere* **2012**, *86*, 853.
- [82] H. Tang, Q. Xiang, M. Lei, J. Yan, L. Zhu, J. Zou, *Chem. Eng. J.* **2012**, *184*, 156.
- [83] S. M. Mitchell, M. Ahmad, A. L. Teel, R. J. Watts, *Environ. Sci.*

- Technol. Lett.* **2013**, *1*, 117.
- [84] K. Park, I. Ali, J. O. Kim, *J. Environ. Manage.* **2018**, *218*, 333.
- [85] J. Zhong, Y. Zhao, L. Ding, H. Ji, W. Ma, C. Chen, J. Zhao, *Appl. Catal. B Environ.* **2018**, *241*, 514.
- [86] M. H. Cao, B. B. Wang, H. S. Yu, L. L. Wang, S. H. Yuan, J. Chen, *J. Hazard. Mater.* **2010**, *179*, 1143.
- [87] Y. Qian, X. Guo, Y. Zhang, Y. Peng, P. Sun, C. H. Huang, J. Niu, X. Zhou, J. C. Crittenden, *Environ. Sci. Technol.* **2016**, *50*, 772.
- [88] M. Filipovic, A. Woldegiorgis, K. Norström, M. Bibi, M. Lindberg, A. H. Österås, *Chemosphere* **2015**, *129*, 39.
- [89] E. F. Houtz, C. P. Higgins, J. A. Field, D. L. Sedlak, *Environ. Sci. Technol.* **2013**, *47*, 8187.
- [90] B. Gomez-Ruiz, S. Gómez-Lavín, N. Diban, V. Boiteux, A. Colin, X. Dauchy, A. Urtiaga, *J. Electroanal. Chem.* **2017**, *798*, 51.
- [91] J. C. D'Eon, M. D. Hurley, T. J. Wallington, S. A. Mabury, *Environ. Sci. Technol.* **2006**, *40*, 1862.
- [92] Y. Wu, Y. Li, A. Tian, K. Mao, J. Liu, *Int. J. Photoenergy* **2016**, *2016*, 1.
- [93] T. Yamamoto, Y. Noma, S.-I. Sakai, Y. Shibata, *Environ. Sci. Technol.* **2007**, *41*, 5660.
- [94] J. Liu, D. J. Van Hoomissen, T. Liu, A. Maizel, X. Huo, S. R. Fernández, C. Ren, X. Xiao, Y. Fang, C. E. Schaefer, C. P. Higgins, S. Vyas, T. J. Strathmann, *Environ. Sci. Technol. Lett.* **2018**, *5*, 289.
- [95] V. Ochoa-Herrera, R. Sierra-Alvarez, A. Somogyi, N. E. Jacobsen, V. H. Wysocki, J. A. Field, *Environ. Sci. Technol.* **2008**, *42*, 3260.
- [96] M. K. Moe, S. Huber, J. Svenson, A. Hagenaaars, M. Pabon, M. Trümper, U. Berger, D. Knapen, D. Herzke, *Chemosphere* **2012**, *89*, 869.

- [97] B. Gomez-Ruiz, S. Gómez-Lavín, N. Diban, V. Boiteux, A. Colin, X. Dauchy, A. Urtiaga, *Chem. Eng. J.* **2017**, 322, 196.
- [98] R. R. Giri, H. Ozaki, T. Okada, S. Taniguchi, R. Takanami, *Chem. Eng. J.* **2012**, 180, 197.
- [99] P. Neta, R. E. Huie, A. B. Ross, *J. Phys. Chem. Ref. Data* **1988**, 17, 1027.
- [100] H. Hori, A. Yamamoto, E. Hayakawa, S. Taniyasu, N. Yamashita, S. Kutsuna, H. Kiatagawa, R. Arakawa, *Environ. Sci. Technol.* **2005**, 39, 2383.
- [101] A. Ghauch, A. Baalbaki, M. Amasha, R. El Asmar, O. Tantawi, *Chem. Eng. J.* **2017**, 317, 1012.
- [102] P. Yin, Z. Hu, X. Song, J. Liu, N. Lin, *Int. J. Environ. Res. Public Health* **2016**, 13, 1.
- [103] S. Kutsuna, K. Koike, H. Hori, *Int. J. Chem. Kinet.* **2009**, 41, 735.
- [104] T. A. Bruton, D. L. Sedlak, *Environ. Sci. Technol.* **2017**, 51, 13878.
- [105] T. Oppenländer, *Photochemical Purification of Water and Air: Advanced Oxidation Processes (AOPs) - Principles, Reaction Mechanisms, Reactor Concepts*, **2003**.
- [106] Z. Song, H. Tang, N. Wang, L. Zhu, *J. Hazard. Mater.* **2013**, 262, 332.
- [107] M. Fischer, P. Warneck, **1996**, 3654, 15111.
- [108] G. V. Buxton, C. L. Greenstock, W. P. Helman, A. B. Ross, *J. Phys. Chem. Ref. Data* **1988**, 17, 513.
- [109] X. Li, G. Liu, J. Fang, S. Yue, Y. Guan, L. Chen, X. Liu, *Environ. Sci. Technol.* **2012**, 46, 7342.
- [110] F. Xiao, R. A. Hanson, S. A. Golovko, M. Y. Golovko, W. A. Arnold, *Environ. Sci. Technol. Lett.* **2018**, 5, 382.
- [111] C. M. Butt, D. C. G. Muir, S. A. Mabury, *Environ. Toxicol. Chem.*

- 2014**, 33, 243.
- [112] R. F. McFeeters, *J. Food Prot.* **1998**, 61, 885.
- [113] S. A. Styler, A. L. Myers, D. J. Donaldson, *Environ. Sci. Technol.* **2013**, 47, 6358.
- [114] D. A. Ellis, J. W. Martin, A. O. De Silva, S. A. Mabury, M. D. Hurley, M. P. Sulbaek Andersen, T. J. Wallington, *Environ. Sci. Technol.* **2004**, 38, 3316.
- [115] M. H. Kim, N. Wang, K. H. Chu, *Appl. Microbiol. Biotechnol.* **2014**, 98, 1831.
- [116] S. a Gauthier, S. a Mabury, *Environ. Toxicol. Chesistry* **2005**, 24, 1837.
- [117] J. Liu, S. Mejia Avendaño, *Environ. Int.* **2013**, 61, 98.
- [118] K. C. Harding-Marjanovic, E. F. Houtz, S. Yi, J. A. Field, D. L. Sedlak, L. Alvarez-Cohen, *Environ. Sci. Technol.* **2015**, 49, 7666.
- [119] K. A. Barzen-Hanson, S. E. Davis, M. Kleber, J. A. Field, *Environ. Sci. Technol.* **2017**, 51, 12394.
- [120] G. Munoz, M. Desrosiers, S. V. Duy, P. Labadie, H. Budzinski, J. Liu, S. Sauvé, *Environ. Sci. Technol.* **2017**, 51, 1231.
- [121] L. J. Trouborst, *Aqueous Photolysis of 6:2 Fluorotelomer Sulfonamide Alkylbetaine*, **2016**.
- [122] D. M. J. Shaw, G. Munoz, E. M. Bottos, S. V. Duy, S. Sauvé, J. Liu, J. D. Van Hamme, *Sci. Total Environ.* **2019**, 647, 690.
- [123] S. Banzhaf, M. Filipovic, J. Lewis, J. Sparrenbom, Charlotte, R. Barthel, *Ambio* **2016**, 46, 335.
- [124] J. Liu, S. Mejia Avendaño, *Environ. Int.* **2013**, 61, 98.
- [125] H. Park, C. D. Vecitis, J. Cheng, N. F. Dalleska, B. T. Mader, M. R. Hoffmann, *Photochem. Photobiol. Sci.* **2011**, 10, 1945.
- [126] S. Yang, J. Cheng, J. Sun, Y. Hu, X. Liang, *PLoS One* **2013**, 8, 6.

- [127] Y. Gu, W. Dong, C. Luo, T. Liu, *Environ. Sci. Technol.* **2016**, *50*, 10554.
- [128] Y. Gu, T. Liu, H. Wang, H. Han, W. Dong, *Sci. Total Environ.* **2017**, *607–608*, 541.
- [129] Y. Qu, C. Zhang, F. Li, J. Chen, Q. Zhou, *Water Res.* **2010**, *44*, 2939.
- [130] J. R. Bolton, K. G. Bircher, W. Tumas, C. A. Tolman, *Pure Appl. Chem.* **2001**, *73*, 627.
- [131] S. Dominguez, M. J. Rivero, P. Gomez, R. Ibañez, I. Ortiz, *J. Ind. Eng. Chem.* **2016**, *37*, 237.





# CONCLUSIONS



#### 4.1. Final remarks and future work

This thesis was focus on the study of using several materials and advanced technologies for the treatment of the persistent poly- and perfluoroalkyl substances in model solutions and real wastewaters. Specifically, this study has led to the following conclusions.

##### Electrochemical oxidation

This work initially aims at investigating the roles of the different BDD anodes on the oxidation of PFOA model solution, since the literature showed a wide diversity of PFASs degradation kinetics by the diverse morphologies of this anodic material. In this context, a comparative study of two commercial electrodes, microcrystalline BDD/Si and ultrananocrystalline BDD/Nb anodes, was studied in terms of morphology, chemical composition and electrochemical performance to elucidate the relationship of the anode features with the PFASs electrolysis. The reported results showed that the electrochemical oxidation of PFOA by BDD anode was highly influenced by chemical and morphological characteristics of the surface, and the following considerations can be withdrawn:

- The MCD anode led to the complete degradation of PFOA in 4 h, at any applied current density in the range of 1-5 mA.cm<sup>-2</sup>. Conversely, remarkable lower PFOA removal ratios were achieved by the UNCD anode, as only 21% PFOA removal was achieved in 4 h working at 5 mA.cm<sup>-2</sup>.
- The higher sp<sup>3</sup> carbon content and lower boron content and H-terminated carbon content of the MCD anode tend to favor a faster

and more efficient PFOA degradation. In contrast, the surface features and the higher conductivity of the UNCD anode limited its electrochemical activity for PFOA degradation.

- The different electrochemical behaviors of commercial BDD anodes strongly impacted on the process energy consumption. The energy needed for PFOA removal from a  $0.24 \text{ mmol.L}^{-1}$  solution was  $1.4 \text{ kWh.m}^{-3}$  and  $52.4 \text{ kWh.m}^{-3}$ , for MCD and UNCD anodes, respectively.

Secondly, the practical feasibility and versatility of the microcrystalline BDD anode was investigated through the treatment of a complex mixture of PFASs contained in the influent and effluent of an industrial wastewater treatment utility that receives the sewage of a manufacturer of fluorinated compounds. PFASs are poorly removed by the conventional treatments currently used in WWTPs, and even, the biodegradation of some labile PFAS precursors may contribute to increase the content of persistent PFCAs. As a result, WWTP effluents have been suggested to be one of the major pathways of PFASs emission sources to the aquatic environment. This work gains insights into the evaluation of electrolysis of PFASs mixtures present over a wider concentration range and under the effect of complex matrix composition, since the electrochemical treatment of industrial wastewaters polluted by elevated concentrations of PFASs was practically unexplored. The results herein reported showed the effectiveness of BDD anode to reduce PFASs content in both influent and effluent wastewaters. Particularly, BDD anodic oxidation was able to reduce the PFASs content by 97.1% after 8 h of electrochemical treatment of the influent WWTP wastewater conducted at a current density of  $50 \text{ mA.cm}^{-2}$ . The high initial content of TOC ( $722 \text{ mg.L}^{-1}$ ) in this sample was

also decreased by 80%, regardless the diverse chemical composition of the organic matter. Moreover, the electrochemical treatment of WWTP effluent allowed the nearly complete elimination of PFASs content at 50 mA.cm<sup>-2</sup> after 8 h. In this case, the TOC concentration was reduced to 12 mg.L<sup>-1</sup>, due to less organic load present in this stream. Although the different initial organic background of industrial wastewaters, electrochemical treatment by BDD achieved similar degradation kinetics of the main PFASs in both samples. Based on the results, it was suggested that 6:2 FTAB and M4 were partially degraded into 6:2 FTSA, which was simultaneously generated and broken under these conditions. Moreover, the degradation of fluorotelomers induced the formation of PFCAs, that were further decomposed into shorter-chain PFCAs, and finally, mineralized as it was also supported by the increase of the fluoride. Therefore, BDD anodes demonstrated the effective removal of the complex mixture of PFASs along with the reduction of the major organic components from industrial wastewaters. Moreover, the BDD/Si anodic material offered a robust stability. The electrochemical cell used in the present study had been in operation at laboratory scale for more than 12 years, under a variety of wastewaters and contaminants, a factor that proves the robustness of BDD electrooxidation technology.

#### Heterogeneous photocatalysis

The photocatalytic degradation of PFOA model solution was studied using a novel composite based on TiO<sub>2</sub> and reduced graphene oxide (rGO) synthesized by the hydrothermal method. The proper synthesis of TiO<sub>2</sub>-rGO catalyst was thoroughly analyzed using microscopic and spectroscopic techniques. Results indicated that TiO<sub>2</sub> nanoparticles were

well loaded and disperse on the graphene plane, where GO was reduced after the bonding with the TiO<sub>2</sub>.

The efficient photoactivity of the prepared TiO<sub>2</sub>-rGO composite was successfully confirmed for PFOA degradation, under UV–vis irradiation. After 12 h of irradiation, PFOA removal ratio was as high as  $93 \pm 7\%$ , using a  $0.1 \text{ g.L}^{-1}$  concentration of the composite catalyst. This results was 4-fold higher than the TiO<sub>2</sub>-mediated photocatalysis ( $24 \pm 11\%$ ), under the same experimental conditions. The outstanding photoactivity of TiO<sub>2</sub>-rGO, which overcomes the limited performance of TiO<sub>2</sub> against PFOA, can be attributed to:

- The excellent electrical properties of the reduced graphene oxide, acting as an electron sink. This property can reduce the recombination of electron/hole pairs, with the electron transfer to rGO which further allows greater generation of oxidizing radicals. In addition, the excellent electron mobility of rGO could promote the electron transfer from PFOA molecule that favors the initial degradation steps.
- The structure and morphology of the composite with the uniform distribution of TiO<sub>2</sub> nanoparticles on rGO sheets surface could reduce the TiO<sub>2</sub> agglomeration, providing more available active sites for the photocatalytic process.
- The lower band gap energy of the TiO<sub>2</sub>-rGO can give the ability to absorb visible light, which promote a more efficient use of irradiated light than TiO<sub>2</sub> catalyst.

Moreover, the progress of shorter-chain PFCAs as well as fluoride release elucidated the step-by-step PFOA decomposition mechanism by gradually

losing one  $-CF_2-$  unit in each step, that is converted into  $CO_2$  and  $F^-$ .

### Homogeneous photochemical techniques

Finally, individual and sequential UV reductive/oxidative systems were proposed for the degradation of a mixture of PFASs contained in an AFFF formulation. The precise chemical compositions of AFFF formulations are proprietary, nevertheless, different perfluorocarboxylates, perfluorosulfantes, fluorotelomer carboxylates and fluorotelomer sulfonates were identified. PFOS present a notably higher initial content in the sample, among the identified PFASs. Moreover, the sample contained high content of unknown PFASs precursors, as it was revealed with the total fluorine content of AFFF obtained by  $^{19}F$ -NMR, that corresponded only to the  $30 \pm 5\%$  of total F calculated from the initial concentration of PFASs detected. The photochemical techniques consisted of: (i) an oxidative treatment based of UV irradiation of sodium persulfate to generate sulfate radicals, and (ii) the UV photolysis of sulfite as the reductive technique, to promote the generation of hydrated electrons.

The results demonstrated that each photochemical system exhibited different performance for each PFAS group. Whereas fluorotelomer carboxylates seem to be inert to the reductive treatment, their concentration increased over the UV-activated persulfate treatment. Fluorotelomer sulfonates were effectively oxidized by sulfate radicals, while the levels of these compounds rose during the reduction. It was suggested that one sulfonamide-based precursors present in the AFFF formulation may be transformed into fluorotelomers FTs detected by different degradation pathways in oxidative and reductive treatments. In contrast, the degradation trends of PFASs were similar between reductive and oxidative

strategies. However, PFCAs were effectively degraded by  $e_{aq}^-$  species, while their concentrations partially increased during the oxidation, due to the high transformation of unknown precursors to fluorotelomers, and consequently to PFCAs, which were also decomposed step-by-step to shorter-chain PFCAs. As a result, it can be concluded that  $e_{aq}^-$  are more reactive with perfluorinated compounds (PFASs and PFCAs), and  $SO_4^{\cdot-}$  radicals could react more rapidly with PFAS precursors and fluorotelomers that contain unfluorinated carbons.

Furthermore, as the efficacy of reduction and oxidation processes seemed to be affected by the molecular structure of PFASs, sequential UV oxidative/reductive treatments were applied for facilitating the degradation of the PFASs. Tests of different sequential treatments showed the most promising combination to be a sequence of UV-sulfite followed by UV-persulfate, which achieved the highest removal of the total PFASs content in AFFF. Indeed, a 96% elimination of PFOS was obtained after 48h in this sequence. When UV-sulfite is used as second stage, it was less effective applied after the persulfate treatment, than the individual treatment. Although a tentative proposal of PFASs precursors have been explained, further research investigating potential PFASs precursors in the AFFF mixture and the possible routes of oxidation and reduction of PFASs will be addressed.

Finally, from an economic point of view, the energy consumption required for the different technologies was evaluated. The results indicated that the electrochemical technology achieves higher removal rates of PFASs at lower values of energy consumption, compared to photochemical strategies. However, the initial concentration of the contaminants highly impacted on the energy requirements of BDD technology. The energy

required for the removal of the PFASs ( $\sim 1.5 \text{ mg.L}^{-1}$ ) in industrial wastewaters was 200 times higher than for synthetic PFOA solution ( $100 \text{ mg.L}^{-1}$ ) prepared in the laboratory. Still, the large-scale implementation of the electrochemical process will require of new strategies to reduce its energy consumption and operation costs. PFASs preconcentration by means of membrane separation is envisaged as possible strategies.

Future research should deal with the understanding of the reaction pathways of PFASs by means of the different technologies in order to get insight in the most likely rate-limiting step in the degradation mechanism. In the case of photochemical processes, the strategies should be conducted towards more sustainable light sources, such as, light emitting diodes (LEDs) which appears a less toxic, durable and more efficient alternative. Moreover, the recovery of the catalyst in an additional stage or the use of catalytic-membrane photoreactors would lead to enhance the practical feasibility of this technology.

## **4.2. Conclusiones y trabajo futuro**

Esta tesis doctoral se ha centrado en el estudio del tratamiento de sustancias poli- y perfluoroalquílicas persistentes, de disoluciones modelo y aguas residuales reales, mediante distintos materiales y tecnologías avanzadas. Las principales conclusiones derivadas de este trabajo se detallan a continuación.

### Oxidación electroquímica

Este estudio inicialmente tiene como objetivo investigar el papel del ánodo BDD en la degradación de PFOA en disoluciones modelo. El trabajo viene motivado por las grandes diferencias ya reportadas en las cinéticas de

degradación de PFASs mediante este material anódico con distintas morfologías. De este modo, se realizó un estudio comparativo de dos electrodos comerciales, un ánodo BDD/Si microcristalino y un ánodo BDD/Nb ultrananocristalino, atendiendo a la morfología, composición química y comportamiento electroquímico para aclarar la relación de las características de la superficie anódica con la electrólisis de PFASs. Los resultados obtenidos mostraron que el comportamiento del ánodo de BDD está altamente influenciado por las características morfológicas y químicas de la superficie anódica. Además, se pueden destacar las siguientes conclusiones:

- El ánodo MCD dio lugar a la degradación completa de PFOA en 4h, para las distintas  $j$  aplicadas en el rango de 1-5 mA.cm<sup>-2</sup>. Por el contrario, las tasas de eliminación de PFOA obtenidas con el ánodo UNCD son notablemente más bajas, alcanzando el 21% de degradación tras 4 h, para una densidad de corriente de 5 mA.cm<sup>-2</sup>.
- El mayor contenido de carbono sp<sup>3</sup>, la menor concentración de boro y de terminaciones C-H del ánodo MCD, tienden a favorecer una degradación de PFOA más rápida y eficiente. Sin embargo, las características de la superficie y la alta conductividad que presenta el ánodo UNCD limitan la actividad electroquímica para la degradación de PFOA.
- Las diferentes respuestas electroquímicas de los ánodos comerciales influyen altamente en el consumo energético del proceso. Así, los requerimientos energéticos para la eliminación de PFOA de la disolución modelo (0.24 mmol.L<sup>-1</sup>) se estimaron como 1.4 kWh.m<sup>-3</sup> y 52.4 kWh.m<sup>-3</sup>, respectivamente.

Tras estos resultados, la viabilidad práctica y versatilidad del ánodo de BDD microcristalino fueron estudiadas a través del tratamiento de una mezcla compleja de PFASs presentes en la corriente de entrada (afluente) y corriente de salida (efluente) de una planta de tratamiento de aguas residuales, que recibe aguas residuales de fábricas de compuestos perfluorados. Actualmente, los PFASs son prácticamente inertes a los procesos de estas plantas de tratamiento, y además, algunos de los compuestos precursores de PFASs pueden ser biodegradados contribuyendo al incremento de compuestos más persistentes como los PFCAs. Como resultado el efluente de estas plantas es considerado como una de las principales fuentes de contaminación de PFASs al medio acuático. En este contexto, este trabajo tiene como objetivo el estudio del proceso electroquímico de una mezcla de PFASs que se encuentra en un rango de concentraciones muy amplio, y bajo el efecto de una matriz acuosa compleja. Además, la degradación electroquímica de estos compuestos en altas concentraciones que se encuentran en aguas residuales industriales no se ha explorado previamente. Los resultados obtenidos en este trabajo mostraron la alta efectividad de la electro-oxidación mediante ánodo de BDD para la eliminación de PFASs tanto en las aguas residuales de entrada y de salida de la planta. Más concretamente, la oxidación anódica mediante BDD fue capaz de reducir el contenido de PFASs en un 97.1% en el influente, tras 8h bajo una densidad de corriente de  $50 \text{ mA}\cdot\text{cm}^{-2}$ . Además, el alto contenido de TOC de esta muestra ( $722 \text{ mg}\cdot\text{L}^{-1}$ ) también fue eliminado en un 80% al final del tratamiento, independientemente de la composición química de la materia orgánica. Por otro lado, durante el tratamiento electroquímico del efluente, el contenido total de PFAS fue casi completamente eliminado tras 8 h a una densidad de corriente de  $50 \text{ mA}\cdot\text{cm}^{-2}$ . En este caso, la carga total de materia orgánica fue reducido hasta

12 mg.L<sup>-1</sup> (89%), dado su menor contenido de TOC inicialmente. A pesar de que la carga orgánica inicial es muy distinta en las aguas residuales industriales, el tratamiento electroquímico con BDD dio lugar a cinéticas de degradación de los principales PFASs muy similares en ambas muestras. Además, en base a los resultados obtenidos, se propusieron diferentes vías de degradación de los PFASs. Así, los compuestos 6:2 FTAB y M4, pueden ser parcialmente degradados en 6:2 FTSA, que bajo estas condiciones fue generado y simultáneamente descompuesto. Además, la degradación de los fluorotelomeros sulfonados da lugar a la formación de PFCAs, que posteriormente son descompuestos a homólogos de menor cadena hasta la completa mineralización, apoyado por la liberación de F<sup>-</sup> a lo largo del tratamiento. Por lo tanto, la electro-oxidación mediante ánodo de BDD demostró la eliminación efectiva de la mezcla compleja de PFASs junto con la reducción de la materia orgánica de las aguas residuales industriales. Además, el material BDD/Si ofrece una gran estabilidad, dado que esta celda ha operado en escala laboratorio durante más de 12 años, con una amplia variedad de aguas residuales y contaminantes, un factor clave que resalta la robustez de esta tecnología.

### Fotocatálisis heterogénea

La degradación fotocatalítica de las disoluciones modelo de PFOA fue estudiada mediante el uso de un nuevo catalizador compuesto basado en TiO<sub>2</sub> y óxido de grafeno reducido (rGO), sintetizado mediante el método hidrotermal.

Inicialmente, la correcta preparación del catalizador compuesto TiO<sub>2</sub>-rGO fue analizado a través de distintas técnicas microscópicas y espectroscópicas. Los resultados mostraron que las nanopartículas de TiO<sub>2</sub>

fueron correctamente depositadas a lo largo de las láminas de rGO, donde el GO fue reducido tras el enlace con  $\text{TiO}_2$ .

La alta actividad fotocatalítica del material compuesto  $\text{TiO}_2$ -rGO para la degradación de PFOA fue confirmada, bajo la irradiación UV-Vis. Así, tras 12 h de irradiación, el ratio de eliminación de PFOA fue de  $93 \pm 7\%$ , empleando una concentración de catalizador de  $0.1 \text{ g.L}^{-1}$ . Este resultado fue 4 veces mayor que la eliminación de PFOA obtenida en el proceso fotocatalítico con  $\text{TiO}_2$  ( $24 \pm 11\%$ ), bajo las mismas condiciones experimentales. La alta efectividad del  $\text{TiO}_2$ -rGO para la degradación de PFOA, que logra superar las limitaciones que presentaba el  $\text{TiO}_2$ , se debe principalmente a las siguientes propiedades:

- Las excepcionales propiedades electricas del rGO que haec que actue como sumidero de electrones. Esta característica hace disminuir la recombinacion de los pares electrón/hueco, con la transferencia del electron hasta el rGO, que puede dar lugar a una mayor formación de radicales oxidantes. Además, esta movilidad de electrones que presenta el rGO también puede promover la liberación de e- del PFOA que favorece las etepas iniciales de degradación.
- La estructura y morfología que presenta el composite, es decir, una distribución uniforme de las nanoparticulas sobre la superficie de las láminas del rGO, puede disminuir la aglomeración del  $\text{TiO}_2$  y proporcionar una mayor disponibilidad de sitios activos para el proceso fotocatalítico.
- La menor energía de la banda prohibida (band gap) del  $\text{TiO}_2$ -rGO puede dar lugar a la absorción de la luz visible, y dar lugar a un mayor aprovechamiento de la luz irradiada en comparación con el  $\text{TiO}_2$ .

Por otro lado, el progreso de los PFCAs de menos cadena, así como, la liberación de fluoruro apoyan el mecanismo de descomposición de PFOA por etapas, mediante la eliminación de una unidad  $\text{CF}_2$  en cada etapa, que es convertido en  $\text{CO}_2$  y  $\text{F}^-$ .

### Técnicas fotoquímicas homogéneas

Finalmente, diferentes estrategias fotoquímicas, oxidativas y reductoras, fueron propuestas para la degradación de una mezcla de PFASs presentes en formulaciones de AFFF. Las composiciones químicas de las formulaciones AFFF son generalmente privadas, sin embargo, se identificaron diferentes perfluorocarboxilados, perfluorosulfonados, fluorotelomeros carboxilados y fluorotelomeros sulfonados. PFOS, presentaba la mayor concentración inicial entre los PFASs identificados. Además, la disolución de AFFF contenía también compuestos precursores de PFASs desconocidos, como reveló la medida de F total de la disolución obtenido mediante la técnica  $^{19}\text{F}$ -RMN, que sólo correspondía con el  $30 \pm 5\%$  de F presente en los PFASs identificados. Los tratamientos fotoquímicos consistieron en: (i) oxidación mediante la radiación UV de persulfato de sodio, para generar radicales sulfato, y (ii) la fotólisis de sulfito en el caso de la reducción, que da lugar a la formación de electrones hidratados.

Los resultados mostraron diferentes comportamientos de los grupos de PFASs en función del sistema fotoquímico. Mientras que los fluorotelomeros carboxilados tienden a ser inertes en el proceso reductor, su concentración aumentaba en el tratamiento con persulfato activado con luz ultravioleta. Por otro lado, los fluorotelomeros sulfonados desaparecían en el tratamiento oxidativo, y en el caso de la reducción con sulfito, su

concentración iba aumentando a lo largo del tratamiento. Estos resultados apoyan la idea de que puede existir una sulfonamida precursora de PFASs en la muestra de AFFF, que puede transformado en los FTs detectados mediante diferentes vías de degradación para los procesos oxidativos o reductores. Por otro lado, las tendencias de degradación de los PFASs fueron similares entre los dos tipos de tratamientos. Sin embargo, los PFCAs fueron altamente degradados mediante las especies  $e_{aq}^-$ , mientras que su concentración aumentó durante el tratamiento con persulfato. Esto fue debido a la descomposición de los precursores desconocidos y fluorotelomeros en los PFCAs, que simultáneamente se iban degradando en compuestos de menor cadena, por el mecanismo de etapas. Como resultado, cabe destacar que  $e_{aq}^-$  tienden a ser más reactivos con los compuestos pefluorados (PFASs and PFCAs), mientras que los radicales pueden reaccionar más rápidamente con los compuestos precursores y fluorotelomeros, ya que contienen carbonos no fluorados.

Además, dado que la eficacia de cada tratamiento es afectada por la estructura molecular de los PFASs, se propusieron tratamientos consecutivos de las técnicas de oxidación y reducción para lograr mayor degradación de estos contaminantes. Los diferentes experimentos mostraron que la combinación más adecuada era la reducción con sulfito seguido de la oxidación de persulfato, que dio lugar a una mayor tasa de eliminación del contenido total de PFASs. Además, se logró un 96% de degradación de PFOS tras 48h de la secuencia de tratamientos, que era el compuesto más abundante en la muestra de AFFF. Se observó que cuando la técnica UV-sulfito era utilizada como segunda etapa, tras la oxidación con persulfato, era menos efectiva que como tratamiento individual. Sin embargo, mayor investigación será necesaria para averiguar los potenciales precursores presentes en la muestra AFFF, así como, las vías de

degradación de los PFASs que tienen lugar en los tratamientos oxidativos y reductores.

Finalmente, desde el punto de vista económico, se calcularon los consumos energéticos por las diferentes tecnologías. Estos resultados mostraron que la tecnología de electrooxidación logra altas tasas de degradación de los contaminantes PFASs con menores requerimientos energéticos que las técnicas fotoquímicas. Sin embargo, la concentración inicial de los contaminantes tuvo un gran impacto en los requisitos energéticos de la tecnología BDD. La energía requerida para la eliminación de los PFASs ( $\sim 1.5 \text{ mg.L}^{-1}$ ) en aguas residuales industriales fue 200 veces mayor que para la disolución sintética de PFOA ( $100 \text{ mg.L}^{-1}$ ), preparada en el laboratorio. Aun así, la implementación a gran escala del proceso electroquímico requerirá nuevas estrategias para reducir su consumo de energía y los costes de operación. La preconcentración de PFASs mediante el uso de membranas podrían ser una posible estrategia.

Las investigaciones futuras deberían abordar el estudio de las reacciones de degradación de los PFAS mediante las diferentes tecnologías, con el fin de conocer las etapas limitantes de los mecanismos de degradación. En el caso de los procesos fotoquímicos, las estrategias deben dirigirse hacia fuentes de luz más sostenibles, como los diodos emisores de luz (LED), que son una alternativa menos tóxica, más duradera y eficiente. Además, la recuperación del catalizador o el uso de reactores con el catalizador integrado en membranas podrían mejorar la viabilidad práctica de este tratamiento.







**SCIENTIFIC  
PUBLICATIONS**





5.1. Scientific publication 1.

**Comparison of microcrystalline and ultrananocrystalline boron doped diamond anodes: Influence on perfluorooctanoic acid electrolysis**

Authors:

Beatriz Gomez-Ruiz, Nazely Diban, Ane Urtiaga

Department of Chemical and Biomolecular Engineering. University of Cantabria. Av. de Los Castros s/n. 39005 Santander. Spain

---

*Accepted 21 March 2018*

*Separation and Purification Technology*

*Volume 208 (2019), Pages 169-177*

DOI: <https://doi.org/10.1016/j.seppur.2018.03.044>



## Comparison of microcrystalline and ultrananocrystalline boron doped diamond anodes: Influence on perfluorooctanoic acid electrolysis

Beatriz Gomez-Ruiz, Nazely Diban\*, Ane Urtiaga

Department of Chemical and Biomolecular Engineering, University of Cantabria, Av. de Los Castros s/n, 39005 Santander, Spain

### ARTICLE INFO

#### Keywords:

Boron doped diamond (BDD)  
Microcrystalline  
Ultrananocrystalline  
Electrolysis  
perfluorooctanoic acid (PFOA)

### ABSTRACT

This work aims to study the effect of the distinctive chemical and structural surface features of boron doped diamond (BDD) anodes on their electrochemical performance for perfluorooctanoic acid (PFOA) degradation. Commercial BDD anodes were compared: (i) a microcrystalline (MCD) coating on silicon; and (ii) an ultrananocrystalline (UNCD) coating on niobium. MCD gave rise to the complete PFOA ( $0.24 \text{ mmol L}^{-1}$ ) degradation in 4 h, at any applied current density in the range  $1\text{--}5 \text{ mA cm}^{-2}$ . On the contrary, only 21% PFOA removal was achieved when using UNCD at  $5 \text{ mA cm}^{-2}$  under comparable experimental conditions. Similarly, the total organic carbon (TOC) was reduced by 89% using MCD, whereas only 13% TOC decrease was obtained by UNCD. In order to explain the dissimilar electrochemical activities, the morphological and chemical characterization of the electrode materials was developed by means of FESEM microscopy, XPS and Raman spectroscopy. The UNCD anode surface showed characteristic ultrananocrystalline grain size (2–25 nm), higher boron doping and greater content of H-terminated carbon, whereas the MCD anode was less conductive but contained higher  $\text{sp}^3$  carbon on the anode surface. Overall, the MCD electrode features allowed more efficient PFOA electrolysis than the UNCD anode. As a result of their distinctive performance, the energy needed for the maximum PFOA degradation (after 4 h) using MCD anode was only  $1.4 \text{ kWh m}^{-3}$ , while the estimated energy consumption for the UNCD anode would be 37-fold higher. It is concluded that the use of the MCD anode involves considerable energy costs savings.

### 1. Introduction

In the last two decades, the use of conducting diamond electrodes has grown rapidly due to their extraordinary performance for electrolysis of refractory organic pollutants [1–3]. In pure diamond, each carbon atom is covalently bonded to four other  $\text{sp}^3$  hybridized carbons forming an extremely robust and electrical insulator crystalline structure. For most electrochemical applications, some carbon atoms in the lattice are substituted with a dopant to provide electrical conductivity and reduce the wide band gap of diamond. Boron is one of the most interesting doping elements which can act as an electron acceptor and provides diamond with *p*-type semiconductivity at room temperature [1,4,5].

Boron-doped diamond (BDD) film electrodes have gained attention for water treatment by anodic oxidation, due to their unique properties compared to other electrode materials [6–9]. The production and weak adsorption of hydroxyl radicals on the BDD anode result in a low electrochemical activity for the oxygen evolution reaction [3], leading to powerful oxidation conditions for the removal of organic compounds

[10–12]. Particularly, BDD electrochemical oxidation has recently demonstrated its efficiency for the abatement of per- and poly-fluoroalkyl substances (PFASs) in aqueous media [13–15]. PFASs, including perfluorooctanoic acid (PFOA) and perfluorooctane sulfonate (PFOS) have been released to the environment because of their use in industrial manufacturing and applications in consumer goods. Persistent PFASs have been detected in industrial effluents, landfill leachates, groundwater, and even in drinking water, causing their bioaccumulation [16,17].

Despite the use of BDD as anode material, the observed rates of PFASs removal were very different among the reported works [13,15,18–24]. Table S1 (in the Supplementary Information) gathers the reported values of the observed kinetic constants alongside the experimental conditions. Nevertheless, the wide diversity of the experimental conditions, such as area ( $5.5\text{--}140 \text{ cm}^2$ ), treated volume ( $0.04\text{--}2 \text{ L}$ ), applied current density ( $0.15\text{--}50 \text{ mA cm}^{-2}$ ), the initial concentration of PFASs ( $0.0007\text{--}8 \text{ mM}$ ), and the observed kinetic constants for PFASs degradation hindered the direct comparison of the previous research. Also, it is worth mentioning that the BDD suppliers

\* Corresponding author.

E-mail address: [diban@unican.es](mailto:diban@unican.es) (N. Diban).

<https://doi.org/10.1016/j.seppur.2018.03.044>

Received 2 February 2018; Received in revised form 20 March 2018; Accepted 21 March 2018  
Available online 22 March 2018

1383-5866/ © 2018 Elsevier B.V. All rights reserved.

were different in most of the reported studies, and the relevant characteristics of the BDD coating were not fully detailed, which could explain the diverse electrochemical responses of BDD encountered in the literature.

Many important features of the BDD coatings are known to influence their electrochemical performance as electrodes, including the boron doping concentration, the surface morphology and roughness, the grain size, the content of non-diamond impurities, the surface termination (H or O), and the  $sp^3/sp^2$  carbon ratio of the diamond [5,9,25–28]. The grain size and the surface morphology of BDD electrode depend basically on the operating conditions of the chemical vapor deposition (CVD) synthesis [4,29–32]. CVD leads to the following categories of BDD electrodes: microcrystalline diamond (MCD), nanocrystalline diamond (NCD) and ultrananocrystalline diamond (UNCD). MCD films exhibit grain sizes larger than 1  $\mu\text{m}$  and roughness values that exceed 100 nm [4,33]. However, some applications require much smoother surfaces implying that the grain microsize has to be reduced to the nanoscale. NCD coatings exhibit grain sizes between 10 nm and 1  $\mu\text{m}$ , with low to moderate amounts of  $sp^2$ -bonded carbon trapped at defects or grain boundaries. UNCD is the newest material of the diamond coatings family which has attracted significant interest due to its high uniformity, high boundary density and ultra-smooth surface morphology [33–36]. UNCD possesses extremely low grain size (< 10 nm) and roughness (< 100 nm) [4,33]. Though, the small grain size and high grain boundary density of UNCD can facilitate the incorporation of graphitic carbon [35].

In this context, the present work aims to investigate and compare the effect of the surface and crystalline features of two commercial BDD anodes on their electrochemical performance for PFOA electrolysis. The BDD samples used in this study were an UNCD electrode from Advanced Diamond Technologies and a MCD electrode supplied by Adamant Technologies. Great attention has been paid to the effect of the diamond carbon content, boron doping level and the hydrogen contained in the surface, which can play a fundamental role in determining the electrical conductivity and the global electrochemical response of the BDD electrodes.

## 2. Materials and methods

### 2.1. Electrode materials and chemical reagents

All chemicals used in the experiments were reagent grade or higher and were used as received without further purification. PFOA ( $\text{C}_7\text{F}_{15}\text{COOH}$ , 96% purity) was purchased from Sigma Aldrich Chemicals. Ammonium acetate ( $\text{CH}_3\text{COONH}_4$ ) and methanol (UHPLC-MS) were obtained from Scharlau. Sodium sulfate (Panreac) 5  $\text{g L}^{-1}$  was used as electrolyte in every electro-oxidation test. All solutions were prepared using ultrapure water (Q-POD Millipore). PFOA aqueous solution with initial concentration 0.24  $\text{mmol L}^{-1}$  were prepared.

The commercial MCD anode was purchased from Adamant Technologies (Neuchatel, Switzerland) as part of a flow-by cell (Diacell 106). The UNCD anode was obtained from Advanced Diamond Technologies (Romeoville, U.S.A.). The MCD anode was formed by a diamond coating of thickness 2–3  $\mu\text{m}$ , synthesized by hot filament CVD on a monocrystalline p-Silicon circular substrate, with 70  $\text{cm}^2$  of geometrical area. The UNCD anode was made of a boron doped ultrananocrystalline diamond coating of 2  $\mu\text{m}$  film thickness and 3–5 nm average grain size, on a niobium substrate (42  $\text{cm}^2$  of geometrical area). Additionally, three commercial BDD electrodes were purchased from NeoCoat SA (Switzerland) for boron doping calibration (100, 2500 and 10,000 ppm of boron, respectively). The latter electrodes were fabricated by hot filament CVD to give a polycrystalline diamond film with 2–3  $\mu\text{m}$  thickness on a p-Silicon substrate, similarly to the MCD anode previously described.

**Table 1**

Description of the experimental conditions and anode geometry for the electro-oxidation experiments.

Characteristic	MCD system	UNCD system
Anode geometry	Circular	Rectangular
Anode surface area ( $\text{cm}^2$ )	70	42
Inter-electrode gap (mm)	5	8
Feed volume (L)	1	0.5
Flow-rate ( $\text{m}^3 \text{s}^{-1}$ )	$5 \cdot 10^{-5}$	$1.1 \cdot 10^{-4}$
Linear velocity ( $\text{m s}^{-1}$ )	0.11 <sup>a</sup>	0.16
Anode substrate	Silicon	Niobium
Cathode	Stainless steel	Tungsten

<sup>a</sup> Linear velocity was calculated at the central position of the circular electrode.

### 2.2. Electrochemical oxidation of PFOA by BDD electrodes

The electrochemical performance of MCD and UNCD anodes was analyzed by the study of PFOA electrolysis in aqueous solutions. The diagram of the experimental set-up used for the electrooxidation experiments is provided as supplementary information (Fig. S1) [14]. Electrolysis tests were carried out in two undivided electrochemical cells, both of them consisting of two parallel electrodes. The feed solution was stored in a feed tank, pumped through the inter-electrode channel at a high linear velocity and recirculated to the feed reservoir. Table 1 collects the details of the experimental conditions applied for each electrochemical cell. The feed volume was adapted to get similar anode area/volume ratios for both experimental systems. The cell was connected to a power supply (Agilent 6654 A) and comparative experiments for MCD and UNCD anodes were conducted under galvanostatic control at  $j = 5 \text{ mA cm}^{-2}$ . Moreover, different current densities were applied for MCD ( $j = 1$  and  $2 \text{ mA cm}^{-2}$ ) and UNCD ( $j = 10$  and  $20 \text{ mA cm}^{-2}$ ) to study the current density effect on the PFOA and total organic carbon (TOC) removal rates. The applied current densities were selected to allow appropriate evaluation of PFOA degradation kinetic during a 4-hour experiment accordingly to the dissimilar electrochemical responses observed for UNCD and MCD anodes, respectively. Every experiment was conducted in batch mode at constant temperature of  $293 \pm 2 \text{ K}$ . The initial PFOA concentration of the prepared solution was set at 0.24  $\text{mmol L}^{-1}$  to represent a concentration within the range reported in the literature dealing with PFASs electrochemical oxidation (Table S1, supplementary information). Treated samples were withdrawn from the feed tank at regular time intervals and preserved at 4 °C until analysis. The cell voltages during the electro-oxidation experiments at 5  $\text{mA cm}^{-2}$  were 5.6 and 4.9 V, for MCD and UNCD systems, respectively.

### 2.3. BDD anodes characterization

The surface morphology of the BDD anodes was determined using field emission scanning electron microscopy (FESEM, JEOL JSM, 7000-F) at 10 kV. The Raman spectra were taken at room temperature under atmospheric pressure in backscattering geometry with a Horiba T64000 triple spectrometer using the 514.5 line of a Coherent Innova Spectrum 70C  $\text{Ar}^+ \text{-Kr}^+$  laser and a nitrogen-cooled CCD (Jobin-Yvon Symphony) with a confocal microscope and a 100 $\times$  objective for detection. The power on the sample was kept below 4 mW to avoid laser-heating effects on the probed material and the concomitant softening of the observed Raman peaks. Lorentzian fitting of the Raman spectra was done using Origin 8 software. The relative  $sp^3/sp^2$  band ratios were determined by deconvolution of the spectra obtained from X-ray photoelectron spectroscopy (XPS), using an SPECS (Berlin, Germany) system equipped with a Phoibos 150 1D-DLD analyser and monochromatic Al K $\alpha$  radiation (1486.6 eV). Data analysis was carried out using Casa XPS 2.3.16 Software to fit the signals to Gauss-Lorentzian curves, after

removing the background (Shirley).

#### 2.4. Analytical procedures

PFOA concentration in the MCD experiments, was determined by HPLC-TQD mass spectrometry (Acquity, Waters), and the X-Bridge BEH C18 (2.5  $\mu\text{m}$ , 2.1  $\times$  75 mm) column. The eluents were: (i) an aqueous solution containing ammonium acetate ( $\text{CH}_3\text{COONH}_4$ ) 2  $\text{mmol L}^{-1}$  and 5% of methanol, and (ii) pure methanol. The eluent flow rate was 0.15  $\text{mL min}^{-1}$ . The limit of quantification (LOQ) was 1  $\mu\text{g L}^{-1}$ . For experiments using the UNCD anode, the PFOA content was analyzed using HPLC-DAD (Water 2695) equipped with a X Bridge C18 column (5  $\mu\text{m}$ , 250 mm  $\times$  4.6 mm, Waters). A mixture of methanol (65%) and di-hydrogen phosphate (35%) was used as mobile phase in isocratic mode with a flow rate of 0.5  $\text{mL min}^{-1}$ . The wavelength of the detector was set at 204 nm. The LOQ was 7.4  $\text{mg L}^{-1}$  [37]. Total organic carbon (TOC) analyses were performed using a TOC-V CPH (Shimadzu). Fluoride was analyzed by ion chromatography (Dionex 120 IC) provided with an IonPac As-HC column and using a 9  $\text{mmol L}^{-1}$   $\text{Na}_2\text{CO}_3$  solution as eluent, that was circulated at a flowrate of 1  $\text{mL min}^{-1}$ , based on Standard Methods 4110B [38]. The LOQ for fluoride analysis was 0.03  $\text{mg L}^{-1}$ .

### 3. Results and discussion

#### 3.1. PFOA electrolysis

Fig. 1 reports the effect of the applied current density on the PFOA removal rate using MCD (Fig. 1a) and UNCD (Fig. 1b) anodes. Different electrochemical responses were observed for both materials. MCD anode allowed a sharp abatement of PFOA, which was almost completely degraded in only 4 h, independently of the applied current density.

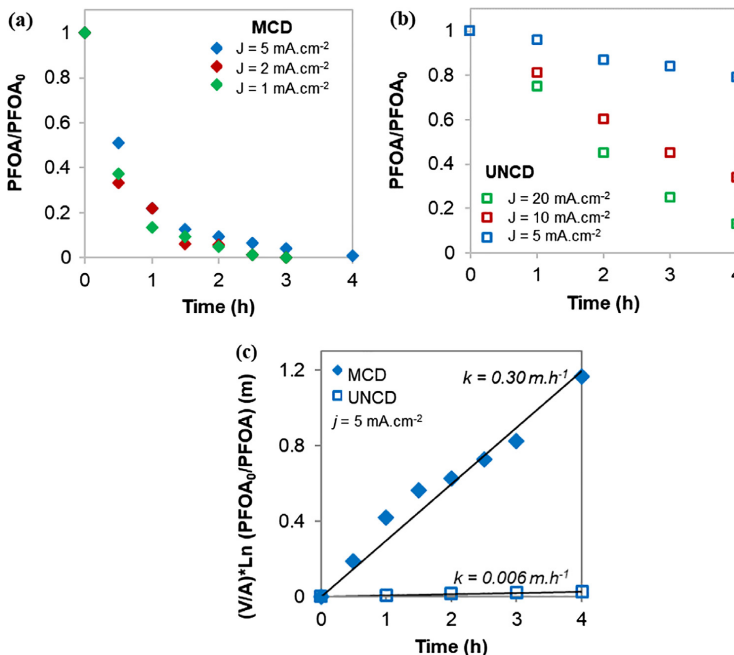


Fig. 1. Influence of the applied current density on PFOA removal with the treatment time, using: (a) MCD ( $j = 1, 2$  and  $5 \text{ mA cm}^{-2}$ ) and (b) UNCD ( $j = 5, 10$  and  $20 \text{ mA cm}^{-2}$ ). (c) Fitting of the experimental data obtained at  $j = 5 \text{ mA cm}^{-2}$  to the kinetic model (Eq. (2)) for both electrodes. The experimental standard deviation of MCD anode (a) was in the range of 10–15% and therefore experimental curves at  $j = 1\text{--}5 \text{ mA cm}^{-2}$  had no significant difference. In the case of UNCD (b), the standard deviation of 3–7% demonstrated that the effect of the current density under the range 5–20  $\text{mA cm}^{-2}$  on PFOA electro-oxidation was statistically significant.  $[\text{PFOA}]_0 = 0.24 \text{ mmol L}^{-1}$ .

Therefore, for the MCD anode, increasing  $j$  in the range 1–5  $\text{mA cm}^{-2}$  had the effect of increasing the energy consumption of the process. On the contrary, the UNCD anode provided significantly slower PFOA degradation kinetics. When using UNCD, 21, 66 and 87% PFOA removals were achieved at  $j = 5, 10$  and  $20 \text{ mA cm}^{-2}$ , respectively. It is worth mentioning that the enhancement of PFOA degradation by sodium sulfate electrolyte as a promoter of secondary oxidant species was considered to be negligible at the low range of current densities applied in the present study [37,39]. Consequently, the remarkable lower PFOA removal ratios alongside the substantial effect of the applied current density observed for the UNCD film resulted in its less efficient electrochemical performance compared to the MCD anode.

The comparison of experimental systems for MCD and UNCD anodes was performed by means of the apparent kinetic rate. The PFOA mass balance in the electrochemical system is written as follows:

$$V \frac{\partial C}{\partial t} = -k A C \quad (1)$$

where  $V$  is the volume of the treated solution (L),  $C$  is the PFOA concentration ( $\text{mmol L}^{-1}$ ) in the feed tank,  $t$  is the electro-oxidation time (h),  $k$  is the apparent first order kinetic constant of PFOA degradation ( $\text{m h}^{-1}$ ) and  $A$  is the electrode surface area ( $\text{m}^2$ ). The integration of Eq. (1) during the length of the experiment ( $t$ ) results in Eq. (2).

$$(V/A) \text{Ln} \left( \frac{C_0}{C} \right) = -k t \quad (2)$$

PFOA removal data using MCD and UNCD electrodes, at the same applied current density  $j = 5 \text{ mA cm}^{-2}$ , were fitted to Eq. (2) in Fig. 1c. The definition of  $k$  allows to remove the effect of the anode area and treated volume for comparison. Table 2 collects the values of  $k$  for MCD and UNCD anodes at the different applied current densities that were tested. In the MCD system, the PFOA decays were fitted to first-order kinetics, and the values of the kinetic constants remained very similar when increasing the applied current densities. This behavior has been

**Table 2**

Apparent kinetic constants  $k$  ( $\text{m h}^{-1}$ ) for the PFOA electro-oxidation on BDD anodes and the comparison with previous studies using similar electrodes. Reference [22] studied the degradation of PFHxA instead of PFOA.

MCD/Si (this study)		UNCD/Nb (this study)		UNCD/Nb [15]		MCD/Si (bipolar) [22]	
$j$ ( $\text{mA cm}^{-2}$ )	$k$ ( $\text{m h}^{-1}$ )	$j$ ( $\text{mA cm}^{-2}$ )	$k$ ( $\text{m h}^{-1}$ )	$j$ ( $\text{mA cm}^{-2}$ )	$k$ ( $\text{m h}^{-1}$ )	$j$ ( $\text{mA cm}^{-2}$ )	$k$ ( $\text{m h}^{-1}$ )
1	0.31	5	0.006	3	0.0054	5	0.126
2	0.36	10	0.027	15	0.026		
5	0.30	20	0.048	50	0.086		

previously described in the literature; the degradation of the perfluoroalkyl pollutant occurred through a fast series of reactions in which both direct electron transfer and oxidation by electro-generated hydroxyl radicals took place, and the overall kinetics were controlled by the mass transport of PFOA from the liquid bulk to the anode surface [40,41]. On the other hand, the PFOA decomposition trend obtained by means of UNCD anode at  $j = 5 \text{ mA cm}^{-2}$  could be described by either zero<sup>th</sup>-order or first-order kinetics. Moreover, the values of the kinetic constant were much lower compared to the ones obtained in the MCD system, and they gradually raised when increasing  $j$ . This electrochemical performance pointed out the limited availability of active sites on the surface of UNCD anode for direct electron transfer and hydroxyl radical production, which play the main roles in PFOA electrochemical degradation [23,24].

The kinetic constants obtained in the present study for the UNCD anode are in agreement with the data reported by Schaefer et al. [15] for PFOA electrolysis using an UNCD electrode manufactured by the same provider (Table 2). Furthermore, Soriano et al. [22] studied the electrochemical removal of perfluorohexanoic acid (PFHxA), which contains two fluorinated carbons less than PFOA in the perfluoroalkyl chain, using an electrochemical cell that contained two parallel flow-by compartments made of a central bipolar BDD/Si electrode and two BDD/Si anode and cathode. In the latter case [22], the provider of the BDD electrodes was the same as the manufacturer of the MCD anode used in the present study. The reported kinetic constant for PFHxA ( $870 \text{ mg L}^{-1}$ ) removal was  $0.13 \text{ m h}^{-1}$  at  $j = 5 \text{ mA cm}^{-2}$ , that is moderately slower than the PFOA degradation constant using the MCD anode in the present work ( $0.30 \text{ m h}^{-1}$ ), although  $k$  values were still within the same order of magnitude. The comparison of the kinetic constants of both MCD and UNCD anodes together with the results reported in the literature indicates that the PFOA degradation rates provided by UNCD/Nb electrodes were much slower than in case of using MCD/Si.

In addition, PFOA mineralization was confirmed by the progress of TOC disappearance and the fluoride release using MCD and UNCD anodes (Fig. 2a). Similarly to PFOA removal trends, the reduction of

TOC was influenced by the type of anode. At  $j = 5 \text{ mA cm}^{-2}$  and  $t = 4 \text{ h}$ , TOC was reduced by 89% using MCD, whereas only 13% TOC decrease was obtained using the UNCD anode. The effective cleavage of C–F bonds was verified by the release of fluoride in the solution (Fig. 2b). The final  $\text{F}^-$  concentration was  $0.7$  and  $0.3 \text{ mmol L}^{-1}$  for MCD and UNCD systems, respectively, after 4 h of the treatment at  $j = 5 \text{ mA cm}^{-2}$ . These results are in agreement with the higher PFOA decomposition rate on the MCD electrode.

Moreover, previous research [20,42] discussed the role of the fluoride released upon PFOA degradation on the anode surface fluorination. This mechanism could improve PFOA degradation, as reported for F-doped Ti/SnO<sub>2</sub> electrodes [43]. Thus, in order to investigate the influence of fluoride, additional tests were carried out with the MCD anode at  $j = 5 \text{ mA cm}^{-2}$ , by adding sodium fluoride to the feed solution. Similar first-order PFOA removal rates ( $0.27$  and  $0.26 \text{ m h}^{-1}$ , respectively) were observed when adding  $20$  and  $50 \text{ mg L}^{-1}$  of fluoride, that were similar to the degradation kinetics obtained without any extra fluoride addition. In the same way, TOC depletion was not accelerated by the addition of the different contents of  $\text{F}^-$  into the reacting media. Moreover, to contrast if higher current densities than those used in the present system could promote the fluorine formation, a test was done at  $20 \text{ mA cm}^{-2}$ . The kinetics observed in Fig. S2 (Supplementary information) for TOC removal, did not reflect any improvement to those experiments done at lower  $j$ . Therefore, the PFOA electrochemical oxidation by means of MCD anodes was not enhanced by the fluoride released into the solution during the degradation process.

### 3.2. Characterization of the BDD electrodes and its influence on PFOA electrolysis

According to the literature [5,26,44], the anodic reactions on BDD electrodes could be influenced by (i) boron doping level, (ii) morphological features and (iii) diamond carbon content, as it has been described for other organic compounds. Therefore, due to the different electrochemical response of the two commercial BDD anodes that have been found in this study as well as the diverse results of PFAS removal

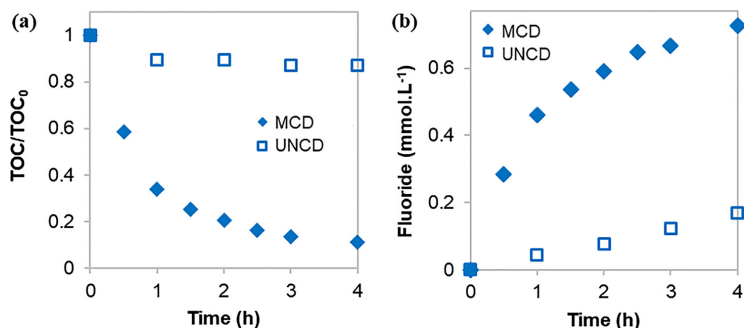


Fig. 2. Evolution of: (a) TOC/TOC<sub>0</sub> and (b) fluoride concentration with the electrolysis time, using MCD and UNCD anodes at  $j = 5 \text{ mA cm}^{-2}$ .  $[\text{PFOA}]_0 = 0.24 \text{ mmol L}^{-1}$ .

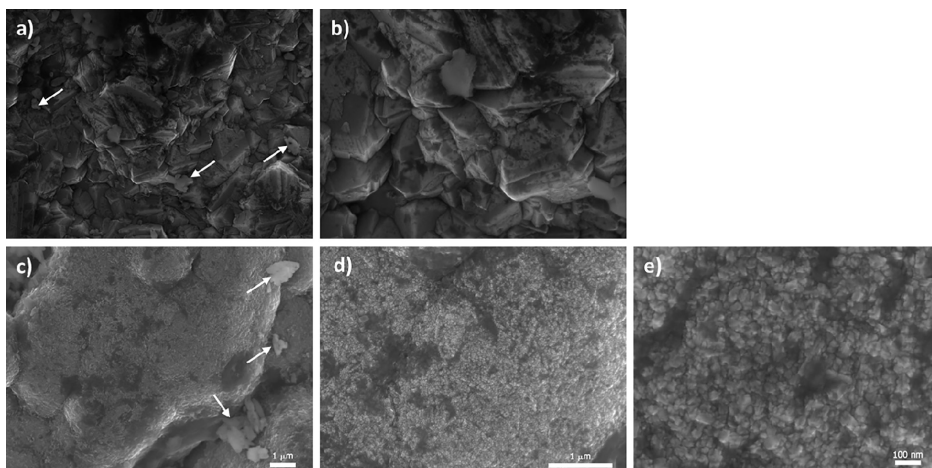


Fig. 3. FESEM surface images of MCD at  $\times 10,000$  (a) and  $\times 25,000$  magnification (b), and UNCD at  $\times 10,000$  (c),  $\times 25,000$  (d) and  $\times 100,000$  magnification (e). Scale bars indicated for each magnification. Arrows indicate dirtiness of salt deposits on the anode surface after the experiments.

rates reported in the literature (Table S1), the surface chemical and morphological characterization of MCD and UNCD anodes was studied to elucidate its effect on PFOA electrolysis.

Fig. 3 shows FESEM surface images of the MCD and UNCD anodes. The FESEM images confirm the information provided by the manufacturers. At  $\times 10,000$  and  $\times 25,000$  magnifications MCD shows the expected microcrystalline structure with crystal grains in the range of approximately 1–3  $\mu\text{m}$  while at the same magnifications, the crystals cannot be appreciated in the UNCD anode. Nevertheless, at  $\times 100,000$  magnification nanocrystal grains ranging approximately between 2 and 25 nm could be observed in UNCD surface [45]. The surface images present well faceted microcrystalline diamond for MCD and line-granular ultrananocrystalline diamond for UNCD film [35]. Moreover, it is worth mentioning that the diamond grains were homogeneously distributed over the anode surface and no cracking defects were appreciated.

Fig. 4 presents Raman spectra obtained for MCD (Fig. 4a) and UNCD (Fig. 4b) anodes [35,46]. The values of the peaks were determined by deconvolution of Raman spectra using Lorentzian functions (green lines). MCD Raman spectra showed a sharp characteristic peak of microcrystals of diamond facet  $\{111\}$  at  $1329\text{ cm}^{-1}$  slightly shifted from the typical  $1333\text{ cm}^{-1}$ , characteristic of pure diamond microcrystals. Indeed, its actual position depends on the boron concentration in the diamond lattice, and moves to lower wavenumbers with increasing boron concentration, as reported by [47,48]. The characteristic peaks at  $1350$  and  $1550\text{ cm}^{-1}$  of D ( $\text{sp}^2$  carbon impurities) and G (non-diamond  $\text{sp}^2$ -bonded carbon atoms in the grain boundaries, C–H bending bonds) bands respectively could be also observed (peaks at  $1387$  and  $1547\text{ cm}^{-1}$  in Fig. 4a).

On the contrary, UNCD surface (Fig. 4b) presents a wide peak at  $1327\text{ cm}^{-1}$  combining the  $\text{sp}^2$  diamond at  $1333\text{ cm}^{-1}$  and a more dominant D band ( $1310$ – $1450\text{ cm}^{-1}$ ) coming from the presence of disordered carbon at the grain boundary [35,49]. Besides G band characteristic of  $\text{sp}^2$  carbon at  $1535\text{ cm}^{-1}$ , as well as the G' band at  $2515\text{ cm}^{-1}$  could be identified in UNCD anode. The peak at  $1175\text{ cm}^{-1}$  which was formerly [49] ascribed wrongly to transpolyacetylene (typically at  $1150\text{ cm}^{-1}$ ), has been demonstrated to actually correspond to  $\text{CH}_x$  bonds in the grain boundaries of nanocrystalline diamonds [50]. The UNCD spectrum in Fig. 4b is a typical Raman spectrum of ultrananocrystalline diamonds using a laser excitation at  $514\text{ nm}$ . According

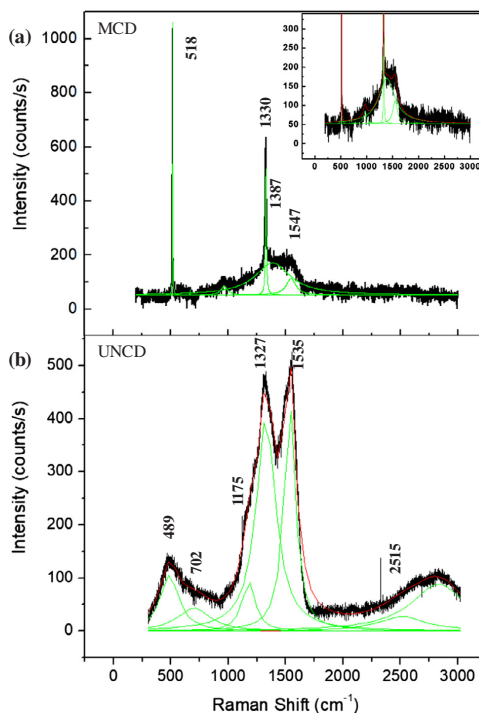


Fig. 4. Raman spectra of (a) MCD and (b) UNCD electrodes. The values of the peaks were determined by deconvolution of Raman spectra using Lorentzian functions within the software Origin 8 (green lines). (For interpretation of the references to colour in this figure legend, the reader is referred to the web version of this article.)

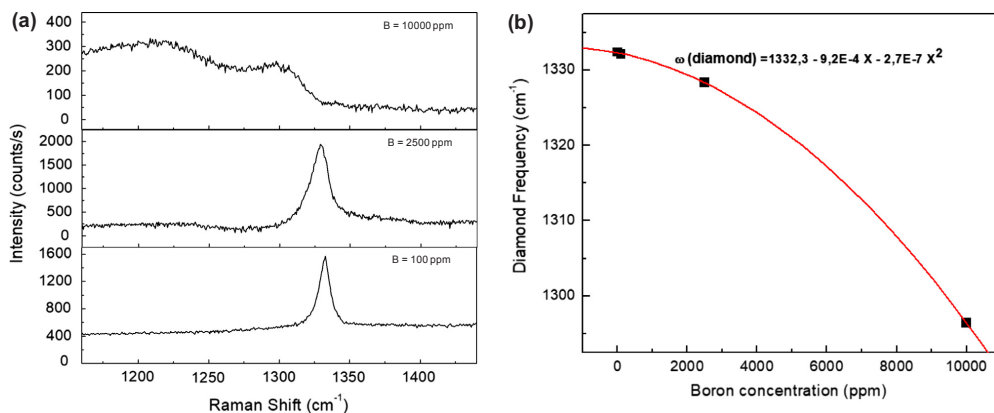


Fig. 5. (a) Raman spectra of microcrystalline BDD standards with different boron concentration: 10,000 ppm, 2500 ppm and 100 ppm. (b) Diamond frequency ( $\text{cm}^{-1}$ ) as a function of the boron concentration (ppm) in BDD standards obtained from Raman spectroscopy.

to the literature [4], the small diamond grain size in the UNCD electrode produced a large presence of graphite in the boundary layers that scattered phonons to make the D peak intensity at  $1357 \text{ cm}^{-1}$  being  $\sim 57$  times larger than the diamond peak at  $1333 \text{ cm}^{-1}$ .

The displacement of the diamond peak to lower frequencies in microcrystalline BDD materials is proportional to the increase of boron content, according to May et al. [46]. This property has been applied in the present work to determine the concentration of boron in the diamond lattice of the MCD electrode. A calibration curve was built using 3 commercial microcrystalline BDD electrodes (NeoCoat, Switzerland) as standards with known boron concentrations of 100, 2500 and 10,000 ppm, respectively. Fig. 5a shows the Raman spectra for each BDD standard and the displacement of the Raman shift of the diamond peak for each standard was determined. The pure diamond peak frequency was used as reference (0 boron concentration,  $1333 \text{ cm}^{-1}$ ). The calibration curve that relates the boron concentration with the diamond Raman vibration frequency in  $\text{cm}^{-1}$  is represented in Fig. 5b. From this calibration curve, the boron concentration for the MCD electrode was calculated as 1676 ppm. Similarly for boron doped ultrananocrystalline diamonds, it has been reported [35] that the D band peak shifted from  $1355 \text{ cm}^{-1}$  at B/C ratios of 0 ppm towards  $1300 \text{ cm}^{-1}$  at B/C ratios of 6000 ppm. A comparison between the Raman spectrum of the UNCD anode and the Raman spectra of ultrananocrystalline BDDs at different boron doping levels reported by Zeng et al. [35] indicated that our UNCD anode would have a boron content of approximately 3000 ppm.

For further surface characterization, Fig. 6 depicts the XPS C 1s spectra of the MCD and UNCD anodes. The peak at  $284.5 \pm 0.1 \text{ eV}$  was labelled as C-C<sub>1</sub> and the component C-C<sub>2</sub> was shifted +0.9 eV. These peaks were attributed to hydrogenated and non-hydrogenated carbon diamond, respectively [51,52]. The peak at  $283.4 \pm 0.3 \text{ eV}$  was ascribed to C=C sp<sup>2</sup> carbon or graphitic defects at the diamond surface and oxygenated carbon species were detected at higher binding energies: 286.5, 287.5 and 289.3 eV for single oxidized components (C-O) such as i.e. -C-OH and -C-O-C- bonds, and further oxidized groups as -C=O or -COOH [51]. The oxidized carbon species typically appear after usage as a result of anode ageing. The B-C peak of boron doped diamonds that should appear at approximately 282.6 eV is not usually observed in these materials due to the presence of surface defects that affect the surface Fermi level [52]. It can be seen that the major component of the MCD surface is C-C<sub>2</sub> or sp<sup>3</sup> crystal diamond carbon (56.0%), the contribution of C-C<sub>1</sub> or hydrogenated diamond was 16.1%, the total oxygenated species were 23.3% and graphitic defects counted up to 4.6% of the total carbon of the MCD anode. On

the other hand, the major component of UNCD anode is hydrogenated diamond carbon (C-C<sub>1</sub>) with 35.2%, non-hydrogenated diamond (C-C<sub>2</sub>) accounted for 31.1%, the graphitic carbon was 5.4% and oxidized species were 28.3% of the total carbon. Hydrogen-terminated diamond (C-C<sub>1</sub>) is produced during the BDD synthesis under H<sub>2</sub>-rich conditions to avoid the formation of graphitic carbon at grain boundaries [4]. The higher content of (C-C<sub>1</sub>) of the UNCD is related to the smaller (ultrananano) grain size and consequently higher grain boundary density [52]. The amount of oxygenated species on both diamond films was comparable (23.3 vs 28.3% for the MCD and UNCD anodes, respectively), which is related to the formation of hydroxyl radicals during the uses of the materials for anodic oxidation [9].

Overall the following remarkable differences about BDD films characterization can be highlighted: (i) the sp<sup>3</sup> diamond relative carbon abundance on the MCD surface is 1.8 times higher than on UNCD surface, (ii) lower boron doping level was found in MCD material compared to UNCD anode, and (iii) the hydrogen-terminated diamond on MCD is 2.2 times lower than in UNCD.

Thus, some studies have demonstrated that higher content of sp<sup>3</sup> carbon resulted in more rapid and efficient contaminant decay by electrochemical oxidation [5,25,26]. Assuming that the sp<sup>3</sup> diamond is the direct responsible of the formation of hydroxyl radicals on the anode surface for electrooxidation applications, a lower abundance on sp<sup>3</sup> diamond carbon would imply lower hydroxyl radical generation per unit anode surface area [25,26]. The sp<sup>2</sup> or graphitic carbon content is very similar in both anodes (MCD = 4.6% and UNCD = 5.4%) and thus, the lower PFOA degradation efficiency of UNCD anode encountered in the present work cannot be justified by differences in the grain boundary graphitic defects. The introduction of boron atoms into the diamond lattice is the main mechanism responsible for the conductivity and the density of active sites on the surface [53]. The anodic materials herein compared present a boron doping level of 1600 (MCD) and 3000 ppm (UNCD). However, despite the higher boron doping level of UNCD anode, the PFOA degradation efficiency was not improved, possibly related to the distortions or defects added into the lattice hindering the electrochemical activity [54,55]. The presence of H-terminated carbon also favors the p-type electrical conductivity on the conductive diamond film surface and enhance the surface hydrophobicity, electron affinity and conductivity [56]. However, the superficial hydrogen content can be progressively changed to O-terminated surface during the electro-oxidation treatments, which would cause the anode surface oxidation and its consequent passivation.

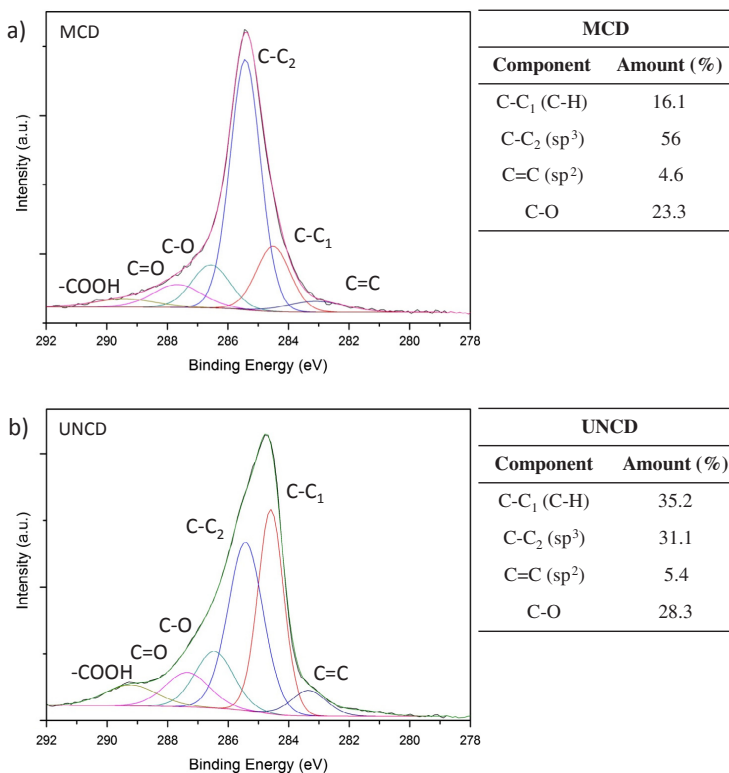


**Fig. 6.** XPS C1s spectra of (a) MCD and (b) UNCD electrodes.  $-\text{COOH}$ ,  $\text{C}=\text{O}$  and  $\text{C}-\text{O}$  were assigned to oxygenated carbon species.  $\text{C}-\text{C}_1$  and  $\text{C}-\text{C}_2$  corresponded to hydrogenated and non-hydrogenated carbon diamond, respectively, and  $\text{C}=\text{C}$  sp<sup>2</sup> refers to the graphitic defects in the diamond surface. Peaks were fitted to the spectra using Gauss-Lorentzian functions.

According to the XPS and Raman analysis, UNCD possessed higher boron doping and more H-terminated superficial carbon content than MCD material, a sum of characteristics that could improve the UNCD p-type superficial conductivity [53,57]. This assumption was verified by the cyclic voltammetry (CV) of PFOA solution using sodium sulfate electrolyte, of both BDD anodes. Fig. S3 given in the Supplementary Data shows that higher current densities were recorded for the UNCD electrode (Fig. S3b), because of its more elevated electrical conductivity. Moreover, a distinctive feature is observed for the MCD anode, as its cyclic voltammogram (Fig. S3a) shows the PFOA direct oxidation peak at a potential close to 2.6 V, which is neither observed in the CV with the single  $\text{Na}_2\text{SO}_4$  electrolyte solution, nor in the case of UNCD anode (Fig. S3b).

Overall, the higher sp<sup>3</sup> carbon content, lower hydrogen terminated carbon and lower conductivity of the MCD film seem to favor the faster and more efficient PFOA degradation. On the contrary, the surface features, such as extremely small grain size, lower sp<sup>3</sup> carbon abundance and higher conductivity, of the UNCD electrode provided a limited electrochemical activity for the PFOA removal.

Finally, the practical feasibility of the electrochemical technology is often linked to the energy consumption. The energy consumption ( $W$ ,  $\text{kWh m}^{-3}$ ) is directly related to the specific electrical charge ( $Q$ ,  $\text{kAh m}^{-3}$ ) and the cell potential ( $v$ ), as described in equation (3) [58]:

$$W = Q \cdot v = \frac{jAt}{V} \cdot v \quad (3)$$

Due to the different electrochemical behavior exhibited by the MCD and UNCD anodes, the energy consumption has been calculated for the maximum PFOA degradation rate obtained in each system, which was 99% and 87% after 4 h of treatment, respectively. In this way, the energy consumption estimated for PFOA removal using MCD was only  $1.4 \text{ kWh m}^{-3}$  ( $j = 1 \text{ mA cm}^{-2}$ ). On the contrary, using UNCD anode would imply shifting to a higher current density ( $j = 20 \text{ mA cm}^{-2}$ ) that implies an estimated consumption of  $52.4 \text{ kWh m}^{-3}$ . These results confirmed that the differences on BDD surface features can influence on the reaction time and the current density needed for the contaminant removal which impacts directly on the energy costs of the electrochemical process.

Additionally, to determine the efficiency of the electro-oxidation process, the decrease in pollutant concentration during electrolysis can be represented against specific electrical charge ( $Q$ ). To illustrate this point, the variation of PFOA degradation rate with  $Q$  was plotted in Fig. S4 in the Supplementary material. It can be seen that for the MCD system, the increase in current density from  $2 \text{ mA cm}^{-2}$  to  $5 \text{ mA cm}^{-2}$  significantly decreased the oxidation efficiency. Therefore, current densities higher than  $5 \text{ mA cm}^{-2}$  only lead to a massive loss of current efficiency in this process. During PFOA electrolysis by UNCD anode (Fig. S4b), the concentration decreased with the increase of specific electrical charge with similar trends for all the applied current densities from 5 to  $20 \text{ mA cm}^{-2}$ . In conclusion, to achieve satisfactory PFOA removal rates, e.g.: 90% removal, the specific electrical charge passed

was two orders of magnitude larger for UNCD anode than MCD electrode.

#### 4. Conclusions

This work reports a morphological, chemical and electrochemical comparison of two BDD electrodes that are commercialized for anodic oxidation. Attending to their crystal size the electrodes are classified as microcrystalline diamond (MCD) and ultrananocrystalline diamond (UNCD). The relationship of the anode surface features with their performance in the electrolysis of perfluorooctanoic acid (PFOA) was analyzed. The following considerations can be withdrawn from the reported results:

- Electrochemical oxidation of PFOA by means of the MCD anode was significantly more efficient than when using the UNCD electrode. The MCD anode led to the complete degradation of the persistent pollutant in 4 h, at any applied current density in the range of 1–5 mA cm<sup>-2</sup>. Conversely, remarkable lower PFOA removal ratios were achieved by the UNCD anode, as only 21% PFOA removal was achieved in 4 h working at 5 mA cm<sup>-2</sup>.
- FESEM microscopy confirmed the micro and ultrananocrystalline structure for MCD and UNCD anodes, respectively. Moreover, the higher sp<sup>3</sup> carbon content and lower boron content and H-terminated carbon content of the MCD, revealed by Raman and XPS spectroscopy, seem to favor faster and more efficient PFOA degradation. On the contrary, the ultrananocrystalline surface features and the higher conductivity of UNCD anode limited the electrochemical activity for PFOA electrolysis.
- Different electrochemical behaviors of the MCD and UNCD BDD anodes strongly impacted the process energy consumption. The energy needed for PFOA removal from a 0.24 mmol L<sup>-1</sup> solution was 1.4 kWh m<sup>-3</sup> and 52.4 kWh m<sup>-3</sup>, for MCD and UNCD anodes, respectively.

#### Acknowledgements

Financial support from the projects CTM2013-44081-R, CTM2016-75509-R and to the Spanish Excellence Network E3TECH (CTQ2015-71650-RDT) (MINECO, SPAIN-FEDER 2014–2020) is gratefully acknowledged. B. Gomez also thanks the FPI research scholarship (BES-2014-071045). Dr. J. Carrillo-Abad is gratefully acknowledged for performing the cyclic voltammograms included in supplementary data.

#### Appendix A. Supplementary material

Supplementary data associated with this article can be found, in the online version, at <https://doi.org/10.1016/j.seppur.2018.03.044>.

#### References

- [1] E. Brillas, C.A. Martínez-Huitle, *Synthetic Diamond Films*, John Wiley & Sons Inc, Hoboken, NJ, USA, 2011.
- [2] R.G. Compton, J.S. Foord, F. Marken, Electroanalysis at diamond-like and doped-diamond electrodes, *Electroanalysis* 15 (2003) 1349–1363, <http://dx.doi.org/10.1002/elan.200302830>.
- [3] M.A. Rodrigo, P. Cañizares, A. Sánchez-Carretero, C. Sáez, Use of conductive-diamond electrochemical oxidation for wastewater treatment, *Catal. Today* 151 (2010) 173–177, <http://dx.doi.org/10.1016/j.cattod.2010.01.058>.
- [4] J.H.T. Luong, B. Male, J.D. Glennon, K.B. Male, J.D. Glennon, Boron-doped diamond electrode: synthesis, characterization, functionalization and analytical applications, *Analyst* 134 (2009) 1965–1979, <http://dx.doi.org/10.1039/b910206j>.
- [5] F.L. Souza, C. Sáez, M.R.V. Lanza, P. Cañizares, M.A. Rodrigo, The effect of the sp<sup>3</sup>/sp<sup>2</sup> carbon ratio on the electrochemical oxidation of 2,4-D with p-Si BDD anodes, *Electrochim. Acta* 187 (2016) 119–124, <http://dx.doi.org/10.1016/j.electacta.2015.11.031>.
- [6] J.M. Peralta-Hernández, M. Méndez-Tovar, R. Guerra-Sánchez, C.A. Martínez-Huitle, J.L. Nava, A brief review on environmental application of boron doped diamond electrodes as a new way for electrochemical incineration of synthetic dyes, *Int. J. Electrochem. Sci.* 2012 (2012) 1–18, <http://dx.doi.org/10.1155/2012/154316>.

- [7] A. Fernandes, D. Santos, M.J. Pacheco, L. Ciriaco, A. Lopes, Nitrogen and organic load removal from sanitary landfill leachates by anodic oxidation at Ti/Pt/PbO<sub>2</sub>, Ti/Pt/SnO<sub>2</sub>-Sb<sub>2</sub>O<sub>4</sub> and Si/BDD, *Appl. Catal. B Environ.* 148–149 (2014) 288–294, <http://dx.doi.org/10.1016/j.apcatb.2013.10.060>.
- [8] A. Kraft, Doped diamond: a compact review on a new, versatile electrode material – open access library, *Int. J. Electrochem. Sci.* 2 (2007) 355–385, <http://dx.doi.org/10.1021/jo62183k>.
- [9] T.A. Ivandini, Y. Einaga, Polycrystalline boron-doped diamond electrodes for electrocatalytic and electrosynthetic applications, *Chem. Commun.* 53 (2017) 1338–1347, <http://dx.doi.org/10.1039/C6CC08681K>.
- [10] I. Sirés, E. Brillas, M.A. Oturan, M.A. Rodrigo, M. Panizza, Electrochemical advanced oxidation processes: today and tomorrow. A review, *Environ. Sci. Pollut. Res.* 21 (2014) 8336–8367, <http://dx.doi.org/10.1007/s11356-014-2783-1>.
- [11] C. Di Dong, T.S. Chen, C.W. Chen, K.L. Huang, Electrochemical degradation of diethyl phthalate under different operating conditions, *Int. J. Electrochem. Sci.* 11 (2016) 5009–5020, <http://dx.doi.org/10.20964/2016.06.077>.
- [12] A.M. Urriaga, G. Pérez, R. Ibáñez, I. Ortiz, Removal of pharmaceuticals from a WWTP secondary effluent by ultrafiltration/reverse osmosis followed by electrochemical oxidation of the RO concentrate, *Desalination* 331 (2013) 26–34, <http://dx.doi.org/10.1016/j.desal.2013.10.010>.
- [13] A.M. Trautmann, H. Schell, K.R. Schmidt, K.M. Mangold, A. Tiehm, Electrochemical degradation of perfluoroalkyl and polyfluoroalkyl substances (PFASs) in groundwater, *Water Sci. Technol.* 71 (2015) 1569–1575, <http://dx.doi.org/10.2166/wst.2015.143>.
- [14] B. Gomez-Ruiz, S. Gómez-Lavín, N. Diban, V. Boiteux, A. Colin, X. Dauchy, A. Urriaga, Efficient electrochemical degradation of poly- and perfluoroalkyl substances (PFASs) from the effluents of an industrial wastewater treatment plant, *Chem. Eng. J.* 322 (2017), <http://dx.doi.org/10.1016/j.cej.2017.04.040>.
- [15] C.E. Schaefer, C. Andaya, A. Burant, C.W. Condee, A. Urriaga, T.J. Strathmann, C.P. Higgins, Electrochemical treatment of perfluoroctanoic acid and perfluorooctane sulfonate: insights into mechanisms and application to groundwater treatment, *Chem. Eng. J.* (2017), <http://dx.doi.org/10.1016/j.cej.2017.02.107>.
- [16] Pravedourou Konstantinos, Ian T. Cousins, Robert C. Buck, S.H. Korzenowski, Critical review sources, fate and transport of fate, *Environ. Sci. Technol.* 40 (2006) 32–44, <http://dx.doi.org/10.1021/es0512475>.
- [17] X.C. Hu, D.Q. Andrews, A.B. Lindstrom, T.A. Bruton, L.A. Schaidler, P. Grandjean, R. Lohmann, C.C. Carignan, A. Blum, S.A. Balan, C.P. Higgins, E.M. Sunderland, Detection of poly- and perfluoroalkyl substances (PFASs) in U.S. drinking water linked to industrial sites, military fire training areas, and wastewater treatment plants, *Environ. Sci. Technol. Lett.* 3 (2016) 344–350, <http://dx.doi.org/10.1021/acs.estlett.6b00260>.
- [18] K.E. Carter, J. Farrell, Oxidative destruction of perfluorooctane sulfonate using boron-doped diamond film electrodes, *Environ. Sci. Technol.* 42 (2008) 6111–6115, <http://dx.doi.org/10.1021/es703273s>.
- [19] H. Xiao, B. Lv, G. Zhao, Y. Wang, M. Li, D. Li, Hydrothermally enhanced electrochemical oxidation of high concentration refractory perfluorooctanoic acid, *J. Phys. Chem. A* 115 (2011) 13836–13841, <http://dx.doi.org/10.1021/jp207519j>.
- [20] T. Ochiai, Y. Iizuka, K. Nakata, T. Murakami, D.A. Tryk, Y. Koide, Y. Morito, A. Fujishima, Efficient decomposition of perfluorocarboxylic acids in aqueous suspensions of a TiO<sub>2</sub> photocatalyst with medium-pressure ultraviolet lamp irradiation under atmospheric pressure, *Ind. Eng. Chem. Res.* 50 (2011) 10943–10947, <http://dx.doi.org/10.1021/ie1017496>.
- [21] H. Lin, J. Niu, J. Xu, H. Huang, D. Li, Z. Yue, C. Feng, Highly efficient and mild electrochemical mineralization of long-chain perfluorocarboxylic acids (C9–C10) by Ti/SnO<sub>2</sub>-Sb-Ce, Ti/SnO<sub>2</sub>-Sb/Ce-PbO<sub>2</sub>, and Ti/BDD electrodes, *Environ. Sci. Technol.* 47 (2013) 13039–13046, <http://dx.doi.org/10.1021/es4034414>.
- [22] Á. Soriano, D. Gorri, A. Urriaga, Efficient treatment of perfluorohexanoic acid by nanofiltration followed by electrochemical degradation of the NF concentrate, *Water Res.* 112 (2017) 147–156, <http://dx.doi.org/10.1016/j.watres.2017.01.043>.
- [23] Q. Zhuo, S. Deng, B. Yang, J. Huang, B. Wang, T. Zhang, G. Yu, Degradation of perfluorinated compounds on a boron-doped diamond electrode, *Electrochim. Acta* 77 (2012) 17–22, <http://dx.doi.org/10.1016/j.electacta.2012.04.145>.
- [24] Z. Liao, J. Farrell, Electrochemical oxidation of perfluorobutane sulfonate using boron-doped diamond film electrodes, *J. Appl. Electrochem.* 39 (2009) 1993–1999, <http://dx.doi.org/10.1007/s10800-009-9909-z>.
- [25] D. Medeiros De Araújo, P. Cañizares, C.A. Martínez-Huitle, M.A. Rodrigo, Electrochemical conversion/combustion of a model organic pollutant on BDD anode: Role of sp<sup>3</sup>/sp<sup>2</sup> ratio, *Electrochem. Commun.* 47 (2014) 37–40, <http://dx.doi.org/10.1016/j.elecom.2014.07.017>.
- [26] E. Guínea, F. Centellas, E. Brillas, P. Cañizares, C. Sáez, M.A. Rodrigo, Electrochemical properties of diamond in the oxidation of a persistent pollutant, *Appl. Catal. B Environ.* 89 (2009) 645–650, <http://dx.doi.org/10.1016/j.apcatb.2009.01.028>.
- [27] S. Fierro, K. Abe, C. Comminellis, Y. Einaga, Influence of doping level on the electrochemical oxidation of formic acid on boron doped diamond electrodes, *J. Electrochem. Soc.* 158 (2011), <http://dx.doi.org/10.1149/2.050112jes>.
- [28] S. García-Segura, E. Vieira dos Santos, C.A. Martínez-Huitle, Role of sp<sup>3</sup>/sp<sup>2</sup> ratio on the electrocatalytic properties of boron-doped diamond electrodes: a mini review, *Electrochem. Commun.* 59 (2015) 52–55, <http://dx.doi.org/10.1016/j.elecom.2015.07.002>.
- [29] J. Zhang, J.W. Zimmer, R.T. Howe, R. Maboudian, Characterization of boron-doped micro- and nanocrystalline diamond films deposited by water-scale hot filament chemical vapor deposition for MEMS applications, *Diam. Relat. Mater.* 17 (2008) 23–28, <http://dx.doi.org/10.1016/j.diamond.2007.09.010>.
- [30] E. Yasu, N. Ohashi, T. Ando, J. Tanaka, M. Kamio, Y. Sato, H. Kiyota, Hall mobility and carrier concentration of boron-doped homoepitaxially grown diamond (001) films, *Diam. Relat. Mater.* 4 (1994) 59–61, <http://dx.doi.org/10.1016/0925->

- 9635(94)90069-8.
- [31] H. Nagasaka, Y. Teranishi, Y. Kondo, T. Miyamoto, T. Shimizu, Growth rate and electrochemical properties of boron-doped diamond films prepared by hot-filament chemical vapor deposition methods, *E – J. Surf. Sci. Nanotechnol.* 14 (2016) 53–58, <http://dx.doi.org/10.1380/ejsnt.2016.53>.
- [32] M.R. Baldan, A.F. Azevedo, A.B. Couto, N.G. Ferreira, Cathodic and anodic pre-treated boron doped diamond with different  $sp^2$  content: morphological, structural, and impedance spectroscopy characterizations, *J. Phys. Chem. Solids* 74 (2013) 1830–1835, <http://dx.doi.org/10.1016/j.jpcs.2013.07.015>.
- [33] J.V. Macpherson, A practical guide to using boron doped diamond in electrochemical research, *Phys. Chem. Chem. Phys.* 17 (2015) 2935–2949, <http://dx.doi.org/10.1039/c4cp04022h>.
- [34] S. Ohmagari, T. Yoshitake, A. Nagano, R. Ohtani, H. Setoyama, E. Kobayashi, T. Hara, K. Nagayama, Formation of p-type semiconducting ultrananocrystalline diamond/hydrogenated amorphous carbon composite films by boron doping, *Jpn. J. Appl. Phys.* 49 (2010), <http://dx.doi.org/10.1143/JJAP.49.031302>.
- [35] H. Zeng, A.R. Konicek, N. Moldovan, F. Mangolini, T. Jacobs, I. Wylie, P.U. Arumugam, S. Siddiqui, R.W. Carpick, J.A. Carlisle, Boron-doped ultrananocrystalline diamond synthesized with an H-rich/Ar-lean gas system, *Carbon* N. Y. 84 (2015) 103–117, <http://dx.doi.org/10.1016/j.carbon.2014.11.057>.
- [36] B.P. Chaplin, I. Wyle, H. Zeng, J.A. Carlisle, J. Farrell, Characterization of the performance and failure mechanisms of boron-doped ultrananocrystalline diamond electrodes, *J. Appl. Electrochem.* 41 (2011) 1329–1340, <http://dx.doi.org/10.1007/s10800-011-0351-7>.
- [37] A. Urriaga, C. Fernández-González, S. Gómez-Lavín, I. Ortiz, Kinetics of the electrochemical mineralization of perfluorooctanoic acid on ultrananocrystalline boron doped conductive diamond electrodes, *Chemosphere* 129 (2015) 20–26, <http://dx.doi.org/10.1016/j.chemosphere.2014.05.090>.
- [38] APHA (American Public Health Association), Standard Methods for the Examination of Water and Wastewater, 20th Ed., Washington DC, 1998. doi: ISBN 9780875532356.
- [39] A. Urriaga, A. Soriano, J. Carrillo-Abad, BDD anodic treatment of 6:2 fluorotelomer sulfonate (6:2 FTSA). Evaluation of operating variables and by-product formation, *Chemosphere* (2018). [10.1016/j.chemosphere.2018.03.027](https://doi.org/10.1016/j.chemosphere.2018.03.027).
- [40] M. Mascia, A. Vacca, S. Palmas, A.M. Polcaro, Kinetics of the electrochemical oxidation of organic compounds at BDD anodes: modelling of surface reactions, *J. Appl. Electrochem.* 37 (2007) 71–76, <http://dx.doi.org/10.1007/s10800-006-9217-9>.
- [41] M. Panizza, G. Siné, I. Duo, L. Ouattara, C. Comminelli, Electrochemical polishing of boron-doped diamond in organic media, *Electrochem. Solid-State Lett.* 6 (2003) D17–D19, <http://dx.doi.org/10.1149/1.1619646>.
- [42] B. Guan, J. Zhi, X. Zhang, T. Murakami, A. Fujishima, Electrochemical route for fluorinated modification of boron-doped diamond surface with perfluorooctanoic acid, *Electrochem. Commun.* 9 (2007) 2817–2821, <http://dx.doi.org/10.1016/j.elecom.2007.10.003>.
- [43] B. Yang, C. Jiang, G. Yu, Q. Zhuo, S. Deng, J. Wu, H. Zhang, Highly efficient electrochemical degradation of perfluorooctanoic acid (PFOA) by F-doped Ti/SnO<sub>2</sub> electrode, *J. Hazard. Mater.* 299 (2015) 417–424, <http://dx.doi.org/10.1016/j.jhazmat.2015.06.033>.
- [44] P. Cañizares, C. Sáez, A. Sánchez-Carretero, M.A. Rodrigo, Influence of the characteristics of p-Si BDD anodes on the efficiency of peroxodiphosphate electro-synthesis process, *Electrochem. Commun.* 10 (2008) 602–606, <http://dx.doi.org/10.1016/j.elecom.2008.01.038>.
- [45] Advanced Diamond Technologies, 2016. < <http://www.thindiamond.com/uncd-technology/what-is-uncd/> > (accessed November 20, 2017).
- [46] P.W. May, W.J. Ludlow, M. Hannaway, P.J. Heard, J.A. Smith, K.N. Rosser, Raman and conductivity studies of boron-doped microcrystalline diamond, faceted nanocrystalline diamond and cauliflower diamond films, *Diam. Relat. Mater.* 17 (2008) 105–117, <http://dx.doi.org/10.1016/j.diamond.2007.11.005>.
- [47] P. Szirmai, T. Pichler, O.A. Williams, S. Mandal, C. Bäuerle, F. Simon, A detailed analysis of the Raman spectra in superconducting boron doped nanocrystalline diamond, *Phys. Status Solidi* 249 (2012) 2656–2659, <http://dx.doi.org/10.1002/psbb.201200461>.
- [48] W. Gajewski, P. Achatz, O.A. Williams, K. Haenen, E. Bustarret, M. Stutzmann, J.A. Garrido, Electronic and optical properties of boron-doped nanocrystalline diamond films, *Phys. Rev. B – Condens. Matter Mater. Phys.* 79 (2009) 1–14, [10.1103/PhysRevB.79.045206](https://doi.org/10.1103/PhysRevB.79.045206).
- [49] H. Kuzmany, R. Pfeiffer, N. Salk, B. Günther, The mystery of the 1140  $\text{cm}^{-1}$  Raman line in nanocrystalline diamond films, *Carbon* N. Y. 42 (2004) 911–917, <http://dx.doi.org/10.1016/j.carbon.2003.12.045>.
- [50] V. Mortel, L. Zhang, M. Eckert, J. D’Haen, A. Soltani, M. Moreau, D. Troadec, E. Neyts, J.C. De Jaeger, J. Verbeeck, A. Bogaerts, G. Van Tendeloo, K. Haenen, P. Wagner, Grain size tuning of nanocrystalline chemical vapor deposited diamond by continuous electrical bias growth: experimental and theoretical study, *Phys. Status Solidi Appl. Mater. Sci.* 209 (2012) 1675–1682, <http://dx.doi.org/10.1002/psa.201200581>.
- [51] M. Wang, N. Simon, G. Charrier, M. Bouttemy, A. Etcheberry, M. Li, R. Boukherroub, S. Szunerits, Distinction between surface hydroxyl and ether groups on boron-doped diamond electrodes using a chemical approach, *Electrochem. Commun.* 12 (2010) 351–354, <http://dx.doi.org/10.1016/j.elecom.2009.12.029>.
- [52] D. Ballutaud, N. Simon, H. Girard, E. Rzepka, B. Bouchet-Fabre, Photoelectron spectroscopy of hydrogen at the polycrystalline diamond surface, *Diam. Relat. Mater.* 15 (2006) 716–719, <http://dx.doi.org/10.1016/j.diamond.2006.01.004>.
- [53] R. Bogdanowicz, A. Fabiańska, L. Golunski, M. Sobaszek, M. Gnyba, J. Ryl, K. Darowicki, T. Ossowski, S.D. Janssens, K. Haenen, E.M. Siedlecka, Influence of the boron doping level on the electrochemical oxidation of the azo dyes at Si/BDD thin film electrodes, *Diam. Relat. Mater.* 39 (2013) 122–127, <http://dx.doi.org/10.1016/j.diamond.2013.08.004>.
- [54] S.C. Ramos, A.F. Azevedo, M.R. Baldan, N.G. Ferreira, Effect of methane addition on ultrananocrystalline diamond formation: morphology changes and induced stress, *J. Vac. Sci. & Technol. A – Vacuum Surfaces Film.* 28 (2010) 27–32, [10.1116/1.3259885](https://doi.org/10.1116/1.3259885).
- [55] Y. Feng, J. Lv, J. Liu, N. Gao, H. Peng, Y. Chen, Influence of boron concentration on growth characteristic and electro-catalytic performance of boron-doped diamond electrodes prepared by direct current plasma chemical vapor deposition, *Appl. Surf. Sci.* 257 (2011) 3433–3439, <http://dx.doi.org/10.1016/j.apsusc.2010.11.041>.
- [56] L.S. Andrade, G.R. Salazar-Banda, R.C. Rocha-Filho, O. Fatibello-Filho, B. Cathodic pretreatment of boron-doped diamond electrodes and their use in electroanalysis, in: E. Brillas, C.A. Martínez-Huitle (Eds.), *Synth. Diam. Film. Prep. Electrochem. Charact. Appl.*, John Wiley & Sons, Inc., Hoboken, NJ, USA, 2011.
- [57] G.R. Salazar-Banda, L.S. Andrade, P.A.P. Nascente, P.S. Pizani, R.C. Rocha-Filho, L.A. Avaca, On the changing electrochemical behaviour of boron-doped diamond surfaces with time after cathodic pre-treatments, *Electrochim. Acta* 51 (2006) 4612–4619, <http://dx.doi.org/10.1016/j.electacta.2005.12.039>.
- [58] Á. Anglada, A. Urriaga, I. Ortiz, Contributions of electrochemical oxidation to waste-water treatment: fundamentals and review of applications, *J. Chem. Technol. Biotechnol.* 84 (2009) 1747–1755, <http://dx.doi.org/10.1002/jctb.2214>.

## **SUPPORTING INFORMATION**

### **Comparison of microcrystalline and ultrananocrystalline boron doped diamond anodes: Influence on perfluorooctanoic acid electrolysis**

**Authors:**

**Beatriz Gomez-Ruiz, Nazely Diban\*, Ane Urtiaga**

Department of Chemical and Biomolecular Engineering. University of Cantabria. Av.  
de Los Castros s/n. 39005 Santander. Spain

\* Corresponding Author: [dibann@unican.es](mailto:dibann@unican.es)

Submitted to

Separation and Purification Technology

March 2018

**Table S1.** Summary of the BDD-electrochemical oxidation for PFASs degradation in aqueous media.

Reference	EXPERIMENTAL CONDITIONS				ELECTROCHEMICAL PERFORMANCE	
	Characteristics of BDD	Configuration	$J$ (mA.cm <sup>-2</sup> )	Feed Volume (L)	[PFAS] <sub>initial</sub> (mM)	$k'$ (h <sup>-1</sup> )
Carter and Farrell, 2008 [18]	One bipolar and two monopolar p-Si/BDD electrodes (Adamant Technologies). Total anode area: 25 cm <sup>2</sup>	Parallel plate flow-through reactor	20	2	0.4 mM PFOS	7.8
Liao and Farrell, 2009 [24]	One bipolar and two monopolar p-Si/BDD electrodes (Adamant Technologies). Total anode area: 25 cm <sup>2</sup>	Flow-through reactor	10	0.35 or 0.6	0.4 mM PFBS	(>90 % degradation, 1h)
Ochiai et al., 2011 [20]	BDD electrode (Condias). Anode area: 77.4 cm <sup>2</sup>	Single compartment flow cell	0.15	0.3	8 mM PFOA	0.8
Xiao et al., 2011 [19]	Si/BDD electrode, boron doping of 1300 ppm and thickness of the diamond film is about 1 μm (CVD). Anode area: 5.5 cm <sup>2</sup>	Teflon-lined stainless steel autoclave cell	20	0.4	0.48 mM PFOA	0.108
Zhuo et al., 2012 [23]	Si/BDD (Chinese Academy of Science). Anode area: 8.5 cm <sup>2</sup>	Three-electrode cell	23.24	0.04	0.114 mM PFBA 0.114 mM PFHxA 0.114 mM PFOA 0.114 mM PFDeA	1.992 2.01 2.568 2.73 0.834 1.338 2.142

					0.114 mM PFBS 0.114 mM PFHxS 0.114 mM PFOS
Lin et al., 2013 [21]	Ti/BDD electrode (HF CVD) (Condias). Anode area: 25 cm <sup>2</sup>	Undivided electrochemical cell	10	0.1	0.25 mM PFNA 0.25 mM PFDA
Trautmann et al., 2015 [13]	Nb/BDD electrode (Condias). Anode area: 35 cm <sup>2</sup>	Undivided electrochemical cell	2.3	1	0.0097 mM PFBS 0.0275 mM PFHxS 0.030 mM PFOS
Schaefer et al., 2017 [15]	Nb/Ultrananocrystalline diamond coating (Advanced Diamond Technologies). Anode area: 38 cm <sup>2</sup>	Single compartment flow-by cell	3, 15 and 50 50 15 15	0.25	0.036 mM PFOA 0.020 mM PFOS 0.0007 mM PFOA 0.0012 mM PFOS
Soriano et al., 2017 [22]	One bipolar and two monopolar p-Si/BDD electrodes (Adamant Technologies). Anode area: 140 cm <sup>2</sup>	Undivided cell with two parallel flow-by compartments	50	1	2.17 mM PFHxA

Abbreviations: *j*: applied current density; *k*: degradation kinetic constant; HF CVD: Hot-filament chemical vapor deposition; CVD: Chemical vapor deposition

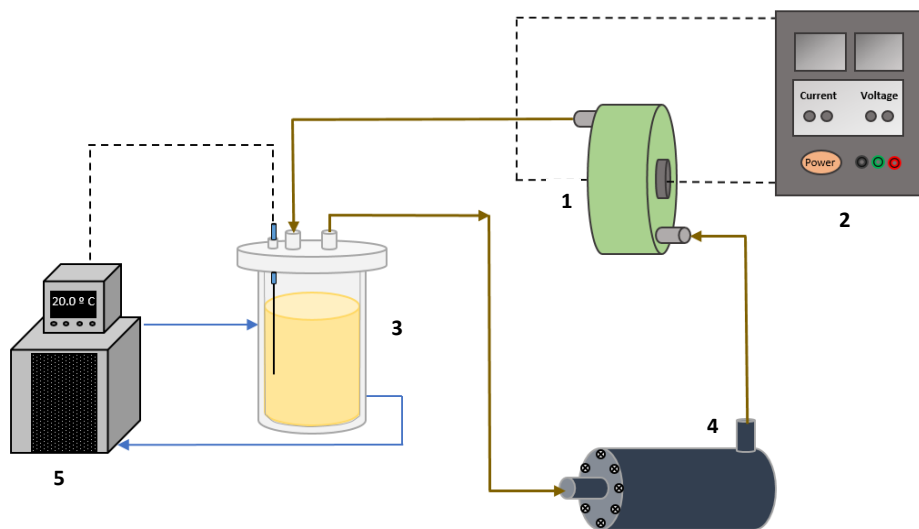


**Figure S1.** Electro-oxidation experimental system (1: Single Compartment Electrochemical Cell, 2: Power Supply, 3: Feed Tank, 4: Pump, 5: Refrigeration System).

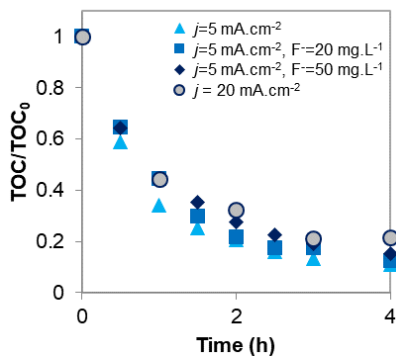


**Figure S2.** Influence of fluoride added in the reacting media on TOC removal with the electro-oxidation time using MCD anode at  $j = 5 \text{ mA.cm}^{-2}$  with no addition of  $F^-$  (▲), at  $j = 5 \text{ mA.cm}^{-2}$  adding  $20 \text{ mg.L}^{-1}$  of  $F^-$  (■), at  $j = 5 \text{ mA.cm}^{-2}$  adding  $50 \text{ mg.L}^{-1}$  of  $F^-$  (◆) and at  $j = 20 \text{ mA.cm}^{-2}$  with no addition of  $F^-$  (○).  $[PFOA]_0 = 0.24 \text{ mmol.L}^{-1}$

Cyclic voltammeteries were performed in a three-electrode cell using 50 mL PFOA (0.24 mmol.L<sup>-1</sup>) and 5 g.L<sup>-1</sup> Na<sub>2</sub>SO<sub>4</sub> as electrolyte. Ag/AgCl saturated KCl electrode was used as the reference electrode and the counter electrode was a Pt foil. MCD and UNCD were used as working electrodes. For these tests, 1x1 cm<sup>2</sup> samples of the commercial electrodes were obtained by fracture of the original ones.

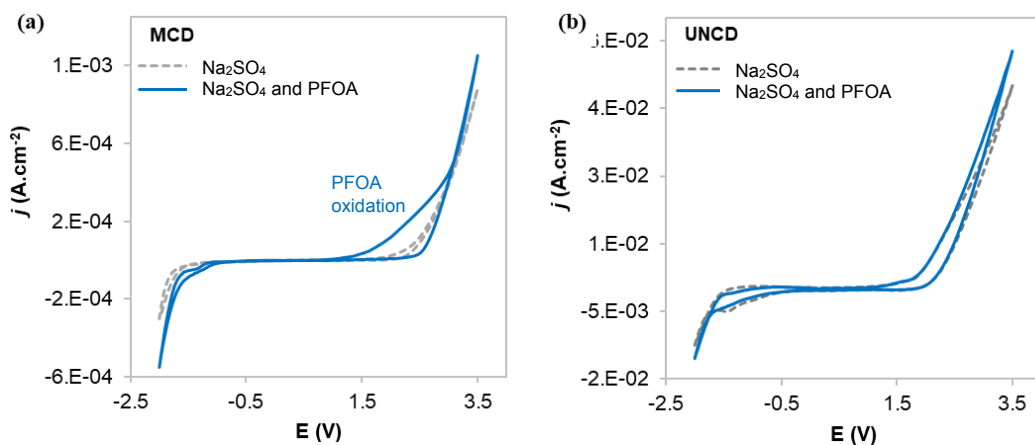


**Figure S3.** Cyclic voltammogram of 0.24 mmol.L<sup>-1</sup> of PFOA (blue lines) in 5 g.L<sup>-1</sup> Na<sub>2</sub>SO<sub>4</sub> solutions for (a) MCD and (b) UNCD anodes, obtained at 100 mV.s<sup>-1</sup> of scan rate. Cyclic voltammograms of single Na<sub>2</sub>SO<sub>4</sub> (dotted lines) are included for comparison.

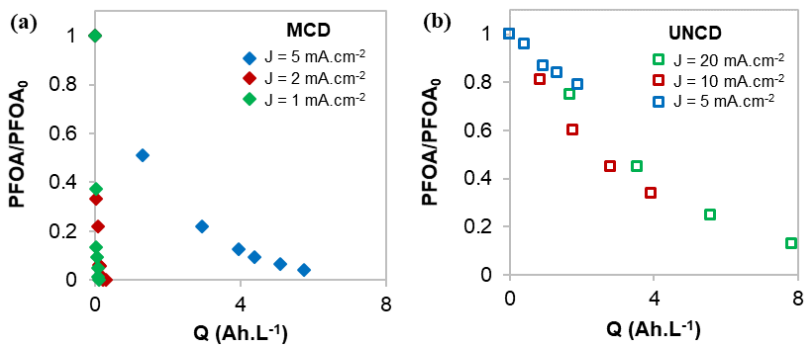


**Figure S4.** PFOA dimensionless evolution as a function of specific electrical charge ( $Q$ ) using: (a) MCD anode ( $j = 1, 2$  and  $5 \text{ mA}\cdot\text{cm}^{-2}$ ) and (b) UNCD anode ( $j = 5, 10$  and  $20 \text{ mA}\cdot\text{cm}^{-2}$ ).  $[\text{PFOA}]_0 = 0.24 \text{ mmol}\cdot\text{L}^{-1}$



## 5.2. Scientific publication 2.

**Boron doped diamond electrooxidation of 6:2 fluorotelomers and perfluorocarboxylic acids. Application to industrial wastewaters treatment**

Authors:

Beatriz Gomez-Ruiz<sup>a</sup>, Sonia Gómez-Lavín<sup>a</sup>, Nazely Diban<sup>a</sup>, Virginie Boiteux<sup>b</sup>, Adeline Colin<sup>b</sup>, Xavier Dauchy<sup>b</sup>, Ane Urtiaga<sup>a</sup>

- a) Department of Chemical and Biomolecular Engineering.  
University of Cantabria. Av. de Los Castros s/n. 39005 Santander.  
Spain
- b) ANSES, Nancy Laboratory for Hydrology, Water Chemistry  
Department, 40 rue Lionnois, 54000 Nancy, France

---

*Accepted 18 May 2017*

*Journal of Electroanalytical Chemistry*

*Volume 798 (2017), Pages 51-57*

DOI: <https://doi.org/10.1016/j.jelechem.2017.05.033>



# Boron doped diamond electrooxidation of 6:2 fluorotelomers and perfluorocarboxylic acids. Application to industrial wastewaters treatment



Beatriz Gomez-Ruiz<sup>a</sup>, Sonia Gómez-Lavín<sup>a</sup>, Nazely Diban<sup>a</sup>, Virginie Boiteux<sup>b</sup>, Adeline Colin<sup>b</sup>, Xavier Dauchy<sup>b</sup>, Ane Urriaga<sup>a,\*</sup>

<sup>a</sup> Department of Chemical and Biomolecular Engineering, Universidad de Cantabria, Av. de Los Castros s/n, 39005 Santander, Spain

<sup>b</sup> ANSES, Nancy Laboratory for Hydrology, Water Chemistry Department, 40 rue Lionnois, 54000 Nancy, France

## ARTICLE INFO

### Keywords:

Poly- and perfluoroalkyl substances (PFASs)  
6:2 FTSA and 6:2 FTAB  
Perfluorocarboxylic acids  
Electrochemical oxidation  
Boron doped diamond anode  
Industrial wastewater

## ABSTRACT

The aim of this study was to determine the viability of electrochemical oxidation to degrade and mineralize poly- and perfluoroalkyl substances (PFASs) in wastewaters from an industrial facility dedicated to the production of side-chain-fluorinated polymers and fluorotelomer-based products for fire-fighting foams. 6:2 fluorotelomer sulfonamide alkylbetaine (6:2 FTAB, 1111 µg/L), 6:2 fluorotelomer sulfonic acid (6:2 FTSA, 242.5 µg/L) and 6:2 fluorotelomer sulfonamide propyl N,N dimethylamine (M4, 34.4 µg/L) were the most abundant PFASs in the industrial wastewater, that also contained perfluorocarboxylic acids (ΣPFCAs, 12.2 µg/L), high TOC and chloride as main anion. 2 L samples were treated in bench scale experiments performed at a current density of 50 mA/cm<sup>2</sup>, in a commercial cell equipped with a boron doped diamond (BDD) anode (70 cm<sup>2</sup>). 97.1% of the initial PFASs content was removed after 8 h of electrochemical treatment. Furthermore, the TOC removal (82.5%) and the fluoride release confirmed the PFASs mineralization. Based on the evolution of the different PFASs, electrochemical degradation pathways were proposed. Fluorotelomers sulfonamides 6:2 FTAB and M4 would be degraded into 6:2 FTSA, which conversely would give rise to PFHpA and preferentially PFHxA. The latter PFCAs were transformed into shorter-chain PFCAs, and eventually into CO<sub>2</sub> and fluoride. The reported results support the technical viability of BDD electrooxidation for the treatment of PFASs in industrial wastewater.

## 1. Introduction

Poly- and perfluoroalkyl substances (PFASs) have been synthesized and widely used in different industrial and commercial applications since the 1950s, including oil and water repellent surface coatings for packing and textiles, surfactants and aqueous fire-fighting foams [1]. PFASs have been detected globally in wildlife and humans, and this group of substances is now recognized as a worldwide health threat. Recent studies reported that PFASs exceed recommended safety levels in public drinking water supplies for 6 million people in the United States [2] and that as many as 100 million people could be at risk from exposure to these chemicals. The United States Environmental Protection Agency established health advisory levels for PFOA and PFOS in drinking water at 0.07 µg/L, both individually and combined [3]. The European Water Directive (2013/39/EU) defined the environmental quality standard (EQS) for the annual average value of PFOS at  $6.5 \times 10^{-4}$  µg/L in inland surface waters [4].

PFASs are released into the environment during their industrial production and application, and as a result of leaching from the PFASs-

containing consumer products [5]. Eventually, PFASs enter wastewater treatment plants (WWTP), which together with landfill sites have been suggested as the major point sources of PFASs to surface waters and to the atmosphere [6–8]. Groundwater contamination is often encountered at or near firefighting training areas where aqueous film-forming foams (AFFFs) have been used [9].

Monitoring of PFASs in WWTP utilities have shown the inefficiency of conventional water treatment technologies to remove PFASs [10,11]. Therefore, there is a need to develop innovative water treatment technologies that enable the removal of this group of persistent and hazardous substances. Electrochemical oxidation is among the most promising technologies for PFASs degradation. It is a versatile option that benefits from working at mild operation conditions and provides high removal efficiency [12–16].

Most of the previous research on PFASs electrochemical treatment was focused on testing different anodic materials, and was conducted with model solutions of a single compound, usually PFOA. In this way, “non-active” anodes such as SnO<sub>2</sub>, PbO<sub>2</sub> and boron doped diamond (BDD) provided high mineralization ratios of some perfluorocarboxylic

\* Corresponding author.

E-mail address: [urriaga@unican.es](mailto:urriaga@unican.es) (A. Urriaga).

<http://dx.doi.org/10.1016/j.jelechem.2017.05.033>

Received 1 March 2017; Received in revised form 11 May 2017; Accepted 18 May 2017  
Available online 19 May 2017

1572-6657/ © 2017 Elsevier B.V. All rights reserved.

(PFCAs) and perfluoroalkane sulfonic acids (PFASs) [13–15,17–20]. In contrast, a poor performance for PFOA degradation was obtained when using “active” anodes, such as Pt, Ti/Ru-IrO<sub>2</sub>, and Ti/SnO<sub>2</sub>-Sb/MnO<sub>2</sub> [14,21]. In order to enhance the treatment efficiency, some studies paid attention to the influence of the operating conditions, such as cell potential, current density and pH, as it has been recently reviewed [22]. However, very few studies have reported the treatment of PFASs in real water samples under environmental conditions. Within this group of pioneering studies, Schaefer et al. [9,23] and Trautmann et al. [24] demonstrated the ability of electrochemical oxidation to remove PFOA, PFOS and other shorter-chain PFCAs and PFASs from groundwaters impacted by the use of AFFFs. Zhang et al. [25] studied the electrochemical treatment of municipal WWTP effluents and reported the efficient removal of PFAS traces. A recently reported study has contributed to a significant scientific progress on the technology for the treatment of industrial wastewaters by obtaining excellent results in the removal of perfluorohexanoic acid (PFHxA) using a hybrid process that combined nanofiltration and electrochemical oxidation using commercial BDD cells [26].

However, the treatment of industrial wastewaters polluted by elevated concentrations of fluorotelomers is still unexplored. More studies need to be conducted to focus on the feasibility and effectiveness of the electrochemical process to remediate PFASs mixtures present over a wider concentration range and under the effect of complex matrix composition with higher organic load background. The lack of studies about the treatment of industrial effluents with a high PFASs load is remarkable, particularly when production of PFASs is recognized as one of the main PFASs emission sources to the environment [1].

The aim of the present study was to investigate the efficiency of electrochemical oxidation to degrade and mineralize a mixture of PFASs of a highly polluted raw industrial wastewater that was generated in a chemical production facility. For this purpose, a bench scale commercial cell provided with a BDD anode was selected. A group of ten PFASs, that included 6:2 fluorotelomer sulfonamide alkylbetaine (6:2 FTAB) and 6:2 fluorotelomer sulfonic acids (6:2 FTSA) as major contributor to the load of PFASs, was monitored along the electrochemical treatment. At the same time, the formation and disappearance of five perfluorocarboxylic acids was analyzed in order to elucidate the degradation pathway followed by fluorotelomers and PFCAs. In addition, the electrochemical treatment allowed the mineralization of the organic pollutant load, using total organic carbon (TOC) as global indicator and the release of fluoride as individual indicator of PFASs mineralization.

## 2. Materials and methods

### 2.1. Materials and water sample

One raw industrial wastewater grab sample (50 L) was collected from the influent to an industrial wastewater treatment utility. The WWTP received the sewage of 4 different manufacturing plants, and only one of them produced side-chain-fluorinated polymers and fluorotelomer-based products, such as 6:2 FTAB and 6:2 FTSA for fire-fighting foams [27]. Its flow accounted for 3 to 17% of the overall WWTP influent flowrate.

The characteristics of the industrial wastewater are summarized in Table 1. The main anions, chloride and sulfate, provided the wastewater with the conductivity required for the electrochemical treatment. Ten individual PFASs were found over the limit of quantification (LOQ) of the analytical method, among the group of 29 PFASs that were included in the monitoring program. The chemical structure of these compounds is provided in Fig. 1, in which the proposed degradation pathways were gathered and will be discussed later. The PFASs profile was dominated by the presence of 6:2 FTAB, 6:2 FTSA and 6:2 fluorotelomer sulfonamide propyl N,N dimethylamine. The latter

**Table 1**  
Characteristics of the raw industrial wastewater and initial PFASs concentration ( $\mu\text{g/L}$ ).

Physico-chemical parameters	
Suspended solids (mg/L)	125
Conductivity (mS/cm)	6.7
pH	8.4
Organic pollutants	
COD (mg/L)	2944
TOC (mg/L)	722
Inorganic compounds	
Sulfate (mM)	1.03
Chloride (mM)	28.4
Ammonium (mM)	5
Fluoride (mM)	< 0.002
Perfluorinated compounds	
PFBS ( $\mu\text{g/L}$ )	0.974
PFBA ( $\mu\text{g/L}$ )	0.496
PFPeA ( $\mu\text{g/L}$ )	3.154
PFHxA ( $\mu\text{g/L}$ )	5.291
PFHpA ( $\mu\text{g/L}$ )	2.793
PFOA ( $\mu\text{g/L}$ )	0.449
6:2 FTSA ( $\mu\text{g/L}$ )	242.496
8:2 FTSA ( $\mu\text{g/L}$ )	0.874
M4 ( $\mu\text{g/L}$ )	34.361
6:2 FTAB ( $\mu\text{g/L}$ )	1111

compound was designated as M4, following the simplified nomenclature reported by Moe et al. [28]. Several PFCAs were also identified, such as PFHxA, perfluoropentanoic acid (PFPeA), perfluoroheptanoic acid (PFHpA), perfluorobutanoic acid (PFBA). On the other hand, perfluorobutane sulfonic acid (PFBS) was the only compound of the group of perfluorosulfonates that was detected in the industrial wastewater. The following list of PFASs were included in the analytical method but were not detected over the LOQ: perfluorohexane sulfonic acid, perfluoroheptane sulfonic acid, perfluoroctane sulfonic acid, perfluorodecanesulfonic acid, perfluorononanoic acid, perfluorodecanoic acid, perfluoroundecanoic acid, perfluorododecanoic acid, perfluorotridecanoic acid, perfluorotetradecanoic acid, 4:2 fluorotelomer sulfonic acid, 6:2, 8:2 and 10:2 fluorotelomer carboxylic acids, 5:3 polyfluorinated acid, 6:2, 8:2 and 10:2 unsaturated fluorotelomer carboxylic acids and perfluorooctane sulfonamide.

### 2.2. Electrochemical experiments

Bench scale electro-oxidation experiments were performed in an undivided cell (Diacell 106, Adamant Technologies, Switzerland) consisting of two circular parallel electrodes: a BDD anode and a stainless steel cathode, each one with a surface area of 70 cm<sup>2</sup> and an electrode gap of 5 mm (Fig. 2). The cell was connected to a power supply (Agilent 6654 A) and experiments were conducted in galvanostatic conditions at a current density of 50 mA/cm<sup>2</sup>. The average cell potential was 11.7 V. The industrial wastewater was filtered using 0.45  $\mu\text{m}$  nitrocellulose filters (Millipore). 2 L samples were used as feed in the experiments that were conducted in batch mode at constant temperature of 20 °C. Treated samples were collected in polypropylene containers, and preserved at 4 °C until delivery for analysis. Each point of the kinetic data was obtained as a single electrochemical experiment, a procedure that allowed to keep the volume constant along the experimental time.

### 2.3. Analytical methods

Detailed protocol of the PFASs analysis has been previously published [29]. Briefly, non-filtered water samples were diluted prior to extraction, purification and pre-concentration by a solid-phase extraction (SPE) procedure (Strata X-AW® (200 mg, 6 mL) cartridge

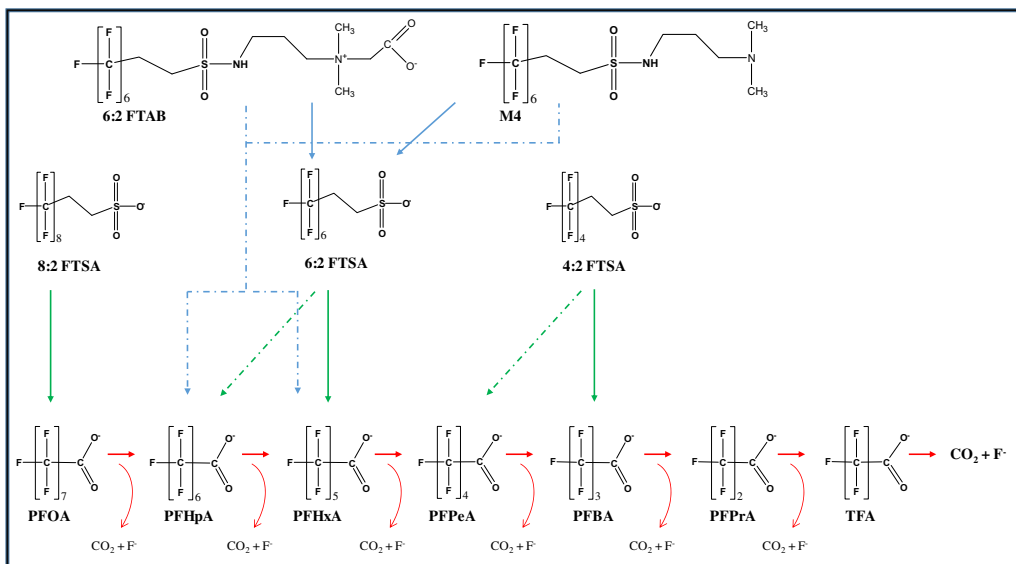


Fig. 1. Proposal for the electrochemical degradation pathway of the group of PFASs observed in the industrial wastewater case of study. Solid lines represent the main degradation pathways, whereas dotted lines show alternative pathways that may also take place.

(Phenomenex, Torrance, CA)). Recovery rates of the SPE procedure were reported elsewhere [29]. An ultra-high performance liquid chromatography coupled to tandem mass spectrometry (UHPLC-MS/MS) in negative electrospray ionisation (ESI) mode was employed to separate and detect targeted compounds (Waters Xevo TQ-MS tandem mass spectrometer (Waters Corporation, Milford, MA, USA)). Twelve labelled internal standards (IS) were used to provide an adequate correction compensating for matrix effects. Considering the initial dilutions, the LOQ in wastewater samples were 0.05 µg/L for 6:2 FTAB and M4, and 0.4 and 1 µg/L for the other PFASs depending on the analytes.

TOC was determined using a TOC-V CPH (Shimadzu) analyzer. Chemical oxygen demand (COD) was measured following the Standard Method 5220D [30]. Ion chromatography was used for anion analysis following the procedure that was detailed elsewhere [26]. Total

ammonium nitrogen (TAN) was determined according to Standard Method 4500-NH<sub>3</sub>. Finally, free chlorine and total chlorine were determined by DPD Ferrous Titrimetric Method. pH was measured using a portable pH-meter.

### 3. Results and discussion

The principal objective of this work was to study the viability and efficiency of the electrochemical oxidation to remediate industrial wastewaters heavily polluted by PFASs. As a whole, the BDD electrochemical treatment achieved 97.1% elimination of the overall ΣPFASs, that was reduced from 1400 µg/L to a final content of 41 µg/L.

Fig. 3 depicts the electrochemical oxidation of the predominant fluorotelomers (6:2 FTAB, 6:2 FTSA and M4). The three compounds include an alkyl chain formed by 8 carbon atoms, 6 of which are fully

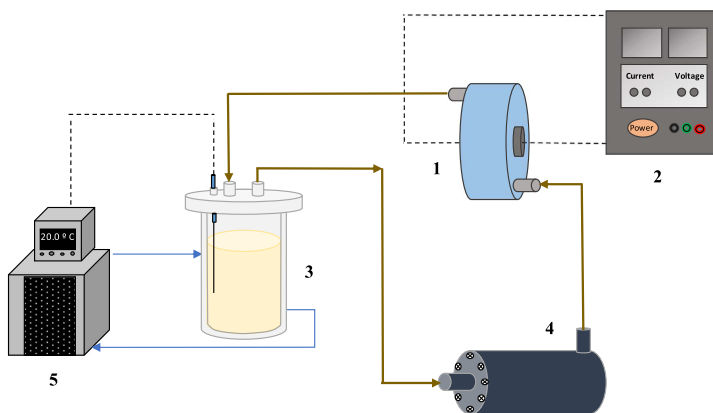


Fig. 2. Electro-oxidation system (1: electro-oxidation cell, 2: power supply, 3: feed tank, 4: pump, 5: cooling system).

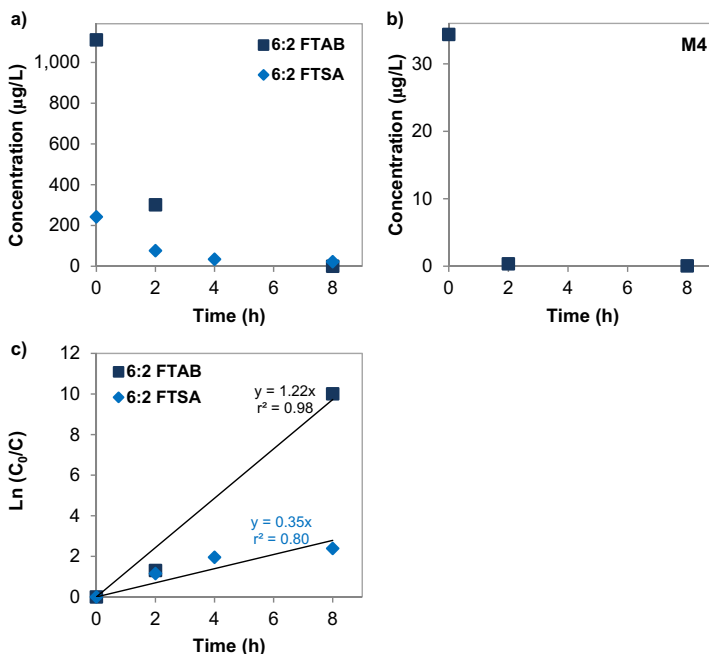


Fig. 3. Change with the treatment time of the main fluorotelomers: a) 6:2 FTAB and 6:2 FTSA, b) M4 and c) fitting of 6:2 FTAB and 6:2 FTSA removal data to a first-order kinetic model.  $j = 50 \text{ mA/cm}^2$ .

substituted by fluorine atoms (see Fig. 1). 6:2 FTAB was the most abundant PFASs in the wastewater sample, with an initial content higher than 1000 µg/L. The electrochemical treatment allowed a fast decrease of 6:2 FTAB that was reduced to 302 µg/L in only 2 h, and a concentration lower than 0.05 µg/L after 8 h of treatment. 6:2 FTAB and 6:2 FTSA removal data were fitted to a first-order kinetic model, as shown in the logarithm plot of Fig. 3c. The resulting pseudo first-order kinetic constant for 6:2 FTAB removal was  $1.22 \text{ h}^{-1}$ , which is significantly faster than the kinetic constant for 6:2 FTSA removal,  $0.35 \text{ h}^{-1}$ . By inspection of the chemical structures depicted in the Fig. 1, the cleavage of the S–N bond by the electrogenerated oxidants would promote the partial conversion of 6:2 FTAB and M4 into 6:2 FTSA, which in these conditions would be simultaneously generated and broken. The formation of 6:2 FTSA as a degradation product of 6:2 FTAB in abiotic conditions has been recently reported. D'Agostino et al. [31] postulated a degradation pathway that involved the activation of molecular oxygen by Fe(II) ions contained in the aqueous solutions to form reactive oxygen species. Formation of 6:2 FTSA through reaction of hydroxyl radicals ( $\cdot\text{OH}$ ) with the sulfur center of the sulfonamide, as was observed for gas phase *N*-methyl perfluorobutane sulfonamide ethanol, has also been described [32].

Fig. 4 shows the change with the treatment time of the PFCAs that were detected in the wastewater sample: PFOA, PFHpA, PFHxA, PFPeA and PFBA. PFOA was initially at low concentration (0.44 µg/L) which passed to 0.96 µg/L at the end of the experiment. This increase was assigned to the decomposition of 8:2 FTSA, that was present in the feed sample at a concentration of 0.87 µg/L. Fang et al. [33] reported the chemical oxidation of 8:2 FTSA into PFOA using hydrogen peroxide and potassium permanganate. These findings support the increase of PFOA observed in the present study during the electrochemical treatment of the industrial wastewaters. PFHxA was the compound with the highest increase in concentration, changing from the initial 5.3 µg/L to a

maximum of 28 µg/L after 6 h of treatment. The peak of PFHxA concentration coincided with the complete depletion of 6:2 FTSA and 6:2 FTAB. In contrast, PFHpA increased only during the initial 2 h, and the variation was not as marked as for PFHxA. The progress of PFHpA and PFHxA revealed that PFHxA is the main product obtained in the degradation of 6:2 fluorotelomers. Our experimental analysis in real industrial wastewaters seems to be in accordance with the mechanisms for 6:2 FTSA splitting reported by Park et al. [34], who found a 25/75 formation ratio of PFHpA/PFHxA upon 6:2 FTSA degradation using heat activated persulfate oxidation. Similarly, the UV-activated hydrogen peroxide oxidation of 6:2 FTSA resulted in a 2-fold formation of PFHxA over PFHpA generation, as reported by Yang et al. [35]. Regarding PFPeA and PFBA (Fig. 4d and e), both compounds followed increasing trends up to 6 h of treatment, in coincidence with the time at which PFHxA started to decrease. This behavior points to the simultaneous formation and consumption of the shorter chain PFCAs.

The evolution of the PFASs analyzed in this work can be described by the degradation pathways gathered in Fig. 1. 6:2 fluorotelomers degradation [35,36] would start with the attack of electrogenerated  $\cdot\text{OH}$  radicals to the C–C and C–H bonds of the two unfluorinated carbons, causing the desulfonation and forming  $\text{C}_6\text{F}_{13}\text{COO}^-$  and  $\text{C}_6\text{F}_{11}\text{COO}^-$ . The degradation of 8:2 FTSA was expected to follow a similar pathway to form PFOA as main secondary product. Once the PFCAs have been formed, the following degradation steps would start with the electron transfer from the carboxyl group to the anode to generate the  $\text{C}_n\text{F}_{2n+1}\text{COO}\cdot$  radical (Eq. (1)). Next, this highly unstable radical would undergo Kolbe decarboxylation to form a perfluoroalkyl radical ( $\text{C}_n\text{F}_{2n+1}\cdot$ ) (Eq. (2)). Then, the electrogenerated hydroxyl radical reacts with the perfluoroalkyl radical to form a perfluoroalcohol  $\text{C}_n\text{F}_{2n+1}\text{OH}$  (Eq. (3)), which is a thermally unstable species that would undergo intramolecular rearrangement to form the perfluoro carbonyl fluoride and release fluoride anion (Eq. (4)). Finally, the latter species

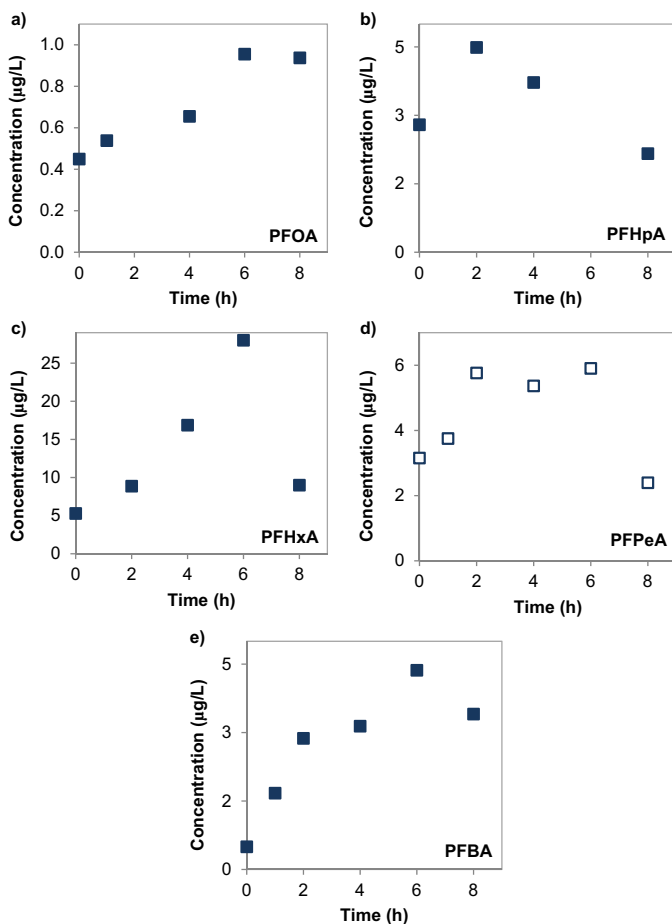
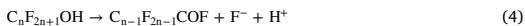
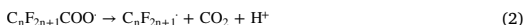


Fig. 4. Change with the treatment time of the main PFCAs: a) PFOA, b) PFHpA, c) PFHxA, d) PFPeA and e) PFBA.  $j = 50 \text{ mA/cm}^2$ .

hydrolyses to give the one-carbon-shorter-chain perfluorocarboxylic acid,  $\text{C}_{n-1}\text{F}_{2n-1}\text{COO}^-$  (Eq. (5)) [14,19,21,36].



The  $\text{C}_{n-1}\text{F}_{2n-1}\text{COO}^-$  repeats the above steps and decomposes into shorter-chain PFCAs by gradually losing a  $\text{CF}_2$  unit. Nevertheless, more studies using model solutions of single fluorinated compounds would be needed to completely assess the proposed degradation pathway.

The change of TOC and the fluoride release with time, shown in Fig. 5, were indicators of mineralization of the overall organic pollutants load. The high TOC content of the industrial wastewaters (see Table 1) revealed that the analyzed PFASs contributed with < 0.1% to the total organic load. Nevertheless, the electrochemical

treatment successfully removed > 80% of TOC after 8 h (Fig. 5), a demonstration of the effectiveness of BDD anodic oxidation for the removal of recalcitrant organic compounds in a variety of chemical compositions. Fig. 5 also shows the evolution of fluoride concentration. Initially,  $\text{F}^-$  concentrations were below the LOQ of the analytical method. Then, the appearance of fluoride was due to PFASs degradation. After 8 h of electrochemical treatment, fluoride increased to 0.012 mM, a value that is significantly below the initial fluoride contained in the analyzed PFASs, 0.034 mM. This difference could be explained by the formation of other shorter-chain PFASs not included as target species or due to the possible fluoride adsorption on the BDD electrode during the mineralization of PFASs, as it has been previously reported when PFOA was electrochemically degraded on BDD [17,37].

The transformation of chloride into other inorganic chlorine species was also evaluated. Fig. 6 shows the evolution of chloride, free chlorine, chlorate and perchlorate. The experimental data show that chloride was transformed into free chloride that was simultaneously oxidized to chlorate. However, the findings recently reported by Schafer et al. [23] demonstrated that chloride in solution had a negligible effect on the kinetics of PFOA and PFOS electrochemical treatment using BDD

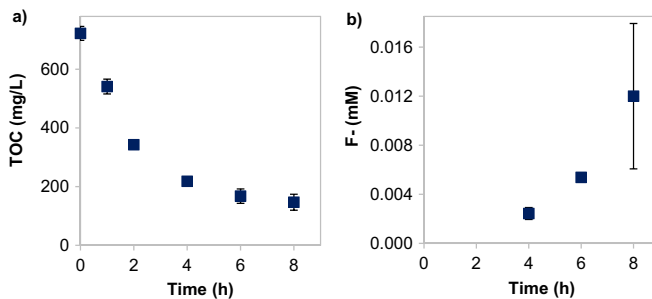


Fig. 5. Reduction of TOC and fluoride release during electrochemical oxidation of the industrial wastewater.  $j = 50 \text{ mA/cm}^2$ . The LOQ of fluoride analysis was 0.002 mM. Data shown as the average of duplicate experiments.

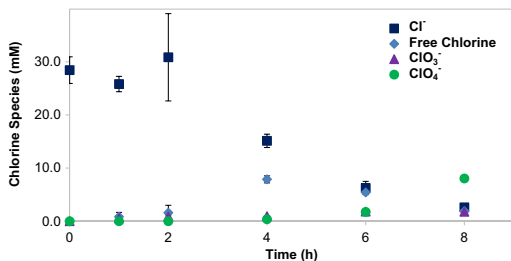


Fig. 6. Change with the treatment time of inorganic chlorine species (chloride, free chlorine, chlorate and perchlorate) during electrochemical oxidation of the industrial wastewater.  $j = 50 \text{ mA/cm}^2$ .

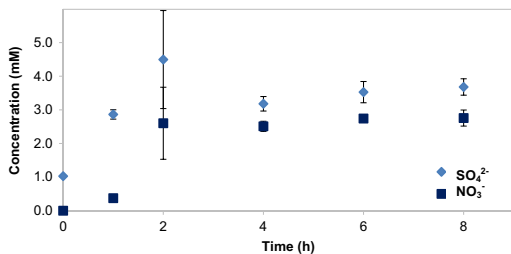


Fig. 7. Change with the treatment time of nitrate and sulfate concentration during electrochemical oxidation of the industrial wastewater.  $j = 50 \text{ mA/cm}^2$ .

anodes. On the other hand, the operating conditions must be carefully selected in order to avoid the formation of undesirable perchlorate [38,39]. It is important to note that in the present study the oxidation of chlorate to perchlorate was significantly delayed and started after 6 h of electrochemical treatment, a behavior that can be explained by the preferential consumption of the electrogenerated hydroxyl radicals for the oxidation of organic compounds. It is not only after most of the organic load and chloride have been oxidized, that hydroxyl radicals are available for perchlorate formation [40,41]. As a result, the formation of undesirable perchlorate was avoided in the period in which > 91% of the initial PFASs content had been degraded.

Nitrate formation was observed during the first 2 h to reach a plateau at 2.8 mM, a value that is lower than the initial 5 mM ammonium concentration of the industrial wastewater (Fig. 7). This result is showing that ammonium was partially converted into gaseous nitrogen, as it typically occurs in the BDD electrochemical removal of ammonium from wastewaters that also contain organic pollutants and

chloride [41–43]. The oxidation of nitrogen in 6:2 FTAB and M4 cannot explain itself the change of nitrate concentration, as it would only contribute to 0.15% of the observed nitrate increase. Similarly, there was a net formation of sulfate that was attributed to the oxidation of unknown sulfur compounds contained in the industrial wastewater (Fig. 7). Nevertheless, the sulfur content of 6:2 FTSA, 6:2 FTAB and M4 could contribute to a maximum of 0.1% of the change in sulfate concentration. Therefore, nitrate and sulfate formation due to the degradation of fluorotelomers contained in the industrial wastewater was observed to be negligible.

One of the key points for the practical feasibility of electrochemical water treatment lies in the reduction of their energy demands. In the present study, the energy consumption for 97% PFASs removal was estimated at 164 kWh/m<sup>3</sup>. In contrast, the extraordinary technical efficiency of BDD electrochemical oxidation has not been reported by any other technique.

#### 4. Conclusions

The present study demonstrated the electrochemical degradation of PFASs contained in the wastewaters generated in an industrial facility dedicated to the production of side-chain-fluorinated polymers and fluorotelomer-based products for fire-fighting foams. The effectiveness of a commercial BDD anode was assessed by studying the evolution of ten PFASs. The most abundant PFASs were 6:2 FTAB, 6:2 FTSA and M4. The BDD anode was able to reduce the PFASs content by 97.1% after 8 h of electrochemical degradation conducted at a current density of 50 mA/cm<sup>2</sup>. While fluorotelomers were completely removed, the degradation of these fluorotelomer compounds gave rise to the formation of PFCAs, being PFHxA the most abundant. However, PFHxA was also converted into shorter chain PFCAs, and eventually mineralized, as it was confirmed by the TOC removal and the release of fluoride. This research contributes to get insight about the electrochemical degradation pathways of fluorotelomers contained in real industrial wastewaters. Future studies should be carried out to verify the suggested mechanisms and determine the presence and the role of possible unknown PFASs.

#### Acknowledgements

This work was supported by the Spanish Ministry of Economy and Competitiveness (CTM2013-44081-R and CTM2016-75509-R). B. Gomez also thanks the FPI postgraduate research grant (BES-2014-071045).

#### References

- [1] K. Prevedouros, I.T. Cousins, R.C. Buck, S.H. Korzeniowski, Critical review sources, fate and transport of fate, *Environ. Sci. Technol.* 40 (2006) 32–44.

- [2] X.C. Hu, D.Q. Andrews, A.B. Lindstrom, T.A. Bruton, L.A. Schaidler, P. Grandjean, R. Lohmann, C.C. Carignan, A. Blum, S.A. Balan, C.P. Higgins, E.M. Sunderland, Detection of poly- and perfluoroalkyl substances (PFASs) in U.S. drinking water linked to industrial sites, military fire training areas, and wastewater treatment plants, *Environ. Sci. Technol. Lett.* 3 (2016) 344–350.
- [3] USEPA, Drinking Water Health Advisory for Perfluorooctanoic Acid (PFOA), (2016), pp. 1–103 <https://www.epa.gov/ground-water-and-drinking-water/drinking-water-health-advisories-pfoa-and-pfos>.
- [4] The European Parliament and the Council of the European Union, Directives of 12 August 2013 amending Directives 2000/60/EC and 2008/105/EC as regards priority substances in the field of water policy, *Off. J. Eur. Union* 2013 (2013) 1–17 <http://eur-lex.europa.eu/legal-content/EN/TXT/?uri=celex:32013L0039>.
- [5] I. Fuentes, S. Gómez-Lavín, M.P. Elizalde, A. Urtiaga, Perfluorinated alkyl substances (PFASs) in northern Spain municipal solid waste landfill leachates, *Chemosphere* 168 (2017) 399–407.
- [6] L. Ahrens, Polyfluoroalkyl compounds in the aquatic environment: a review of their occurrence and fate, *J. Environ. Monit.* 13 (2011) 20–31.
- [7] I. Weinberg, A. Dreyer, R. Ebinghaus, Waste water treatment plants as sources of polyfluorinated compounds, polybrominated diphenyl ethers and musk fragrances to ambient air, *Environ. Pollut.* 159 (2011) 125–132.
- [8] E.F. Houtz, R. Sutton, J.S. Park, M. Sedlak, Poly- and perfluoroalkyl substances in wastewater: significance of unknown precursors, manufacturing shifts, and likely AFFF impacts, *Water Res.* 95 (2016) 142–149.
- [9] C.E. Schaefer, C. Andaya, A. Urtiaga, E.R. McKenzie, C.P. Higgins, Electrochemical treatment of perfluorooctanoic acid (PFOA) and perfluorooctane sulfonic acid (PFOS) in groundwater impacted by aqueous film forming foams (AFFFs), *J. Hazard. Mater.* 295 (2015) 170–175.
- [10] N. Ratola, A. Cincinelli, A. Alves, A. Katsoyiannis, Occurrence of organic micro-contaminants in the wastewater treatment process. A mini review, *J. Hazard. Mater.* 239–240 (2012) 1–18.
- [11] E. Sinclair, K. Kannan, Mass loading and fate of perfluoroalkyl surfactants in wastewater treatment plants, *Environ. Sci. Technol.* 40 (2006) 1408–1414.
- [12] Á. Anglada, A. Urtiaga, I. Ortiz, D. Mantzavinos, E. Diamadopoulos, Boron-doped diamond anodic treatment of landfill leachate: evaluation of operating variables and formation of oxidation by-products, *Water Res.* 45 (2011) 828–838.
- [13] K.E. Carter, J. Farrell, Oxidative destruction of perfluorooctane sulfonate using boron-doped diamond film electrodes, *Environ. Sci. Technol.* 42 (2008) 6111–6115.
- [14] H. Lin, J. Niu, S. Ding, L. Zhang, Electrochemical degradation of perfluorooctanoic acid (PFOA) by Ti/SnO<sub>2</sub>-Sb, Ti/SnO<sub>2</sub>-Sb/PbO<sub>2</sub> and Ti/SnO<sub>2</sub>-Sb/MnO<sub>2</sub> anodes, *Water Res.* 46 (2012) 2281–2289.
- [15] J. Niu, H. Lin, J. Xu, H. Wu, Y. Li, Electrochemical mineralization of perfluorocarboxylic acids (PFCAs) by Ce-doped modified porous nanocrystalline PbO<sub>2</sub> film electrode, *Environ. Sci. Technol.* 46 (2012) 10191–10198.
- [16] G. Pérez, R. Ibáñez, A.M. Urtiaga, I. Ortiz, Kinetic study of the simultaneous electrochemical removal of aqueous nitrogen compounds using BDD electrodes, *Chem. Eng. J.* 197 (2012) 475–482.
- [17] T. Ochiai, Y. Iizuka, K. Nakata, T. Murakami, D.A. Tryk, A. Fujishima, Y. Koide, Y. Morito, Efficient electrochemical decomposition of perfluorocarboxylic acids by the use of a boron-doped diamond electrode, *Diam. Relat. Mater.* 20 (2011) 64–67.
- [18] A. Urtiaga, C. Fernández-González, S. Gómez-Lavín, I. Ortiz, Kinetics of the electrochemical mineralization of perfluorooctanoic acid on ultrananocrystalline boron doped conductive diamond electrodes, *Chemosphere* 129 (2015) 20–26.
- [19] Q. Zhuo, S. Deng, B. Yang, J. Huang, B. Wang, T. Zhang, G. Yu, Degradation of perfluorinated compounds on a boron-doped diamond electrode, *Electrochim. Acta* 77 (2012) 17–22.
- [20] H. Zhao, J. Gao, G. Zhao, J. Fan, Y. Wang, Y. Wang, Fabrication of novel SnO<sub>2</sub>-Sb/carbon aerogel electrode for ultrasonic electrochemical oxidation of perfluorooctanoate with high catalytic efficiency, *Appl. Catal. B Environ.* 136–137 (2013) 278–286.
- [21] Q. Zhuo, S. Deng, B. Yang, J. Huang, G. Yu, Efficient electrochemical oxidation of perfluorooctanoate using a Ti/SnO<sub>2</sub>-Sb-Bi anode, *Environ. Sci. Technol.* 45 (2011) 2973–2979.
- [22] J. Niu, Y. Li, E. Shang, Z. Xu, J. Liu, Electrochemical oxidation of perfluorinated compounds in water, *Chemosphere* 146 (2016) 526–538.
- [23] C.E. Schaefer, C. Andaya, A. Burant, C.W. Condee, A. Urtiaga, T.J. Strathmann, C.P. Higgins, Electrochemical treatment of perfluorooctanoic acid and perfluorooctane sulfonate: insights into mechanisms and application to groundwater treatment, *Chem. Eng. J.* (2017).
- [24] A.M. Trautmann, H. Schell, K.R. Schmidt, K.M. Mangold, A. Tiehm, Electrochemical degradation of perfluoroalkyl and polyfluoroalkyl substances (PFASs) in groundwater, *Water Sci. Technol.* 71 (2015) 1569–1575.
- [25] C. Zhang, J. Tang, C. Peng, M. Jin, Degradation of perfluorinated compounds in wastewater treatment plant effluents by electrochemical oxidation with Nano-ZnO coated electrodes, *J. Mol. Liq.* 221 (2016) 1145–1150.
- [26] Á. Soriano, D. Gorri, A. Urtiaga, Efficient treatment of perfluorohexanoic acid by nanofiltration followed by electrochemical degradation of the NF concentrate, *Water Res.* 112 (2017) 147–156.
- [27] X. Dauchy, V. Boiteux, C. Bach, A. Colin, J. Hemard, C. Rosin, J.F. Munoz, Mass flows and fate of per- and polyfluoroalkyl substances (PFASs) in the wastewater treatment plant of a fluorochromal manufacturing facility, *Sci. Total Environ.* 576 (2017) 549–558.
- [28] M.K. Moe, S. Huber, J. Svenson, A. Hagenaars, M. Pabon, M. Trümper, U. Berger, D. Knapen, D. Herzke, The structure of the fire fighting foam surfactant Forafac®1157 and its biological and photolytic transformation products, *Chemosphere* 89 (2012) 869–875.
- [29] V. Boiteux, C. Bach, V. Sagres, J. Hemard, A. Colin, C. Rosin, J.-F. Munoz, X. Dauchy, Analysis of 29 per- and polyfluorinated compounds in water, sediment, soil and sludge by liquid chromatography-tandem mass spectrometry, *Int. J. Environ. Anal. Chem.* 96 (2016) 705–728.
- [30] APHA (American Public Health Association), Standard Methods for the Examination of Water and Wastewater, (1998) 20th Ed. Washington DC. (ISBN 9780875523235).
- [31] L.A. D'Agostino, S.A. Mabury, Aerobic biodegradation of two fluorotelomer sulfonamide-based aqueous film forming foam components produces perfluoroalkyl carboxylates, *Environ. Toxicol. Chem.* (2017), <http://dx.doi.org/10.1002/etc.3750> (in press).
- [32] J.C. D'Eon, M.D. Hurley, T.J. Wallington, S.A. Mabury, Atmospheric chemistry of N-methyl perfluorobutane sulfonamidoethanol, C<sub>4</sub>F<sub>9</sub>SO<sub>2</sub>N(CH<sub>3</sub>)CH<sub>2</sub>CH<sub>2</sub>OH: kinetics and mechanism of reaction with OH, *Environ. Sci. Technol.* 40 (2006) 1862–1868.
- [33] C. Fang, M. Megharaj, R. Naidu, Chemical oxidation of some AFFFs leads to the formation of 6:2FTS and 8:2FTS, *Environ. Toxicol. Chem.* 34 (2015) 2625–2628.
- [34] S. Park, L.S. Lee, V.F. Medina, A. Zull, S. Waisner, Heat-activated persulfate oxidation of PFOA, 6:2 fluorotelomer sulfonate, and PFOS under conditions suitable for in-situ groundwater remediation, *Chemosphere* 145 (2016) 376–383.
- [35] X. Yang, J. Huang, K. Zhang, G. Yu, S. Deng, B. Wang, Stability of 6:2 fluorotelomer sulfonate in advanced oxidation processes: degradation kinetics and pathway, *Environ. Sci. Pollut. Res.* 21 (2014) 4634–4642.
- [36] Q. Zhuo, X. Li, F. Yan, B. Yang, S. Deng, J. Huang, G. Yu, Electrochemical oxidation of 1H,1H,2H,2H-perfluorooctane sulfonic acid (6:2 FTS) on DSA electrode: operating parameters and mechanism, *J. Environ. Sci. (China)* 26 (2014) 1733–1739.
- [37] B. Guan, J. Zhi, X. Zhang, T. Murakami, A. Fujishima, Electrochemical route for fluorinated modification of boron-doped diamond surface with perfluorooctanoic acid, *Electrochem. Commun.* 9 (2007) 2817–2821.
- [38] A.M. Polcaro, A. Vacca, M. Mascia, S. Palmas, J. Rodríguez Ruiz, Electrochemical treatment of waters with BDD anodes: kinetics of the reactions involving chlorides, *J. Appl. Electrochem.* 39 (2009) 2083–2092.
- [39] M.E.H. Bergmann, T. Lourthouk, W. Schmidt, J. Hartmann, M. Fischer, G. Nüsseke, D. Gerngroß, Laboratory- and technical-scale comparison of chlorate and perchlorate formation during drinking water electrolysis: a field study, *J. Appl. Electrochem.* 45 (2015) 765–778.
- [40] D.K. Hubler, J.C. Baygens, B.P. Chaplin, J. Farrell, Understanding chlorite, chlorate and perchlorate formation when generating hypochlorite using boron doped diamond film electrodes, *ECS Trans.* 58 (2013) 21–32.
- [41] G. Pérez, J. Saiz, R. Ibáñez, A.M. Urtiaga, I. Ortiz, Assessment of the formation of inorganic oxidation by-products during the electrocatalytic treatment of ammonium from landfill leachates, *Water Res.* 46 (2012) 2579–2590.
- [42] A. Urtiaga, I. Ortiz, A. Anglada, D. Mantzavinos, E. Diamadopoulos, Kinetic modeling of the electrochemical removal of ammonium and COD from landfill leachates, *J. Appl. Electrochem.* 42 (2012) 779–786.
- [43] A. Kapalka, L. Joss, A. Anglada, C. Cominelli, K.M. Udert, Direct and mediated electrochemical oxidation of ammonia on boron-doped diamond electrode, *Electrochem. Commun.* 12 (2010) 1714–1717.





5.3. Scientific publication 3.

**Efficient electrochemical degradation of poly- and perfluoroalkyl substances (PFASs) from the effluents of an industrial wastewater treatment plant**

Authors:

Beatriz Gomez-Ruiz<sup>a</sup>, Sonia Gómez-Lavín<sup>a</sup>, Nazely Diban<sup>a</sup>, Virginie Boiteux<sup>b</sup>, Adeline Colin<sup>b</sup>, Xavier Dauchy<sup>b</sup>, Ane Urtiaga<sup>a</sup>

- a) Department of Chemical and Biomolecular Engineering. University of Cantabria. Av. de Los Castros s/n. 39005 Santander. Spain
- b) ANSES, Nancy Laboratory for Hydrology, Water Chemistry Department, 40 rue Lionnois, 54000 Nancy, France

---

*Accepted 6 April 2017*

*Chemical Engineering Journal*

*Volume 322 (2017), Pages 196-204*

DOI: <https://doi.org/10.1016/j.cej.2017.04.040>



## Efficient electrochemical degradation of poly- and perfluoroalkyl substances (PFASs) from the effluents of an industrial wastewater treatment plant

Beatriz Gomez-Ruiz<sup>a</sup>, Sonia Gómez-Lavín<sup>a</sup>, Nazely Diban<sup>a</sup>, Virginie Boiteux<sup>b</sup>, Adeline Colin<sup>b</sup>, Xavier Dauchy<sup>b</sup>, Ane Urtiaga<sup>a,\*</sup>

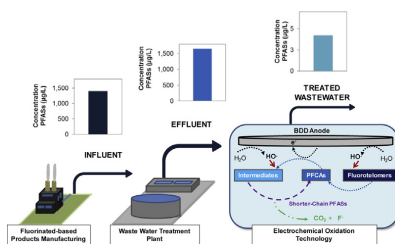
<sup>a</sup> Department of Chemical and Biomolecular Engineering, Universidad de Cantabria, Av. de Los Castros s/n, 39005 Santander, Spain

<sup>b</sup> ANSES, Nancy Laboratory for Hydrology, Water Chemistry Department, 40 rue Lionnois, 54000 Nancy, France

### HIGHLIGHTS

- Industrial wastewaters with a high PFASs content,  $\Sigma$ PFASs = 1642  $\mu\text{g/L}$ , were treated.
- The most abundant PFASs were fluorotelomers 6:2 FTAB and 6:2 FTSA.
- Boron doped diamond anode allowed 99.7% PFASs removal.
- TOC decay and fluoride release revealed PFASs mineralization.
- Fluorotelomer sulfonamides decomposed into PFCAs via FTSA formation.

### GRAPHICAL ABSTRACT



### ARTICLE INFO

#### Article history:

Received 12 January 2017

Received in revised form 5 April 2017

Accepted 6 April 2017

Available online 7 April 2017

#### Keywords:

Perfluoroalkyl substances (PFASs)

6:2 Fluorotelomers

Perfluorocarboxylates

Electrochemical oxidation

Boron doped diamond anode (BDD)

Industrial wastewater

### ABSTRACT

This paper reports the electrochemical treatment of poly- and perfluoroalkyl substances (PFASs) in the effluent from an industrial wastewater treatment plant (WWTP). While most of the previous research focused on the electrochemical degradation of perfluorooctanoic acid and perfluorooctane sulfonate in model solutions, this work studies the simultaneous removal of 8 PFASs at environmentally relevant concentrations in real industrial emissions, which also contained organic matter and inorganic anions. The overall PFASs content in the WWTP effluent was 1652  $\mu\text{g/L}$ , which emphasized the need to develop innovative technologies for the management of PFASs emissions. 6:2 fluorotelomer sulfonamide alkybetaine (6:2 FTAB) and 6:2 fluorotelomer sulfonate (6:2 FTSA) were the major contributors (92% w/w) to the overall PFASs content, that also contained significant amounts of short-chain perfluorocarboxylic acids (PFCAs). Using a boron doped diamond (BDD) anode of 0.0070  $\text{m}^2$ , the effluent (2 L) was treated by applying a current density of 50  $\text{mA}/\text{cm}^2$  for 10 h, that resulted in 99.7% PFASs removal. The operation at lower current densities (5 and 10  $\text{mA}/\text{cm}^2$ ) evidenced the initial degradation of 6:2 fluorotelomers into perfluoroheptanoic and perfluorohexanoic acids, that were later degraded into shorter chain PFCAs. The high TOC removal, >90%, and the fluoride release revealed that PFASs mineralization was effective. These results highlight the potential of the electrochemical technology for the treatment of PFASs contained in industrial wastewaters, which nowadays stands as the main source of this group of persistent pollutants into the environment.

© 2017 Elsevier B.V. All rights reserved.

\* Corresponding author.

E-mail address: [urtiaga@unican.es](mailto:urtiaga@unican.es) (A. Urtiaga).

## 1. Introduction

Poly- and perfluoroalkyl substances (PFASs) have been synthesized and widely used in industrial and commercial applications since the 1950s [1]. Releases of perfluoroalkyl carboxylic acids (PFCAs) into the environment during the period 1950–2004 were estimated to be 3200–7300 tons. The contribution of direct sources that result from the manufacture and use of PFCAs were estimated to be in the range 3200–6900 ton, most of them used as processing aids in the manufacture of fluoropolymers [2,3]. Therefore, historically PFASs emissions are dominated by industrial manufacturing processes.

Recently, perfluorooctane sulfonate (PFOS) and perfluorooctanoic acid (PFOA) have been subjected to increasingly intense research due to their potential toxicity and the extent of their environmental distribution [4]. PFOS and its salts are included in the Annex B of the Stockholm Convention on Persistent Organic Pollutants (POPs) [5]. In addition, PFOS is part of the OSPAR List of Chemicals for Priority Action [6] and is also listed as a priority substance in the field of European water policy according to Directive 2013/39/EC [7]. U.S. EPA has also established the health advisory level at 70 parts per trillion of combined PFOA and PFOS in drinking water [8].

The scientific community is now facing the challenge of developing new technologies for the treatment at source of PFASs emissions, and where necessary, to abate the pollution already introduced in the environment. Many of the already published studies emphasize the low efficiency of the conventional water treatment technologies for the elimination of PFASs [9]. It is thought that PFASs removal takes place by adsorption onto sludge, although the biodegradation of some precursors might contribute to the observed increase of PFCAs concentrations in wastewater treatment processes [10], as it happens in AFFF (Aqueous Film Forming Foams) impacted soils and groundwaters [11]. Several studies have reported that activated carbon adsorption and reverse osmosis remove significant amounts of PFASs [10,12–16]. However, these are physical separation technologies that transfer the contaminants from the water phase to a second phase that still needs to be treated, and that work properly only for long-chain PFASs. Because of this reason, advanced oxidation processes [17] such as persulfate addition [18], photocatalysis [19–20], and particularly electrochemical oxidation are receiving growing attention [21]. Electrochemical oxidation has the advantages of mild temperature and pressure operating conditions, versatility and ease of operation [22–25]. Furthermore, the efficiency of this process has already been assessed for landfill leachates [26], recalcitrant compounds in industrial wastewater [27], pharmaceuticals in reverse osmosis concentrates [28], and other emerging contaminants contained in the secondary effluents of wastewater treatment plants (WWTP) [29–31].

The ability of electrochemical technologies for PFASs degradation is now under intensive research. Most of the previous studies were focused on the selection of the anodic material. “Non-active” anodes such as SnO<sub>2</sub>, PbO<sub>2</sub> and boron doped diamond (BDD), provided high mineralization of PFOA and some perfluoroalkane sulfonic acids [24,32–35]. The electrochemical efficiency of the anode material depends on its electron transfer ability, as well as on its hydroxyl radical (HO•) generation capacity. To improve the treatment efficiency some studies paid attention to the optimization of the experimental conditions, such as cell potential, current density and pH, as it has been recently reviewed [34]. Even though previous studies of electrochemical degradation of PFASs have shown promising results, most of the studies were performed using model solutions of single PFASs upon addition of an electrolyte, and using initial concentrations in the range of ten to hundred milligrams per liter, which are much higher than the

concentrations usually found in polluted groundwater or even in industrial effluents. Very few studies dealt with real water samples under environmental conditions. Exceptions include the recent studies that demonstrated the electrochemical degradation of PFOA and PFOS in groundwaters impacted by the use of AFFFs [35,36]. Particularly, the removal of PFASs from heavily contaminated industrial wastewaters has not been reported yet.

The present innovative work analyzes the electrooxidation of PFASs in real effluents from an industrial WWTP. This water treatment facility was selected based on the wide variety and the high amount of PFASs contained in the effluent, as it will be shown later on. BDD anodic material was selected due to its high stability, low adsorption capacity, high overpotential for oxygen generation and long life span, and moreover, because of its proven capacity to degrade non-biodegradable organic compounds [26]. Both the influent and the effluent streams of the industrial WWTP were physico-chemically characterized. The electrochemical degradation and mineralization of 8 PFASs were evaluated in the WWTP effluent, together with the reduction of major organic pollution parameters such as total organic carbon (TOC). The formation and degradation of intermediate PFCAs, which were generated as degradation products of the most abundant fluorotelomers, is also reported. In addition, the effect of the applied current density (*j*), on the rate of PFASs degradation is also reported.

## 2. Materials and methods

### 2.1. Materials and wastewater samples

Grab samples, 50 l each, of the influent (I) and effluent (E) streams from an industrial WWTP located in France were obtained in one sampling campaign in 2015. It is worthy to note that both I and E samples were simultaneously collected, so the effluent sample did not come from the influent sample, as the residence time in the treatment plant (nine days) was not taken into account. Four manufacturing plants discharge their wastewater into the WWTP, but only one of them produces side-chain-fluorinated polymers and fluorotelomer based products for fire-fighting foams. This chemicals manufacturer contributes with 3–17% to the overall flow treated in the industrial WWTP. More details on the WWTP facility, including the description of the conventional treatment stages, were recently described elsewhere [37]. The same study estimated the PFASs release from this WWTP facility in the range of 21–247 g/day of PFCAs and 1,622–6963 g/day of fluorotelomers, taking into account the variations observed in several sampling campaigns.

Table 1 summarizes the characteristics of I and E samples, including the concentration of the PFAS (ng/L) that were found over the limits of quantification (LOQ) of the analytical procedure. The chemical structure of these compounds is provided in Table 2. The analytical method included perfluoroalkyl carboxylic acids (PFCAs), perfluoroalkane sulfonic acids (PFASs), n:2 fluorotelomer carboxylic acids (n:2 FTCAs), n:2 unsaturated fluorotelomer carboxylic acids (n:2 FTUCAs), n:2 fluorotelomer sulfonic acids (n:2 FTSAs), perfluorooctane sulfonamide (FOSA), 6:2 FTAB and 6:2 fluorotelomer sulfonamide propyl N,N dimethylamine. The latter compound, which has been identified in several previous works [38,39] will be named M4, following the simplified nomenclature reported by Moe et al. (2012) [40]. It can be observed that the concentration of ΣPFASs included in the analytical survey was 1402 µg/L in the influent and 1652 µg/L in the WWTP effluent. Moreover, the conventional water treatment technologies applied at this WWTP resulted in a considerable increase in the concentration of 6:2 FTSA, as well as all PFCAs.

**Table 1**

Main characteristics and initial concentration of PFASs ( $\mu\text{g/L}$ ) in the influent (I) and effluent (E) samples of the industrial WWTP.

	Influent	Effluent
<i>Physico-chemical parameters</i>		
Suspended Solids (mg/L)	125	55
Conductivity (mS/cm)	6.7	6.9
pH	8.4	7.6
<i>Organic Pollutants</i>		
COD (mg/L)	2944	227
TOC (mg/L)	722	99
<i>Inorganic Compounds</i>		
Sulfate (mM)	9	11.3
Chloride (mM)	28.4	38
Fluoride (mM)	<LOQ	<LOQ
<i>PFASs</i>		
PFBA (ng/L)	496	7544
PFPeA (ng/L)	3154	52,500
PFHxA (ng/L)	5291	24,827
PFHpA (ng/L)	2793	37,847
PFOA (ng/L)	449	2063
6:2 FTSA (ng/L)	242,496	382,200
8:2 FTSA (ng/L)	874	<LOQ
6:2 FTCA (ng/L)	328	<LOQ
6:2 FTAB (ng/L)	1,111,000	1,143,000
M4 (ng/L)	34,361	2414

LOQ: limit of quantification. The LOQ for fluoride was 0.002 mM. The LOQs for 8:2 FTSA and 6:2 FTCA were 2000 and 5000 ng/L, respectively.

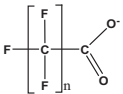
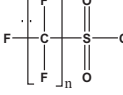
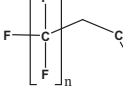
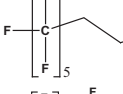
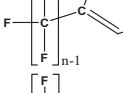
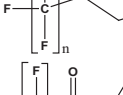
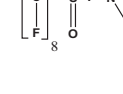
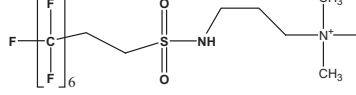
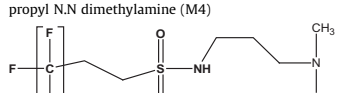
The most abundant PFASs in the influent was 6:2 FTAB (6:2 Fluorotelomer sulphonamide alkylbetaine) followed by 6:2 FTSA (6:2 Fluorotelomer sulphonic acid), and M4. As it can be seen in Table 2 the bio-oxidative breakdown of 6:2 FTAB and M4 at the S-NH position can give rise to both 6:2 FTSA and PFHxA (Perfluorohexanoic acid) [41–43]. An explanation for the observed increase in the PFHpA (Perfluorheptanoic acid) concentration is not readily available, although it could be due to the bio-degradation of unknown 8:2 fluorotelomer compounds not included as target analytes in the current research [17,44]. It is also worthy to mention that a recent study by Dauchy et al. [37] on the characterization of PFASs mass flow rates in the same WWTP recognized the presence of PFHpA precursors by means of an oxidative conversion analytical method [44]. These results emphasize the low efficiency of the conventional water treatment technologies for the removal of PFASs, and the need to develop advanced treatments specially designed for PFASs degradation.

## 2.2. Electrochemical experiments

Electro-oxidation treatment was applied to the effluent sample. Experiments were performed at laboratory scale in an undivided flow-by cell (Diacell 106, Adamant Technologies, Switzerland) formed by two circular parallel electrodes: a BDD anode and a stainless steel cathode, each one with a surface area of  $70\text{ cm}^2$  and an electrode gap of 5 mm. The cell was connected to a power supply (Agilent 6654 A) and experiments were performed under galvanostatic conditions. Fig. S1 shows a diagram of the experimental set-up, and further details can be found in previous works [26,28]. Aliquots (volume = 2 L) of the E sample were introduced in the feed jacketed glass tank (temperature =  $20\text{ }^\circ\text{C}$ ), and the fluid was circulated at a flowrate of 3 L/min, from the feed tank to the electrooxidation cell and back to the tank. Most of the experiments were performed at a current density of  $50\text{ mA/cm}^2$ . In these conditions, the voltage developed by the cell varied in the range 13.9–15.3 V. In addition, different current densities (2, 5 and  $10\text{ mA/cm}^2$ ) were applied to assess their effect on the removal rate of PFASs and TOC from the WWTP effluent. The salts content of the effluent sample was enough to provide the adequate conductivity

**Table 2**

Chemical structure by compound class, of PFASs included in the analytical method.

Compound name	Chemical structure	n
Perfluoroalkyl carboxylic acids (PFCA)		3–13
Perfluoroalkane sulfonic acids (PFSA)		4, 6–8, 10
Fluorotelomer carboxylic acids (n:2 FTCA)		6, 8, 10
5:3 Polyfluorinated acid (5:3 Acid)		
Unsaturated fluorotelomer carboxylic acids (n:2 FTUCA)		6,8,10
Fluorotelomer sulfonic acids (n:2 FTSA)		4,6,8
Perfluorooctane sulfonamide (FOSA)		
6:2 Fluorotelomer sulfonamide alkylbetaine (6:2 FTAB)		6:2
Fluorotelomer sulfonamide propyl N,N dimethylamine (M4)		

for the electrochemical treatment. Treated liquid samples were collected in polypropylene containers, and stored in the refrigerator at  $4\text{ }^\circ\text{C}$  until they were delivered for analysis. Gas phase sampling was not considered, even though it could contain small amount of short-chain volatile PFCA as final products of the electrochemical treatment. Each point of the kinetic experiments shown in Figs. 3 and 4 was obtained as a single electrochemical experiment. This way of operation allowed to keep constant the feed volume along the electrochemical treatment time. Preliminary experiments using a model solution of PFOA ( $100\text{ mg/L}$ ) were conducted in the absence of current, to check that the concentration of PFOA was maintained within  $\pm 5\%$  of the initial value, thus showing that adsorption of PFASs in the experimental system could be minimized.

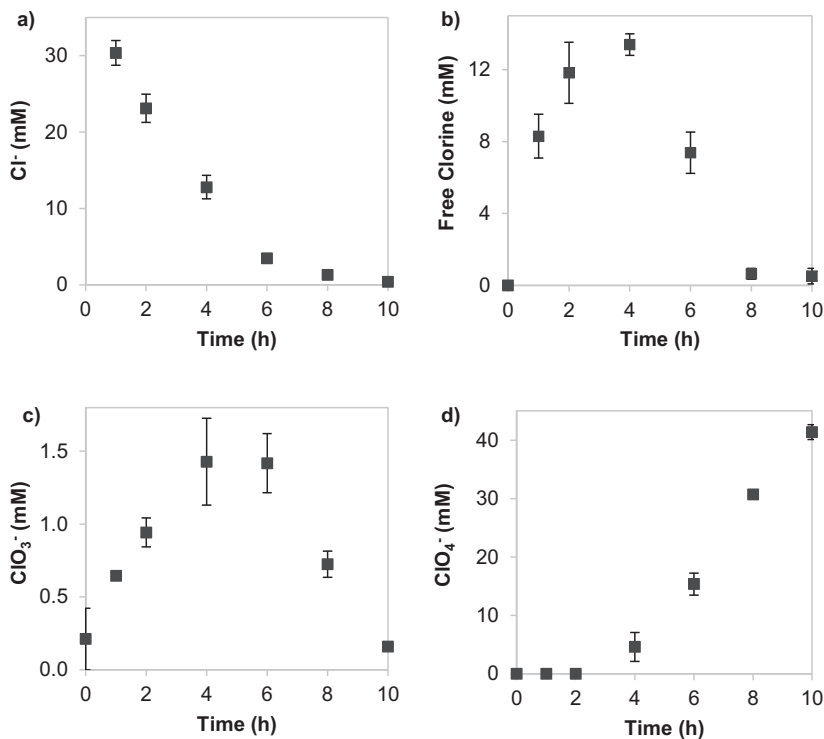


**Fig. 1.** Evolution of inorganic chlorine species a) chloride, b) free chlorine, c) chlorate and d) perchlorate, with electro-oxidation time, under  $j = 50 \text{ mA/cm}^2$  of applied current density to the effluent (E) sample. Average values of duplicate experiments are shown.

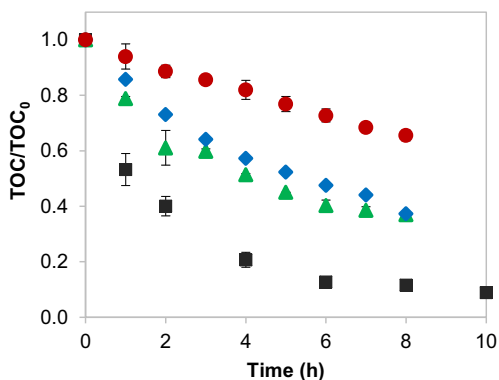


**Fig. 2.** Evolution of TOC/TOC<sub>0</sub> ratios during electrooxidation of the effluent sample, where TOC<sub>0</sub> is the initial TOC concentration in the E sample (99 mg/L). (■)  $j = 50 \text{ mA/cm}^2$ , (▲)  $j = 10 \text{ mA/cm}^2$ , (◆)  $j = 5 \text{ mA/cm}^2$ , (●)  $j = 2 \text{ mA/cm}^2$ .

### 2.3. Analytical methods

TOC analyses were performed using a TOC-V CPH (Shimadzu). Chemical oxygen demand (COD) was determined by the closed

reflux and colorimetric method following the procedure 5220D from Standard Methods [45]. Anions were determined by ion chromatography (Dionex 120 IC) provided with an IonPac As-HC column, using a solution of 9 mM of  $\text{Na}_2\text{CO}_3$  as eluent, with a flowrate of 1 mL/min and a pressure of 2000 psi, based on Standard Methods 4110B. Free chlorine was determined following the N, N-Diethyl-p-phenylene diamine (DPD) Ferrous Titrimetric Method according to Standard Methods 4500-Cl. pH was measured using a portable pH-meter.

The detailed protocol of the PFASs analysis has been recently published [46]. Briefly, non-filtered water samples were diluted prior to extraction, purification and pre-concentration by a solid-phase extraction (SPE) procedure (Strata X-AW<sup>®</sup> (200 mg, 6 mL) cartridge (Phenomenex, Torrance, CA)). Recovery rates of the SPE procedure were reported elsewhere [46]. An ultra-high performance liquid chromatograph coupled to tandem mass spectrometer (UHPLC-MS/MS) in negative electrospray ionisation (ESI) mode was employed to separate and detect targeted compounds (Waters Xevo TQ-MS tandem mass spectrometer (Waters Corporation, Milford, MA, USA)). Table S2 lists the MS/MS transitions, cone voltages and collision energies applied for the different target analytes and isotope labelled standards. Twelve labelled internal standards (IS) were used to provide an adequate correction compensating for matrix effects. Due to initial dilutions, LOQs were between 2 and 5  $\mu\text{g/L}$  in water samples depending on the analytes (see Table S1 of supporting information).

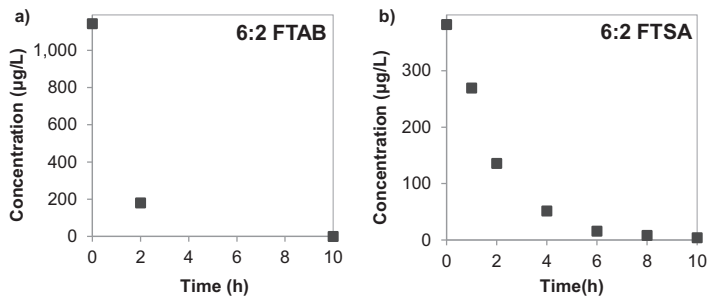


Fig. 3. Evolution of the main fluorotelomers a) 6:2 FTAB and b) 6:2 FTSA with electro-oxidation time,  $j = 50 \text{ mA/cm}^2$ , of effluent (E) sample.

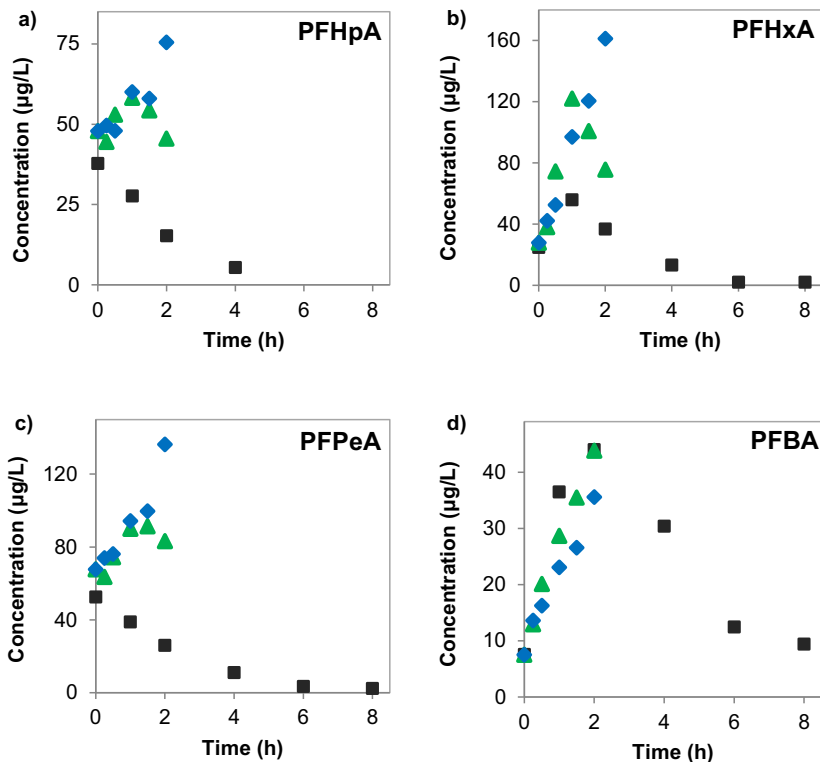


Fig. 4. Influence of the applied current density on the concentration of a) PFHpA, b) PFHxA, c) PFPeA and d) PFBA with electro-oxidation time, in effluent (E) sample. (■)  $j = 50 \text{ mA/cm}^2$  (cell voltage =  $14.6 \pm 0.5 \text{ V}$ ), (▲)  $j = 10 \text{ mA/cm}^2$  (cell voltage =  $5.4 \pm 0.02 \text{ V}$ ), (◆)  $j = 5 \text{ mA/cm}^2$  (cell voltage =  $4.5 \pm 0.07 \text{ V}$ ).

### 3. Results and discussion

#### 3.1. Evolution of chloride and TOC

The unknown nature of the industrial wastewaters under study and the complexity of their matrix components suggested to study the evolution with time of the major pollutants. TOC acts as an indicator of mineralization of the overall organic pollutants load.

Particular attention was paid to chlorine species, in order to identify the operating conditions that would prevent the formation of undesirable perchlorate.

Fig. 1 reports the evolution of the concentration of chlorine species with time. Firstly, the depletion of chloride (Fig. 1,a) as a result of its anodic oxidation generated the increase of free chlorine (Fig. 1,b). During the formation of free chlorine, that occurred in the initial 4 h, the sample slightly reduced its bulk pH from 7.36

to 6.47. Therefore, hypochlorous acid was the most abundant chlorine species in solution. Free chlorine is not expected to promote the degradation of PFASs, e.g.: Schaefer et al. [47] showed that the presence of chloride had a minimal effect on the observed rate constants for PFOA removal from groundwaters, by BDD electrochemical treatment, compared to the absence of chloride. After 4 h of treatment, free chloride started to decrease (Fig. 1,b), in coincidence with the depletion of its chloride precursor and the formation of more oxidized chlorine species, such as chlorate (Fig. 1,c) and perchlorate (Fig. 1,d). Nevertheless, it is also observed that the formation of hazardous perchlorate was avoided in a period up to 4 h of electrochemical treatment when most of the PFASs were degraded, as it will be shown below. The total concentration of all chlorine species at 10 h ( $42.4 \pm 0.9$  mM) was quite similar to the value at the beginning of the experiment ( $38.2 \pm 1.6$  mM), and the small increase could be assigned both to the experimental error or to the release of chloride upon oxidation of organochlorinated compounds [22].

The TOC removal of the industrial WWTP effluent is given in Fig. 2. A reduction of  $91.1 \pm 0.31\%$  was achieved when working at a current density of  $50 \text{ mA/cm}^2$ , showing the good performance of the BDD anodes for the mineralization of recalcitrant organic pollutants. If we look back to Table 1, the treatment applied in the WWTP achieved a significant removal of both COD and TOC, so the remaining TOC in the effluent was mostly assigned to non-identified soluble organic compounds that are refractory to traditional physico-chemical and biological treatments. The effect of the applied current density on the TOC removal was examined at 2, 5, 10 and  $50 \text{ mA/cm}^2$ . At the low current regime ( $2 \text{ mA/cm}^2$ ) the TOC development was slow, and showed zero order kinetics, which is typically observed when electrolysis is under current control. By increasing the applied current density to  $50 \text{ mA/cm}^2$  the observed kinetics changed to first order, which is usually found when the electrolysis is under mass transport control [48,49]. The use of intermediate current densities (5 and  $10 \text{ mA/cm}^2$ ) originated TOC removal rates which fell in the middle, that in the case of  $5 \text{ mA/cm}^2$  showed an initial zero order trend followed by a first order trend after 3 h of treatment. The complex reaction scheme involved in the BDD electrooxidation of chloride-rich waters requires a detailed analysis of the operating conditions that enable the removal of TOC and at the same time the minimization of undesirable chlorinated species. Our previous studies using BDD electrodes to oxidize landfill leachates have documented that waters that initially contained high levels of dissolved organic carbon scavenged the chlorine produced from chloride oxidation and thus limited perchlorate formation [50]. In the present study, the formation of perchlorate was hindered at operation times before 4 h when working at  $50 \text{ mA/cm}^2$ , which resulted in a TOC removal of 79%.

### 3.2. Electrochemical oxidation of PFASs

This section is focused on the degradation and transformation of the group of PFASs found in the effluent of the industrial WWTP. Figs. 3 and 4 show the evolution with time of the concentration of those PFASs which were detected in higher amounts. The detail about the concentration of all the compounds included in the analytical procedure is provided in the supplementary material (Table S1 of supplementary material).

The development of the major fluorotelomers, 6:2 FTAB and 6:2 FTSA is depicted in Fig. 3. Due to the use of a specific calibration method, which is costly and time-consuming (standard addition, details are described by Boiteux et al. [46]), 6:2 FTAB was determined only in three samples, which corresponded to the initial effluent and two samples that were electrooxidized for 2 and

10 h. The  $\text{CH}_2\text{-CH}_2$  unit between the perfluoroalkyl chain and the sulfonate end group makes fluorotelomers much more susceptible to oxidation than PFCAs. Looking at the chemical structures in Table 2, it is possible to foresee that 6:2 FTAB was partially degraded into 6:2 FTSA which in these conditions would be simultaneously generated and broken. However, the kinetics of 6:2 FTSA elimination was faster than its formation kinetics, as 6:2 FTSA follows a decreasing trend all the time. The removal of both 6:2 FTAB and 6:2 FTSA followed first-order kinetic trends, typically observed in BDD electro-oxidation processes that are governed by mass transfer limitations. In a previous work, BDD electrodes were recognized as strong generators of HO. at the anode surface during the electrooxidation of PFOA [51], a process that was enhanced at higher values of the applied current density. The concentration data shown in Fig. 3 were fitted to a first-order kinetic model,  $C = C_0 e^{-kt}$ , where  $C$  is the concentration of the compound at a given time  $t$ ,  $C_0$  is the initial concentration and  $k$  is the apparent kinetic constant. The values of  $k$  for 6:2 FTAB and 6:2 FTSA removal were  $0.923$  and  $0.469 \text{ h}^{-1}$ , respectively. The lower kinetic constant of 6:2 FTSA disappearance supports the assumption of simultaneous electrochemical formation and degradation of this compound. The electrochemical degradation of fluorotelomers has not been fully investigated in the literature yet. Among the very few studies, Zhuo et al. [52] reported the use of a  $\text{Ti/SnO}_2\text{-Sb}_2\text{O}_5\text{-Bi}_2\text{O}_3$  anode for the degradation of 6:2 FTSA, that provided a rate constant of  $0.074 \text{ h}^{-1}$ . However, the comparison is not straightforward, as the applied current and systems dimensions were different. Furthermore, in the present study, PFASs were simultaneously treated with other major pollutants (the analyzed PFASs contributed only with 0.5% to the initial TOC) that could have hindered the kinetics of fluorotelomers degradation.

The degradation of 6:2 FTAB and 6:2 FTSA gave rise to the formation of PFCAs, as it is shown in Fig. 4. Initially, electrochemical experiments were performed at 5 and  $10 \text{ mA/cm}^2$ , and for shorter degradation times, up to 2 h. After checking that PFASs degradation was incomplete, it was decided to work at a higher current density ( $50 \text{ mA/cm}^2$ ) and for longer times, in order to assure complete PFASs degradation. It should be reminded, that additionally to the PFASs content, electro-oxidation is also acting on other recalcitrant organic pollutants that are consuming most of the applied current for their degradation and mineralization.

Paying attention to Table 1, the most abundant PFCAs in the effluent sample were PFHpA ( $C_0 = 37.85 \text{ }\mu\text{g/L}$ ), PFHxA ( $C_0 = 24.83 \text{ }\mu\text{g/L}$ ), PFPeA (Perfluoropentanoic acid) ( $C_0 = 52.50 \text{ }\mu\text{g/L}$ ) and PFBA (Perfluorobutanoic acid) ( $C_0 = 7.54 \text{ }\mu\text{g/L}$ ). The low initial concentration of PFOA ( $C_0 = 2.06 \text{ }\mu\text{g/L}$ ) could be related to the low concentration of 8:2 fluorotelomers and other PFOA precursors in the WWTP influent. The development of PFCAs during the electro-oxidation treatment (Fig. 4) varied according to the applied current density. For the lowest values of the applied current,  $5 \text{ mA/cm}^2$ , the progress of all PFCAs showed increasing concentrations with time, indicating that these compounds were formed at a faster rate than they were degraded. Based on the very few previous studies dealing with the degradation of 6:2 FTSA, which include the use of  $\text{Ti/SnO}_2\text{-Sb}_2\text{O}_5\text{-Bi}_2\text{O}_3$  anode [52], heat activated persulfate oxidation [53] and with hydrogen peroxide activated by UV light [54], 6:2 FTSA was transformed into a mixture of PFHpA and PFHxA, where the proportions of each PFCa coming from 6:2 FTSA degradation seem to strongly depend on the oxidation technique implemented [44]. 6:2 FTSA degradation would start with the attack of hydroxyl radical at the positions of the two unfluorinated carbons. Further reaction with hydroxyl radical caused the desulfonation, cleaving the bond between the end group of the sulfonate and the polyfluorinated tail. After that, the polyfluorinated tail could be carboxylized at the end to form PFHpA and PFHxA

[54]. Furthermore, these PFCAs obtained after breakdown of the main 6:2 fluorotelomers was broken into shorter-chain perfluorocarboxylates through a step by step mechanism that involved the loose of one electron to the anode to form a perfluoroalkyl carboxyl radical, which was later decarboxylated and defluorinated by hydroxyl radical mediated reaction. In each step, the PFCa molecule loses a  $\text{CF}_2$  unit, and generates  $\text{CO}_2$  and fluoride ions [33,34]. This proposal of degradation pathway, which includes the above mentioned previous literature contributions, is described in Fig. S2 of the supplementary material [44,53,54].

Increasing the applied current density to  $10 \text{ mA/cm}^2$  had the effect of reducing the maximum peak of PFCAs concentration. A further increase to  $50 \text{ mA/cm}^2$  reinforced this effect and therefore, increasing trends were observed only for PFHxA and PFBA. According to these observations, it could be concluded that on the one hand PFHxA is the main initial degradation product of the major 6:2 fluorotelomers. On the other hand, PFBA is, among the measured compounds, at the end of the degradation pathway of longer chain PFCAs, and tends to accumulate at all the applied current conditions under study. Further degradation of PFBA into shorter PFCAs or transfer to the gas phase of volatile PFPrA and trifluoroacetic acid are expected to have occurred too.

Fig. 5 depicts the evolution of the total concentration of PFASs. Solid bars represent the sum of 6:2 FTAB and M4 that were measured only at times 0, 2 and 10 h. Dotted bars gather the sum of 6:2 FTSA, PFCAs, and other minor PFASs. The remaining concentration of all the detected PFASs at  $t = 10 \text{ h}$  was  $4.22 \text{ }\mu\text{g/L}$ , that represents a reduction of 99.74% of the initial total PFASs content. The energy consumption required for the 99.74% PFASs removal was estimated as  $256 \text{ kWh/m}^3$ , which is significantly reduced to  $153 \text{ kWh/m}^3$  when the target PFASs removal rate is set at 98% (treatment time 6 h). Therefore, energy consumption, that is strongly dependent on the target PFASs removal rate [55], and the potential formation of disinfection by-product could be considered the main drawbacks of the electrochemical treatment. In this way it is demonstrated that the electrochemical treatment of the industrial WWTP effluent with BDD anodes allows the effective removal of PFASs at the same time that the general TOC content is nearly completely eliminated. Moreover, the Si/BDD anodic material offered a robust stability. The electrochemical cell used in the present study had been in operation at laboratory scale for more than 10 years. Its degradation efficiency was periodically checked using a phenol degradation test, that proved its stability after more than 4000 h of discontinuous operation and acid/caustic cleaning in a wide range of applied current densities, and under a

variety of wastewaters and contaminants [22,27,30,56], a factor that proves the robustness of BDD electrooxidation technology.

The data about the release of fluoride anions is given in Fig. 6. The fluoride content in solution, given by the black dots, increased progressively, in coincidence with the disappearance of the analyzed PFASs. The total fluorine in solution, calculated as the sum of fluorine contained in the analyzed PFASs plus fluoride in solution, is also shown in Fig. 6 as open circles. After 10 h of electrochemical treatment, the fluoride concentration in solution was  $0.053 \text{ mM}$ . The defluorination factor at  $t = 10 \text{ h}$  was calculated according to equation 1, where  $C_{F-}$  is the final concentration of fluoride ions in the solution (mM),  $C_{0,i}$  is the initial concentration of each PFASs and  $n_{F,i}$  is the stoichiometry factor of the fluoride anion for each PFAS.

$$D_{F-} (\%) = \frac{C_{F-}}{\sum C_{0,i} \cdot n_{F,i}} \cdot 100 \quad (1)$$

The calculated defluorination factor was 126%. This value, higher than 100%, supports the assumption that other unknown fluorotelomers were also degraded during electrochemical oxidation of the effluent. Similarly, previous works highlighted the presence of unidentified perfluorinated compounds in various types of samples by the determination of total fluorine and total oxidizable precursors [37,44,57,58].

#### 4. Conclusions

Results herein reported highlight the potential of electrochemical technology for the treatment of poly and perfluoroalkyl substances (PFASs) contained in industrial wastewaters coming from the manufacturing of fluorotelomer-based products and side-chain-fluorinated polymers. In this work, the use of a commercial BDD anode reduced the PFASs contained in the effluent from an industrial WWTP by 99.7%, as the concentrations decreased from  $1652 \text{ }\mu\text{g/L}$  in the feed water (effluent of the WWTP) to  $4.2 \text{ }\mu\text{g/L}$  in the electrochemically treated water. The only compound, among a group of 29 analyzed PFASs, that was detected in the final sample of the electrooxidation treatment was 6:2 FTSA, since all the other perfluorinated compounds were found below the LOQ of the analytical method. It was evidenced that the degradation of fluorotelomers induced the formation of PFCAs, that nevertheless were further degraded into shorter chain PFCAs and finally miner-

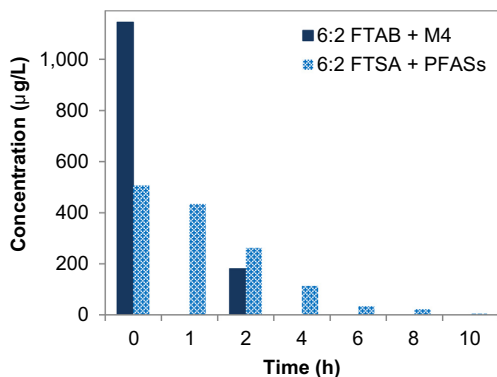


Fig. 5. Evolution of total concentration of PFASs with electro-oxidation time under  $j = 50 \text{ mA/cm}^2$ , in effluent (E) sample.

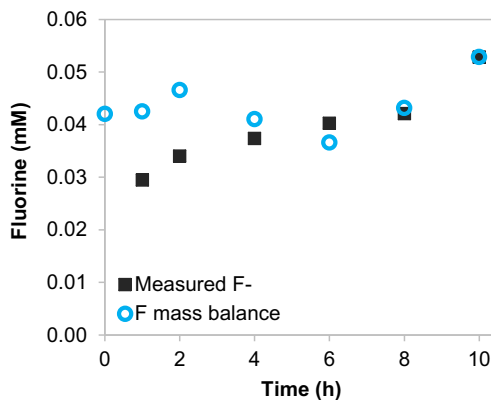


Fig. 6. Evolution of fluoride concentration in solution and total fluorine mass balance with electro-oxidation time, under  $j = 50 \text{ mA/cm}^2$ , in effluent (E) sample.

alized, as it was also supported by the increase of the fluoride content and the TOC decay.

However, further research will be focused on the optimization of the electrochemical process considering that variation of the PFASs concentration in the feed water will likely act as a source of uncertainty. Moreover, one of the key points for the economic viability of electrochemical technologies lies in the reduction of their energy demands. In the present study, the energy consumption for 99.74% PFASs removal was estimated at 256 kWh/m<sup>3</sup>. Therefore, the large scale implementation of the electrochemical process will require of new strategies to reduce its high energy consumption and operation costs. PFASs treatment at source before mixing with other diluting water streams and PFASs pre-concentration by means of membrane separation are envisaged as possible strategies.

## Acknowledgements

Financial support of project CTM2013-44081-R (MINECO, SPAIN-FEDER 2014–2020) is acknowledged. B. Gomez also thanks the FPI grant (BES-2014-071045).

## Appendix A. Supplementary data

Additional information regarding the analytical procedure, evolution with time of PFASs during electrochemical experiments, PFASs degradation pathways and names, acronyms and optimised UHPLC-MS/MS.

Supplementary data associated with this article can be found, in the online version, at <http://dx.doi.org/10.1016/j.cej.2017.04.040>.

## References

- V. Nania, G.E. Pellegrini, L. Fabrizi, G. Sesta, P.D. Sanctis, D. Lucchetti, M.D. Pasquale, E. Coni, Monitoring of perfluorinated compounds in edible fish from the Mediterranean Sea, *Food Chem.* 115 (2009) 951–957.
- H.J. Lehmler, Synthesis of environmentally relevant fluorinated surfactants – A review, *Chemosphere* 58 (2005) 1471–1496.
- K. Prevedourou, I.T. Cousins, R.C. Buck, S.H. Korzeniowski, Sources, fate and transport of perfluorocarboxylates, *Environ. Sci. Technol.* 40 (2006) 32–44.
- B.M. Braune, R.J. Letcher, Perfluorinated sulfonate and carboxylate compounds in eggs of seabirds breeding in the Canadian Arctic: temporal trends (1975–2011) and interspecies comparison, *Environ. Sci. Technol.* 47 (2013) 616–624.
- Stockholm Convention Secretariat, Decision SC-4/17: listing of perfluorooctane sulfonic acid, its salts and perfluorooctane sulfonyl fluoride, Stockholm Convention Secretariat, 1–4, 2009. <http://chm.pops.int/TheConvention/Overview/TextoftheConvention/tabid/2232/> (accessed 16.07.26).
- OSPAR Commission, List of chemicals for priority action. Reference number 2004–12, 1–6, 2011. <http://www.ospar.org/documents?v=7027> (accessed 16.07.26).
- European Chemical Agency, ECHA. Candidate list of substances of very high concern for authorization, 2013. [aue.es/candidate-list-table](http://aue.es/candidate-list-table) (accessed 16.07.26).
- U.S. Environmental Protection Agency, Fact Sheet PFOA and PFOS drinking water health advisories, EPA 800-F-16-003, 2016. <https://www.epa.gov/ground-water-and-drinking-water/supporting-documents/drinking-water-health-advisories-pfoa-and-pfos> (accessed 16.07.26).
- J. Yu, J. Hu, S. Tanaka, S. Fujii, Perfluorooctane sulfonate (PFOS) and perfluorooctanoic acid (PFOA) in sewage treatment plants, *Water Res.* 43 (2009) 2399–2408.
- T.D. Appleman, C.P. Higgins, O. Quiñones, B.J. Vanderford, C. Kolstad, J.C. Zeigler-Holady, E.R.V. Dickenson, Treatment of poly- and perfluoroalkyl substances in U.S. full-scale water treatment systems, *Water Res.* 51 (2014) 246–255.
- E.F. Houtz, C.P. Higgins, J.A. Field, D.L. Sedlak, Persistence of perfluoroalkyl acid precursors in AFFF-impacted groundwater and soil, *Environ. Sci. Technol.* 47 (2013) 8187–8195.
- K.E. Carter, J. Farrell, Removal of perfluorooctane and perfluorobutane sulfonate from water via carbon adsorption and ion exchange, *Sep. Sci. Technol.* 45 (2010) 762–767.
- C. Eschauer, E. Beerendonk, P. Scholte-Veenendaal, P. De Voogt, Impact of treatment processes on the removal of perfluoroalkyl acids from the drinking water production chain, *Environ. Sci. Technol.* 46 (2012) 1708–1715.
- S. Takagi, F. Adachi, K. Miyano, Y. Koizumi, H. Tanaka, M. Mimura, I. Watanabe, S. Tanabe, K. Kannan, Perfluorooctane sulfonate and perfluorooctanoate in raw and treated tap water from Osaka, Japan, *Chemosphere* 72 (2008) 1409–1412.
- J. Thompson, G. Eaglesham, J. Reungtoot, Y. Poussade, M. Bartkow, M. Lawrence, J.F. Mueller, Removal of PFOS, PFOA and other perfluoroalkyl acids at water reclamation plants in South East Queensland Australia, *Chemosphere* 82 (2011) 9–17.
- C.Y. Tang, Q.S. Fu, A.P. Robertson, C.S. Criddle, J.O. Leckie, Use of reverse osmosis membranes to remove perfluorooctane sulfonate (PFOS) from semiconductor wastewater, *Environ. Sci. Technol.* 40 (2006) 7343–7349.
- T. Anumol, S. Dagnino, D.R. Vandervort, S.A. Snyder, Transformation of polyfluorinated compounds in natural waters by advanced oxidation processes, *Chemosphere* 144 (2016) 1780–1787.
- H. Hori, A. Yamamoto, E. Hayakawa, S. Taniyasu, N. Yamashita, S. Kutsuna, H. Katagawa, R. Arakawa, Efficient decomposition of environmentally persistent perfluorocarboxylic acids by use of persulfate as a photochemical oxidant, *Environ. Sci. Technol.* 39 (2005) 2383–2388.
- X. Li, P. Zhang, L. Jin, T. Shao, Z. Li, J. Cao, Efficient photocatalytic decomposition of perfluorooctanoic acid by indium oxide and its mechanism, *Environ. Sci. Technol.* 46 (2012) 5528–5534.
- S. Chen, Y. Lo, C. Lee, Huang, Photocatalytic decomposition of perfluorooctanoic acid by transition-metal modified titanium dioxide, *J. Hazard. Mater.* 288 (2015) 168–175.
- I. Sirés, E. Brillas, M.A. Oturan, M.A. Rodrigo, M. Panizza, Electrochemical advanced oxidation processes: today and tomorrow. A review, *Environ. Sci. Pollut. Res.* 21 (2014) 8336–8367.
- Á. Anglada, A. Urriaga, I. Ortiz, D. Mantzavinos, E. Diamadopoulos, Boron-doped diamond anodic treatment of landfill leachate: evaluation of operating variables and formation of oxidation by-products, *Water Res.* 45 (2011) 828–838.
- J. Niu, H. Lin, J. Xu, H. Wu, Y. Li, Electrochemical mineralization of perfluorocarboxylic acids (PFCAs) by Ce-doped modified porous nanocrystalline PbO<sub>2</sub> film electrode, *Environ. Sci. Technol.* 46 (2012) 10191–10198.
- H. Lin, J. Niu, S. Ding, L. Zhang, Electrochemical degradation of perfluorooctanoic acid (PFOA) by Ti/SnO<sub>2</sub>-Sb, Ti/SnO<sub>2</sub>-Sb/PbO<sub>2</sub> and Ti/SnO<sub>2</sub>-Sb/MnO<sub>2</sub> anodes, *Water Res.* 46 (2012) 2281–2289.
- K.E. Carter, J. Farrell, Oxidative destruction of perfluorooctane sulfonate using boron-doped diamond film electrodes, *Environ. Sci. Technol.* 42 (2008) 6111–6115.
- Á. Anglada, A. Urriaga, I. Ortiz, Contributions of electrochemical oxidation to waste-water treatment: fundamentals and review of applications, *J. Chem. Technol. Biotechnol.* 84 (2009) 1747–1755.
- A. Urriaga, P. Fernandez-Castro, P. Gómez, I. Ortiz, Remediation of wastewaters containing tetrahydrofuran. Study of the electrochemical mineralization on BDD electrodes, *Chem. Eng. J.* 239 (2014) 341–350.
- G. Pérez, A.R. Fernández-Alba, A.M. Urriaga, I. Ortiz, Electro-oxidation of reverse osmosis concentrates generated in tertiary water treatment, *Water Res.* 44 (2010) 2763–2772.
- A. Cano, C. Barrera, S. Cotillas, J. Llanos, P. Cañizares, M.A. Rodrigo, Use of DiaCell modules for the electro-disinfection of secondary-treated wastewater with diamond anodes, *Chem. Eng. J.* 306 (2016) 433–440.
- A.M. Urriaga, G. Pérez, R. Ibáñez, I. Ortiz, Removal of pharmaceuticals from a WWTP secondary effluent by ultrafiltration/reverse osmosis followed by electrochemical oxidation of the RO concentrate, *Desalination* 331 (2013) 26–34.
- C.E. Schaefer, C. Andaya, A. Urriaga, Assessment of disinfection and by-product formation during electrochemical treatment of surface water using a Ti/IrO<sub>2</sub> anode, *Chem. Eng. J.* 264 (2015) 411–416.
- T. Ochiai, Y. Iizuka, K. Nakata, T. Murakami, D.A. Tryk, A. Fujishima, Y. Koide, Y. Morito, Efficient electrochemical decomposition of perfluorocarboxylic acids by the use of a boron-doped diamond electrode, *Diamond Relat. Mat.* 20 (2011) 64–67.
- Q. Zhuo, S. Deng, B. Yang, J. Huang, B. Wang, T. Zhang, G. Yu, Degradation of perfluorinated compounds on a boron-doped diamond electrode, *Electrochim. Acta* 77 (2012) 17–22.
- J. Niu, Y. Li, E. Shang, Z. Xu, J. Liu, Electrochemical oxidation of perfluorinated compounds in water, *Chemosphere* 146 (2016) 526–538.
- A.M. Trautmann, H. Schell, K.R. Schmidt, K. Mangold, A. Tiehm, Electrochemical degradation of perfluoroalkyl and polyfluoroalkyl substances (PFASs) in groundwater, *Water Sci. Technol.* 71 (2015) 1569–1575.
- C.E. Schaefer, C. Andaya, A. Urriaga, E.R. McKenzie, C.P. Higgins, Electrochemical treatment of perfluorooctanoic acid (PFOA) and perfluorooctane sulfonic acid (PFOS) in groundwater impacted by aqueous film forming foams (AFFFs), *J. Hazard. Mater.* 295 (2015) 170–175.
- X. Dauchy, Y. Boiteux, C. Bach, A. Colin, J. Hemard, C. Rosin, J. Munoz, Mass flows and fate of per- and polyfluoroalkyl substances (PFASs) in the wastewater treatment plant of a fluorochemical manufacturing facility, *Sci. Total Environ.* 576 (2017) 549–558.
- B.J. Place, J.A. Field, Identification of novel fluorochemicals in aqueous film-forming foams used by the US military, *Environ. Sci. Technol.* 46 (2012) 7120–7127.
- LA. D'Agostino, S.A. Mabury, Identification of novel fluorinated surfactants in aqueous film forming foams and commercial surfactant concentrates, *Environ. Sci. Technol.* 48 (2014) 121–129.
- M.K. Moe, S. Huber, J. Svenson, A. Hagenars, M. Pabon, M. Trümper, U. Berger, D. Knapen, D. Herzke, The structure of the fire fighting foam surfactant Forafac<sup>®</sup> 1157 and its biological and photolytic transformation products, *Chemosphere* 89 (2012) 869–875.

- [41] B. Weiner, L.W.Y. Yeung, E.B. Marchington, L.A. D'Agostino, S.A. Mabury, Organic fluorine content in aqueous film forming foams (AFFFs) and biodegradation of the foam component 6:2 fluorotelomermercaptoalkylamido sulfonate (6:2 FTSAS), *Environ. Chem.* 10 (2013) 486–493.
- [42] N. Wang, J. Liu, R.C. Buck, S.H. Korzeniowski, B.W. Wolstenholme, P.W. Folsom, L.M. Sulecki, 6:2 Fluorotelomer sulfonate aerobic biotransformation in activated sludge of waste water treatment plants, *Chemosphere* 82 (2011) 853–858.
- [43] K.C. Harding-Marjanovic, E.F. Houtz, S. Yi, J.A. Field, D.L. Sedlak, L. Alvarez-Cohen, Aerobic biotransformation of fluorotelomer thioether amido sulfonate (Lodyne) in AFFF-amended microcosms, *Environ. Sci. Technol.* 49 (2015) 7666–7674.
- [44] E.F. Houtz, D.L. Sedlak, Oxidative conversion as a means of detecting precursors to perfluoroalkyl acids in urban runoff, *Environ. Sci. Technol.* 46 (2012) 9342–9349.
- [45] APHA (American Public Health Association), *Standard Methods for the Examination of Water and Wastewater*, 20th Ed., Washington DC, 1998. ISBN 9780875532356.
- [46] V. Boiteux, C. Bach, V. Sagres, J. Hemard, A. Colin, C. Rosin, J. Munoz, X. Dauchy, Analysis of 29 per- and polyfluorinated compounds in water, sediment, soil and sludge by liquid chromatography–tandem mass spectrometry, *Int. J. Environ. Anal. Chem.* 96 (2016) 705–728.
- [47] C.E. Schaefer, C. Anday, A. Burant, C.W. Condee, A. Urriaga, T.J. Strathmann, C.P. Higgins, Electrochemical treatment of perfluorooctanoic acid and perfluorooctane sulfonate: insights into mechanisms and application to groundwater treatment, *Chem. Eng. J.* 317 (2017) 424–432.
- [48] M. Panizza, P.A. Michaud, G. Cerisola, Ch. Cominellis, Anodic oxidation of 2-naphthol at boron-doped diamond electrodes, *J. Electroanal. Chem.* 507 (2001) 206–214.
- [49] A. Urriaga, I. Ortiz, A. Anglada, D. Mantzavinos, E. Diamadopoulos, Kinetic modeling of the electrochemical removal of ammonium and COD from landfill leachates, *J. Appl. Electrochem.* 42 (2012) 779–786.
- [50] G. Pérez, J. Saiz, R. Ibañez, A.M. Urriaga, I. Ortiz, Assessment of the formation of inorganic oxidation by-products during the electrocatalytic treatment of ammonium from landfill leachates, *Water Res.* 46 (2012) 2579–2590.
- [51] A. Urriaga, C. Fernández-González, S. Gómez-Lavín, I. Ortiz, Kinetics of the electrochemical mineralization of perfluorooctanoic acid on ultrananocrystalline boron doped conductive diamond electrodes, *Chemosphere* 129 (2015) 20–26.
- [52] Q. Zhuo, X. Li, F. Yan, B. Yang, S. Deng, J. Huang, G. Yu, Electrochemical oxidation of 1H,1H,2H,2H-perfluorooctane sulfonic acid (6:2 FTS) on DSA electrode: Operating parameters and mechanism, *J. Environ. Sci.* 26 (2014) 1733–1739.
- [53] S. Park, L.S. Lee, V.F. Medina, A. Zull, S. Waisner, Heat-activated persulfate oxidation of PFOA, 6:2 fluorotelomer sulfonate, and PFOS under conditions suitable for in-situ groundwater remediation, *Chemosphere* 145 (2016) 376–383.
- [54] X. Yang, J. Huang, K. Zhang, G. Yu, S. Deng, B. Wang, Stability of 6:2 fluorotelomer sulfonate in advanced oxidation processes: Degradation kinetics and pathway, *Environ. Sci. Pollut. R.* 21 (2014) 4634–4642.
- [55] Á. Soriano, D. Gorri, A. Urriaga, Efficient treatment of perfluorohexanoic acid by nanofiltration followed by electrochemical degradation of the NF concentrate, *Water Res.* 112 (2017) 147–156.
- [56] A. Cabeza, A.M. Urriaga, I. Ortiz, Electrochemical treatment of landfill leachates using a boron-doped diamond anode, *Ind. Eng. Chem. Res.* 46 (2007) 1439–1446.
- [57] L.W.Y. Yeung, Y. Miyake, S. Taniyasu, Y. Wang, H. Yu, M.K. So, G. Jiang, Y. Wu, J. Li, J.P. Giesy, N. Yamashita, P.K.S. Lam, Perfluorinated compounds and total and extractable organic fluorine in human blood samples from China, *Environ. Sci. Technol.* 42 (2008) 8140–8145.
- [58] Y. Miyake, N. Yamashita, P. Rostkowski, M.K. So, S. Taniyasu, P.K.S. Lam, K. Kannan, Determination of trace levels of total fluorine in water using combustion ion chromatography for fluorine: a mass balance approach to determine individual perfluorinated chemicals in water, *J. Chromatogr. A* 1143 (2007) 98–104.

## **SUPPORTING INFORMATION**

### **Efficient electrochemical degradation of poly- and perfluoroalkyl substances (PFASs) from the effluents of an industrial wastewater treatment plant**

#### **Authors:**

Beatriz Gomez-Ruiz<sup>a</sup>, Sonia Gómez-Lavín<sup>a</sup>, Nazely Diban<sup>a</sup>, Virginie Boiteux<sup>b</sup>, Adeline  
Colin<sup>b</sup>, Xavier Dauchy<sup>b</sup>, Ane Urriaga<sup>a,\*</sup>

a) Department of Chemical and Biomolecular Engineering. Universidad de Cantabria.  
Av. de Los Castros s/n. 39005 Santander. Spain.

\* Corresponding author: [urriaga@unican.es](mailto:urriaga@unican.es)

b) ANSES, Nancy Laboratory for Hydrology, Water Chemistry Department, 40 rue  
Lionnois, 54000 Nancy, France.

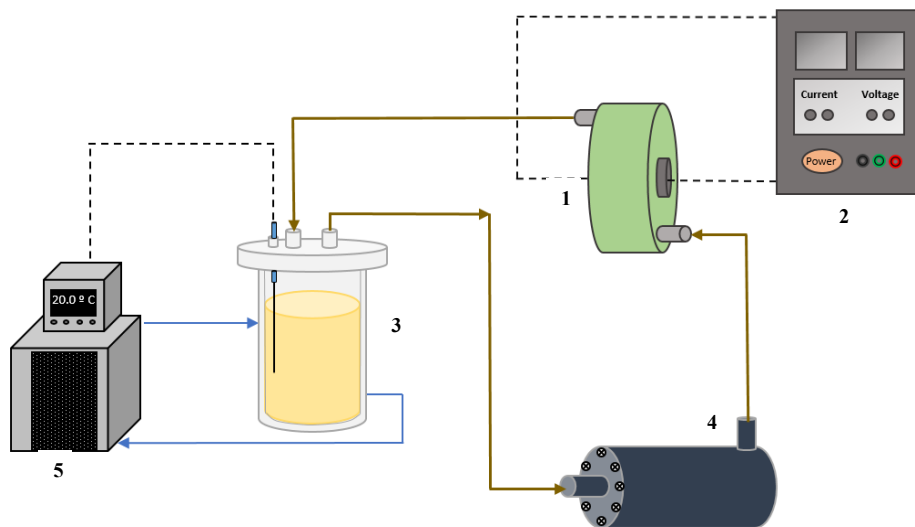


**Figure S1.** Electro-oxidation experimental system (1: Electro-oxidation Cell, 2: Power Supply, 3: Feed Tank, 4: Pump, 5: Refrigeration System).

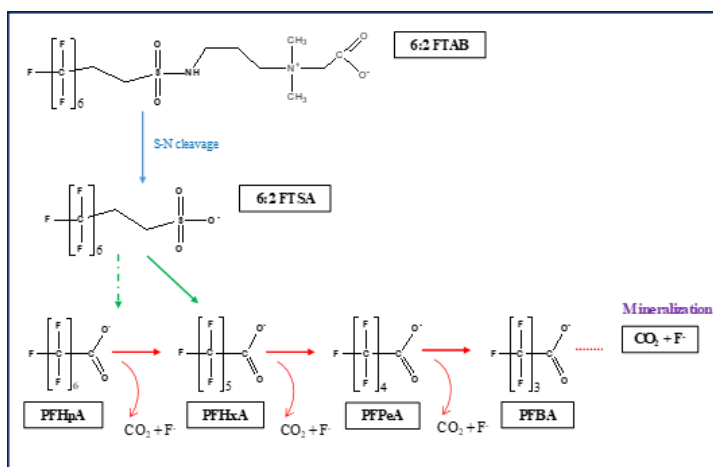


**Figure S2.** Electrochemical oxidation pathways for the predominant PFASs contained in the wastewater sample according to the literature.

**Table S1.** Evolution of PFASs concentration (ng/L) with time during electrochemical experiment of E sample at a current density of 50 mA/cm<sup>2</sup>.

Analyte	E_t=0h	E_J=50mA/cm <sup>2</sup> _t=1h	E_J=50mA/cm <sup>2</sup> _t=2h	E_J=50mA/cm <sup>2</sup> _t=4h	E_J=50mA/cm <sup>2</sup> _t=6h	E_J=50mA/cm <sup>2</sup> _t=8h	E_J=50mA/cm <sup>2</sup> _t=10h
PFBS	<2,000	<2,000	<2,000	<2,000	<2,000	<2,000	<2,000
PFHXS	<2,000	<2,000	<2,000	<2,000	<2,000	<2,000	<2,000
PFHpS	<2,000	<2,000	<2,000	<2,000	<2,000	<2,000	<2,000
PFOS	<2,000	<2,000	<2,000	<2,000	<2,000	<2,000	<2,000
PFDS	<2,000	<2,000	<2,000	<2,000	<2,000	<2,000	<2,000
PFBA	7,544	36,476	44,002	30,393	12,432	9,405	<2,000
PFPeA	52,500	38,808	26,012	11,066	3,518	2,376	<2,000
PFHxA	24,827	56,002	36,870	13,233	2,121	2,156	<2,000
PFHpA	37,847	27,676	15,301	5,478	<2,000	<2,000	<2,000
PFOA	2,063	1,694	<2,000	<2,000	<2,000	<2,000	<2,000
PFNA	<2,000	<2,000	<2,000	<2,000	<2,000	<2,000	<2,000
PFDA	<2,000	<2,000	<2,000	<2,000	<2,000	<2,000	<2,000
PFUnDA	<2,000	<2,000	<2,000	<2,000	<2,000	<2,000	<2,000
PFDoDA	<2,000	<2,000	<2,000	<2,000	<2,000	<2,000	<2,000
PFTriDA	<5,000	<5,000	<5,000	<5,000	<5,000	<5,000	<5,000
PFTeDA	<5,000	<5,000	<5,000	<5,000	<5,000	<5,000	<5,000
4:2FTSA	<2,000	<2,000	<2,000	<2,000	<2,000	<2,000	<2,000
6:2FTSA	382,200	269,600	135,800	51,480	15,603	8,228	4,224
8:2FTSA	<2,000	<2,000	<2,000	<2,000	<2,000	<2,000	<2,000
FOSA	<5,000	<5,000	<5,000	<5,000	<5,000	<5,000	<5,000
6:2 FTCA	<5,000	4,323	4,246	2,376	<5,000	<5,000	<5,000
8:2 FTCA	<5,000	<5,000	<5,000	<5,000	<5,000	<5,000	<5,000
10:2 FTCA	<5,000	<5,000	<5,000	<5,000	<5,000	<5,000	<5,000
5:3 ACID	<5,000	<5,000	<5,000	<5,000	<5,000	<5,000	<5,000
6:2 FTUCA	<5,000	<5,000	<5,000	<5,000	<5,000	<5,000	<5,000
8:2 FTUCA	<5,000	<5,000	<5,000	<5,000	<5,000	<5,000	<5,000
10:2 FTUCA	<5,000	<5,000	<5,000	<5,000	<5,000	<5,000	<5,000
6:2 FTAB	1,143,000	N.M.*	180,544	N.M.	N.M.	N.M.	<25
M4	2,414	N.M.	<25	N.M.	N.M.	N.M.	<25

\* N.M.: Not measured

\*\* The limits of quantification were 25, 2,000 or 5,000 ng/L for the PFASs, as shown in the table

**Table S2.** Name, acronym and optimised UHPLC-MS/MS parameters for target analytes and IS.

Compound name	Acronym	IS	UHPLC-MS/MS			
			Precursor ion (m/z)	Product ions (m/z)	Cone voltage (V)	CE <sup>a</sup> (eV)
<b>Perfluoroalkane Sulphonic Acids</b>	<b>PFSA</b> s					
Perfluorobutane sulphonate anion	PFBS	mPFHxA	299	<b>99</b> / 80	40	31 / 30
Perfluorohexane sulphonate anion	PFHxS	mPFOA	399	<b>99</b> / 80	45	31 / 33
Perfluoroheptane sulphonate anion	PFHpS	mPFOA	449	<b>99</b> / 80	54	34 / 40
Perfluorooctane sulphonate anion	PFOS	mPFOS	499	<b>99</b> / 80	60	38 / 39
Perfluorodecane sulphonate anion	PFDS	mPFDoDA	599	<b>99</b> / 80	66	46 / 42
<b>Perfluoroalkyl Acids</b>	<b>PFC</b> As					
Perfluorobutanoate	PFBA	mPFBA	213	<b>169</b> / 213	12	10 / 2
Perfluoropentanoate	PFPeA	mPFHxA	263	<b>219</b> / 263	12	9 / 2
Perfluorohexanoate	PFHxA	mPFHxA	313	<b>269</b> / 119	16	10 / 17
Perfluoroheptanoate	PFHpA	mPFHxA	363	<b>319</b> / 169	16	10 / 19
Perfluorooctanoate	PFOA	mPFOA	413	<b>369</b> / 169	16	10 / 19
Perfluorononanoate	PFNA	mPFOA	463	<b>419</b> / 219	16	10 / 17
Perfluorodecanoate	PFDA	mPFDA	513	<b>469</b> / 219	16	10 / 18
Perfluoroundecanoate	PFUnDA	mPFUnDA	563	<b>519</b> / 269	16	12 / 20
Perfluorododecanoate	PFDoDA	mPFDoDA	613	<b>569</b> / 269	16	15 / 16
Perfluorotridecanoate	PFTTrDA	mPFDoDA	663	<b>619</b> / 169	18	15 / 20
Perfluorotetradecanoate	PFTeDA	mPFDoDA	713	<b>669</b> / 369	18	12 / 28
<b>Fluorotelomers</b>	<b>FT</b> s					
4:2 Fluorotelomer sulphonate anion	4:2 FTSA	m6:2 FTSA	327	<b>307</b> / 80	36	16 / 26
6:2 Fluorotelomer sulphonate anion	6:2 FTSA	m6:2 FTSA	427	<b>407</b> / 80	38	20 / 34
8:2 Fluorotelomer sulphonate anion	8:2 FTSA	m6:2 FTSA	527	<b>507</b> / 80	46	24 / 32
Perfluorooctane sulphonamide	FOSA	mPFDoDA	498	<b>78</b> / 478	42	30 / 20
6:2 Fluorotelomer carboxylic acid	6:2 FTCA	m6:2 FTCA	377	<b>293</b> / 313	14	18 / 6
8:2 Fluorotelomer carboxylic acid	8:2 FTCA	m8:2 FTCA	477	<b>393</b> / 413	12	14 / 8
10:2 Fluorotelomer carboxylic acid	10:2 FTCA	m8:2 FTCA	577	<b>493</b> / 513	14	12 / 8
5:3 Acid	5:3 ACID	m6:2 FTCA	341	<b>237</b> / 271	20	12 / 24
6:2 Fluorotelomer unsaturated	6:2 FTUCA	m8:2	357	<b>293</b> / 243	16	18 / 34

carboxylic acid		FTUCA				
8:2 Fluorotelomer unsaturated carboxylic acid	8:2 FTUCA	m8:2 FTUCA	457	<b>393</b> / 343	16	12 / 38
10:2 Fluorotelomer unsaturated carboxylic acid	10:2 FTUCA	m10:2 FTUCA	557	<b>493</b> / 243	20	16 / 36
6:2 Fluorotelomer sulphonamide alkylbetaine	6:2 FTAB	addition standard	569	<b>549</b> / 223	50	30 / 24
6:2 Fluorotelomer sulphonamide propyl N.N dimethylamine	M4	addition standard	511	<b>491</b> / 165	48	30 / 36
<b>Internal labelled standard</b>	<b>IS</b>					38
Perfluoro-n-[1,2,3,4- <sup>13</sup> C <sub>4</sub> ]octane sulphonate anion	mPFOS		503	<b>99</b>	60	10
Perfluoro- n-[ <sup>13</sup> C <sub>4</sub> ]butanoate	mPFBA		217	<b>172</b>	14	10
Perfluoro- n-[1,2- <sup>13</sup> C <sub>2</sub> ]hexanoate	mPFHxA		315	<b>207</b>	13	10
Perfluoro- n-[1,2,3,4- <sup>13</sup> C <sub>4</sub> ]octanoate	mPFOA		417	<b>372</b>	16	10
Perfluoro- n-[1,2- <sup>13</sup> C <sub>2</sub> ]decanoate	mPFDA		515	<b>470</b>	16	15
Perfluoro- n-[1,2- <sup>13</sup> C <sub>2</sub> ]undecanoate	mPFUnDA		565	<b>520</b>	15	12
Perfluoro- n-[1,2- <sup>13</sup> C <sub>2</sub> ] Perfluorododecanoate	mPFDoDA		615	<b>570</b>	16	26
6:2 Fluorotelomer-[1,2- <sup>13</sup> C <sub>2</sub> ] sulphonate anion	m6:2 FTSA		429	<b>409</b>	40	24
6:2 Fluorotelomer-[1,2- <sup>13</sup> C <sub>2</sub> ]carboxylic acid	m6:2 FTCA		379	<b>294</b>	12	14
8:2 Fluorotelomer-[1,2- <sup>13</sup> C <sub>2</sub> ]carboxylic acid	m8:2 FTCA		479	<b>394</b>	14	14
8:2 Fluorotelomer-[1,2- <sup>13</sup> C <sub>2</sub> ] unsaturated carboxylic acid	m8:2 FTUCA		459	<b>394</b>	18	14
10:2 Fluorotelomer-[1,2- <sup>13</sup> C <sub>2</sub> ] unsaturated carboxylic acid	m10:2 FTUCA		559	<b>494</b>	24	16 / 26

Bold means transitions used for quantification; <sup>a</sup> Collision Energy





5.4. Scientific publication 4.

**Photocatalytic degradation and mineralization of  
perfluorooctanoic acid (PFOA) using a composite TiO<sub>2</sub>-rGO  
catalyst**

Authors:

Beatriz Gomez-Ruiz, Paula Ribao, Nazely Diban, Maria J. Rivero,  
Inmaculada Ortiz, Ane Urriaga

Department of Chemical and Biomolecular Engineering. University of  
Cantabria. Av. de Los Castros s/n. 39005 Santander. Spain

---

*Accepted 25 November 2017*

*Journal of Hazardous Materials*

*Volume 344 (2018), Pages 950-957*

DOI: <https://doi.org/10.1016/j.jhazmat.2017.11.048>



ELSEVIER

Contents lists available at ScienceDirect

## Journal of Hazardous Materials

journal homepage: [www.elsevier.com/locate/jhazmat](http://www.elsevier.com/locate/jhazmat)

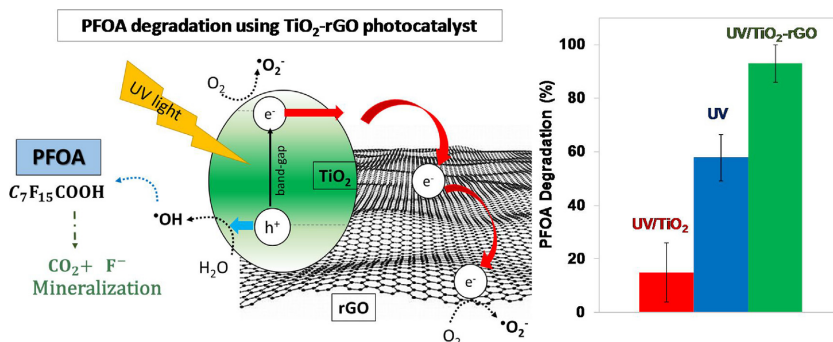
# Photocatalytic degradation and mineralization of perfluorooctanoic acid (PFOA) using a composite $\text{TiO}_2$ –rGO catalyst

Beatriz Gomez-Ruiz, Paula Ribao, Nazely Diban, Maria J. Rivero, Inmaculada Ortiz, Ane Urriaga\*

Department of Chemical and Biomolecular Engineering, Universidad de Cantabria, Av. de Los Castros s/n, 39005 Santander, Spain



## GRAPHICAL ABSTRACT



## HIGHLIGHTS

- Photocatalytic decomposition of PFOA using a  $\text{TiO}_2$ -rGO catalyst was studied.
- $\text{TiO}_2$ -rGO catalyst ( $0.1 \text{ g L}^{-1}$ ) allowed  $93 \pm 7\%$  PFOA removal under UV–vis irradiation.
- Formation of intermediate PFCAs and  $\text{F}^-$  elucidated the PFOA degradation mechanism.
- Faster degradation kinetics were observed for shorter carbon-chain PFCAs.

## ARTICLE INFO

## Article history:

Received 20 June 2017

Received in revised form

24 November 2017

Accepted 25 November 2017

Available online 28 November 2017

## Keywords:

Perfluorooctanoic acid

PFOA

 $\text{TiO}_2$ -rGO

## ABSTRACT

The inherent resistance of perfluoroalkyl substances (PFASs) to biological degradation makes necessary to develop advanced technologies for the abatement of this group of hazardous substances. The present work investigated the photocatalytic decomposition of perfluorooctanoic acid (PFOA) using a composite catalyst based on  $\text{TiO}_2$  and reduced graphene oxide (95%  $\text{TiO}_2$ /5% rGO) that was synthesized using a facile hydrothermal method. The efficient photoactivity of the  $\text{TiO}_2$ -rGO ( $0.1 \text{ g L}^{-1}$ ) composite was confirmed for PFOA ( $0.24 \text{ mmol L}^{-1}$ ) degradation that reached  $93 \pm 7\%$  after 12 h of UV–vis irradiation using a medium pressure mercury lamp, a great improvement compared to the  $\text{TiO}_2$  photocatalysis ( $24 \pm 11\%$  PFOA removal) and direct photolysis ( $58 \pm 9\%$ ). These findings indicate that rGO provided the suited properties of  $\text{TiO}_2$ -rGO, possibly as a result of acting as electron acceptor and avoiding the high recombination electron/hole pairs.

\* Corresponding author.

E-mail address: [urriaga@unican.es](mailto:urriaga@unican.es) (A. Urriaga).

Titanium dioxide  
Graphene oxide  
Photocatalysis

The release of fluoride and the formation of shorter-chain perfluorocarboxylic acids, that were progressively eliminated in a good match with the analysed reduction of total organic carbon, is consistent with a step-by-step PFOA decomposition via photogenerated hydroxyl radicals. Finally, the apparent first order rate constants of the TiO<sub>2</sub>-rGO UV-vis PFOA decompositions, and the intermediate perfluorocarboxylic acids were found to increase as the length of the carbon chain was shorter.

© 2017 Elsevier B.V. All rights reserved.

## 1. Introduction

The presence of poly- and perfluoroalkyl substances (PFASs) in industrial emissions, drinking water sources and groundwaters is of increasing concern due to their extreme persistence and potential toxicity [1–3]. As a result, the Stockholm Convention on Persistent Organic Pollutants restricted the use and production of perfluorooctanesulfonate (PFOS) and its salts, and at present perfluorooctanoic acid (PFOA) and PFOA related compounds are under review for listing under the Convention [4]. The United States Environmental Protection Agency established health advisory levels for PFOA and PFOS in drinking water at 0.07 µg L<sup>-1</sup>, both individually and combined [5].

Due to the inherent resistance of PFOA, PFOS and related compounds to biological degradation [6–8], there is an intense research on chemical oxidation/reduction technologies to degrade PFASs in water, including direct photolysis, photochemical oxidation, photochemical reduction, photocatalytic oxidation, electrochemical oxidation, persulfate oxidation and sonochemical pyrolysis [9–18]. Among these technologies, direct photolysis is an alternative that operates at ambient temperature and pressure and it does not require additional chemicals. However, the studies published so far have shown that PFOA was only efficiently decomposed using a light source emitting at wavelengths from deep UV-region to 220 nm [19,20] or under elevated irradiation intensity [21]. Therefore, direct photolysis application is constrained by the high energy demand needed to obtain the intensity of the active irradiating light and the long treatment times.

A literature survey about the photocatalytic PFOA degradation in aqueous media is summarized in Table S1 (Supplementary Material). Despite the suitable properties of TiO<sub>2</sub> catalyst, such as non-toxicity, photostability and low cost [22–24], the majority of the previous studies revealed the low PFOA degradation rate achieved by TiO<sub>2</sub> photocatalysis, which was comprised in the range 7–44% in most of the studies [12,21,25–33]. The limited performance of TiO<sub>2</sub> is attributed to its relatively large band-gap, high recombination rate of electron-hole pairs and limited use of visible light spectrum. Nevertheless, the comparison of previous research is hindered by the diversity of the applied experimental conditions, e.g.: light intensity (0.45–9.5 mW cm<sup>-2</sup>), wavelength spectrum emitted by the light source (200–600 nm), reactor volume (0.12–3 L) and treatment time. The reaction medium has been also widely varied, in terms of PFOA concentration, background electrolytes and O<sub>2</sub> or N<sub>2</sub> supply [34]. Yet, the catalyst dosage was quite homogeneous in all the reviewed research, and was varied in the range of 0.25–2 g L<sup>-1</sup>. The highest reported PFOA removal rates, 98%, could be associated to the use of high intensity irradiation, a factor that would accelerate the degradation rates [21,34].

Recently, different strategies have been proposed to overcome TiO<sub>2</sub> limitations, such as the synthesis of titanate nanotubes (TNTs) out of a commercial TiO<sub>2</sub> catalyst, that doubled the PFOA degradation rate [21]. Other approaches consisted of modifying the process conditions. Within this group, TiO<sub>2</sub>-mediated photocatalysis combined with perchloric acid [26] or ultrasonication [35], achieved 2-fold and almost 5-fold improvements in the PFOA degradation

rate, respectively. The addition of oxalic acid also accelerated PFOA decomposition using TiO<sub>2</sub> under nitrogen atmosphere [27]. However, these methods would involve adding different substances to the polluted water. A more promising strategy is focused on the synthesis of new composite catalysts that combine the photocatalytic of TiO<sub>2</sub> with transition metals, e.g.: Fe, Nb, Cu, Pb [12,30,36] or with noble metal nanoparticles Ag, Pt or Pd [31]. Transition and noble metals have demonstrated to act as electron traps preventing the high electron-hole recombination, to successfully improve the photocatalytic features of TiO<sub>2</sub>-doped composites [37]. Also Song et al. [32] showed that the use of composites of TiO<sub>2</sub> with multiple wall carbon nanotubes (TiO<sub>2</sub>-MWCNT) enhanced the photocatalytic PFOA decomposition.

Among the new strategies to enhance the efficiency of photocatalysts, the combination of TiO<sub>2</sub> with graphene materials has been reported to increase the lifetime of electron-hole pairs, by reducing charge recombination, due to the excellent electron trapping and electrical conductivity properties of graphene. It is also thought that graphene provides a superior photoresponse by extending the excitation wavelength compared to bare TiO<sub>2</sub> [37–40]. The effective photocatalytic activity of the composite catalysts based on TiO<sub>2</sub> and graphene or graphene oxide has been demonstrated for the degradation of dyes as model of organic pollutants [39,41–44], and in a few seminal studies dealing with more complex organic contaminants, such as, dodecylbenzenesulfonate [45], diphenhydramine [46] or phenols [40]. A notable gap is that TiO<sub>2</sub>-graphene composite photocatalysts have not been tested yet for the degradation of neither PFOA nor other PFASs.

This study aims to explore the photocatalytic degradation of PFOA by means of a composite catalyst of TiO<sub>2</sub> and reduced graphene oxide (TiO<sub>2</sub>-rGO). Photocatalysis experiments under UV-vis irradiation examined the effect of TiO<sub>2</sub>-rGO catalyst concentration on PFOA removal and defluorination, and evaluated the generation of shorter-chain perfluorinated intermediate products, as well as the total organic carbon reduction. Results were compared with bare TiO<sub>2</sub> and direct photolysis conditions to gain insight into factors influencing the significant photocatalytic enhancement that was provided by the TiO<sub>2</sub>-rGO material. Finally, this work assessed the effect of the alkyl chain length on the kinetics of the photocatalytic degradation of perfluorocarboxylic acids by means of TiO<sub>2</sub>-rGO composite catalyst.

## 2. Materials and methods

### 2.1. Chemical reagents

All chemicals were reagent grade or higher and were used as received without further purification. PFOA (C<sub>7</sub>F<sub>13</sub>COOH, 96% purity), perfluoroheptanoic acid (PFHpA, C<sub>6</sub>F<sub>13</sub>COOH, 99% purity), perfluorohexanoic acid (PFHxA, C<sub>5</sub>F<sub>11</sub>COOH, 96% purity), perfluoropentanoic acid (PFPeA, C<sub>4</sub>F<sub>9</sub>COOH, 97% purity) were purchased from Sigma Aldrich Chemicals. TiO<sub>2</sub> (P25, 20% rutile and 80% anatase, 50 m<sup>2</sup> g<sup>-1</sup>, 21 nm) was obtained from Evonik Degussa. Graphite powder was supplied by Acros Organics. Sulfuric acid 95–98% (H<sub>2</sub>SO<sub>4</sub>), chloride acid 37% (HCl), potassium permanganate

( $\text{KMnO}_4$ ), sodium nitrate ( $\text{NaNO}_3$ ), phosphoric acid (85%) and sodium di-hydrogen phosphate anhydrous were provided by Pan-reac. Hydrogen peroxide ( $\text{H}_2\text{O}_2$ , 30% v/v) and Methanol (UHPLC–MS grade) were obtained from Scharlau. All solutions were prepared using ultrapure water (Q-POD Millipore).

## 2.2. Synthesis of composite $\text{TiO}_2$ -rGO catalyst

The first step was the synthesis of graphene oxide (GO) using the modified Hummers method [47] by the oxidation of graphite powder with  $\text{NaNO}_3$ ,  $\text{H}_2\text{SO}_4$  and  $\text{KMnO}_4$ . The oxidized graphite was centrifuged and washed with ultrapure water and with an aqueous HCl solution. The remaining solid was ultrasonicated to achieve exfoliated graphene oxide nanosheets. After that, the sample was centrifuged and the supernatant was collected and dried in an oven overnight, obtaining GO as a solid [46].

$\text{TiO}_2$ -rGO composites were synthesized using the hydrothermal method and following the procedure reported in the literature [37,48]. In brief, commercial  $\text{TiO}_2$  was added into 150 mL GO dispersion in ultrapure water. The content of GO was controlled to be 5% wt. in the  $\text{TiO}_2$ -rGO composites. After stirring for 2 h, the solution was placed in a 200 mL Teflon-lined stainless steel auto-clave and maintained at  $120^\circ\text{C}$  for 3 h, to achieve simultaneously the reduction of GO and the loading of  $\text{TiO}_2$  on the reduced GO sheets. The resulting composite was recovered by centrifugation, rinsed with ultrapure water, and fully dried at  $50^\circ\text{C}$  overnight.

The successful synthesis of the composite  $\text{TiO}_2$ -rGO was examined by means of Attenuated Total Reflectance Fourier Transformed Infrared (ATR-FTIR) spectroscopy (Fig. S1, Supplementary material). The intensity increase of the ATR-FTIR bands between 500 and  $900\text{ cm}^{-1}$  for  $\text{TiO}_2$ -rGO in contrast to the  $\text{TiO}_2$  material was indicating the formation of Ti–O–C bonds in addition to the typical Ti–O–Ti bonds present in  $\text{TiO}_2$ . Furthermore, Transmission Electron Microscopy (TEM) results (Fig. S2 in Supplementary material) demonstrated the homogeneous distribution of the  $\text{TiO}_2$  catalysts on the rGO surface. Energy dispersive X-ray (EDX) spectroscopy of two distinct zones of the  $\text{TiO}_2$ -rGO material were done to qualitatively discern between  $\text{TiO}_2$  and GO presence. Both ATR-FTIR and TEM-EDX results are similar to those reported by Ribao et al. [37]. X-ray diffraction analysis (Fig. S3 in Supplementary material) showed that the crystalline phase of the commercial P25  $\text{TiO}_2$  was maintained in the  $\text{TiO}_2$ -rGO composite after the hydrothermal synthesis. Therefore, it can be deemed that  $\text{TiO}_2$ -rGO composites were successfully prepared via hydrothermal synthesis. Finally, the specific surface area ( $S$ ) of the catalyst materials was calculated by the Brunauer-Emmett-Teller (BET) method from the nitrogen adsorption-desorption isotherm data employing the ASAP 2000 surface area analyzer (Micromeritics).

## 2.3. Photocatalytic experiments

The schematic of experimental setup is shown in the Supplementary material, Fig. S4. Photocatalytic experiments were conducted in a 1 L Heraeus Laboratory UV Reactor mounted on an Agimatic-S magnetic stirring plate (JP Selecta, Spain). A water/ethylene-glycol cooling jacket (PolyScience Digital Temperature Controller) was used to keep the reactor temperature at  $293$ – $298\text{ K}$ . A medium-pressure mercury lamp (Heraeus Noblelight TQ 150 W z1) with an emission spectrum between 200 and  $600\text{ nm}$  (Fig. S5, Supplementary material) was used as irradiation source. The lamp was placed in a quartz sleeve in the centre of the reactor. It is noteworthy that the quartz sleeve of the lamp did not absorb light in the UV wavelength range of interest. PFOA aqueous solutions  $0.24\text{ mmol L}^{-1}$  were used as feed in all experiments. The initial pH of the PFOA solution was 3.8 and it was not adjusted during the experiments. The  $\text{TiO}_2$ -rGO catalyst doses were 0.05, 0.1 and  $0.5\text{ g L}^{-1}$ .

Samples were withdrawn from the reactor at different time intervals and filtered through  $0.45\text{ }\mu\text{m}$  polypropylene filters to remove the catalyst particles before analysis. A HD2102.1 photo/radiometer (Delta OHM) provided with VIS-NIR, UVA, UVB and UVC detectors allowed measuring the light intensity received on the outer wall of the glass reactor.

## 2.4. Analytical methods

The concentration of PFOA and its degradation products, PFHpA, PFHxA, PFPeA were analysed using HPLC–DAD (Water 2695) system equipped with a X Bridge C18 column ( $5\text{ }\mu\text{m}$ ,  $250\text{ mm} \times 4.6\text{ mm}$ , Waters). The separation column was set in an oven at  $40^\circ\text{C}$ . A mixture of methanol (65%) and di-hydrogen phosphate (35%) was used as mobile phase in isocratic mode with a flow rate of  $0.5\text{ mL min}^{-1}$ . The wavelength of the detector was set at  $204\text{ nm}$ . The limit of quantification (LOQ) was  $10\text{ mg L}^{-1}$  for PFOA and  $5\text{ mg L}^{-1}$  for PFHpA, PFHxA and PFPeA.

TOC analyses were performed using a TOC-V CPH (Shimadzu). Fluoride was analyzed by ion chromatography (Dionex 120 IC) provided with an IonPac As-HC column and using a  $9\text{ mM Na}_2\text{CO}_3$  solution as eluent, that was circulated at a flowrate of  $1\text{ mL min}^{-1}$ , based on Standard Methods 4110B (Standard Methods, 1998). The LOQ for fluoride analysis was  $0.03\text{ mg L}^{-1}$ . The possible fluoride incorporation onto the  $\text{TiO}_2$ -rGO surface was investigated by X-ray photoelectron spectroscopy (XPS), using a SPECS (Berlin, Germany) system equipped with a Phoibos 150 1D-DLD analyser and monochromatic Al  $K_{\alpha}$  radiation ( $1486.6\text{ eV}$ ).

## 3. Results and discussion

### 3.1. Photocatalytic decomposition of PFOA

The photocatalytic degradation of PFOA using the  $\text{TiO}_2$ -rGO composite and commercial  $\text{TiO}_2$  was studied. Moreover, the removal of PFOA by direct photolysis under UV irradiation was also studied for comparison. The intermediate products formed upon PFOA degradation were analysed, and PFOA mineralization rate was monitored using the progress of TOC and the released fluoride as indicators. The adsorption of PFOA in the experimental system was negligible (less than 1%) after 12 h of contact of the feed solution inside the glass reactor. The amount of PFOA adsorbed on the  $\text{TiO}_2$  and  $\text{TiO}_2$ -rGO ( $0.5\text{ g L}^{-1}$ ) were found to be  $6.4 \pm 0.6\%$  and  $8.4 \pm 0.4\%$ , respectively, after 12 h of contact under stirring in dark conditions. These values of adsorption could be explained by the higher BET specific surface area of  $\text{TiO}_2$ -rGO,  $S_{\text{TiO}_2\text{-rGO}} = 62.2\text{ m}^2\text{ g}^{-1}$ , compared to  $\text{TiO}_2$ ,  $S_{\text{TiO}_2} = 50\text{ m}^2\text{ g}^{-1}$  [48]. Similar values of PFOA adsorption on  $\text{TiO}_2$  and metal-modified  $\text{TiO}_2$  have been reported [31]. The electrostatic attraction between the negatively charged perfluorooctanoate anion and the positively charged surface of  $\text{TiO}_2$  particles in acidic solution could have favoured the adsorption [12,26], that nevertheless reached only a minor fraction of the initial content.

Next, the influence of the photocatalytic media was assessed. Fig. 1 allows the comparison of the disappearance of PFOA with time by means of direct photolysis (without catalyst) and when using  $\text{TiO}_2$  and  $\text{TiO}_2$ -rGO as photocatalysts. In every experiment, a volume of  $0.8\text{ L}$  of an aqueous PFOA solution ( $0.24\text{ mmol L}^{-1}$ ) was irradiated. It is observed that the application of UV light in the absence of any catalyst produced a significant PFOA degradation that reached  $58 \pm 9\%$  removal after 12 h of irradiation. These results are in agreement with available data reported elsewhere [9,21]. PFOA molecule strongly absorbs light with wavelengths from deep UV-region to  $220\text{ nm}$ , and presents weak absorption in the  $220$ – $270\text{ nm}$  range of light wavelengths [19]. In line with

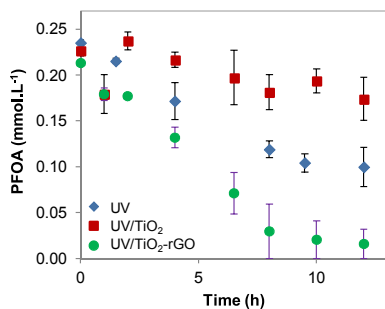


Fig. 1. Evolution of PFOA concentration ( $\text{mmol L}^{-1}$ ) with irradiation time by photolysis and photocatalysis using  $\text{TiO}_2$  and  $\text{TiO}_2$ -rGO; photocatalyst loading:  $0.1 \text{ g L}^{-1}$ .

these properties, some authors reported high PFOA photoabatement using a vacuum UV lamp with a monochromatic emission at 185 nm, although the kinetics of PFOA removal were significantly reduced when using the more common emission at 254 nm [49,50]. However, the comparison of literature data about the direct photolysis of PFOA is hindered by the diversity of the applied experimental conditions, range of UV emission wavelength and power of the UV lamp [21]. In line with the previous discussion, it was concluded that the medium-pressure mercury lamp used in the present study promoted PFOA degradation by means of the deep UV-region of its emission spectrum.

The addition of the  $\text{TiO}_2$  catalyst (Fig. 1, UV- $\text{TiO}_2$ ) had the effect of decreasing the PFOA removal to only  $24 \pm 11\%$ , after 12 h of irradiation. Although PFOA could have been partially adsorbed on the  $\text{TiO}_2$  surface (6.4% adsorption was observed in the dark experiments), the little release of fluoride ( $0.14 \text{ mmol L}^{-1}$ ) and the detection of a small amount of PFHpA ( $0.023 \text{ mmol L}^{-1}$ ) confirmed that PFOA had been partially degraded into shorter-chain perfluorocarboxylic acids. The lower degradation rate of PFOA observed upon the addition of  $\text{TiO}_2$  can be assigned to a light screening effect by the  $\text{TiO}_2$  particles, that would have significantly reduced the penetration of the UV light into the reaction medium [51]. In contrast, the use of the  $\text{TiO}_2$ -rGO composite (Fig. 1, UV- $\text{TiO}_2$ -rGO) enhanced PFOA degradation compared to direct photolysis and  $\text{TiO}_2$ -mediated photocatalysis.  $93 \pm 7\%$  of the initial PFOA was removed after 12 h of irradiation, 4-fold higher than in  $\text{TiO}_2$ -mediated photocatalysis for the same reaction time. This high degradation has been previously demonstrated in the literature using  $\text{TiO}_2$  catalysts modified with metals such as Pb [36]. Moreover, a control experiment using GO nanoplatelets showed that graphene oxide particles did not produce a significant variation

of PFOA concentration, at the same time no degradation products were detected in solution. This result pointed out a synergistic effect between the reduced graphene oxide (rGO) layers and  $\text{TiO}_2$  nanoparticles during the photocatalytic degradation of PFOA. The effect can be ascribed to the good transparency of one-atom thickness rGO sheets towards the UV-vis spectrum, that can decrease the light screening phenomena caused by  $\text{TiO}_2$  particles, and therefore, facilitate a more efficient utilization of light and avoid the electron-hole recombination [39,52].

The irradiance received on the outer wall of the reactor was measured to get an indirect evaluation of the light screening phenomena. The results are displayed in Fig. 2, using a background PFOA ( $0.24 \text{ mmol L}^{-1}$ ) aqueous solution in all cases. The radiation received when using  $\text{TiO}_2$  suspensions was significantly lower than through  $\text{TiO}_2$ -rGO suspensions, for every ultraviolet light range tested and for each catalyst concentration. If we focus on the UV-A range (315–400 nm) and  $0.1 \text{ g L}^{-1}$  catalyst dose, where the  $\text{TiO}_2$  catalyst can absorb photons to generate the electron/hole pairs, the irradiance through  $\text{TiO}_2$  suspensions was approximately one-tenth of the irradiance received through the  $\text{TiO}_2$ -rGO solution. These results confirm that  $\text{TiO}_2$  particles were promoting the UV light screening and hindered UV-A light penetration through the PFOA solution. While the  $\text{TiO}_2$ -rGO composite ( $0.1 \text{ g L}^{-1}$ ) still reduced the light transmission compared to the absence of catalyst, the suitable photocatalytic properties of the prepared  $\text{TiO}_2$ -rGO composite overcame the UV light screening, as the achieved PFOA degradation yield (93%) was much higher than the degradation percentage obtained under direct photolysis conditions (58%), as it was reported in Fig. 1.

Some studies have already shown that the combination of  $\text{TiO}_2$  with rGO leads to a reduction in the band gap energy to 2.72 eV [48], a feature that would provide the composite  $\text{TiO}_2$ -rGO with the ability of visible light adsorption, and a more efficient utilization of light than  $\text{TiO}_2$  (band gap 3.2 eV). On the other hand, Kamat and co-workers [53,54] have shown that photo-electrons generated by  $\text{TiO}_2$  under UV irradiation can be transferred to rGO thanks to the excellent electron conductivity of graphene materials, thus avoiding the electron/hole recombination [43,55]. Therefore, rGO sheets would act as an electron-trap similar to the reported behaviour of the metallic nanoparticles in metal-modified  $\text{TiO}_2$  photocatalysts [31,37]. The electron conduction throughout the  $\text{TiO}_2$ -rGO photocatalyst may further allow higher generation of superoxide and hydroxyl radicals [37,56], which in turn will enhance the oxidation of PFOA molecules.

The structure and morphology of  $\text{TiO}_2$ -rGO could also have a significant role in the photocatalytic process. It is well known that the spherical-like  $\text{TiO}_2$  nanoparticles aggregate to form larger particles [46,56]. Sun et al. [57] demonstrated that UV irradiation of  $\text{TiO}_2$  nanoparticles suspended in water accelerated particle

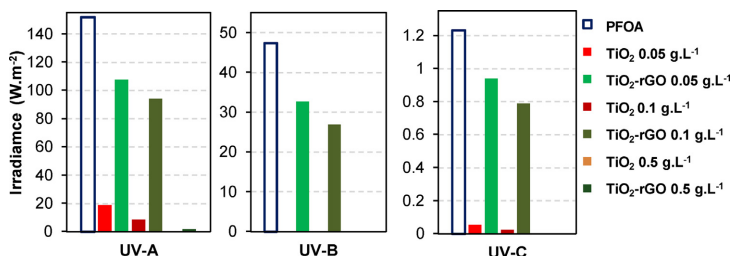


Fig. 2. Irradiance measurements ( $\text{W m}^{-2}$ ) on the outer wall of the reactor using  $\text{TiO}_2$  (0.05, 0.1 and  $0.5 \text{ g L}^{-1}$ , red bars) and  $\text{TiO}_2$ -rGO suspensions (0.05, 0.1 and  $0.5 \text{ g L}^{-1}$ , green bars) in a PFOA ( $0.24 \text{ mmol L}^{-1}$ ) aqueous solution, in the regions: UV-A (315–400 nm), UV-B (280–315 nm) and UV-C (110–280 nm). (For interpretation of the references to colour in this figure legend, the reader is referred to the web version of this article.)

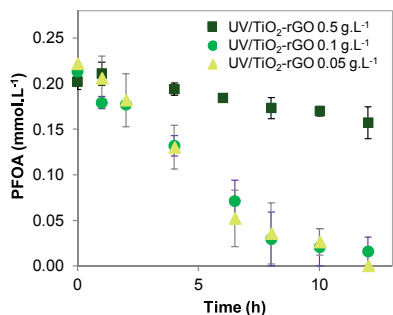


Fig. 3. Influence of the TiO<sub>2</sub>-rGO loading on the PFOA concentration (mmol L<sup>-1</sup>) with the irradiance time. TiO<sub>2</sub>-rGO concentrations were 0.05, 0.1 and 0.5 g L<sup>-1</sup>.

aggregation, that hindered the TiO<sub>2</sub> photocatalytic degradation of Rhodamine B. However, the TiO<sub>2</sub>-rGO composite prepared in the present study presented a homogeneous distribution of TiO<sub>2</sub> nanoparticles spread on the platform of a graphene oxide nanosheet (Fig. S2, Supplementary material). This structure may have limited TiO<sub>2</sub> particles agglomeration with the benefit of a more efficient use of the UV light by the composite particles.

Results for experiments performed at different TiO<sub>2</sub>-rGO catalyst concentrations are provided in Fig. 3. The concentration of the catalyst was first increased from 0.1 g L<sup>-1</sup> to 0.5 g L<sup>-1</sup>, as the latter value is a common dose in TiO<sub>2</sub> photocatalytic experiments, according to the literature survey (Table S1). However, increasing the catalyst dose had the effect of reducing significantly the rate of PFOA removal. Considering that TiO<sub>2</sub> is the major component (95%

wt.) of the composite catalyst, the higher concentration of TiO<sub>2</sub> at the highest catalyst dose may have facilitated the UV light screening, as it can be seen in Fig. 2. In contrast, the reduction of the catalyst dose to 0.05 g L<sup>-1</sup> had a minimal effect on PFOA removal in comparison to 0.1 g L<sup>-1</sup> catalyst concentration, in agreement with the similar values of light transmission for 0.05 g L<sup>-1</sup> and 0.1 g L<sup>-1</sup> TiO<sub>2</sub>-rGO concentrations (Fig. 2).

### 3.2. PFOA mineralization and intermediate degradation products

Generation of shorter chain PFCAs that were formed as intermediates from PFOA degradation is presented in Fig. 4a, working with a catalyst concentration of 0.1 g L<sup>-1</sup>. The corresponding fluoride generation for the same experiment is shown in Fig. 4b, that also presents the total fluorine in the reactor calculated as the sum of fluoride anions in solution and the fluorine contained as part of the quantified PFCAs. Finally, Fig. 4c presents the reduction of TOC together with the TOC calculated from the organic compounds that were found in the analytical survey. Lines plotted in Fig. 4a and c correspond to simulated values that were obtained using the model and kinetic parameters that will be described next in this section.

PFOA removal can be described by a first order rate kinetic law. Several studies have reported that PFOA oxidation by hydroxyl radicals proceeds via a stepwise mechanism in which C–C bond cleavage occurs between the carbon chain and the carboxylate group, coupled with fluoride elimination, resulting in the intermediate generation of shorter chain PFCAs [30]. Consistent with this mechanism, in the present work the generation of shorter chain PFCAs was observed. The order of appearance and the concentrations observed in solution support the stepwise degradation mechanism, in which PFOA would have lost one –CF<sub>2</sub> group to give PFHpA, and consecutively PFHxA and PFPeA. The next molecule in the degradation pathway would be perfluorobutanoic acid (PFBA)

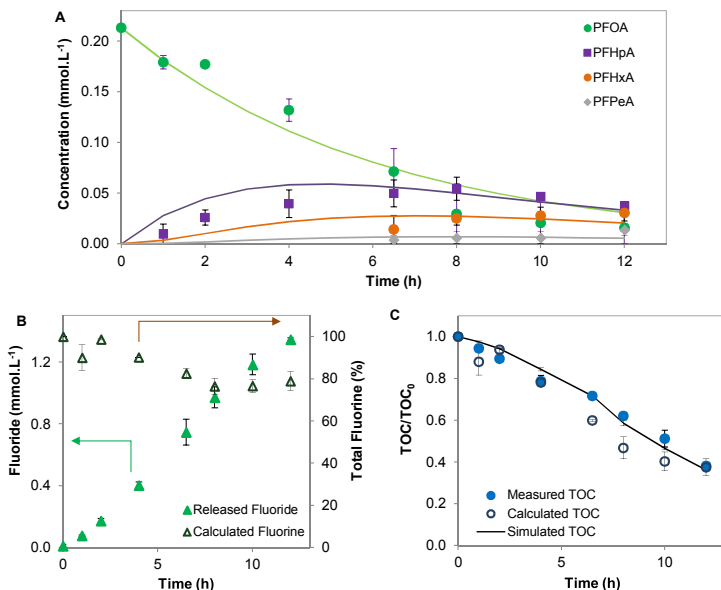
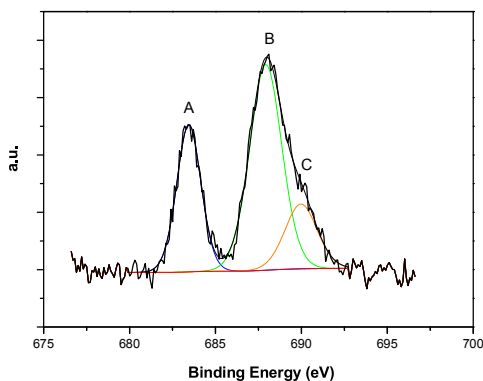


Fig. 4. Evolution of (A) PFOA, PFHpA, PFHxA and PFPeA (mmol L<sup>-1</sup>), and their simulated concentrations using the pseudo-first order estimated kinetic parameters (solid line); (B) fluoride (mmol L<sup>-1</sup>) in solution and calculated total fluorine (%), and (C) measured TOC/TOC<sub>0</sub>, calculated TOC/TOC<sub>0</sub> from the analyzed PFCAs, and simulated TOC/TOC<sub>0</sub> using the simulated PFCAs concentrations. Experimental data obtained using 0.1 g L<sup>-1</sup> of TiO<sub>2</sub>-rGO. TOC<sub>0</sub> was the initial value in each experiment.



**Fig. 5.** XPS spectrum in the F-1s region of TiO<sub>2</sub>-rGO surface after PFOA photocatalytic degradation. A peak is attributed to inorganic fluorinated species. B and C peaks are assigned to organic fluorinated compounds.

that was detected although at concentrations below the LOD (Limit Of Detection) of the analytical technique. Volatile perfluoropropionic acid (PFPrA) and trifluoroacetic acid (TFA) were not observed in the liquid phase.

TOC was reduced by 62% during the photocatalytic decomposition of PFOA. The difference between the PFOA reduction (93%) and TOC decrease can be ascribed to the presence of intermediate degradation products. It is worth mentioning the good match between the analyzed TOC and the TOC calculated from the quantified concentrations of PFOA, PFHpA, PFHxA, and PFPeA. The coincident trends prove the step-by-step PFOA degradation pathway in which shorter-chain perfluorocarboxylates are the intermediate products.

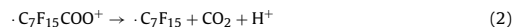
The gradual increase of fluoride in the aqueous solution demonstrated that the cleavage of the C–F bonds was effective during PFCAs degradation. Total fluorine measurements showed a net loss of fluorine of 20% after 12 h of photocatalytic treatment. The loss of fluorine may be attributed to two factors: i) fluoride adsorption on the surface of the TiO<sub>2</sub> fraction of the composite catalysts, which is positively charged in acidic conditions [28,29,58], and ii) the volatilization of the shortest PFCAs obtained as end products of the PFOA degradation chain [33].

In order to verify the possible fluoride incorporation onto the photocatalyst surface, XPS analysis of the TiO<sub>2</sub>-rGO particles surface was performed, using both fresh and used samples of the photocatalytic material. The XPS survey spectra and elemental composition for both materials is provided as Fig. S6 and Table S2 (Supplementary material). As expected, fluorine was only detected on the TiO<sub>2</sub>-rGO sample that had been used as catalyst for PFOA photocatalytic degradation. The mass percentual elemental composition of the fresh TiO<sub>2</sub>-rGO sample was 13.8/58.1/28.1 as C/O/Ti, while in the used catalyst the elemental composition was 13.1/53.2/26.9/6.8 as C/O/Ti/F.

Fig. 5 shows the section of the high resolution XPS spectrum of used TiO<sub>2</sub>-rGO particles, where the F-1s region has been magnified. Three deconvoluted peaks at 684.2 (A), 688.8 (B) and 691.0 eV (C) can be observed: the first peak was related to negatively charged monovalent fluoride (F<sup>-</sup>); and the signals around 688–691 eV could be assigned to fluorine bonded to carbon, as it happens in the C–F bonds of PFOA and its perfluorinated degradation intermediates that may have been adsorbed on the catalyst surface [28,29]. Moreover, F-1s spectra for TiO<sub>2</sub>-rGO composite before use was not detected (Fig. S6). Similar peak distribution and binding energies for raw and used TiO<sub>2</sub>-rGO catalysts samples confirmed that the pho-

tocatalyst surface remained unchanged after its use in the PFOA photodegradation experiments. Based on the above results, part of the fluoride anions that were released during PFOA abatement were absorbed onto the TiO<sub>2</sub>-rGO photocatalyst, to account for 6.8% of the total mass of the catalyst sample used in the XPS analyses (Table S2). As this adsorption rate did not represent the total fluorine loss, the volatilization of the shortest PFCAs could have also contributed to the 20% of fluorine loss observed in Fig. 4b.

Fig. 6 presents the proposed mechanism and pathway of PFOA decomposition in the TiO<sub>2</sub>-rGO mediated photocatalysis and the role of rGO in the mechanism. Previous studies considered different possibilities for the initiation of the PFOA molecule oxidation: i) direct reaction of PFOA with the photogenerated holes of the photocatalyst surface [26,29,31,34], ii) indirect reaction with hydroxyl radicals [21,30,36,59,60] or iii) combination of both mechanisms. Thereby, the degradation of PFOA could start from terminal carboxylic end, where the photogenerated hydroxyl radicals can attack the first alkyl C atom adjacent to the –COOH group, leading to the cleavage of C–C bond between the perfluorinated alkyl chain –C<sub>7</sub>F<sub>15</sub> and –COOH by the formation of perfluorinated alkyl radicals, which can then react with water to produce the unstable perfluorinated alcohol C<sub>7</sub>F<sub>15</sub>OH (reactions (1)–(3)). After that, C<sub>7</sub>F<sub>15</sub>OH would eliminate HF to form C<sub>6</sub>F<sub>13</sub>COF (Eq. (4)). The active C<sub>6</sub>F<sub>13</sub>COF undergoes hydrolysis in the solution, resulting in the formation of PFHpA with the release of CF<sub>2</sub> unit (Eq. (5)).



On the other hand, other possible initiation of PFOA degradation could be the direct reaction of C<sub>7</sub>F<sub>15</sub>COO<sup>-</sup> with the holes. This step would involve the electron transfer from the dissociated PFOA to the valence band of the photocatalyst, generating the C<sub>7</sub>F<sub>15</sub>COO<sup>•</sup> radical that subsequently would undergo Kolbe decarboxylation, to give perfluoroalkyl radical C<sub>7</sub>F<sub>15</sub><sup>•</sup> and CO<sub>2</sub> [34]. The next degradation pathways would be similar to reactions (3)–(5).

Correspondingly, the intermediates will be decomposed stepwisely into shorter-chain PFCAs, and eventually to CO<sub>2</sub> and F<sup>-</sup>. Although the reaction mechanism seems to be mostly driven by HO<sup>•</sup> radical attack, the formation of the reactive species such as radical superoxide anion (O<sub>2</sub><sup>•-</sup>) may also be associated with the PFOA degradation.

### 3.3. Kinetic model for PFOA and its degradation products

In a first attempt to quantify the kinetics of PFOA photocatalytic degradation by the TiO<sub>2</sub>-rGO composite catalyst, the concentrations of PFOA and intermediate products were fitted to the following first-order rate equation [20,26,28–30,33]:

$$\frac{d[C_n]}{dt} = k_{n+1} [C_{n+1}] - k_n [C_n] \quad (6)$$

where *n* is the carbon atoms number in each PFOA molecule, *C* is the concentration in the solution (mmol L<sup>-1</sup>), *t* is the time (h), *k* the observed degradation rate constant (h<sup>-1</sup>) of each PFOA.

Concentration data shown in Fig. 4a (0.1 g L<sup>-1</sup> TiO<sub>2</sub>-rGO) were used for the estimation of kinetic parameters. The obtained values of the apparent kinetic constants can be ordered as *k*<sub>PFPrA</sub> > *k*<sub>PFHxA</sub> > *k*<sub>PFHpA</sub> > *k*<sub>PFOA</sub>, with values of 2.14, 0.54, 0.27 and 0.163 h<sup>-1</sup>, respectively. These results point to a clear influence of the length of the perfluoroalkyl chain on the degradation rate. Similarly to our process, Qian et al. [10] reported that the rate constant

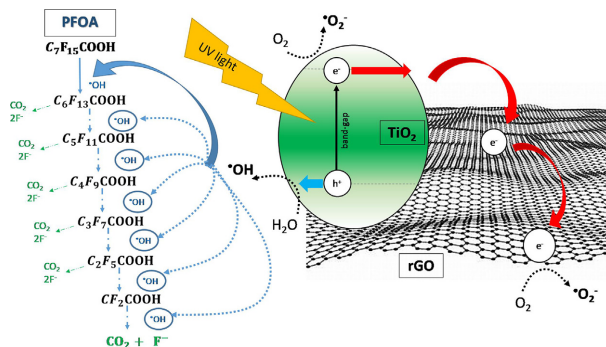


Fig. 6. Photocatalytic pathways of PFOA decomposition using the  $\text{TiO}_2$ -rGO catalyst.

of PFCAs UV-persulfate decomposition distinctly increased when the carbon-chain of the PFCAs was shorter.

Eq. (6) and the reported  $k$  values were used to simulate the concentration of PFCAs, as depicted by the solid lines included in Fig. 4a. Similarly, simulated PFCAs concentrations were employed to calculate TOC evolution, which is also shown as solid line in Fig. 4b. The good agreement between measured and simulated TOC supports the validity of the kinetic constants obtained from the fitting of the experimental results.

#### 4. Conclusions

This study reports for the first time the effective photocatalytic degradation of perfluorooctanoic acid (PFOA) using a composite catalyst based on  $\text{TiO}_2$  and reduced graphene oxide (rGO) successfully synthesized by a hydrothermal method.

The efficient photoactivity of the prepared  $\text{TiO}_2$ -rGO composite was positively confirmed for PFOA degradation under UV-vis irradiation. After 12 h of irradiation, the PFOA removal ratio was as high as  $93 \pm 7\%$ , using a  $0.1 \text{ g L}^{-1}$  concentration of the composite catalyst. The PFOA degradation ratio obtained using  $\text{TiO}_2$ -rGO was 4-fold higher than the  $\text{TiO}_2$ -mediated photocatalysis, under the same experimental conditions. It is hypothesized that reduced graphene oxide can efficiently capture the electrons/hole pair photogenerated by the  $\text{TiO}_2$ , thus reducing the electron/hole pair recombination, that would promote the PFCAs degradation by means of active radicals or direct oxidation by the photogenerated holes. The progress of shorter-chain perfluorocarboxylic acids as well as fluoride release elucidated the step-by-step PFOA decomposition mechanism by gradually losing a  $\text{CF}_2$  unit in each step, generating  $\text{CO}_2$  and  $\text{F}^-$ . The PFOA mineralization was also demonstrated with the 60% TOC reduction. Furthermore, the effect of the alkyl chain length on the kinetics of PFCAs was revealed, showing that shorter chain PFCAs degraded faster than their longer chain homologues.

It is concluded that  $\text{TiO}_2$ -rGO composite catalyst offers an unprecedented effectiveness for the degradation of recalcitrant PFCAs, to become a promising alternative for the photocatalytic degradation of this group of persistent organic pollutants.

#### Acknowledgements

Financial support from projects CTM2013-44081-R, CTM2015-69845-R and CTM2016-75509-R (MINECO, SPAIN-FEDER 2014–2020) is acknowledged. B. Gomez thanks the FPI scholarship (BES-2014-071045).

#### Appendix A. Supplementary data

Supplementary data associated with this article can be found, in the online version, at <https://doi.org/10.1016/j.jhazmat.2017.11.048>.

#### References

- [1] H.J. Lehmler, Synthesis of environmentally relevant fluorinated surfactants – A review, *Chemosphere* 58 (2005) 1471–1496.
- [2] F. Xiao, M.F. Simcik, T.R. Halbach, J.S. Gulliver, Perfluorooctane sulfonate (PFOS) and perfluorooctanoate (PFOA) in soils and groundwater of a U.S. metropolitan area: migration and implications for human exposure, *Water Res.* 72 (2014) 64–74.
- [3] S. Fujii, C. Polprasert, S. Tanaka, N.P.H. Lien, Y. Qiu, New POPs in the water environment: distribution bioaccumulation and treatment of perfluorinated compounds—a review paper, *J. Water Supply Res. Technol.—AQUA* 56 (2007) 313–326.
- [4] Secretary-General of the United Nations, The Stockholm convention on persistent organic pollutants, 4 (2009) 1–63. <http://chm.pops.int/TheConvention/Overview/TextoftheConvention/tabid/2232/>.
- [5] USEPA, Drinking Water Health Advisory for Perfluorooctanoic Acid (PFOA), (2016) 1–103. <https://www.epa.gov/ground-water-and-drinking-water/drinking-water-health-advisories-pfoa-and-pfos>.
- [6] M.M. Schultz, C.P. Higgins, C.A. Huset, R.G. Luthy, D.F. Barofsky, J.A. Field, Fluorochemical mass flows in a municipal wastewater treatment facility, *Environ. Sci. Technol.* 40 (2006) 7350–7357.
- [7] I. Fierres, S. Gómez-Lavín, M.P. Elizalde, A. Urriaga, Perfluorinated alkyl substances (PFASs) in northern Spain municipal solid waste landfill leachates, *Chemosphere* 168 (2017) 399–407.
- [8] X. Dauchy, V. Boiteux, C. Bach, A. Colin, J. Hemard, C. Rosin, J.F. Muñoz, Mass flows and fate of per- and polyfluoroalkyl substances (PFASs) in the wastewater treatment plant of a fluorochemical manufacturing facility, *Sci. Total Environ.* 576 (2017) 549–558.
- [9] R. Qu, J. Liu, C. Li, L. Wang, Z. Wang, J. Wu, Experimental and theoretical insights into the photochemical decomposition of environmentally persistent perfluorocarboxylic acids, *Water Res.* 104 (2016) 34–43.
- [10] Y. Qian, X. Guo, Y. Zhang, Y. Peng, P. Sun, C.H. Huang, J. Niu, X. Zhou, J.C. Crittenden, Perfluorooctanoic acid degradation using UV-persulfate process: modeling of the degradation and chlorate formation, *Environ. Sci. Technol.* 50 (2016) 772–781.
- [11] Y. Qu, C. Zhang, F. Li, J. Chen, Q. Zhou, Photo-reductive defluorination of perfluorooctanoic acid in water, *Water Res.* 44 (2010) 2939–2947.
- [12] C.R. Estrella, C. Salm, H. Hinode, Photocatalytic decomposition of perfluorooctanoic acid by iron and niobium co-doped titanium dioxide, *J. Hazard. Mater.* 179 (2010) 79–83.
- [13] Á. Soriano, D. Gorri, A. Urriaga, Efficient treatment of perfluorohexanoic acid by nanofiltration followed by electrochemical degradation of the NF concentrate, *Water Res.* 112 (2017) 147–156.
- [14] B. Gomez-Ruiz, S. Gómez-Lavín, N. Diban, V. Boiteux, A. Colin, X. Dauchy, A. Urriaga, Efficient electrochemical degradation of poly- and perfluoroalkyl substances (PFASs) from the effluents of an industrial wastewater treatment plant, *Chem. Eng. J.* 322 (2017) 196–204.
- [15] C.E. Schaefer, C. Andaya, A. Burant, C.W. Condee, A. Urriaga, T.J. Strathmann, C.P. Higgins, Electrochemical treatment of perfluorooctanoic acid and perfluorooctane sulfonate: insights into mechanisms and application to groundwater treatment, *Chem. Eng. J.* 317 (2017) 424–432.

- [16] A. Urriaga, C. Fernández-González, S. Gómez-Lavín, I. Ortiz, Kinetics of the electrochemical mineralization of perfluorooctanoic acid on ultrananocrystalline boron doped conductive diamond electrodes, *Chemosphere* 129 (2015) 20–26.
- [17] H. Hori, A. Yamamoto, E. Hayakawa, S. Taniyasu, N. Yamashita, S. Kutsuna, H. Kitagawa, R. Arakawa, Efficient decomposition of environmentally persistent perfluorocarboxylic acids by use of persulfate as a photochemical oxidant, *Environ. Sci. Technol.* 39 (2005) 2383–2388.
- [18] C.D. Vecitis, H. Park, J. Cheng, B.T. Mader, M.R. Hoffmann, Kinetics and mechanism of the sonolytic conversion of the aqueous perfluorinated surfactants, perfluorooctanoate (PFOA), and perfluorooctane sulfonate (PFOS) into inorganic products, *J. Phys. Chem. A* 112 (2008) 4261–4270.
- [19] H. Hori, E. Hayakawa, H. Einaga, S. Kutsuna, K. Koike, T. Ibusuki, H. Kitagawa, R. Arakawa, Decomposition of environmentally persistent perfluorooctanoic acid in water by photochemical approaches, *Environ. Sci. Technol.* 38 (2004) 6118–6124.
- [20] M.H. Cao, B.B. Wang, H.S. Yu, L.L. Wang, S.H. Yuan, J. Chen, Photochemical decomposition of perfluorooctanoic acid in aqueous periodate with VUV and UV light irradiation, *J. Hazard. Mater.* 179 (2010) 1143–1146.
- [21] Y.C. Chen, S.L. Lo, J. Kuo, Effects of titanate nanotubes synthesized by a microwave hydrothermal method on photocatalytic decomposition of perfluorooctanoic acid, *Water Res.* 45 (2011) 4131–4140.
- [22] M. Pelaez, N.T. Nolan, S.C. Pillai, M.K. Seery, P. Falaras, A.G. Kontos, P.S.M. Dunlop, J.W.J. Hamilton, J.A. Byrne, K.O'Shea, M.H. Entezari, D.D. Dionysiou, A review on the visible light active titanium dioxide photocatalysts for environmental applications, *Appl. Catal. B Environ.* 125 (2012) 331–349.
- [23] S. Dominguez, P. Ribao, M.J. Rivero, I. Ortiz, Influence of radiation and TiO<sub>2</sub> concentration on the hydroxyl radicals generation in a photocatalytic LED reactor. Application to dodecylbenzenesulfonate degradation, *Appl. Catal. B Environ.* 178 (2014) 165–169.
- [24] M. Sanchez, M.J. Rivero, I. Ortiz, Kinetics of dodecylbenzenesulfonate mineralisation by TiO<sub>2</sub> photocatalysis, *Appl. Catal. B Environ.* 101 (2011) 515–521.
- [25] R. Dillert, D. Bahnemann, H. Hidaka, Light-induced degradation of perfluorocarboxylic acids in the presence of titanium dioxide, *Chemosphere* 67 (2007) 785–792.
- [26] S.C. Panchangam, A.Y.C. Lin, K.L. Shaik, C.F. Lin, Decomposition of perfluorocarboxylic acids (PFCAs) by heterogeneous photocatalysis in acidic aqueous medium, *Chemosphere* 77 (2009) 242–248.
- [27] Y. Wang, P. Zhang, Photocatalytic decomposition of perfluorooctanoic acid (PFOA) by TiO<sub>2</sub> in the presence of oxalic acid, *J. Hazard. Mater.* 192 (2011) 1869–1875.
- [28] F. Sansotera, C. Persico, W. Pirola, A. Navarrini, C.L. Di Michele, Decomposition of perfluorooctanoic acid photocatalyzed by titanium dioxide: chemical modification of the catalyst surface induced by fluoride ions, *Appl. Catal. B Environ.* 148 (2014) 29–35.
- [29] S. Gatto, M. Sansotera, F. Persico, M. Gola, C. Pirola, W. Panzeri, W. Navarrini, C.L. Bianchi, Surface fluorination on TiO<sub>2</sub> catalyst induced by photodegradation of perfluorooctanoic acid, *Catal. Today* 241 (2015) 8–14.
- [30] M.J. Chen, S.L. Lo, Y.C. Lee, C.C. Huang, Photocatalytic decomposition of perfluorooctanoic acid by transition-metal modified titanium dioxide, *J. Hazard. Mater.* 288 (2015) 168–175.
- [31] M. Li, Z. Yu, Q. Liu, L. Sun, W. Huang, Photocatalytic decomposition of perfluorooctanoic acid by noble metallic nanoparticles modified TiO<sub>2</sub>, *Chem. Eng. J.* 286 (2016) 232–238.
- [32] C. Song, P. Chen, C. Wang, L. Zhu, Photodegradation of perfluorooctanoic acid by synthesized TiO<sub>2</sub>-MWCNT composites under 365 nm UV irradiation, *Chemosphere* 86 (2012) 853–859.
- [33] X. Li, P. Zhang, L. Jin, T. Shao, Z. Li, J. Cao, Efficient photocatalytic decomposition of perfluorooctanoic acid by indium oxide and its mechanism, *Environ. Sci. Technol.* 46 (2012) 5528–5534.
- [34] M. Sansotera, F. Persico, V. Rizzi, W. Panzeri, C. Pirola, C.L. Bianchi, A. Mele, W. Navarrini, The effect of oxygen in the photocatalytic oxidation pathways of perfluorooctanoic acid, *J. Fluor. Chem.* 179 (2015) 159–168.
- [35] S.C. Panchangam, A.Y.C. Lin, J.H. Tsai, C.F. Lin, Sonication-assisted photocatalytic decomposition of perfluorooctanoic acid, *Chemosphere* 75 (2009) 654–660.
- [36] M.J. Chen, S.L. Lo, Y.C. Lee, J. Kuo, C.H. Wu, Decomposition of perfluorooctanoic acid by ultraviolet light irradiation with Pb-modified titanium dioxide, *J. Hazard. Mater.* 303 (2016) 111–118.
- [37] P. Ribao, M.J. Rivero, I. Ortiz, TiO<sub>2</sub> structures doped with noble metals and/or graphene oxide to improve the photocatalytic degradation of dichloroacetic acid, *Environ. Sci. Pollut. Res.* (2016) 1–10.
- [38] D. Liang, C. Cui, H. Hub, Y. Wang, S. Xu, B. Ying, P. Li, B. Lu, H. Shen, One-step hydrothermal synthesis of anatase TiO<sub>2</sub>/reduced graphene oxide nanocomposites with enhanced photocatalytic activity, *J. Alloys Compd.* 582 (2014) 236–240.
- [39] H. Zhang, X. Lv, Y. Li, Y. Wang, J. Li, P25/graphene composite as a high performance photocatalyst, *ACS Nano* 4 (2009) 380–386.
- [40] H. Adamu, P. Dubej, J.A. Anderson, Probing the role of thermally reduced graphene oxide in enhancing performance of TiO<sub>2</sub> in photocatalytic phenol removal from aqueous environments, *Chem. Eng. J.* 284 (2016) 380–388.
- [41] Y. Liang, H. Wang, H.S. Casalogue, Z. Chen, H. Dai, TiO<sub>2</sub> Nanocrystals grown on graphene as advanced photocatalytic hybrid materials, *Nano Res.* 3 (2010) 701–705.
- [42] H. Zhao, J. Gao, G. Zhao, J. Fan, Y. Wang, Y. Wang, Fabrication of novel SnO<sub>2</sub>-Sb/carbon aerogel electrode for ultrasonic electrochemical oxidation of perfluorooctanoate with high catalytic efficiency, *Appl. Catal. B Environ.* 136–137 (136) (2013) 278–
- [43] P. Wang, J. Wang, X. Wang, H. Yu, J. Yu, M. Lei, Y. Wang, One-step synthesis of easy-recycling TiO<sub>2</sub>-rGO nanocomposite photocatalysts with enhanced photocatalytic activity, *Appl. Catal. B Environ.* 132–133 (132) (2013) 452–
- [44] R.K. Nainani, P. Thakur, Facile synthesis of TiO<sub>2</sub>-RGO composite with enhanced performance for the photocatalytic mineralization of organic pollutants, *Water Sci. Technol.* 73 (2016) 1927–1936.
- [45] B. Neppolian, A. Bruno, C.L. Bianchi, M. Ashokkumar, Graphene oxide based Pt-TiO<sub>2</sub> photocatalyst: ultrasound assisted synthesis, characterization and catalytic efficiency, *Ultrason. Sonochem.* 19 (2012) 9–15.
- [46] L.M. Pastrana-Martínez, S. Morales-Torres, V. Likodimos, J.L. Figueiredo, J.L. Faria, P. Falaras, A.M.T. Silva, Advanced nanostructured photocatalysts based on reduced graphene oxide-TiO<sub>2</sub> composites for degradation of diphenhydramine pharmaceutical and methyl orange dye, *Appl. Catal. B Environ.* 123–124 (2012) 241–256.
- [47] W.S. Hummers, R.E. Offeman, Preparation of graphitic oxide, *J. Am. Chem. Soc.* 80 (1958) 1339.
- [48] J. Li, S.L. Zhou, G.B. Hong, C.T. Chang, Hydrothermal preparation of P25-graphene composite with enhanced adsorption and photocatalytic degradation of dyes, *Chem. Eng. J.* 219 (2013) 486–491.
- [49] J. Chen, P. Zhang, J. Liu, Photodegradation of perfluorooctanoic acid by 185 nm vacuum ultraviolet light, *J. Environ. Sci.* 19 (2007) 387–390.
- [50] R.R. Giri, H. Ozaki, T. Morigaki, S. Taniguchi, R. Takunami, UV photolysis of perfluorooctanoic acid (PFOA) in dilute aqueous solution, *Water Sci. Technol.* 63 (2011) 276–282.
- [51] N.A. Ab Aziz, P. Palaniandy, H.A. Aziz, I. Dahlan, Review of the mechanism and operational factors influencing the degradation process of contaminants in heterogeneous photocatalysis, *J. Chem. Res.* 40 (2016) 704–712.
- [52] H.A. Becerril, J. Mao, Z. Liu, R.M. Stoltenberg, Z. Bao, Y. Chen, Evaluation of solution-processed reduced graphene oxide films as transparent conductors, *ACS Nano* 2 (2008) 463–470.
- [53] G. Williams, B. Seger, P.V. Kamat, TiO<sub>2</sub>-graphene nanocomposites, UV-assisted photocatalytic reduction of graphene oxide, *ACS Nano* 2 (2008) 1487–1491.
- [54] I.V. Lightcap, T.H. Kosel, P.V. Kamat, Anchoring semiconductor and metal nanoparticles on a two-dimensional catalyst map. storing and shuttling electrons with reduced graphene oxide, *Nano Lett.* 10 (2010) 577–583.
- [55] H. Mahmood, A. Habib, M. Mujahid, M. Tanveer, S. Javed, A. Jamil, Band gap reduction of titania thin films using graphene nanosheets, *Mater. Sci. Semicond. Process.* 24 (2014) 193–199.
- [56] M.J. Sampaio, C.G. Silva, A.M.T. Silva, L.M. Pastrana-Martínez, C. Han, S. Morales-Torres, J.L. Figueiredo, D.D. Dionysiou, J.L. Faria, Carbon-based TiO<sub>2</sub> materials for the degradation of microcystin-LA, *Appl. Catal. B Environ.* 170–171 (2010) 715–74–
- [57] J. Sun, L.-H. Guo, H. Zhang, L. Zhao, UV irradiation induced transformation of TiO<sub>2</sub> nanoparticles in water: aggregation and photoreactivity, *Environ. Sci. Technol.* 48 (2014) 11962–11968.
- [58] M.S. Vohra, S. Kim, W. Choi, Effects of surface fluorination of TiO<sub>2</sub> on the photocatalytic degradation of tetramethylammonium, *J. Photochem. Photobiol. A Chem.* 160 (2003) 55–60.
- [59] C. Song, P. Chen, C. Wang, L. Zhu, Photodegradation of perfluorooctanoic acid by synthesized TiO<sub>2</sub>-MWCNT composites under 365 nm UV irradiation, *Chemosphere* 86 (2012) 853–859.
- [60] H. Tang, Q. Xiang, M. Lei, J. Yan, L. Zhu, J. Zou, Efficient degradation of perfluorooctanoic acid by UV–Fenton process, *Chem. Eng. J.* 184 (2012) 156–162.

## **SUPPLEMENTARY DATA**

### **Photocatalytic degradation and mineralization of perfluorooctanoic acid (PFOA) using a composite TiO<sub>2</sub>-rGO catalyst**

#### **Authors:**

Beatriz Gomez-Ruiz, Paula Ribao, Nazely Diban, María J. Rivero, Inmaculada Ortiz,  
Ane Urtiaga\*

Department of Chemical and Biomolecular Engineering. Universidad de Cantabria.

Av. de Los Castros s/n. 39005 Santander. Spain.

\* Corresponding author: [urtiaga@unican.es](mailto:urtiaga@unican.es)

**Table S1.** Summary of the photocatalytic processes for PFOA degradation in aqueous media.

PFOA (mmol.L <sup>-1</sup> )	Photocatalyst	Volume (mL)	UV Lamp Intensity (mW.cm <sup>-2</sup> )	Media	Degradation Ratio (%)	Reference
1.5	TiO <sub>2</sub> (2 g.L <sup>-1</sup> )	500	6.3-6.7 (75 W, 310-400 nm)	0.1 M HClO <sub>4</sub> and O <sub>2</sub> atmosphere	44% at 24h	[25]
0.12	TiO <sub>2</sub> (0.66 g.L <sup>-1</sup> )	3000	0.45 (16 W, 254 nm)	O <sub>2</sub> purge at 140 mL min <sup>-1</sup>	20-22 % at 7 h	[26]
0.1	TiO <sub>2</sub> (0.5 g.L <sup>-1</sup> )	600	150 W, 200-600 nm	Air	7 % at 3 h	[12]
0.12	TiO <sub>2</sub> (0.25 g.L <sup>-1</sup> )	2000	400 W, 254 nm	Air	19 % at 24 h	[21]
0.1	TiO <sub>2</sub> (0.5 g.L <sup>-1</sup> )	400	23 W, 254 nm	O <sub>2</sub> atmosphere	15.9 % at 4 h	[33]
0.07	TiO <sub>2</sub> (0.8 g.L <sup>-1</sup> )	250	300 W, 365 nm	Air, pH=5	37 % at 8 h	[32]
4	TiO <sub>2</sub> (0.66 g.L <sup>-1</sup> )	1000	7.5-9.5 (500 W, 315-400 nm)	Air	30-32 % at 6 h	[28]
4	TiO <sub>2</sub> (0.66 g.L <sup>-1</sup> )	1000	9.5 (500 W, 315-400 nm)	Air	32 % at 4 h	[29]
0.12	TiO <sub>2</sub> (0.5 g.L <sup>-1</sup> )	1000	400 W, 254 nm	Air, HCl and NaOH (pH 5)	14 % at 12 h	[30]
0.14	TiO <sub>2</sub> (0.5 g.L <sup>-1</sup> )	120	5.3 (125 W, 365 nm)	Air, HClO <sub>4</sub> and NaOH (pH 3)	31.1 % at 7 h	[31]
0.024	TiO <sub>2</sub> (0.5 g.L <sup>-1</sup> )	500	5.9-6.1 (23 W, 254 nm)	N <sub>2</sub> atmosphere	12.4 % at 3 h	[27]
4	TiO <sub>2</sub> (0.66 g.L <sup>-1</sup> )	1000	7.5 (500 W, 315-400 nm)	Air	93.7 % at 15 h	[34]

4	TiO <sub>2</sub> (0.66 g.L <sup>-1</sup> )	1000	7.5 (500 W, 315-400 nm)	O <sub>2</sub> atmosphere	97.9 % at 1.5 h	[34]
4	TiO <sub>2</sub> (0.66 g.L <sup>-1</sup> )	1000	7.5 (500 W, 315-400 nm)	N <sub>2</sub> atmosphere	12 % at 1.5 h	[34]
0.12	TNT (0.25 g.L <sup>-1</sup> )	2000	400 W, 254 nm	Air	44 % at 24 h	[21]
0.12	TiO <sub>2</sub> (0.66 g.L <sup>-1</sup> )	3000	0.45 (16 W, 254 nm)	0.15 mmol L <sup>-1</sup> HClO <sub>4</sub> (pH 4), O <sub>2</sub> purge at 140 mL min <sup>-1</sup>	97 % at 7 h	[26]
0.12	TiO <sub>2</sub> (0.66 g.L <sup>-1</sup> )	3000	0.45 (16 W, 254 nm)	O <sub>2</sub> purge at 140 mL min <sup>-1</sup> under ultrasonic irradiation (40kHz)	45 % at 7 h	[35]
0.024	TiO <sub>2</sub> (0.5 g.L <sup>-1</sup> )	500	5.9-6.1 (23 W, 254 nm)	3 mmol L <sup>-1</sup> C <sub>2</sub> H <sub>2</sub> O <sub>4</sub> N <sub>2</sub> atmosphere	86.7 % at 3 h	[27]
0.1	Fe/Nb-TiO <sub>2</sub> (0.5 g.L <sup>-1</sup> )	600	150 W, 200-600 nm	Air	14 % at 3 h	[12]
0.12	Fe-TiO <sub>2</sub> (0.5 g.L <sup>-1</sup> )	1000	400 W, 254 nm	Air, HCl and NaOH (pH 5)	69 % at 12 h	[30]
0.12	Cu-TiO <sub>2</sub> (0.5 g.L <sup>-1</sup> )	1000	400 W, 254 nm	Air, HCl and NaOH (pH 5)	91 % at 12 h	[30]
0.12	Pb-TiO <sub>2</sub> (0.5 g.L <sup>-1</sup> )	1000	400 W, 254 nm	Air, HCl and NaOH (pH 5)	99.9 % at 12 h	[36]
0.14	Ag-TiO <sub>2</sub> (0.5 g.L <sup>-1</sup> )	120	5.3 (125 W, 365 nm)	Air, HClO <sub>4</sub> and NaOH (pH 3)	57.7 % at 7 h	[31]
0.14	Pd-TiO <sub>2</sub> (0.5 g.L <sup>-1</sup> )	120	5.3 (125 W, 365 nm)	Air, HClO <sub>4</sub> and NaOH (pH 3)	94.2 % at 7 h	[31]
0.14	Pt-TiO <sub>2</sub> (0.5 g.L <sup>-1</sup> )	120	5.3 (125 W, 365 nm)	Air, HClO <sub>4</sub> and NaOH (pH 3)	100 % at 7 h	[31]
0.07	(10:1) TiO <sub>2</sub> -MWCNT (1.6 g.L <sup>-1</sup> )	250	300 W, 365 nm	Air, pH =5	94 % at 8 h	[33]

Abbreviations: MWCNT: Multiple Wall Carbon Nano Tube; TNT: Titanate Nano Tube

The prepared TiO<sub>2</sub>-rGO composite was characterized by Attenuated total reflectance - Fourier transform infrared (ATR-FTIR; Spectrum Two spectrometer, Perkin Elmer). Additionally, ATR-FTIR spectra of the GO and commercial TiO<sub>2</sub> materials were performed for comparison (Figure S1).

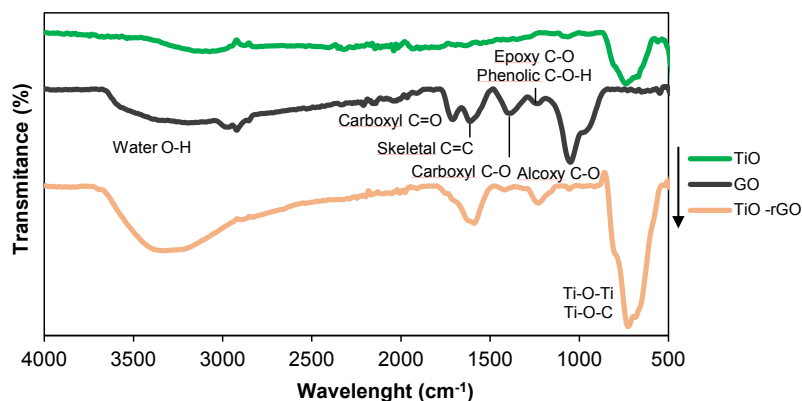
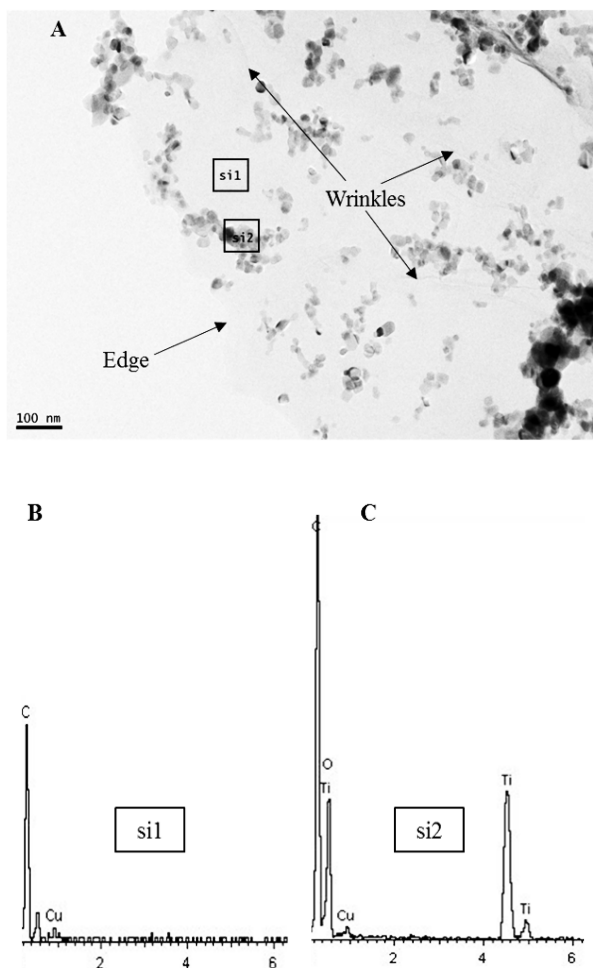


**Fig. S1.** FTIR spectra of TiO<sub>2</sub>, GO and TiO<sub>2</sub>-rGO.

Analysis of Fig. S1:

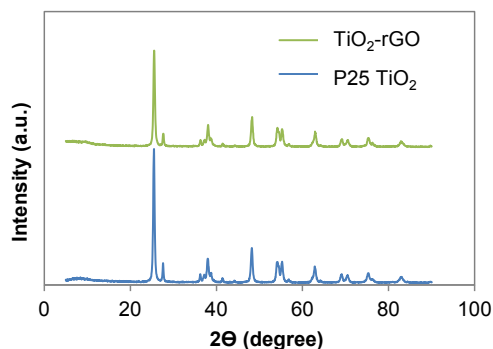
- GO spectrum displayed strong absorption peaks that correspond to different oxygenated functional groups. The peaks at 3400 cm<sup>-1</sup> and 1620 cm<sup>-1</sup> are ascribed to the stretching vibration of water hydroxyl groups and the skeletal vibration of C=C, respectively. The peaks at 1732, 1380, 1220 and 1055 cm<sup>-1</sup> are attributed to carboxylates C=O stretching, carboxyl C-O, epoxide C-O-C or phenolic C-O-H and alkoxy C-O, respectively.
- TiO<sub>2</sub>-rGO samples still show skeletal vibration peak of C=C; however, there is no presence of peaks associated to carboxyl and alkoxy functional groups. This fact implies that GO was partially reduced during the hydrothermal synthesis of the composite catalyst. Moreover, the important intensity increase of the band range between 500-900 cm<sup>-1</sup> in the spectrum of TiO<sub>2</sub>-rGO in comparison to the TiO<sub>2</sub> spectrum could be related to the possible formation of Ti-O-C bonds additional to the Ti-O-Ti bonds typically occurring in TiO<sub>2</sub>.

Fig. S2A shows Transmission electron microscopy (TEM; JEOL, JEM-2100 electron microscope) images of the prepared  $\text{TiO}_2$ -rGO composites. It is observed that  $\text{TiO}_2$  nanoparticles were well loaded on the graphene plane, which presents a flake-like structure with some wrinkles. Figs. S2B and S2C present the energy dispersive X-ray (EDX) spectrum collected from Si1 and Si2 areas in Fig. S2A. The composition of the GO sheets (Si1) was mainly carbon. EDX spectrum of Si2 area shows a composition based on titanium and oxygen, evidencing the presence of  $\text{TiO}_2$  on the graphene oxide nanosheets. Copper signal is attributed to the sample holder.



**Fig. S2.** TEM image of the composite  $\text{TiO}_2$ -rGO (A) and EDX scan of zones Si1 (B) and Si2 (C) in the image.

Fig. S3 shows the X-ray diffraction (XRD) data of commercial P25 TiO<sub>2</sub> (blue line) and the synthesized TiO<sub>2</sub>-rGO composite (green line). The crystalline phase of TiO<sub>2</sub> was not modified by the hydrothermal method used to synthesize the TiO<sub>2</sub>-rGO composite.



**Fig. S3.** XRD data of of P25 TiO<sub>2</sub> and TiO<sub>2</sub>-rGO composite. Power X-ray diffraction patterns were recorded with a “Bruker Kappa-APEX-II” X-ray diffractometer, equipped with a Molybdenum Rx tube operating at 50Kv and 30mA.

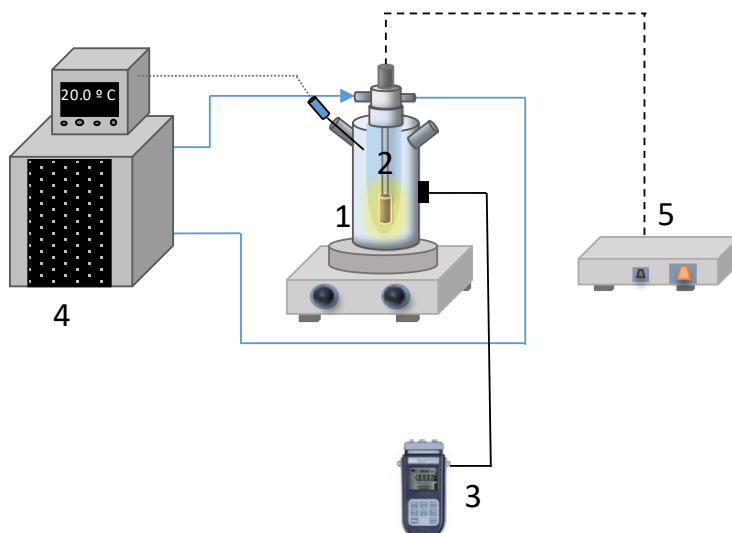


**Fig. S4.** Schematic illustration of the photocatalytic system (1: Photocatalytic Reactor, 2: Medium Pressure Mercury Lamp, 3: Radiometer, 4: Refrigeration System; 5: Power Source). The lamp was placed into a quartz sleeve, which was surrounded by a cooling jacket used to circulate a cooling fluid to maintain the temperature of the reacting media at 20 °C.

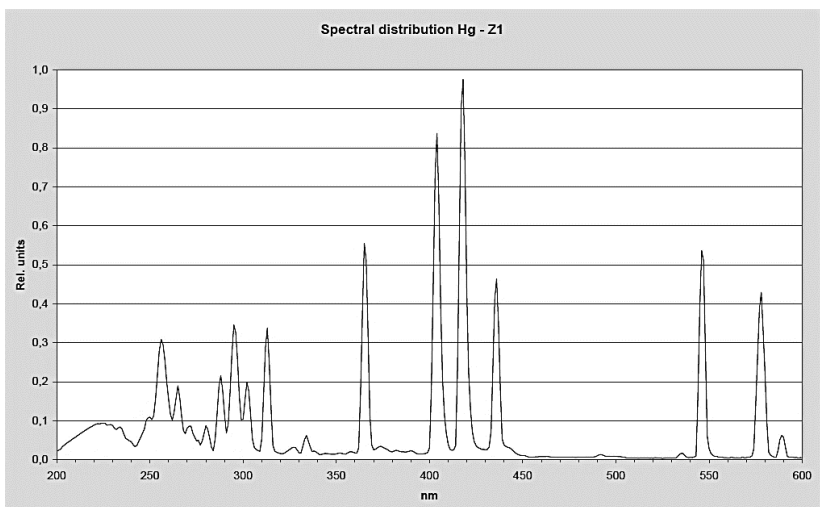


**Fig. S5.** UV-Vis emission spectrum of the medium-pressure mercury lamp

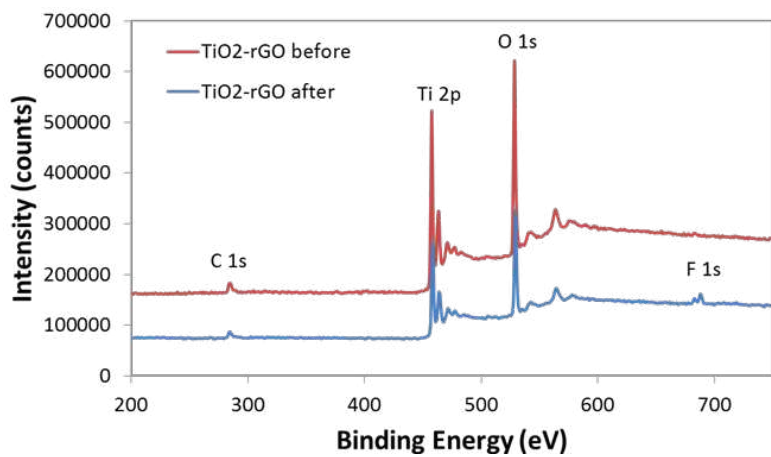


**Fig. S6.** XPS spectra of fresh (red line) and used (blue line)  $\text{TiO}_2$ -rGO catalyst.

**Table S2.** X-ray photoelectron spectroscopy (XPS) data of TiO<sub>2</sub>-rGO photocatalyst before and after the photocatalytic degradation of PFOA for 12 h of UV-Vis irradiation.

Sample	Atomic Species	Peak (eV)	Amount (at%)	Total Amount (%)
TiO <sub>2</sub> -rGO (fresh catalyst)	C	284.6	7.266	<b>13.8</b>
		286.3	4.757	
		288.9	1.811	
	O	529.6	48.51	<b>58.1</b>
		531.2	9.574	
	Ti	458.5	15.762	<b>28.1</b>
		464.2	7.892	
		471.8	3.046	
		477.3	1.381	
	TiO <sub>2</sub> -rGO (used catalyst)	C	284.6	7.313
286.3			2.509	
288.6			1.375	
292.5			1.95	
O		529.8	48.45	<b>53.2</b>
		531.4	4.697	
Ti		458.6	15.202	<b>26.9</b>
		464.3	7.611	
		471.9	2.81	
		477.4	1.24	
F		683.5	1.988	<b>6.8</b> (5.4 mg of F)
		687.9	3.686	
		690.0	1.161	

Regarding the C-1s region in Fig. S6, the main peak at 284.6 eV, which is due to C-C and C-H bonds, and the signals at 286 and 288 eV of the oxygenated species, C-O and COO<sup>-</sup>, were assigned to the partially reduced graphene oxide sheets in the TiO<sub>2</sub>-rGO composite. The XPS results in the Ti-2p region revealed the double signal at 458 and 464 eV of Ti<sup>4+</sup> in the TiO<sub>2</sub> particles. Also, the deconvoluted Ti-2p spectrum showed extra satellite peaks which contributed to the total amount of Ti. The typical zone of O-1s signals showed two peaks, one at 529 eV of the oxygen as oxide and another at 531 eV of the hydroxyl groups. Besides, the peak that was detected at 292.5 eV was assigned to the presence of C-F<sub>2</sub> and C-F<sub>3</sub> bonds on account of absorbed PFOA and its degradation products.





# ANNEXES



**Annex I. Scientific publication in preparation.**

**Degradation of poly- and perfluoroalkyl substances (PFASs) in  
Aqueous Film-Forming Foam by sequential UV  
oxidative/reductive treatments**

Authors:

Beatriz Gomez-Ruiz<sup>1</sup>, Nazely Diban<sup>1</sup>, Ane Urtiaga<sup>1</sup>, Raul Tenorio<sup>2</sup>,  
Juliane Brown<sup>2</sup>, Christopher P. Higgins<sup>2</sup>, Christopher Bellona<sup>2</sup>, Timothy  
J. Strathmann<sup>2</sup>

(1) Department of Chemical and Biomolecular Engineering,  
Universidad de Cantabria. Av. de Los Castros s/n. 39005 Santander.  
Spain.

(2) Department of Civil and Environmental Engineering, Colorado  
School of Mines, 1012 14th Street, Coolbaugh Hall, Golden, USA

**Abstract**

Aqueous film-forming foam (AFFF) containing poly- and perfluoroalkyl substances (PFASs), widely used for firefighting, have resulted in the contamination of water at training sites. In this work, sequential UV oxidative/reductive treatments were applied to accomplish the degradation of a mixture of PFASs contained in AFFF solution. The oxidative treatment consisted of UV irradiation of sodium persulfate solution to generate sulfate radicals ( $\text{SO}_4^{\cdot-}$ ,  $E=+2.5\text{-}3.1$  V). The reductive approach was accomplished by UV irradiation of sulfite to promote the generation of hydrated electrons ( $e_{\text{aq}}^-$ ,  $E=-2.9$  V). The oxidation technique promoted transformation of fluorotelomers sulfonates and unknown PFASs precursors to fluorotelomer carboxylates (FTCA) and perfluorocarboxylates (PFCAs). Additionally, it could be observed a decrease of long-chain PFCAs and PFOS concentrations by  $\text{SO}_4^{\cdot-}$  radicals. Conversely, the highest PFOS and PFCAs removal ratios were observed during UV-sulfite treatment. In contrast, fluorotelomers seemed to be relatively inert to  $e_{\text{aq}}^-$ . Tests of different sequential oxidative/reductive treatments were carried out. As a result of applying UV-persulfate stage followed by UV-sulfite treatment, the total concentration of PFASs in the AFFF solution was not further removed, due to the simultaneous elimination of unknown precursors and the less effectiveness of sulfite treatment as the second stage. However, the sequence of UV-sulfite followed by UV-persulfate was the most promising combination, achieving higher removal of the total content of PFASs and a 96% elimination of PFOS from the AFFF sample, after 48h of irradiation in this sequence.

## Graphical Abstract

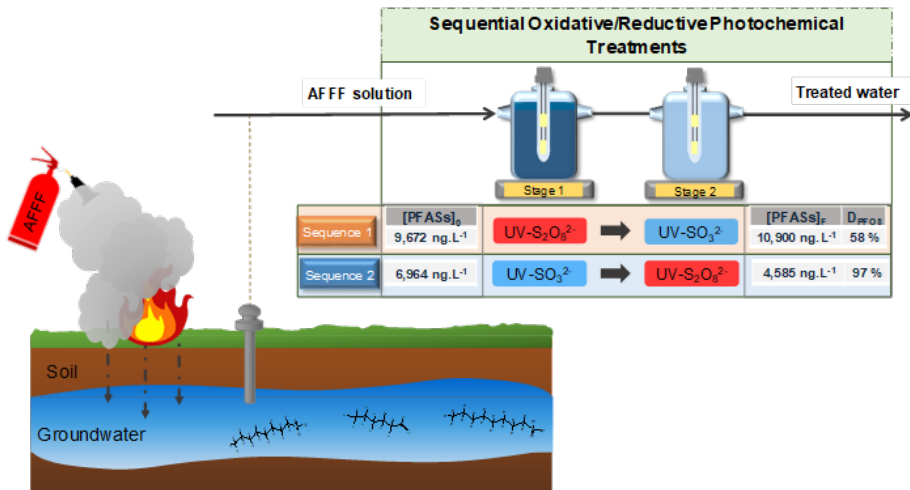


**Figure 3.1.** Graphical abstract of the work “*Degradation of poly- and perfluoroalkyl substances (PFASs) in Aqueous Film-Forming Foam by sequential UV oxidative/reductive treatments*”.

**Keywords:** AFFF, hydrated electrons, hydroxyl radical, sulfate radical, photodegradation

## 1. Introduction

Poly- and perfluoroalkyl substances (PFASs) have been extensively released to the environment due to their wide use in a variety of industrial and household applications for 50 years [1,2]. Furthermore, the extreme environmental persistence, global distribution and bio-accumulation of PFASs, in particular perfluorooctanoic acid (PFOA) and perfluorooctane sulfonic acid (PFOS), have resulted in increasing attention from the regulatory bodies [3,4].

In particular, PFASs are key components in aqueous film-forming foam (AFFF) formulations used for fire suppression because of their superior heat resistance and unique tensioactive properties, facilitating the rapid formation of thin films on the surface of the fuel, thereby preventing contact with oxygen and extinguish fires [5,6]. The extensive use of AFFFs during fire training activities at many civilian airports and military fire training areas has been an important contamination source of PFASs and associated co-contaminants, e.g., hydrocarbon fuels, into groundwater and surface waters surrounding these sites [7–9]. Therefore, the large volume of AFFF used for decades has resulted in a high number of AFFF-impacted sites that need to be assessed and remediated. Additionally, since the information of AFFF composition is proprietary and rarely available, many of the PFASs and nonfluorinated compounds contained in AFFF formulations are still unidentified [10].

To date, adsorption and/or ion exchange processes, such as granular activated carbon or ion exchange resins, are the most common approaches in use for PFASs impacted groundwater remediation. These techniques are effective for removal of long-chain PFASs. However, the adsorbent life

span can make these processes costly, and the PFAS contaminants are transferred to an another matrix that needs to be further treated [11,12].

Therefore, the challenge lies in the cleavage of the strong C-F bonds to achieve the complete mineralization of PFASs in water. Most of the technologies proposed for PFASs destruction have been focused on advanced oxidation processes (AOPs), by means of the generation of hydroxyl radicals, such as UV-H<sub>2</sub>O<sub>2</sub> system. Hori et al. [13] observed slow PFOA degradation rates by means of 1M of H<sub>2</sub>O<sub>2</sub> under UV-Visible irradiation and O<sub>2</sub> atmosphere, whereas no removal of PFOA was observed with 15 mM and even higher H<sub>2</sub>O<sub>2</sub> dosages under UV light by Qian et al. [14]. However, Yang et al. [15] observed nearly complete desulfonation and defluorination of 6:2 FTSA and of the perfluorocarboxylates formed during the UV-H<sub>2</sub>O<sub>2</sub> treatment in air atmosphere. Additionally, other photolytic methods including persulfate photolysis [14] have shown more efficacy on PFASs elimination. Sulfate radicals promoted by activated persulfate seem to be stronger oxidant species than hydroxyl radicals. In this way, Qian et al. [14] and Yin et al. [16] demonstrated significant PFOA degradation by activated-persulfate system and under acidic conditions. Moreover, Bruton et al. [17] evaluated the oxidation of PFASs contained in AFFF-impacted groundwater by heat activated persulfate. Fluorotelomer- and perfluoroalkyl sulfonamide-based polyfluorinated compounds were transformed to perfluorinated carboxylic acids, which underwent further degradation under acidic conditions. Other photochemical strategies, such as heterogeneous photocatalysis by means of new synthetic composite catalysts, e.g., TiO<sub>2</sub> with metals or carbon-based material, have been demonstrated to be a promising alternatives for the degradation of PFOA [18,19]. Overall, some AOPs are able to degrade perfluorocarboxylates, however, reports to date indicate that they are

ineffective with perfluoroalkyl sulfonates, including PFOS [17,20]. Additionally, among these oxidative approaches, electrochemical oxidation has also attracted interest for PFAS degradation. Particularly, BDD anodes can effectively decompose PFAS from aqueous solution, since it can provide high generation of  $\cdot\text{OH}$  and the ability of electron transfer [21–23]

Recently, new reductive strategies have been proposed as alternative for PFAS removal which involve the generation of hydrated electrons ( $e_{\text{aq}}^-$ , standard reduction potential = -2.9 V). Hydrated electrons are powerful reducing agents that enabled the effective degradation of both PFOA and PFOS [24]. It has been reported that PFASs reduction is thermodynamically more favored than PFASs oxidation [25]. The strong electronegativity of fluorine atoms can act as the reductive reaction center for defluorination.  $e_{\text{aq}}^-$  species can be generated by pulse radiolysis of pure water or photolytic methods including inorganic anions mediated photolysis, such as ferrocyanide mediated laser flash photolysis [26] or UV photolysis of KI [27], sulfite [28,29], aminocarboxylates [30,31] or NOM [32,33]. Among the different alternatives, UV photolysis of sulfite is more practical and environmental friendly than the use of KI or ferricyanide as sensitizers. Song et al. [34] reported the feasibility of using the UV-sulfite system to decompose PFOA under  $\text{N}_2$  atmosphere and alkaline conditions. Also, PFOS was successfully decomposed in 30 min using high-pressure mercury lamp at alkaline and 10 mM of sulfite [29]. Additionally, Park et al. [35] studied the effect of the ionic headgroup and the chain length of perfluoroalkyl carboxylates and sulfonates on the reductive defluorination by UV irradiation of KI. As a result, for the same alkyl-chain length, higher degradation rates for PFASs were obtained. Moreover, PFASs reduction

kinetic increase linearly with the chain length, whereas a negligible effect of PFCA chain length on reduction rate was observed.

As the efficacy of reduction and oxidation processes seemed to be affected by the molecular structure of PFASs, this work reports for the first time the sequential UV oxidative/reductive treatments for facilitating the degradation and mineralization of a complex mixture of PFASs contained in AFFF formulation. The AFFF included a PFAS profile defined by perfluorocarboxylates, perfluorosulfantes, and fluorotelomer carboxylates and sulfonates. The oxidative treatment consisted of UV irradiation with persulfate to generate sulfate radicals, whereas the photolysis of sulfite was used to promote hydrated electrons. In this work, individual and sequential treatments, including oxidation followed by reduction and reduction followed by oxidation, were compared. The feasibility of each UV-system and the benefits of the different combinations for the degradation of PFASs were also evaluated.

## **2. Materials and methods**

### **2.1. Materials and AFFF samples**

All chemicals used in the experiments were reagent grade or higher (purity > 98%) and were used as received without further purification. Sodium sulfite ( $\text{Na}_2\text{SO}_3$ ), sodium sulfate ( $\text{Na}_2\text{SO}_4$ ), sodium persulfate ( $\text{Na}_2\text{S}_2\text{O}_8$ ), sodium phosphate monobasic dihydrated ( $\text{NaH}_2\text{PO}_4 \cdot 2\text{H}_2\text{O}$ ), potassium hydrogen phthalate ( $\text{C}_8\text{H}_5\text{KO}_4$ ), 5-5-dithio-bis-(2-nitrobenzoic acid) ( $\text{C}_{14}\text{H}_8\text{N}_2\text{O}_8\text{S}_2$ , DTNB), were purchased from Sigma Aldrich Chemicals. Sodium bicarbonate ( $\text{NaHCO}_3$ ) was obtained by Macron, ACS Reagent. Sodium hydroxide 1N ( $\text{NaOH}$ ) was obtained from Fisher Chemical. Sulfuric acid ( $\text{H}_2\text{SO}_4$ , GR grade, 98%) was purchased by

Millipore. Potassium iodide (KI) was obtained from Alfa Aesar (99%). All solutions were prepared using ultrapure water (Millipore Milli-Q system).

A mixed AFFF waste mixture was obtained from CH2M (Englewood, Colorado). The AFFF mixture was spiked into laboratory water matrices as the target contaminated water. A 1-to-10<sup>6</sup> dilution of the AFFF formulation was prepared to simulate PFAS concentration ( $\mu\text{g.L}^{-1}$  levels) typically found in real AFFF-impacted groundwater. Table 1 lists the composition of the resulting diluted AFFF solution, that was analyzed using the analytical methods reported in section 2.3.

As it is observed, AFFF contained a complex mixture of PFASs that is formed by: perfluoroalkyl carboxylates (PFCAs), perfluoroalkyl sulfonates (PFSAs) and fluorotelomers (FTs). The AFFF composition was consistent with a mixture of 3M AFFF formulation synthesized by electrochemical fluorination (ECF) and fluorotelomer AFFFs obtained by telomerization methods [36]. PFOS was significantly the most abundant compound identified in the model AFFF-impacted water, as it has been observed in other AFFF formulations [8]. Full names, abbreviations and limits of quantification (LOQs) for these PFASs detected in AFFF, are listed in Table S1 in the Supplementary information.

The total fluorine content the AFFF solution was  $0.0135 \text{ mg.L}^{-1}$  which was quantified by Fluorine-19 nuclear magnetic resonance spectroscopy (<sup>19</sup>F-NMR). The F content calculated from the initial concentration of PFASs detected in the AFFF (Table 1) corresponded only to the  $30 \pm 5\%$  of the total fluorine obtained by <sup>19</sup>F-NMR. This result revealed a high content of unknown PFASs or fluorinated precursors in AFFF formulation. These compounds can cause the generation of the PFASs monitored throughout

the treatments, hindering the determination of each PFAS compound removal. In this context, the total content of PFASs at the end of the stages was used to compare the feasibility of the proposed AFFF treatments.

**Table 1.** Initial concentration of PFASs, total organic carbon (TOC) and F content in the 1-to-10<sup>6</sup> diluted AFFF solution

<b>PFASs</b>	<b>C<sub>0</sub> (ng.L<sup>-1</sup>)</b>
PFBA	47 ± 8
PFPeA	41 ± 3
PFHxA	110 ± 76
PFHpA	39 ± 6
PFOA	86 ± 24
PFNA	65 ± 0
PFPrS	91 ± 16
PFBS	17 ± 3
PFPeS	124 ± 16
PFHxS	725 ± 91
PFHpS	104 ± 17
PFOS	4,976 ± 692
PFNS	51 ± 3
6:2 FTCA	22 ± 7
6:2 FTSA	67 ± 29
8:2 FTSA	29 ± 2
6:2 FTUCA	33 ± 17
<b>TOC (mg C.L<sup>-1</sup>)</b>	0.147
<b>F (mg.L<sup>-1</sup>)</b>	0.0135

## 2.2. Photochemical Experiments

The schematic of experimental setup is shown in the Figure S1 (Supplementary Data). Batch photochemical degradation experiments were conducted in an immersion well photoreactor (Ace Glass Inc.) mounted on a magnetic stirring plate (Isotemp, Fisher Scientific). A UV low-pressure mercury lamp (Ace Glass Inc., 18W) emitting at 254 nm, was placed in a quartz sleeve in the center of the reactor, as irradiation source. By flowing a cooling fluid through the outer cooling jacket that encases the lamp and the reactor, the temperature was maintained at  $20 \pm 1$  °C. Treated samples were withdrawn from the reactor at regular time intervals and preserved at 4°C until analysis. PFASs concentrations are shown as the average of duplicate experiments.

Two photochemical systems were studied: (O1) UV irradiation with persulfate (UV-S<sub>2</sub>O<sub>8</sub><sup>2-</sup>) and (R1) UV irradiation with sulfite (UV-SO<sub>3</sub><sup>2-</sup>). Table 2 summarizes the experimental conditions that were established based on the literature [13–16,29,34,37–39]. The same initial concentration of Na<sub>2</sub>S<sub>2</sub>O<sub>8</sub> and Na<sub>2</sub>SO<sub>3</sub> (10 mM) was employed to allow the comparison of treatments efficiency. In each experiment, a volume of 575 mL of a 1-to-10<sup>6</sup> dilution of AFFF was irradiated. Oxidative treatment was carried out under atmospheric air, and the initial pH was adjusted to 3 with 0.5 mM of H<sub>2</sub>SO<sub>4</sub> and 4 mM Na<sub>2</sub>SO<sub>4</sub>, used for ionic strength adjustment. During AFFF impacted water treatments, additions of 10-12 mM Na<sub>2</sub>S<sub>2</sub>O<sub>8</sub> aliquots to the reacting media were needed when the sensitizer concentrations dropped below 50% of their initial value. UV-sulfite tests were performed under N<sub>2</sub> gas and the initial pH was adjusted to 9.5 by NaOH and 5mM NaHCO<sub>3</sub> buffer. Before the test, the mixture was bubbled

with N<sub>2</sub> for an hour to remove dissolved oxygen from solution before switching on the UV lamp.

**Table 2.** Experimental conditions for each photolytic system: UV-S<sub>2</sub>O<sub>8</sub><sup>2-</sup> and UV-SO<sub>3</sub><sup>2-</sup>.

System	Reacting media	Atmosphere	Initial sensitizer concentration (mmol.L <sup>-1</sup> )	Initial AFFF concentration	Treatment time (h)
<b>O1:</b> UV-S <sub>2</sub> O <sub>8</sub> <sup>2-</sup>	Acidic pH <sub>0</sub> H <sub>2</sub> SO <sub>4</sub> + Na <sub>2</sub> SO <sub>4</sub>	Air	10 (Na <sub>2</sub> S <sub>2</sub> O <sub>8</sub> )	1-to-10 <sup>6</sup> dilution	34
<b>R1:</b> UV-SO <sub>3</sub> <sup>2-</sup>	Alkaline pH <sub>0</sub> NaOH + NaHCO <sub>3</sub>	Nitrogen	10 (Na <sub>2</sub> SO <sub>3</sub> )	1-to-10 <sup>6</sup> dilution	24

Individual experiments of each UV-system and sequences of UV oxidative/reductive treatments were performed as follows:

- 1) Control test: UV only
- 2) UV- Persulfate only
- 3) UV- Sulfite only
- 4) Sequence 1: UV- Persulfate followed by UV- Sulfite
- 5) Sequence 2: UV- Sulfite followed by UV- Persulfate

### 2.3. Analytical Methods

Persulfate concentrations were quantified by colorimetric methods following the reported studies by Liang et al. [40]. A modified spectrophotometric method was applied to determine sulfite concentrations [41]. Briefly, sulfite reacts quantitatively with excess DTNB in aqueous solutions buffered at pH 7.0 with NaH<sub>2</sub>PO<sub>4</sub> for 5 min before measuring absorbance at 412 nm. Fluoride determination by ion-selective electrode was unsuccessful due to the low concentrations present

in the diluted AFFF mixture.

PFASs were measured on a SCIEX X500R QToF-MS system (Framingham, MA) using electrospray ionization in negative mode (ESI-) with SWATH® Data-Independent Acquisition for both TOFMS and MS/MS mode, which enables simultaneous tentative identification of >1500 PFASs in the suspect screening list, and including 44 analytes that are quantified against external reference standards. LOQs were analyte, matrix, and run dependent, but were generally 0.6–23 ng.L<sup>-1</sup> (see details on the analytical protocol in the Supplementary Information).

### **3. Results and discussion**

#### **3.1. Direct UV photolysis**

Prior to AFFF experiments, the effect of UV irradiation on AFFF degradation (in the absence of any sensitizer) was also studied in a sequence formed by a first stage in acidic matrix (Figure 1, red colored background) and the second alkaline stage (Figure 1, blue colored background). The value of the pH remained nearly constant during the treatments.

As it can be observed in Figure 1a, the content of PFCAs highly increased during the first 15 h of experiment, particularly PFNA, PFOA and PFHxA. Possible direct photolysis of fluorotelomers or unknown precursors promoted the generation of PFCAs [22,42–44]. However, after 34 h of UV irradiation, the concentrations of longer-chain PFCAs (PFNA and PFOA) decreased likely due to their moderate photolysis [45–47]. PFOA molecule absorbs photons from deep UV-region to 220 nm, and presents weak absorption in the 220–270 nm range of light wavelengths [13]. Qu et al.

[48] also observed that the C-C bond strength between carboxylic carbon and the adjacent carbon increases with the shortened carbon chains of PFCAs, revealing that photolysis rate gradually increases with the alkyl chain length. Additionally, other components in AFFF solution possibly absorb UV light (254 nm) which can generate small concentrations of reactive species.

In contrast, PFSAAs seemed to be relatively inert to direct photolysis (Figure 1b). Only a slow degradation of PFOS ( $14 \pm 10\%$ ) could be observed after 34 h of UV irradiation and acidic conditions. Direct photolysis of PFOS has been previously investigated using a low pressure mercury lamp by Yamamoto et al. [49], who reported that PFOS was slowly photodecomposed by 8 and 68% after 1 and 10 days, respectively. Moreover, this result can be related to the elimination of branched PFOS isomers in the sample, which are more susceptible to degradation due to the presence of one or two  $-\text{CF}_3$  groups branching from the perfluorinated alkyl chain [50,51]. The AFFF sample used in the present work typically contains a ratio of  $\sim 70/30$  of linear/branched PFOS. The concentrations of FTs were depicted in Figure 1c. Overall, the content of FTs increased dramatically during the first 15 h of treatment, particularly 6:2 FTCA. After 34 h of irradiation, 6:2 FTCA achieved its maximum concentration of  $26,000 \text{ ng}\cdot\text{L}^{-1}$ , whereas the concentrations of 6:2 FTSA, 8:2 FTSA and 6:2 FTUCA were photodegraded by 67, 60 and 41%, respectively. It can be suggested that 6:2 FTCA was the main PFAS component in the sample. Therefore, AFFF mixture contains high content of unknown precursors which may firstly form fluorotelomers, and subsequently, PFNA, PFOA and PFHxA under photolytic conditions [44,52,53]. However, this last assumption will be discussed in the section 3.4.

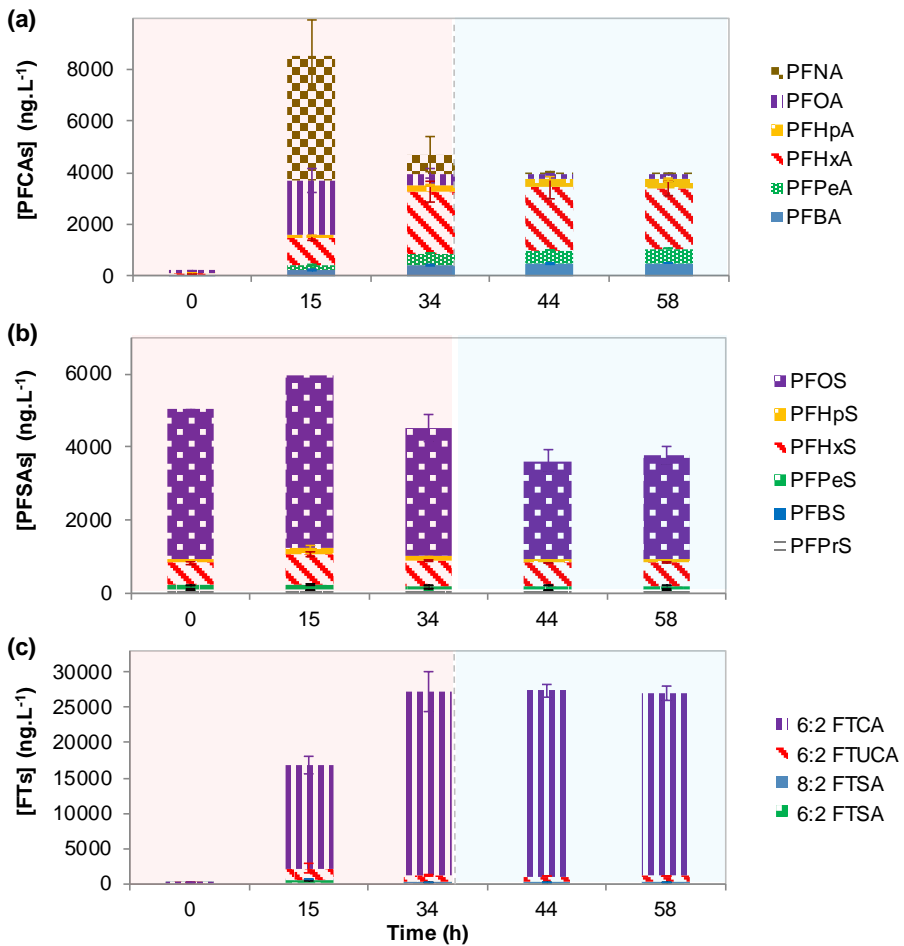


**Figure 1.** Concentration of (a) PFCAs, (b) PFSA and (c) FTs during the photolytic treatment in absence of sensitizers. The first stage (0-34 h) developed under acidic matrix and air is shown in red colored background, whereas the second stage (34-58 h) in alkaline matrix and N<sub>2</sub> is shown in blue colored background. 1-to-10<sup>6</sup> dilution of AFFF. Error bars represent standard deviation derived from duplicated experiments.

Before the second stage of this control sequence, the experimental conditions of the AFFF sample were adjusted to alkaline conditions (see Table 2), to mimic conditions used for UV-SO<sub>3</sub><sup>2-</sup>. Then, during this second UV-only treatment (Figure 1, 34-58 h), no further photodecomposition of the different groups of PFASs was observed. Only minor eliminations of PFNA, PFOA and PFOS during the first 10 h of treatment (34-44 h in the overall experimental cycle) could be detected. Longer-chain PFCAs may be more sensitive to UV irradiation than shorter-chain PFCAs [48]. Nevertheless, the bicarbonate presence in the alkaline matrix may have interfered with PFASs photodegradation, as it has been observed by Giri et al. [54].

### **3.2. Individual photochemical treatments of AFFF**

In this section, the progress of PFASs concentration after the application of each individual treatment (UV- Persulfate and UV- Sulfite) will be explained. Each individual UV system correspond to the first stage of the sequence of treatments proposed. However, the results of PFASs concentrations of the second stage in each sequence will be reported in the next section.

#### UV – Persulfate

The AFFF degradation by UV activated-persulfate is depicted in Figure 2 (0-34 h, red colored background). Figure 2a presents the monitoring of persulfate concentration with time. The results showed the concentration before and after the persulfate spikes into the reacting media. The rate of persulfate decomposition by UV light became gradually slower during the test (Figure 2a). Some species formed during the treatment of AFFF

impacted water may hinder the photoreaction between persulfate and UV light. As a result, the experiments were carried out during 34 h, to completely eliminate the residual persulfate at the end of the treatment.

Persulfate salts dissociate in water to persulfate anion ( $S_2O_8^{2-}$ ) which can be activated photo-chemically or thermally to form two free sulfate radicals ( $SO_4^{\cdot-}$ , standard reduction potential = 2.5-3.1 V [55]) with quantum efficiency of unity (Eq. 1) [56].



$SO_4^{\cdot-}$  is an oxidizing radical that reacts by direct one-electron transfer to form sulfate ion. Sulfate radicals may react with water to form bisulfate and hydroxyl radicals (Eq. 2). Moreover, bisulfate can release protons to the solution due to its low  $pK_a$  (Eq. 3) [57]. This is the main mechanism that caused the pH drop from 3 to 1.4 at the end of persulfate experiment. The  $H^+$  released from the decomposition of some PFASs was considered negligible because of their lower concentration compared to persulfate. Therefore, under acidic conditions,  $SO_4^{\cdot-}$  is the predominant oxidizing species for PFASs degradation reactions during the persulfate process [14,16].



Figure 2b shows the concentrations of PFCAs during the UV-persulfate process. PFCAs progressively increased during the first 10 h of irradiation. Particularly, the concentrations of shorter-chain PFCAs (PFPeA and PFBA) increased in  $1,000 \text{ ng}\cdot\text{L}^{-1}$  during this period, a significantly higher

rate than the results obtained in direct photolysis. These results may indicate that longer PFCAs were simultaneously formed and decomposed step-by-step by  $\text{SO}_4^{\cdot-}$  radicals into shorter-chain PFCAs, as it has been previously reported [14,16,20,58]. After that, PFCAs concentrations partially decreased after 34 h of irradiation time, more noticeable for longer chain PFCAs by the role of sulfate radicals (see Table S2, Supplementary Material).

In the case of PFSAs (Figure 2c), a high 79% PFOS removal ratio was obtained after 34 h of treatment. Even though a possible PFOS sorption to the reactor walls or other physical phenomenon related to AFFF components can take place [17], the progressive decay with time elucidated its degradation under the applied experimental conditions. This finding revealed a higher removal of PFOS by UV-activated persulfate than heat-activated persulfate previously reported [17,20]. It may be related to the high energy introduced by UV photons into the molecular entity that could promote electronically excited states of molecules, giving products probably different from the products of chemical/thermal reactions [59]. Alternatively, intermediates between persulfate or sulfate radicals and other components of AFFF may promote formation of unidentified PFOS-reactive species. Moreover, concentrations of PFHpS, PFHxS and PFPeS also decreased by 43, 28 and 34%, respectively. On the contrary, shorter-chain PFSAs exhibited poorer reactivity during the oxidative treatment.

The progresses of FT carboxylates and FT sulfonates are shown in Figure 2d. 6:2 FTCA notably increased during the first 10 h of treatment ( $1,800 \text{ ng}\cdot\text{L}^{-1}$ ), and then, its concentration only slightly decreased after 34 h. However, these levels of 6:2 FTCA were lower than those obtained by photolysis. This result points out that 6:2 FTCA was formed and

simultaneously degraded by the strong reactive capacity of  $\text{SO}_4^{\cdot-}$  radicals with this compound. Additionally, n:2 FTSA and 6:2 FTUCA were completely decomposed, likely to form PFCAs by UV-activated persulfate [20].

After 34 h of UV activated-persulfate treatment, the total concentration of PFASs (listed in Table S2, Supplementary Material) decreased by 17%. Even though  $\text{SO}_4^{\cdot-}$  radicals were strong oxidizing species for PFASs degradation, the final concentration was still high, likely due to the formation of PFCAs and FTs as degradation products of PFAS precursors in the AFFF sample. Moreover, it is important to note that the high presence of unknown fluorinated precursors in AFFF were highlighted previously, when the total F content in the detected PFASs in the AFFF solution only corresponded to the 30% of the total fluorine content of AFFF obtained by  $^{19}\text{F}$ -NMR.

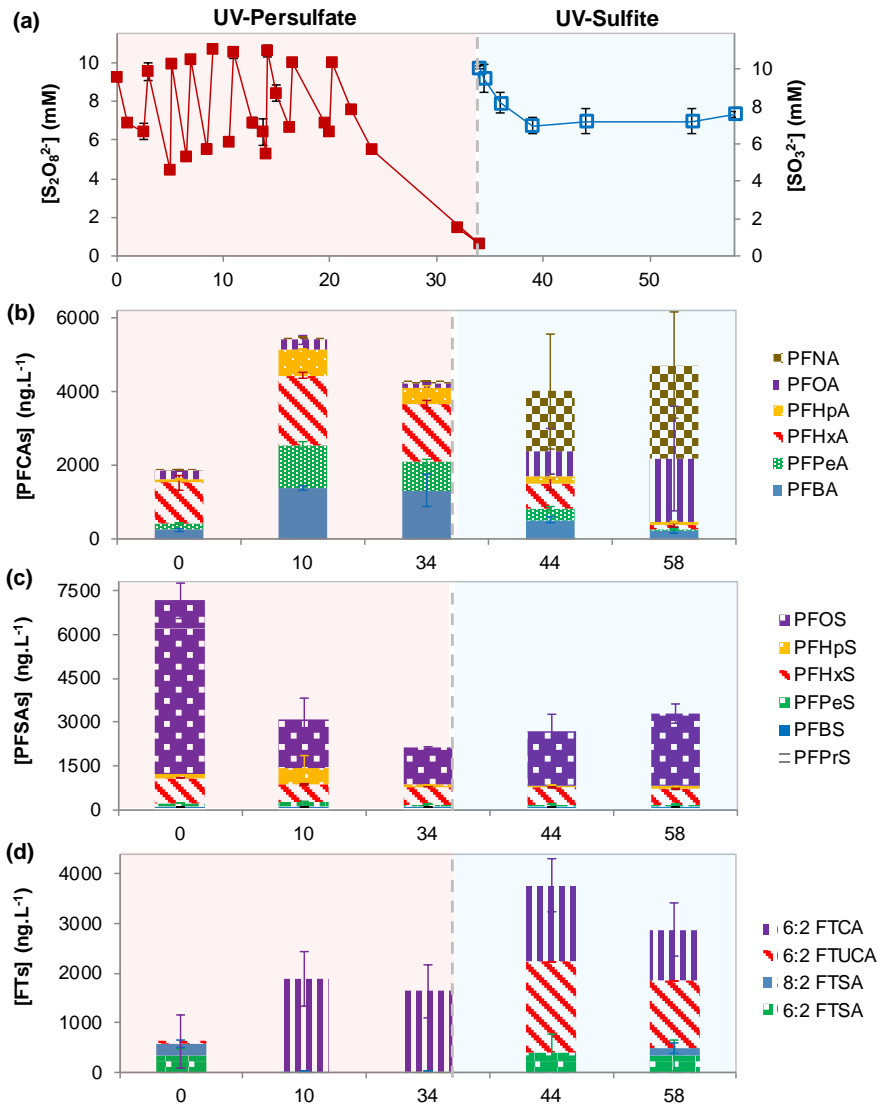


**Figure 2.** Concentration of (a) sensitizers persulfate and sulfite, (b) PFCAs, (c) PFSAs, and (d) FTs during the sequence 2, formed by the first stage of UV- $S_2O_8^{2-}$  (0-34 h, red background) and the second treatment of UV- $SO_3^{2-}$  (34-58 h, blue background). 1-to- $10^6$  dilution of AFFF. Error bars represent standard deviation derived from duplicated experiments.

### UV - Sulfite

The reductive method was developed by UV photolysis of sulfite which involves hydrated electrons ( $e_{aq}^-$ ) generation (Eq. 4), in an alkaline matrix and  $N_2$  atmosphere, in order to avoid the high reactivity of  $e_{aq}^-$  with  $H^+$  and oxygen.



Sulfite decay with UV irradiation time was depicted in Figure 3a (0-24 h, blue colored background). The sulfite concentration remained at ~4mM after 24 h, without any further addition of sensitizer. Increasing the initial sulfite concentration could hinder AFFF degradation due to the formation of  $SO_3^{\bullet-}$  which could react with other  $SO_3^{\bullet-}$  radicals to give  $S_2O_6^{2-}$ , an  $e_{aq}^-$  quencher (Eq. 5-6) [34,60,61].



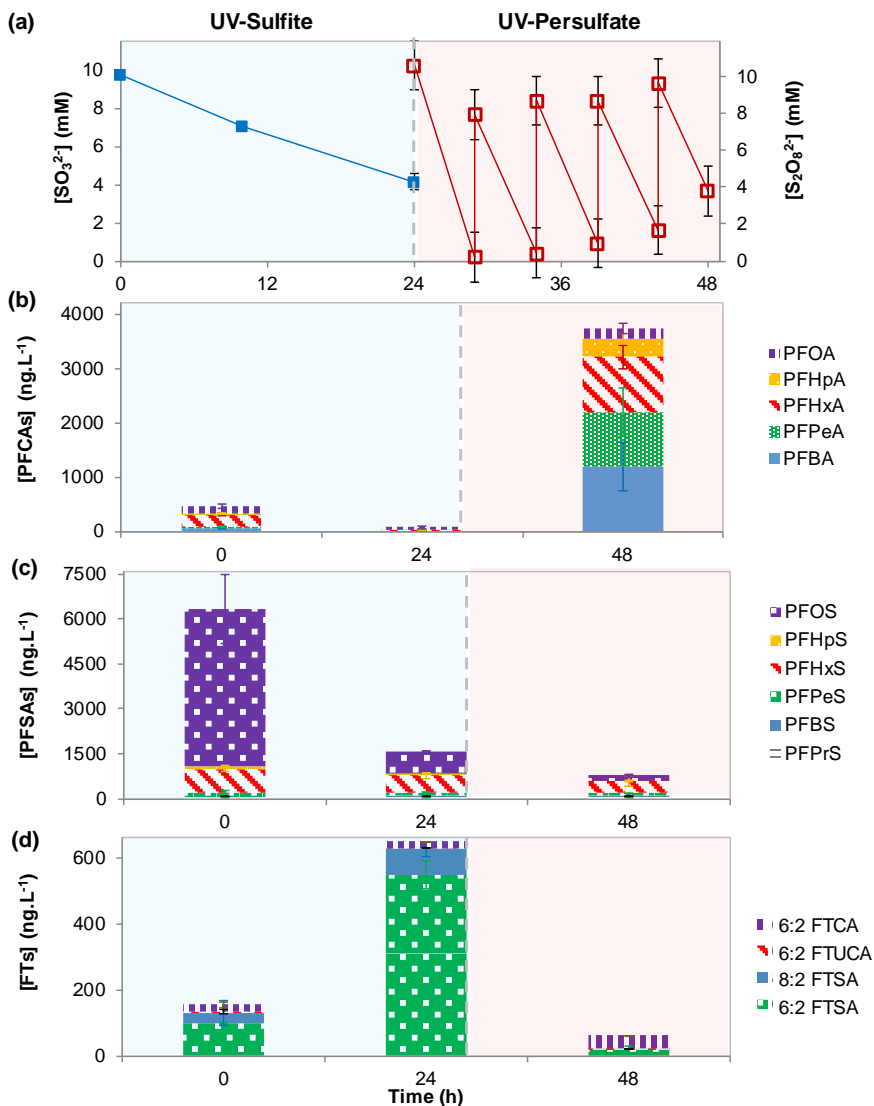
The solution pH increased from 9.6 to 10.3 at the end of the experiment without pH adjustment. The pH increase could be assigned to the minor reaction of  $e_{aq}^-$  with water, which produce  $OH^-$  and  $H^+$ , since this later compound can react with other components of AFFF solution (Eq. 7) [62].



Figure 3 (0-24 h, blue colored background) shows the concentrations of PFCAs (b), PFSAs (c) and FTs (d) during the reductive treatment. In contrast to the oxidative technique,  $e_{aq}^-$ -mediated experiments efficiently allowed higher removal rates of all PFCAs initially contained in the AFFF

solution (Figure 3b). After 24h, PFHxA and PFPeA almost disappeared, whereas PFOA, PFHpA and PFBA exhibited 69, 45 and 75% of degradation, respectively. It must be noted that the overall initial concentration of PFCAs was notably lower than in the initial sample of experiments shown in Figure 3, an indicative of the uncertainty of the composition of the AFFF formulation. In addition, PFCAs concentration did not increase during the treatment time of UV-sulfite system. Although unknown PFASs precursors were degraded into PFCAs over the treatment, the degradation rates of PFCAs were higher than the formation kinetics from the precursors transformation. This behavior contrast with the results obtained in the UV activated persulfate treatment, pointing to differences in the degradation mechanisms by the oxidative and reductive treatments.

The concentrations of PFSA in the treatment are shown in Figure 3c. As it is observed, this reductive test achieved the highest elimination of PFOS (86%) from the AFFF mixture after 24 h. PFHpS, PFHxS and PFPeS, decreased by 42, 26 and 25%, respectively, whereas shorter-chain PFSA remained inert to  $e_{aq}^-$  species formed during the treatment. Figure 3d shows that the concentration of FT carboxylates (6:2 FTCA and 6:2 FTUCA) remained nearly constant, however, the levels of FT sulfonates increased considerably after 24h of irradiation, likely due to the reduction of unknown sulfonamide-based precursors. In addition, control reductive experiments revealed that individual PFOA and PFOS solutions exhibited similar degradation rates compared to those obtained over AFFF treatment. Therefore, although unknown precursors were degraded over the UV-sulfite treatment, the degradation rates of PFCAs and PFSA by hydrated electrons were notably higher than the formation kinetics from the precursors or fluorotelomers transformation.



**Figure 3.** Concentration of (a) sensitizers sulfite and persulfate, (b) PFCAs, (c) PFSAAs, and (d) FTs during the sequence 3, formed by the first stage of UV- $\text{SO}_3^{2-}$  (0-24 h, blue background) and the second treatment of UV- $\text{S}_2\text{O}_8^{2-}$  (24-48 h, red background). 1-to- $10^6$  dilution of AFFF. Error bars represent standard deviation derived from duplicated experiments.

According to the results shown above, it could be highlighted that hydrated electrons reacted more rapidly with perfluorinated compounds (PFCAs and PFASs) than with the fluorotelomers or unknown precursors that contained unfluorinated carbons in their molecules.

After 24h of the reductive process, the  $\Sigma$ PFAS concentrations in the AFFF mixture was decreased to 2,281 ng.L<sup>-1</sup> (Table S3, Supplementary Material), which represented a significantly improved overall removal compared to UV-S<sub>2</sub>O<sub>8</sub><sup>2-</sup> treatment.

### 3.3. Sequential oxidative/reductive treatments of AFFF

#### Sequence 1: UV- Persulfate followed by UV- Sulfite

The AFFF sample treated firstly by UV-activated persulfate was adjusted to the experimental conditions needed for UV-sulfite system (see Table 2). The sulfite concentration represented in Figure 2a (34-58 h, blue colored background) stayed nearly constant after 4 h of the treatment, which could involve lower formation of e<sub>aq</sub><sup>-</sup> during that period.

Figure 2b shows that the high content of C<sub>4</sub>-C<sub>7</sub> PFCAs after the first UV-S<sub>2</sub>O<sub>8</sub><sup>2-</sup> oxidative stage were progressively removed by e<sub>aq</sub><sup>-</sup>, and decreased by 80-90% at the end of this second treatment. However, PFOA and PFNA were significantly formed over the reductive treatment, up to levels of 1,700-2,500 ng.L<sup>-1</sup>. It is thought that C<sub>8</sub> precursors may be inert to e<sub>aq</sub><sup>-</sup> during the first sulfite treatment, whereas these contaminants can be degraded by oxidizing species producing PFOA and PFNA in this second stage.

Figure 2c shows the evolution of PFASs with the irradiation time. PFOS

concentration slightly increased during the reductive treatment. However, an overall 60% PFOS removal resulted from this sequence of treatments. In contrast, shorter-chain PFSA's did not exhibit high interaction with  $e_{aq}^-$  species formed in this second treatment. Figure 2d displays the change of FTs concentrations with time. 6:2 FTCA and 6:2 FTUCA initially increased during the first part of the treatment, and then, slightly decreased after 24 h of treatment. n:2 FTSA compounds seemed to be formed and degraded simultaneously during the treatment. These results pointed out the presence of unknown C<sub>8</sub> sulfonamide-based or fluorotelomer precursors in the second stage, producing mainly PFOS, PFOA and PFNA during the reductive treatment [63,64]. Moreover, previous experiments in the research group revealed the formation of PFOA, PFOS and perfluorooctane sulfonamide as degradation product of the reductive treatment of perfluorooctane sulfonamidoacetic acid (data not shown). These possible mechanisms are reported in Figure 4.

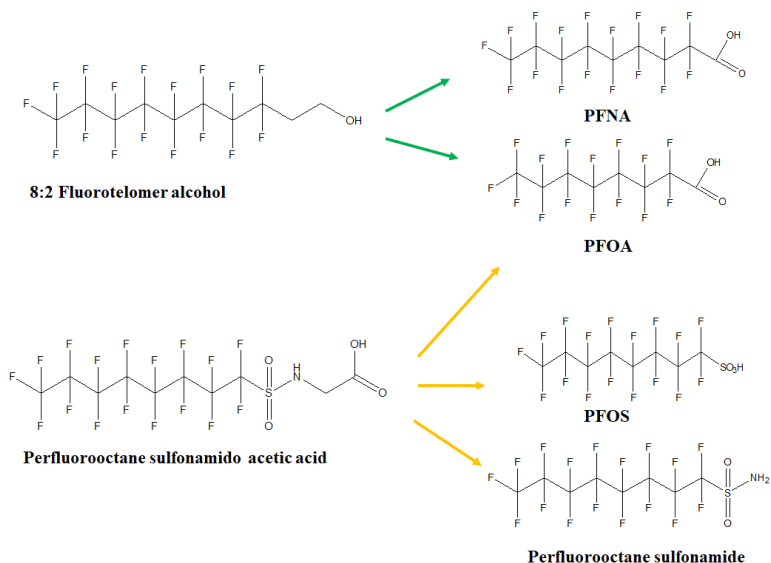


**Figure 4.** Degradation pathways of possible precursors of PFOS, PFOA, PFNA.

Additionally, the lower formation of n:2 FTSA in this second stage than in the UV-sulfite treatment (Figure 3d), revealed the partial removal of C<sub>6</sub> unknown precursors at the first persulfate treatment.

The results of this reductive treatment differed with the individual UV-sulfite treatment applied as the first treatment in the sequence (Fig 3 0-24 h), particularly for long-chain PFCAs and PFSA trends. This response may be attributed to the limited formation of e<sub>aq</sub><sup>-</sup> after 4-5 h of this treatment, since the sulfite concentration stayed constant. Moreover, it is important to note that the AFFF sample contained high sulfate ion concentration (~180 mmol.L<sup>-1</sup>) due to the persulfate spikes over the first stage, which may interfere in the reactions scenario in this second reductive treatment.

Even though the total concentration of PFASs slightly decreased during the first UV-S<sub>2</sub>O<sub>8</sub><sup>2-</sup> stage (Table S2), the transformation of unknown components into the identified PFASs which were also degraded resulted in a similar total content of PFAS at the end of this sequence of oxidative and reductive treatments.

#### Sequence 2: UV- Sulfite followed by UV- Persulfate

The background of the AFFF sample, treated initially by the reductive UV-sulfite treatment, was modified according to the needs of the UV-S<sub>2</sub>O<sub>8</sub><sup>2-</sup> process (see Table 2). It is noteworthy that residual sulfite was totally quenched by an equimolar amount of H<sub>2</sub>O<sub>2</sub> without UV irradiation in 5 min (data not shown) [65], to avoid any interference in the generation of SO<sub>4</sub><sup>-</sup>, since e<sub>aq</sub><sup>-</sup> can also rapidly react with S<sub>2</sub>O<sub>8</sub><sup>2-</sup>. The monitoring of persulfate concentration during the treatment is depicted in Figure 3a (24-48 h, red colored background).

Figure 3b (24-48 h) shows that the total concentrations of PFCAs highly increased, particularly C<sub>4</sub>-C<sub>6</sub> PFCAs, as it was observed in the individual UV-S<sub>2</sub>O<sub>8</sub><sup>2-</sup> treatment. Regarding the progress of the PFSA with time (Figure 3c), the concentrations of longer-chain PFSA progressively decreased during this second treatment, in agreement with the results of UV-S<sub>2</sub>O<sub>8</sub><sup>2-</sup> treatment that were shown in Figure 2b. Additionally, this sequence of UV-sulfite plus UV-persulfate treatments, achieved the highest total removal ratios of 96, 65, 50 and 36 %, for PFOS, PFHpS, PFHxS and PFPeS, respectively, after 48 h of irradiation. The change of FTs concentrations with time is displayed in Figure 3d. Whereas 6:2 FTCA partially increased during the treatment, SO<sub>4</sub><sup>-</sup> radicals can efficiently remove 6:2 FTSA, 8:2 FTSA and 6:2 FTUCA from the AFFF solution, similarly to the effect of the UV- S<sub>2</sub>O<sub>8</sub><sup>2-</sup> displayed in Figure 2d.

In summary, during the first reductive stage, the ΣPFASs content decreased to 2,281 ng.L<sup>-1</sup> after 24h of irradiation time. However, this total concentration of PFASs increased again to 4585 ng.L<sup>-1</sup> after the second persulfate stage of this sequence (Table S3), due to the degradation of unidentified precursors by sulfate radicals.

### **3.4. Overview of AFFF composition and treatments**

Since AFFF compositions are proprietary, some possible PFASs precursors in the AFFF formulation used in the present work were proposed, based on the trends of PFASs during the treatments and data from literature.

#### Fluorotelomers

Firstly, the initial content of the fluorotelomer carboxylates and

fluorotelomer sulfonates on the target screening list studied in the sample was minor among the total PFASs content. However, the important formation of 6:2 fluorotelomer carboxylate during the oxidative treatment, revealed that unknown fluorotelomer-based precursors could be considered the most abundant component in the AFFF sample. The formation of FT carboxylates has been previously related to the photolytic degradation of fluorotelomer alcohols which can exist as both primary contaminants and intermediates. In this way,  $C_n$  fluorotelomer alcohols were degraded into  $C_n$  fluorotelomer carboxylates and PFCAs under UV oxidations [39,66–68]. Moreover, 6:2 FTCA, FTUCA and 5:3 FTCA were also detected as semi-stable intermediates by abiotic and biotic 6:2 FTOH degradation [69], which can also explain the generation of FTUCA as a by-product in the present work. On the other hand, the formation of fluorotelomer sulfonates, particularly 6:2 FTSA, can be associated with the presence of fluorotelomer sulfonamide-based compounds in AFFF, such as fluorotelomer sulfonamide alkylbetaine (FTAB). FTAB, fluorotelomer thioether amido sulfonate (FtTAoS) and fluorotelomer sulfoxide amido sulfonate (FTSAS-sulfoxide) have been recently identified as alternatives to replace PFOS in AFFF formulations [5,17,70,71]. These PFASs precursors and fluorotelomers are more susceptible to oxidative degradation since they contain unfluorinated carbons (i.e.,  $-\text{CH}_2-\text{CF}_2-$  into  $-\text{CH}=\text{CF}-$ ) or individual chemical moieties within their molecular structures [72]. D'Agostino et al. [43] reported the biodegradation 6:2 FTAB produces FTOH, FTCA, FTUCA, 5:3 FTCA and PFHxA and PFPeA. Direct photolysis of 6:2 FTAB gave rise to the generation of 6:2 fluorotelomer sulfonamide (6:2 FTSA<sub>m</sub>), 6:2 fluorotelomer sulfonamide alkylamine (6:2 FTAA), 6:2 FTOH and 6:2 FTUCA and PFHpA, PFHxA and PFPeA, whereas the BDD electrochemical oxidation of industrial

effluents that contain 6:2 FTAB produced 6:2 FTSA and PFCAs (C<sub>7</sub>-C<sub>4</sub>) [53,73]. Bruton et al. [17] observed the transformation of 6:2 FtTAoS in mainly PFHxA, and also PFHpA, PFPeA and PFBA, by heat activated-persulfate. Overall, it has been reported that C<sub>n</sub> sulfonamide-containing compounds can be transformed to equimolar quantities of the corresponding C<sub>n</sub> fluorotelomers or PFCAs [17,53], whereas C<sub>n</sub> fluorotelomers are transformed to a mixture of PFCAs of varying carbon chain length [15,17,20,39,74]. Furthermore, based on the literature and the fluorotelomer trends in the different treatments herein shown, it could be pointed out that high content of an unknown C<sub>6</sub> sulfonamide-based precursor (such as 6:2 FTAB [75]) in the AFFF formulation could give rise to 6:2 FTCA in the oxidative treatment, whereas 6:2 FTSA and 6:2 FTUCA can be formed as by-product during the reductive treatment. This idea is supported by the low generation of 6:2: FTCA during the UV-persulfate treatment used as the second stage (Fig. 3d), when its precursors seems to be eliminated in the first reductive stage. However, future research will be focus on the identification of these kind of sulfonamide precursors in the initial AFFF sample.

### Perfluoroalkyl sulfonates

Within this group of PFASs, PFOS was initially the most abundant component in the AFFF mixture used in this work. On the one hand, PFOS initially increased during the second reductive stage in sequence 1, and then decreased by means of e<sub>aq</sub><sup>-</sup> species. This indicates that AFFF also contains perfluoroalkyl sulfonamide-based precursors, such as perfluorooctane sulfonamide (FOSA) which has been found in AFFF-impacted groundwater [76,77]. This type of precursors can be also transformed into PFCAs (PFOA in this case) and the corresponding

perfluoroalkyl sulfonamide as well [44].

On the other hand, based on the results, it is concluded that both sulfate radicals and hydrated electrons could decompose long-chain PFSA in the UV-persulfate and UV-sulfite treatments. The oxidative degradation pathways of PFOS initiated by  $\text{SO}_4^{\cdot-}$  radicals are not clear at present. However, it has been reported that the first oxidative attack of PFOS may occur at the C-S bond, to form  $\text{C}_8\text{F}_{17}\cdot$  [25,37,49,78]. Yamamoto et al. [49] demonstrated that PFOS can undergo two major degradation pathways, via  $\text{C}_8\text{HF}_{17}$  and  $\text{C}_8\text{F}_{17}\text{OH}$ , under UV irradiation and alkaline 2-propanol. As a result, short-chain fluorinated compounds such as  $\text{C}_7\text{HF}_{15}$  and  $\text{C}_7\text{F}_{15}\text{OH}$  by stepwise removal of  $\text{CF}_2$  were produced, to result in the formation of PFCAs. On the other hand, the reductive route of PFOS by  $e_{\text{aq}}^-$  species could initially start with the formation of  $\text{PFOS}^{2-}$  ( $\text{C}_n\text{F}_{2n+1}\text{SO}_3^{2-}$ ) which would further dissociate and produce different fragments [29,79].  $\text{C}_n\text{F}_{2n+1}^-$  was the most likely produced species which may be transformed to PFOA through defluorination and hydrolysis reactions.

### Perfluoroalkyl carboxylates

The initial content of PFCAs ( $\text{C}_4\text{-C}_9$ ) in the AFFF formulation was relatively low. Two different PFCAs trends were observed over the treatments: (i) formation and degradation of PFCAs in the oxidative system, and (ii) only degradation of PFCAs was obtained by UV-sulfite treatment.

The formation of PFCAs was the last step in the degradation of fluorotelomers or unknown sulfonamide- and fluorotelomer-based precursors in the UV-persulfate treatment. Houtz et al. [10] also observed the presence perfluorohexane sulfonamide amine (PFHxSAM) and

perfluorohexane sulfonamide amino carboxylate responsible for PFHxA production in 3M AFFF. Once PFCAs are formed, the content of PFCAs subsequently decreased with the reaction with  $\text{SO}_4^{\cdot-}$  by the well-known sequential chain-shortening mechanism forming shorter-chain PFCAs, F and  $\text{CO}_2$  [14,16,20,58].

On the other hand,  $e_{\text{aq}}^-$  generated during the UV-sulfite treatment were more reactive with fully fluorinated compounds (PFCAs and PFSA) than with compounds that contained unfluorinated carbons. Qu et al. [27] and Song et al. [34] proposed reductive degradation routes in which PFOA could initially react with  $e_{\text{aq}}^-$  releasing fluorine to form  $\text{C}_7\text{F}_{14}\text{HCOOH}$  and  $\text{C}_7\text{F}_{13}\text{H}_2\text{COOH}$ . Afterward,  $\text{C}_6\text{F}_{13}\cdot$ ,  $\cdot\text{COOH}$  radicals and  $\text{CH}_2$  carbene were generated from  $\text{C}_7\text{F}_{13}\text{H}_2\text{COOH}$  under irradiation. The reaction between  $\text{C}_6\text{F}_{13}\cdot$  and  $\cdot\text{COOH}$  radicals may occur to form shorter chain perfluoroalkyl carboxylate,  $\text{C}_6\text{F}_{13}\text{COOH}$ , which is further degraded in the same manner. Similarly,  $\text{C}_6\text{F}_{13}\cdot$  radical can undergo hydrolysis and HF loss to yield perfluoroalkyl carboxylates, which would be further decomposed by the same mechanism.

#### **4. Conclusions**

This work evaluates the feasibility of sequential UV oxidative/reductive treatments for the degradation of a complex mixture of PFASs contained in a AFFF formulation. The precise chemical compositions of AFFF formulations are proprietary, nevertheless, different perfluorocarboxylates, perfluorosulfantes, fluorotelomer carboxylates and fluorotelomer sulfonates were identified. PFOS present a notably higher initial content in the sample, among the identified PFASs. PFOS present a notably higher initial content in the sample, among the identified PFASs. Moreover, the

sample contained high content of unknown PFASs precursors, as it was revealed with the total fluorine content of AFFF obtained by  $^{19}\text{F}$ -NMR, that corresponded only to the  $30 \pm 5\%$  of total F calculated from the initial concentration of PFASs detected. To the best of our knowledge, this is the first study investigating combinations of consecutive treatments of AFFF.

The results demonstrated that each photochemical system exhibited different performance for each PFAS group. Whereas fluorotelomer carboxylates seem to be inert to the reductive treatment, their concentration increased over the UV-activated persulfate treatment. Fluorotelomer sulfonates were effectively oxidized by sulfate radicals, while the levels of these compounds rose during the reduction. It was suggested that one sulfonamide-based precursors present in the AFFF formulation may be transformed into fluorotelomers FTs detected by different degradation pathways in oxidative and reductive treatments. In contrast, the degradation trends of PFASs were similar between reductive and oxidative strategies. However, PFCAs were effectively degraded by  $e_{\text{aq}}^-$  species, while their concentrations partially increased during the oxidation, due to the high transformation unknown precursors to fluorotelomers, and consequently to PFCAs, which were also decomposed step-by-step to shorter-chain PFCAs. As a result, it can be concluded that  $e_{\text{aq}}^-$  are more reactive with perfluorinated compounds (PFASs and PFCAs), and  $\text{SO}_4^{\bullet-}$  radicals could react more rapidly with PFAS precursors and fluorotelomers that content unfluorinated carbons.

Furthermore, as the efficacy of reduction and oxidation processes seemed to be affected by the molecular structure of PFASs, sequential UV oxidative/reductive treatments were applied for facilitating the degradation of the PFASs. Tests of different sequential treatments showed the most

promising combination to be a sequence of UV-sulfite followed by UV-persulfate, which achieved the highest removal of the total PFASs content in AFFF. Indeed, a 96% elimination of PFOS was obtained after 48h in this sequence. When UV-sulfite is used as second stage, it was less effective applied after the persulfate treatment, than the individual treatment. Further research investigating potential PFASs precursors in the AFFF mixture and the possible routes of oxidation and reduction of PFASs will be addressed.

### **Appendix A. Supplementary data**

Additional information regarding the full name, chemical structure, LOQs for PFASs detected in AFFF and PFASs concentrations after the treatments are gathered.

### **Acknowledgements**

Financial support from projects CTM2016-75509-R (MINECO/FEDER) and the U.S. Air Force Civil Engineering Center (BAA-031 Contract FA8903-16-C-0019-P00001). B. Gómez-Ruiz also acknowledges the PhD research grant (FPI, BES-2014-071045) and the funding of the short-term stay in Colorado School of Mines during the FPI grant period.

### **References**

- [1] R.C. Buck, J. Franklin, U. Berger, J.M. Conder, I.T. Cousins, P. De Voogt, A.A. Jensen, K. Kannan, S.A. Mabury, S.P.J. van Leeuwen, Perfluoroalkyl and polyfluoroalkyl substances in the environment: Terminology, classification, and origins, *Integr. Environ. Assess. Manag.* 7 (2011) 513–541.

- [2] S.H. Prevedouros, Konstantinos; Cousins, Ian T.; Buck, Robert C., Korzeniowski, Critical Review Sources , Fate and Transport of Fate, Environ. Sci. Technol. 40 (2006) 32–44.
- [3] USEPA, Drinking Water Health Advisory for Perfluorooctanoic Acid (PFOA), 2016. <https://www.epa.gov/ground-water-and-drinking-water/drinking-water-health-advisories-pfoa-and-pfos>.
- [4] The European Commission, Commission Regulation (EU) 2017/1000 concerning the Registration, Evaluation, Authorisation and Restriction of Chemicals as regards perfluorooctanoic acid (PFOA), its salts and PFOA-related substances, 2017. <http://eur-lex.europa.eu/legal-content/EN/TXT/PDF/?uri=CELEX:32017R1000&from=EN>.
- [5] G. Munoz, M. Desrosiers, S.V. Duy, P. Labadie, H. Budzinski, J. Liu, S. Sauvé, Environmental Occurrence of Perfluoroalkyl Acids and Novel Fluorotelomer Surfactants in the Freshwater Fish *Catostomus commersonii* and Sediments Following Firefighting Foam Deployment at the Lac-Mégantic Railway Accident, Environ. Sci. Technol. 51 (2017) 1231–1240.
- [6] L.A. D’Agostino, S.A. Mabury, Identification of novel fluorinated surfactants in aqueous film forming foams and commercial surfactant concentrates, Environ. Sci. Technol. 48 (2014) 121–129.
- [7] R.H. Anderson, G.C. Long, R.C. Porter, J.K. Anderson, Occurrence of select perfluoroalkyl substances at U.S. Air Force aqueous film-forming foam release sites other than fire-training areas: Field-validation of critical fate and transport properties, Chemosphere. 150 (2016) 678–685.
- [8] M. Filipovic, A. Woldegiorgis, K. Norström, M. Bibi, M. Lindberg, A.H. Österås, Historical usage of aqueous film forming foam: A case study of the widespread distribution of perfluoroalkyl acids from a military airport to groundwater, lakes, soils and fish, Chemosphere. 129 (2015) 39–45.
- [9] S. Mejia-Avenidaño, G. Munoz, S. Vo Duy, M. Desrosiers, P. Benolt, S. Sauvé, J. Liu, Novel Fluoroalkylated Surfactants in Soils Following Firefighting Foam Deployment during the Lac-Mégantic Railway

- Accident, *Environ. Sci. Technol.* 51 (2017) 8313–8323.
- [10] E.F. Houtz, C.P. Higgins, J.A. Field, D.L. Sedlak, Persistence of perfluoroalkyl acid precursors in AFFF-impacted groundwater and soil, *Environ. Sci. Technol.* 47 (2013) 8187–8195.
- [11] X. Xiao, B.A. Ulrich, B. Chen, C.P. Higgins, Sorption of Poly- and Perfluoroalkyl Substances (PFASs) Relevant to Aqueous Film-Forming Foam (AFFF)-Impacted Groundwater by Biochars and Activated Carbon, *Environ. Sci. Technol.* 51 (2017) 6342–6351.
- [12] I. Ross, J. McDonough, J. Miles, P. Storch, P. Thelakkat Kochunarayanan, E. Kalve, J. Hurst, S. S. Dasgupta, J. Burdick, A review of emerging technologies for remediation of PFASs, *Remediat. J.* 28 (2018) 101–126.
- [13] H. Hori, E. Hayakawa, H. Einaga, S. Kutsuna, K. Koike, T. Ibusuki, H. Kiatagawa, R. Arakawa, Decomposition of environmentally persistent perfluorooctanoic acid in water by photochemical approaches, *Environ. Sci. Technol.* 38 (2004) 6118–6124.
- [14] Y. Qian, X. Guo, Y. Zhang, Y. Peng, P. Sun, C.H. Huang, J. Niu, X. Zhou, J.C. Crittenden, Perfluorooctanoic Acid Degradation Using UV-Persulfate Process: Modeling of the Degradation and Chlorate Formation, *Environ. Sci. Technol.* 50 (2016) 772–781.
- [15] X. Yang, J. Huang, K. Zhang, G. Yu, S. Deng, B. Wang, Stability of 6:2 fluorotelomer sulfonate in advanced oxidation processes: Degradation kinetics and pathway, *Environ. Sci. Pollut. Res.* 21 (2014) 4634–4642.
- [16] P. Yin, Z. Hu, X. Song, J. Liu, N. Lin, Activated persulfate oxidation of perfluorooctanoic acid (PFOA) in groundwater under acidic conditions, *Int. J. Environ. Res. Public Health.* 13 (2016) 1-15.
- [17] T.A. Bruton, D.L. Sedlak, Treatment of Aqueous Film-Forming Foam by Heat-Activated Persulfate under Conditions Representative of in Situ Chemical Oxidation, *Environ. Sci. Technol.* 51 (2017) 13878–13885.
- [18] M. Li, Z. Yu, Q. Liu, L. Sun, W. Huang, Photocatalytic decomposition of perfluorooctanoic acid by noble metallic nanoparticles modified TiO<sub>2</sub>, *Chem. Eng. J.* 286 (2016) 232–238.

- [19] B. Gomez-Ruiz, P. Ribao, N. Diban, M.J. Rivero, I. Ortiz, A. Urriaga, Photocatalytic degradation and mineralization of perfluorooctanoic acid (PFOA) using a composite TiO<sub>2</sub>-rGO catalyst, *J. Hazard. Mater.* 344 (2018) 950–957.
- [20] S. Park, L.S. Lee, V.F. Medina, A. Zull, S. Waisner, Heat-activated persulfate oxidation of PFOA, 6:2 fluorotelomer sulfonate, and PFOS under conditions suitable for in-situ groundwater remediation, *Chemosphere*. 145 (2016) 376–383.
- [21] Á. Anglada, A. Urriaga, I. Ortiz, D. Mantzavinos, E. Diamadopoulou, Boron-doped diamond anodic treatment of landfill leachate: Evaluation of operating variables and formation of oxidation by-products, *Water Res.* 45 (2011) 828–838.
- [22] B. Gomez-Ruiz, S. Gómez-Lavín, N. Diban, V. Boiteux, A. Colin, X. Dauchy, A. Urriaga, Boron doped diamond electrooxidation of 6:2 fluorotelomers and perfluorocarboxylic acids. Application to industrial wastewaters treatment, *J. Electroanal. Chem.* 798 (2017) 51–57.
- [23] C.E. Schaefer, C. Andaya, A. Urriaga, E.R. McKenzie, C.P. Higgins, Electrochemical treatment of perfluorooctanoic acid (PFOA) and perfluorooctane sulfonic acid (PFOS) in groundwater impacted by aqueous film forming foams (AFFFs), *J. Hazard. Mater.* 295 (2015) 170–175.
- [24] B.P. Vellanki, A. Abdel-wahab, B. Batchelor, Advanced Reduction Processes: A New Class of Treatment Processes., *Environ. Eng. Sci.* 30 (2013) 264–271.
- [25] H. Park, C.D. Vecitis, J. Cheng, N.F. Dalleska, B.T. Mader, M.R. Hoffmann, Reductive degradation of perfluoroalkyl compounds with aquated electrons generated from iodide photolysis at 254 nm, *Photochem. Photobiol. Sci.* 10 (2011) 1945.
- [26] L. Huang, W. Dong, H. Hou, Investigation of the reactivity of hydrated electron toward perfluorinated carboxylates by laser flash photolysis, *Chem. Phys. Lett.* 436 (2007) 124–128.

- [27] Y. Qu, C. Zhang, F. Li, J. Chen, Q. Zhou, Photo-reductive defluorination of perfluorooctanoic acid in water, *Water Res.* 44 (2010) 2939–2947.
- [28] X. Li, J. Fang, G. Liu, S. Zhang, B. Pan, J. Ma, Kinetics and efficiency of the hydrated electron-induced dehalogenation by the sulfite/UV process, *Water Res.* 62 (2014) 220–228.
- [29] Y. Gu, W. Dong, C. Luo, T. Liu, Efficient Reductive Decomposition of Perfluorooctanesulfonate in a High Photon Flux UV/Sulfite System, *Environ. Sci. Technol.* 50 (2016) 10554–10561.
- [30] N.N. Noorhasan, V.K. Sharma, D. Cabelli, Reactivity of ferrate(V) ( $\text{Fe}^{\text{V}}\text{O}_4^{3-}$ ) with aminopolycarboxylates in alkaline medium: A premix pulse radiolysis, *Inorganica Chim. Acta.* 361 (2008) 1041–1046.
- [31] M. Zhai, H. Kudoh, G. Wu, R.A. Wach, Y. Muroya, Y. Katsumura, N. Nagasawa, L. Zhao, F. Yoshii, Laser photolysis of carboxymethylated chitin derivatives in aqueous solution. Part 1. Formation of hydrated electron and a long-lived radical, *Biomacromolecules.* 5 (2004) 453–457.
- [32] R.G. Zepp, A.M. Braun, J. Holane, J.A. Leenheer, Photoproduction of Hydrated Electrons from Natural Organic Solutes in Aquatic Environments, *Environ. Sci. Technol.* 21 (1987) 485–490.
- [33] T.E. Thomas-Smith, N.V. Blough, Photoproduction of hydrated electron from constituents of natural waters, *Environ. Sci. Technol.* 35 (2001) 2721–2726.
- [34] Z. Song, H. Tang, N. Wang, L. Zhu, Reductive defluorination of perfluorooctanoic acid by hydrated electrons in a sulfite-mediated UV photochemical system, *J. Hazard. Mater.* 262 (2013) 332–338.
- [35] H. Park, C.D. Vecitis, J. Cheng, W. Choi, B.T. Mader, M.R. Hoffmann, Reductive defluorination of aqueous perfluorinated alkyl surfactants: Effects of ionic headgroup and chain length, *J. Phys. Chem. A.* 113 (2009) 690–696.
- [36] B.J. Place, J.A. Field, Identification of Novel Fluorochemicals in Aqueous Film- Forming Foams (AFFF) Used by the US Military, *Environ. Sci. Technol.* 46 (2012) 7120–7127.

- [37] S. Yang, J. Cheng, J. Sun, Y. Hu, X. Liang, Defluorination of Aqueous Perfluorooctanesulfonate by Activated Persulfate Oxidation, *PLoS One*. 8 (2013) 6–15.
- [38] H. Liu, T.A. Bruton, F.M. Doyle, D.L. Sedlak, In situ chemical oxidation of contaminated groundwater by persulfate: Decomposition by Fe(III)- and Mn(IV)-containing oxides and aquifer materials, *Environ. Sci. Technol.* 48 (2014) 10330–10336.
- [39] S. a Gauthier, S. a Mabury, Aqueous Photolysis of 8:2 Fluorotelomer Alcohol, *Environ. Toxicol. Chesistry*. 24 (2005) 1837–1846.
- [40] C. Liang, C.F. Huang, N. Mohanty, R.M. Kurakalva, A rapid spectrophotometric determination of persulfate anion in ISCO, *Chemosphere*. 73 (2008) 1540–1543.
- [41] R.E. Humphrey, M.H. Ward, W. Hinze, Spectrophotometric Determination of Sulfite with 4,4'-Dithiodipyridine and 5,5'-Dithiobis-(2-Nitrobenzoic Acid), *Anal. Chem.* 42 (1970) 698–702.
- [42] E.F. Houtz, D.L. Sedlak, Oxidative conversion as a means of detecting precursors to perfluoroalkyl acids in urban runoff, *Environ. Sci. Technol.* 46 (2012) 9342–9349.
- [43] L.A. D'Agostino, S.A. Mabury, Aerobic biodegradation of two fluorotelomer sulfonamide-based Aqueous Film Forming Foam components produces perfluoroalkyl carboxylates, *Environ. Toxicol. Chem.* 36 (2017) 2012–2021.
- [44] J.C. D'Eon, M.D. Hurley, T.J. Wallington, S.A. Mabury, Atmospheric Chemistry of N-methyl Perfluorobutane Sulfonamidoethanol, C<sub>4</sub>F<sub>9</sub>SO<sub>2</sub>N(CH<sub>3</sub>)CH<sub>2</sub>CH<sub>2</sub>OH: Kinetics and Mechanism of Reaction with OH, *Environ. Sci. Technol.* 40 (2006) 1862–1868.
- [45] R.R. Giri, H. Ozaki, T. Morigaki, S. Taniguchi, R. Takanami, UV photolysis of perfluorooctanoic acid (PFOA) in dilute aqueous solution, *Water Sci. Technol.* 63 (2011) 276–282.
- [46] J. Chen, P. Zhang, J. Liu, Photodegradation of perfluorooctanoic acid by 185 nm vacuum ultraviolet light, *J. Environ. Sci.* 19 (2007) 387–390.

- [47] Y. Wu, Y. Li, A. Tian, K. Mao, J. Liu, Selective Removal of Perfluorooctanoic Acid Using Molecularly Imprinted Polymer-Modified TiO<sub>2</sub> Nanotube Arrays, *Int. J. Photoenergy*. 2016 (2016) 1–10.
- [48] R. Qu, J. Liu, C. Li, L. Wang, Z. Wang, J. Wu, Experimental and theoretical insights into the photochemical decomposition of environmentally persistent perfluorocarboxylic acids, *Water Res.* 104 (2016) 34–43.
- [49] T. Yamamoto, Y. Noma, S.-I. Sakai, Y. Shibata, Photodegradation of perfluorooctane sulfonate by UV irradiation in water and alkaline 2-propanol, *Environ. Sci. Technol.* 41 (2007) 5660–5665.
- [50] J. Liu, D.J. Van Hoomissen, T. Liu, A. Maizel, X. Huo, S.R. Fernández, C. Ren, X. Xiao, Y. Fang, C.E. Schaefer, C.P. Higgins, S. Vyas, T.J. Strathmann, Reductive Defluorination of Branched Per- and Polyfluoroalkyl Substances with Cobalt Complex Catalysts, *Environ. Sci. Technol. Lett.* 5 (2018) 289–294.
- [51] V. Ochoa-Herrera, R. Sierra-Alvarez, A. Somogyi, N.E. Jacobsen, V.H. Wysocki, J.A. Field, Reductive defluorination of perfluorooctane sulfonate, *Environ. Sci. Technol.* 42 (2008) 3260–3264.
- [52] M.K. Moe, S. Huber, J. Svenson, A. Hagenaaers, M. Pabon, M. Trümper, U. Berger, D. Knapen, D. Herzke, The structure of the fire fighting foam surfactant Forafac®1157 and its biological and photolytic transformation products, *Chemosphere*. 89 (2012) 869–875.
- [53] B. Gomez-Ruiz, S. Gómez-Lavín, N. Diban, V. Boiteux, A. Colin, X. Dauchy, A. Urriaga, Efficient electrochemical degradation of poly- and perfluoroalkyl substances (PFASs) from the effluents of an industrial wastewater treatment plant, *Chem. Eng. J.* 322 (2017) 196–204.
- [54] R.R. Giri, H. Ozaki, T. Okada, S. Taniguchi, R. Takanami, Factors influencing UV photodecomposition of perfluorooctanoic acid in water, *Chem. Eng. J.* 180 (2012) 197–203.
- [55] P. Neta, R.E. Huie, A.B. Ross, Rate constants for reactions of inorganic radicals in aqueous solution, *J.Phys.Chem.Ref.Data.* 17 (1988) 1027–

- 1284.
- [56] H. Hori, A. Yamamoto, E. Hayakawa, S. Taniyasu, N. Yamashita, S. Kutsuna, H. Kiatagawa, R. Arakawa, Efficient decomposition of environmentally persistent perfluorocarboxylic acids by use of persulfate as a photochemical oxidant, *Environ. Sci. Technol.* 39 (2005) 2383–2388.
- [57] A. Ghauch, A. Baalbaki, M. Amasha, R. El Asmar, O. Tantawi, Contribution of persulfate in UV-254 nm activated systems for complete degradation of chloramphenicol antibiotic in water, *Chem. Eng. J.* 317 (2017) 1012–1025.
- [58] S. Kutsuna, K. Koike, H. Hori, Rate constants and conversion ratios for aqueous-phase reactions of  $\text{SO}_4^-$  with  $\text{C}_n\text{F}_{2n+1}\text{C}(\text{O})\text{O}^-$  ( $n = 4-7$ ) at 298 K, *Int. J. Chem. Kinet.* 41 (2009) 735–747.
- [59] T. Oppenländer, *Photochemical Purification of Water and Air: Advanced Oxidation Processes (AOPs) - Principles, Reaction Mechanisms, Reactor Concepts*, 2003.
- [60] M. Fischer, P. Warneck, Photodecomposition and Photooxidation of Hydrogen Sulfite in Aqueous Solution, 3654 (1996) 15111–15117.
- [61] G. V. Buxton, C.L. Greenstock, W.P. Helman, A.B. Ross, Critical Review of rate constants for reactions of hydrated electrons, hydrogen atoms and hydroxyl radicals ( $\cdot\text{OH}/\cdot\text{O}$ ) in Aqueous Solution, *J. Phys. Chem. Ref. Data.* 17 (1988) 513–886.
- [62] X. Li, G. Liu, J. Fang, S. Yue, Y. Guan, L. Chen, X. Liu, Efficient Reductive Dechlorination of Monochloroacetic Acid by Sulfite/UV Process, *Environ. Sci. Technol.* 46 (2012) 7342-7349.
- [63] F. Xiao, R.A. Hanson, S.A. Golovko, M.Y. Golovko, W.A. Arnold, PFOA and PFOS are generated from zwitterionic and cationic precursor compounds during water disinfection with chlorine and ozone (submitted), *Environ. Sci. Technol. Lett.* 5 (2018) 382-388.
- [64] C.M. Butt, D.C.G. Muir, S.A. Mabury, Biotransformation pathways of fluorotelomer-based polyfluoroalkyl substances: A review, *Environ. Toxicol. Chem.* 33 (2014) 243–267.

- [65] R.F. McFeeters, Use and Removal of Sulfite by Conversion to Sulfate in the Preservation of Salt-Free Cucumbers, *J. Food Prot.* 61 (1998) 885–890.
- [66] S.A. Styler, A.L. Myers, D.J. Donaldson, Heterogeneous photooxidation of fluorotelomer alcohols: A new source of aerosol-phase perfluorinated carboxylic acids, *Environ. Sci. Technol.* 47 (2013) 6358–6367.
- [67] D.A. Ellis, J.W. Martin, A.O. De Silva, S.A. Mabury, M.D. Hurley, M.P. Sulbaek Andersen, T.J. Wallington, Degradation of fluorotelomer alcohols: A likely atmospheric source of perfluorinated carboxylic acids, *Environ. Sci. Technol.* 38 (2004) 3316–3321.
- [68] M.H. Kim, N. Wang, K.H. Chu, 6:2 Fluorotelomer alcohol (6:2 FTOH) biodegradation by multiple microbial species under different physiological conditions, *Appl. Microbiol. Biotechnol.* 98 (2014) 1831–1840.
- [69] J. Liu, S. Mejia Avendaño, Microbial degradation of polyfluoroalkyl chemicals in the environment: A review, *Environ. Int.* 61 (2013) 98–114.
- [70] K.C. Harding-Marjanovic, E.F. Houtz, S. Yi, J.A. Field, D.L. Sedlak, L. Alvarez-Cohen, Aerobic Biotransformation of Fluorotelomer Thioether Amido Sulfonate (Lodyne) in AFFF-Amended Microcosms, *Environ. Sci. Technol.* 49 (2015) 7666–7674.
- [71] K.A. Barzen-Hanson, S.E. Davis, M. Kleber, J.A. Field, Sorption of Fluorotelomer Sulfonates, Fluorotelomer Sulfonamido Betaines, and a Fluorotelomer Sulfonamido Amine in National Foam Aqueous Film-Forming Foam to Soil, *Environ. Sci. Technol.* 51 (2017) 12394–12404.
- [72] A. Urriaga, A. Soriano, J. Carrillo-Abad, BDD anodic treatment of 6:2 fluorotelomer sulfonate (6:2 FTSA). Evaluation of operating variables and by-product formation, *Chemosphere.* 201 (2018) 571–577.
- [73] L.J. Trouborst, Aqueous photolysis of 6:2 fluorotelomer sulfonamide alkylbetaine, 2016.
- [74] Q. Zhuo, X. Li, F. Yan, B. Yang, S. Deng, J. Huang, G. Yu, Electrochemical oxidation of 1H,1H,2H,2H-perfluorooctane sulfonic acid

- (6:2 FTS) on DSA electrode: Operating parameters and mechanism, *J. Environ. Sci. (China)*. 26 (2014) 1733–1739.
- [75] D.M.J. Shaw, G. Munoz, E.M. Bottos, S.V. Duy, S. Sauvé, J. Liu, J.D. Van Hamme, Degradation and defluorination of 6:2 fluorotelomer sulfonamidoalkyl betaine and 6:2 fluorotelomer sulfonate by *Gordonia* sp. strain NB4-1Y under sulfur-limiting conditions, *Sci. Total Environ.* 647 (2019) 690–698.
- [76] S. Banzhaf, M. Filipovic, J. Lewis, J. Sparrenbom, Charlotte, R. Barthel, A review of contamination of surface-, ground-, and drinking water in Sweden by perfluoroalkyl and polyfluoroalkyl substances (PFASs), *Ambio*. 46 (2017) 335–346.
- [77] J. Liu, S. Mejia Avendaño, Microbial degradation of polyfluoroalkyl chemicals in the environment: A review, *Environ. Int.* 61 (2013) 98–114.
- [78] S. Wang, Q. Yang, F. Chen, J. Sun, K. Luo, F. Yao, X. Wang, D. Wang, X. Li, G. Zeng, Photocatalytic degradation of perfluorooctanoic acid and perfluorooctane sulfonate in water: A critical review, *Chem. Eng. J.* 328 (2017) 927–942.
- [79] Y. Gu, T. Liu, H. Wang, H. Han, W. Dong, Hydrated electron based decomposition of perfluorooctane sulfonate (PFOS) in the VUV/sulfite system, *Sci. Total Environ.* 607–608 (2017) 541–548.

## **SUPPORTING INFORMATION**

### **Degradation of poly- and perfluoroalkyl substances (PFASs) in Aqueous Film-Forming Foam by sequential UV oxidative/reductive treatments**

#### **Authors:**

Beatriz Gomez-Ruiz<sup>1</sup>, Nazely Diban<sup>1</sup>, Ane Urriaga<sup>1</sup>, Raul Tenorio<sup>2</sup>,  
Juliane Brown<sup>2</sup>, Christopher P. Higgins<sup>2</sup>, Christopher Bellona<sup>2</sup>, Timothy  
J. Strathmann<sup>2</sup>

(1) Department of Chemical and Biomolecular Engineering,  
Universidad de Cantabria. Av. de Los Castros s/n. 39005 Santander.  
Spain.

(2) Department of Civil and Environmental Engineering, Colorado  
School of Mines, 1012 14th Street, Coolbaugh Hall, Golden, USA

**Table S1.** Full names, abbreviations and limits of quantification (LOQs) for PFAS analytes identified in this work.

Compound	Compound Name	Lower LOQ (ng.L <sup>-1</sup> )	Upper LOQ (ng.L <sup>-1</sup> )
<b>Perfluoroalkyl carboxylates (PFCAs)</b>			
PFBA	Perfluoro-n-butanoic acid	18.8	2323
PFPeA	Perfluoro-n-pentanoic acid	0.6	2323
PFHxA	Perfluoro-n-hexanoic acid	0.6	2323
PFHpA	Perfluoro-n-heptanoic acid	2.3	2323
PFOA	Perfluoro-n-octanoic acid	0.6	2323
PFNA	Perfluoro-n-nonanoic acid	1.2	2323
<b>Perfluoroalkyl sulfonates (PFSA)</b>			
PFPrS	perfluoro-1-propanesulfonate	5.8	1161
PFBS	perfluoro-1-butanesulfonate	0.6	2323
PFPeS	perfluoro-1-pentanesulfonate	0.6	2323
PFHxS	perfluoro-1-hexanesulfonate	2.3	2323
PFHpS	perfluoro-1-heptanesulfonate	2.3	2323
PFOS	perfluorooctanesulfonate	1.2	1161
PFNS	perfluoro-1-nonanesulfonate	0.6	1161
<b>Fluorotelomer carboxylates (FTCAs)</b>			
6:2 FTCA	2-Perfluorohexyl ethanoic acid (6:2)	23.2	2323
<b>Fluorotelomer sulfonates (FTSAs)</b>			
6:2 FTSA	1H,1H,2H,2H-perfluorooctane sulfonate (6:2)	0.6	2323
8:2 FTSA	1H,1H,2H,2H-perfluorodecane sulfonate (8:2)	2.3	581
<b>Fluorotelomer unsaturated carboxylates (FTUCAs)</b>			
6:2 FTUCA	2H-Perfluoro-2-octenoic acid (6:2)	2.3	5807

**Table S2.** Initial concentration ( $C_{\text{initial}}$ ) and the variation of each PFAS concentration ( $\Delta C = C_{\text{final}} - C_{\text{initial}}$ ) after individual UV- $S_2O_8^{2-}$  treatment and sequence of UV- $S_2O_8^{2-}$  and UV- $SO_3^{2-}$  systems.

	$C_{\text{initial}}$ (ng.L <sup>-1</sup> )	$\Delta C$ (ng.L <sup>-1</sup> ) UV- $S_2O_8^{2-}$	$\Delta C$ (ng.L <sup>-1</sup> ) UV- $S_2O_8^{2-}$ + UV- $SO_3^{2-}$
<b>PFBA</b>	244 ± 44	1068 ± 406	-2 ± 39
<b>PFPeA</b>	178 ± 38	601 ± 40	-151 ± 21
<b>PFHxA</b>	1103 ± 196	462 ± 88	-984 ± 133
<b>PFHpA</b>	100 ± 6	359 ± 41	-30 ± 6
<b>PFOA</b>	220 ± 15	-112 ± 8	1512 ± 1406
<b>PFNA</b>	39 ± 2	24 ± 1	2482 ± 1429
<b>PFPrS</b>	100 ± 1	-3 ± 0*	-5 ± 4
<b>PFBS</b>	19 ± 0	0 ± 0*	2 ± 0
<b>PFPeS</b>	128 ± 3	-43 ± 2	-50 ± 3
<b>PFHxS</b>	844 ± 3	-239 ± 5	-307 ± 13
<b>PFHpS</b>	131 ± 3	-56 ± 1	-41 ± 2
<b>PFOS</b>	5929 ± 587	-4686 ± 551	-3436 ± 259
<b>6:2 FTCA</b>		1611 ± 154	1028 ± 6
<b>6:2 FTSA</b>	357 ± 119	-333 ± 117	2 ± 192
<b>8:2 FTSA</b>	230 ± 76	-230 ± 76	-94 ± 32
<b>6:2 FTUCA</b>	50 ± 0	-50 ± 0	1303 ± 0
<b>ΣPFASs</b>	9672 ± 1094	-1628 ± 197	1228 ± 2720

\*The drop of PFAS concentration could be associated with the effect of adding extra volume with  $Na_2S_2O_8$  spikes (10mM) into the reacting media (which represented a removal ratio around 6 %).

**Table S3.** Initial concentration ( $C_{\text{initial}}$ ) and the variation of each PFAS concentration ( $\Delta C = C_{\text{final}} - C_{\text{initial}}$ ) after individual UV-SO<sub>3</sub><sup>2-</sup> treatment and sequence of UV-SO<sub>3</sub><sup>2-</sup> and UV-S<sub>2</sub>O<sub>8</sub><sup>2-</sup> systems.

	$C_{\text{initial}}$ (ng.L <sup>-1</sup> )	$\Delta C$ (ng.L <sup>-1</sup> ) UV-SO <sub>3</sub> <sup>2-</sup>	$\Delta C$ (ng.L <sup>-1</sup> ) UV-SO <sub>3</sub> <sup>2-</sup> + UV-S <sub>2</sub> O <sub>8</sub> <sup>2-</sup>
<b>PFBA</b>	58 ± 19	-43 ± 6	1137 ± 426
<b>PFPeA</b>	31 ± 14	-29 ± 14	959 ± 435
<b>PFHxA</b>	217 ± 27	-213 ± 27	818 ± 185
<b>PFHpA</b>	30 ± 10	-13 ± 4	299 ± 81
<b>PFOA</b>	119 ± 45	-82 ± 15	77 ± 50
<b>PFNA</b>			
<b>PFPrS</b>	63 ± 27	20 ± 2	8 ± 6*
<b>PFBS</b>	13 ± 5	7 ± 0	9 ± 0*
<b>PFPeS</b>	149 ± 39	-38 ± 26	-54 ± 27
<b>PFHxS</b>	777 ± 95	-200 ± 2	-388 ± 41
<b>PFHpS</b>	84 ± 15	-35 ± 12	-54 ± 6
<b>PFOS</b>	5269 ± 1151	-4547 ± 1126	-5096 ± 1092
<b>6:2 FTCA</b>	22 ± 7	-3 ± 7	19 ± 7
<b>6:2 FTSA</b>	99 ± 4	447 ± 39	-80 ± 8
<b>8:2 FTSA</b>	31 ± 37	48 ± 16	-30 ± 37
<b>6:2 FTUCA</b>	3 ± 0	1 ± 0	-1 ± 0
<b>ΣPFASs</b>	6964 ± 1497	-4683 ± 1182	-2379 ± 61

\*The drop of PFAS concentration could be associated with the effect of adding extra volume with Na<sub>2</sub>S<sub>2</sub>O<sub>8</sub> spikes (10mM) into the reacting media (which represented a removal ratio around 6 %).

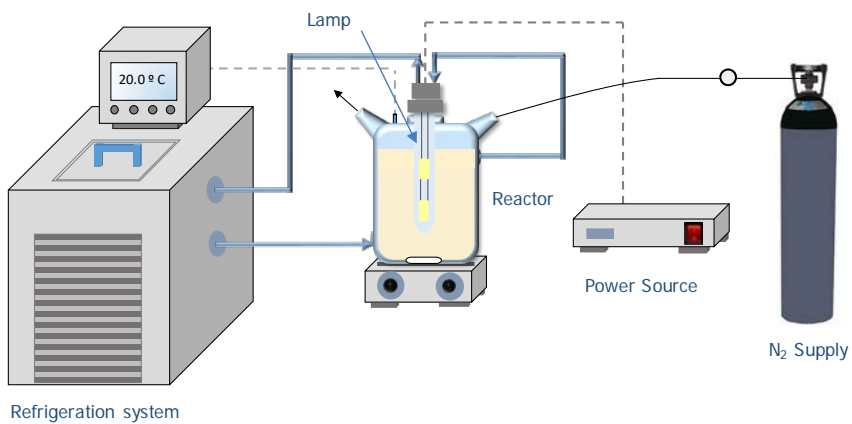


**Figure S1.** Photochemical experimental system formed by the UV reactor, refrigeration system, magnetic stirrer, UV low pressure mercury lamp and N<sub>2</sub> tank (for UV/sulfite experiments).

Prior to AFFF experiments, control tests were carried out to study the sensitizers decay by UV irradiation (Figure S2). After 4h of UV irradiation, complete depletion of persulfate was obtained. However, the concentration of sulfite after 24h of UV irradiation was around the 50% of the initial concentration. According to these results, additional aliquots of 10-12 mM  $\text{Na}_2\text{S}_2\text{O}_8$  were added to the reacting media to maintain a regular content of sensitizers throughout the AFFF tests. On the contrary, no additional aliquots of sulfite were introduced during the reductive experiments.

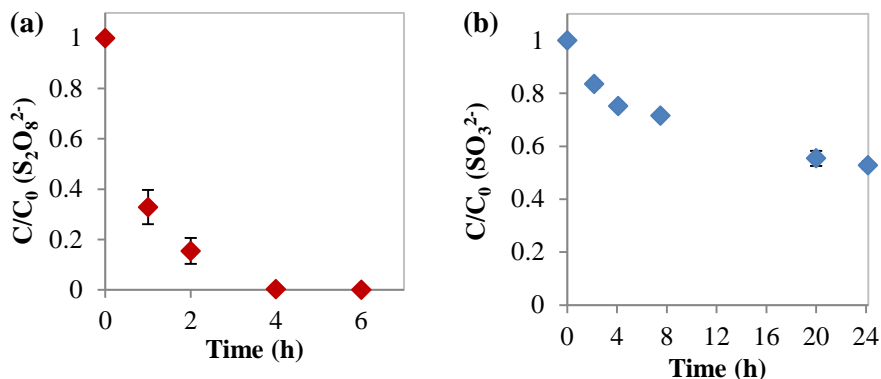


**Figure S2.** Evolution of the dimensionless concentration of each sensitizer: (a) persulfate and (b) sulfite with time under UV irradiation. The initial concentration of sensitizers was 10 mM.



## Annex II. Congress contributions

Urtiaga, A., **Gomez-Ruiz, B.**, Ortiz, I. Electrocatalytic and photo-assisted degradation of perfluorooctanoic acid. 4th European Congress on Environmental Applications of Advanced Oxidation processes (EAAOP-4). Athens (Greece), October 21-24, 2015. *Lecture*



**Gomez-Ruiz, B.**, Diban, N., Urtiaga, A. Oxidación electroquímica del ácido perfluorooctanoico y estudio del efecto de fluoruro mediante ánodo de diamante dopado con boro. XXXVII Reunión del Grupo de Electroquímica GE-RSEQ. ISBN 978-84-16724-13-0. Alicante (Spain), July 17-20, 2016. *Lecture*



**Gomez-Ruiz, B.**, Diban, N., Rivero, M.J., Ortiz, I., Urtiaga, A. Efficient photocatalytic degradation of perfluorooctanoic acid. 6th EuCheMS-Chemistry Congress. Seville (Spain), September 11-15, 2016. *Poster presentation*



Urtiaga, A., **Gomez-Ruiz, B.**, Gómez-Lavín, S., Diban, N., Colin, A., Boiteux, V., Dauchy, X. Rivero, M.J., Ortiz, I., O Electrochemical treatment of poly- and perfluoroalkyl substances (PFASs) from industrial effluents. 11<sup>th</sup> European Symposium on Electrochemical Engineering (ESEE 2017). Prague, June 4-8, 2017. *Lecture*



**Gomez-Ruiz, B.,** Ribao, P., Diban, N., Rivero, M.J., Ortiz, I., Urtiaga, A. Decomposition of perfluorooctanoic acid photocatalyzed by doped TiO<sub>2</sub> structures with graphene oxide under UV-VIS irradiation. 5<sup>th</sup> European Conference on Environmental Applications of Advanced Oxidation Processes (EAAOP-5). Prague, June 25-29, 2017. *Lecture*



**Gomez-Ruiz, B.,** Diban, N., Rivero, M.J., Ortiz, I., Urtiaga, A. Efficient photocatalytic degradation of perfluorooctanoic acid (PFOA) by TiO<sub>2</sub> doped with graphene oxide. 10<sup>th</sup> World Congress of Chemical Engineering. Barcelona (Spain), October 1-5, 2017. *Lecture*



**Gomez-Ruiz, B.,** Diban, N., Urtiaga, A., Tenorio, R., Brown, J., Higgins, C.P., Bellona, C., Strathmann. Degradation of poly- and per-fluoroalkyl substances (PFASs) from AFFF-impacted water by sequential oxidative/reductive treatments. 110th European meeting on Solar Chemistry and Photocatalysis:



Environmental Applications (SPEA10). Almeria (Spain), June 4-8, 2017. *Poster presentation*

**Gomez-Ruiz, B.,** Diban, N., Rivero, M.J., Ortiz, I., Urtiaga, A. Photocatalytic degradation of perfluorocarboxylic acids by TiO<sub>2</sub>-rGO composite. Carbon 2018. Madrid (Spain), July 1-6, 2018. *Lecture*



### **Annex III. Dissemination activities**

**Gomez-Ruiz, B.** European Researchers' Night. Diffusion activities of the Research Groups: DEPRO, PAS, IPS y TAB. Santander, September 2016, 2017, 2018.



**Gomez-Ruiz, B.** Diffusion activities in the Scientific Week at the University of Cantabria. Santander, November 6-17, 2017. November 5-16, 2018.



**Gomez-Ruiz, B.** Mini-lecture: own experiences as Chemical Engineer. International Day of Women and Girls in Science. ETSIT, University of Cantabria. February 11, 2018.



